

Electrocatalysis Induced by Surface Redox Activities on Conductive Metal Oxide Electrodes

THÈSE N° 4619 (2010)

PRÉSENTÉE LE 5 MARS 2010

À LA FACULTÉ SCIENCES DE BASE

GROUPE DE GÉNIE ÉLECTROCHIMIQUE

PROGRAMME DOCTORAL EN CHIMIE ET GÉNIE CHIMIQUE

ÉCOLE POLYTECHNIQUE FÉDÉRALE DE LAUSANNE

POUR L'OBTENTION DU GRADE DE DOCTEUR ÈS SCIENCES

PAR

Stéphane FIERRO

acceptée sur proposition du jury:

Prof. L. Kiwi, présidente du jury
Prof. C. Comninellis, directeur de thèse
Prof. G. Chen, rapporteur
Prof. D. Devilliers, rapporteur
Dr S. Mischler, rapporteur



ÉCOLE POLYTECHNIQUE
FÉDÉRALE DE LAUSANNE

Suisse
2010

Acknowledgements

Je voudrais tout d'abord remercier particulièrement le Pr. Christos Comninellis qui m'a accepté dans son groupe déjà depuis le travail de Master et qui m'a donné l'opportunité d'entreprendre cette thèse. Je tiens à le remercier également pour ses encouragements et pour les conseils précieux qu'il m'a donné durant nos nombreuses discussions ainsi que pour l'encadrement exceptionnel dont j'ai bénéficié pendant ces trois années. Ευχαριστώ πολύ!

Dr. Györgi Fóti a également toujours été disponible pour m'aider dans mes recherches et m'a fait profiter de ses connaissances et de son expérience pour mener à bien ce travail. Merci Györgi.

Je tiens à remercier aussi tous les membres du jury qui ont pris le temps de lire et corriger ce travail: Pr. Guohua Chen, Pr. Didier Devilliers et Dr. MER Stefano Mischler. Merci également au Pr. Liubov Kiwi pour avoir présidé le jury.

Ich möchte auch Pr. Helmut Baltruschat, Dr. Tina Nagel und Dr. Barbora Lanova von der Institut für Physikalische und Theoretische Chemie in der Universität von Bonn danken um mir einen Monat in ihrer Gruppe akzeptiert zu haben. Die DEMS Ergebnisse waren einen Ausgangspunkt dieser Arbeit und ich hatte eine wunderschöne Erfahrung in Bonn und Köln. Ich werde sicherlich ein Tag nach Bonn zurückkommen um ein Kölsch zu trinken! Herzliches Dank für alles.

Un grand merci également au Pr. Milena Koudelka et au Dr. Olivier Frey du SAMLAB à l'université de Neuchâtel pour leur aide précieuse concernant les microélectrodes en iridium.

Un remerciement très spécial également à mon frère Alex pour avoir pris le temps de corriger l'anglais et à Claudia pour la mise en page.

Je remercie aussi Mme Evelyne Toubes et Mme Anne Lene Odegaard pour leur aide concernant les tâches administratives.

Je remercie également les techniciens de l'Institut de génie chimique.

Aussi durant ces trois années, j'ai travaillé dans une ambiance exceptionnelle au sein du groupe de génie électrochimique et ce en grande partie grâce à tous mes collègues: Mériadec, Cyril, Pietro (un remerciement spécial à vous

ABSTRACT

trois pour les escapades à Prague), Aga, Alain, Arnaud, Bahaa, Guillaume, Erika, Lassiné, Nikola, Félicien et Julian.

Je tiens à remercier également les stagiaires et diplômants qui ont contribué à la réussite de ce travail: Manolis (Many thanks my friend), Michaël, Déborah, Sneh, Gabrielle, Thibault et Efthalia.

Et enfin, et surtout, je tiens à remercier du fond du coeur mes parents ainsi que mon grand frère pour leur soutien inconditionnel durant toutes ces années. Ils ont toujours été présents et je ne serais pas arrivé là sans eux. Merci infiniment.

ELECTROCATALYSIS INDUCED BY SURFACE REDOX ACTIVITIES ON CONDUCTIVE METAL OXIDE ELECTRODES

Abstract

Iridium dioxide electrodes form part of the dimensionally stable anodes (DSA®) and this electrode material is widely used in many industrial processes namely water electrolysis, metal electro-winning, cathodic protection and electro-organic synthesis due to the high electrochemical activity and stability of this electrode material.

IrO₂-based electrodes can be prepared using different techniques but the most common is the thermal decomposition of H₂IrCl₆ precursor solution on an inert substrate like titanium.

Within the water stability potential domain, the charging/discharging process is attributed to the slow diffusion of protons within the IrO₂ coating together with the electrical double layer capacitance. In fact the valence state of the Ir surface atoms of the coating varies from +IV to +VI in the potential domain between the on-set potentials of H₂ and O₂ evolution.

Concerning the oxygen evolution reaction, direct evidence was found that the IrO₂ coating participates actively in the reaction using an electrolyte solution containing isotopically labeled H₂¹⁸O. In fact, measurements of the relative amounts of electrogenerated ¹⁶O₂ and ¹⁸O¹⁶O have demonstrated that the hydroxyl radicals coming from water discharge interact strongly with IrO₂ resulting in the formation of the higher oxide (IrO₃) and the decomposition of that oxide produces oxygen. IrO₃ is thus the intermediate involved in the OER on these electrodes.

During the oxidation of organic compounds, direct evidence was found by marking the IrO₂ electrode with ¹⁸O that the higher valence state oxide IrO₃ participates effectively also in this process. In fact, the oxidation of a solution of formic acid on a marked IrO₂ coating containing ¹⁸O has shown that C¹⁶O¹⁸O is evolved proving that the oxidation of organic compounds occurs on IrO₃ with competing side-reaction of oxygen evolution. The low overpotential of the OER allows performing selective electro-oxidation of a wide variety of organic compounds. In fact, the competing side reaction of oxygen evolution

ABSTRACT

'buffers' the potential around values where the oxidation products are not further oxidized showing that the IrO₂ electrode is particularly suited for electro-organic synthesis. However, the current efficiency of the oxidation process remains low due to the competing side reaction of oxygen evolution.

KEYWORDS: IrO₂ electrode, DSA®, oxygen evolution, electro-organic synthesis, voltammetric charge, surface redox electrocatalysis, DEMS measurements

Résumé

Les électrodes au dioxyde d'iridium font partie des anodes dimensionnellement stables (DSA®) et ce matériau d'électrode est largement employé dans plusieurs procédés industriels tels que les électrolyses en milieu aqueux, la récupération de métaux, la protection cathodique et la synthèse électro-organique, car ce matériau possède une grande activité électrochimique ainsi qu'une grande stabilité.

Les électrodes au dioxyde d'iridium peuvent être préparées de différentes manières mais la plus répandue est la décomposition thermique d'une solution du précurseur H_2IrCl_6 sur un substrat inerte tel que le titane.

Dans le domaine de potentiel de stabilité de l'eau, la charge/décharge de l'électrode est attribuée à la diffusion lente de protons à l'intérieur du film d' IrO_2 ainsi qu'au chargement de la double couche électrique. En fait, l'état de valence des atomes d'iridium surfaciques du matériau d'électrode varie entre +IV et +VI dans le domaine de potentiel situé entre les potentiels de départ des dégagements d'hydrogène et d'oxygène.

Concernant la réaction de dégagement d'oxygène, une preuve directe de la participation du film IrO_2 à cette réaction a été trouvée en utilisant une solution d'électrolyte contenant H_2^{18}O . En fait, les mesures des concentrations relatives de $^{16}\text{O}_2$ et $^{18}\text{O}^{16}\text{O}$ électro-générés ont démontré que les radicaux hydroxyles provenant de la décharge de l'eau interagissent fortement avec l' IrO_2 impliquant la formation de l'oxyde d'état de valence supérieur (IrO_3) et la décomposition de cet oxyde produit de l'oxygène. IrO_3 donc est l'intermédiaire impliqué dans le dégagement d'oxygène sur ces électrodes.

Pendant l'oxydation de composés organiques, une preuve directe a été trouvée en marquant une électrode Ti/IrO_2 avec ^{18}O que l'oxyde d'état de valence supérieur IrO_3 participe activement aussi dans ce procédé. En effet, l'oxydation d'une solution d'acide formique sur une électrode Ti/IrO_2 marquée avec ^{18}O a engendré la formation de $\text{C}^{16}\text{O}^{18}\text{O}$ prouvant que l'oxydation de composés organiques se produit sur IrO_3 en compétition avec le dégagement d'oxygène. La faible surtension du dégagement d'oxygène permet l'électro-oxydation sélective d'une grande variété de composés organiques. En fait, la

RESUME

réaction secondaire de dégagement d'oxygène 'tamponne' le potentiel à des valeurs où les produits d'oxydation ne sont pas minéralisés ce qui montre que cette électrode est particulièrement appropriée pour la synthèse électro-organique. Cependant, l'efficacité du courant de la réaction d'oxydation reste faible en raison de la forte compétition avec le dégagement d'oxygène.

MOTS-CLÉS: électrode à l'IrO₂, DSA®, dégagement d'oxygène, synthèse electro-organique, charge voltamétrique, électrocatalyse redox de surface, mesures DEMS.

Table of contents

Chapter 1 : Introduction	13
References.....	16
Chapter 2 : Bibliography.....	19
2.1 Dimensionally Stable Anodes (DSA®): Preparation, properties and applications..	20
2.2 The spin coating deposition technique.....	21
2.3 General mechanism of organics oxidation on ‘active’ and ‘non-active’ type electrodes with competing side reaction of oxygen evolution.....	26
2.3.1 ‘Active’ type electrodes	28
2.3.2 ‘Non-active’ type electrodes.....	29
2.4 Differential Electrochemical Mass Spectrometry (DEMS)	30
2.4.1 DEMS setup.....	31
Interface to vacuum.....	31
The DEMS cell	31
Vacuum system.....	33
2.4.2 DEMS results analysis.....	34
2.5 Theoretical model for the oxidation of organic compounds during electrolysis experiments based on the maximum oxidation rate	36
2.5.1 Electrolysis under current control ($j_{\text{applied}} < j_{\text{lim}}$)	37
2.5.2 Electrolysis under mass transport control ($j_{\text{applied}} > j_{\text{lim}}$)	38
2.6 References	40
Chapter 3 : Preparation and morphological characterization of Ti/IrO₂ and p-Si/IrO₂ electrodes	43
3.1 Introduction.....	44
3.2 Experimental details	46
3.3 Results and discussion.....	47
3.3.1 Morphological and voltammetric charge studies of Ti/IrO ₂ electrodes.....	47
3.3.2 Morphological and voltammetric charge study of Ti/IrO ₂ electrodes prepared using the spin coating deposition method	51

TABLE OF CONTENT

3.3.3 p-Si as substrate	58
3.4 Conclusions	61
3.5 References	62
Chapter 4 : Surface redox activities and charging/discharging process on p-Si/IrO₂ electrodes.....	63
4.1 Introduction.....	64
4.2 Experimental details	66
4.3 Results and discussion.....	67
4.3.1 The charging/discharging process.....	67
4.3.2 Surface redox activities of p-Si/IrO ₂ electrodes.....	76
Open circuit potential.....	76
Cyclic voltammetry measurements on p-Si/IrO ₂	77
Proposed surface reactions for p-Si/IrO ₂ electrodes.....	83
4.4 Conclusions	83
4.5 References	84
Chapter 5 : Active intermediates involved in the oxygen evolution reaction (OER) on IrO₂ electrodes: Voltammetric and DEMS study	87
5.1 Introduction.....	88
5.2 Experimental details	90
5.2.1 Differential electrochemical mass spectrometry (DEMS).....	90
5.2.2 Voltammetric experiments	92
5.2.3 Ohmic drop correction.....	92
5.3 Results and discussion.....	93
5.3.1 DEMS measurements.....	93
5.3.2 Tafel slope measurement for the oxygen evolution reaction on p-Si/IrO ₂ electrodes.....	102
5.4 Conclusions	105
5.5 References	105
Chapter 6 : Active intermediates involved in the oxidation of organic compounds on Ti/IrO₂ electrodes: DEMS study.....	107

6.1	Introduction.....	108
6.2	Experimental details	109
	Differential electrochemical mass spectrometry (DEMS).....	109
6.3	Results and discussion.....	110
	DEMS measurements using Ti/IrO ₂	110
6.4	Conclusions	117
6.5	References	118
Chapter 7 : Voltammetric study of the oxidation of model organic compounds on p-Si/IrO₂ electrodes119		
7.1	Introduction.....	120
7.2	Experimental details	121
	Voltammetric experiments using p-Si/IrO ₂	121
7.3	Results and discussion.....	122
	Model for organics oxidation on p-Si/IrO ₂ electrodes.....	122
	Estimation of the kinetic parameters of organic oxidation on p-Si/IrO ₂ electrodes using formic acid, <i>i</i> -propanol, 2-butanol and phenol as model compounds.....	127
	Theoretical I-V curves of formic acid oxidation on p-Si/IrO ₂ electrodes	132
7.4	Conclusions	134
7.5	References	135
Chapter 8 : Selective oxidation of organic compounds on IrO₂ electrodes 137		
8.1	Introduction.....	138
8.2	Experimental details	140
	Preparative electrolysis experiments.....	140
	Electrolysis using a single compartment electrochemical cell.....	141
	Determination of the average mass transfer coefficient for both reactors.....	145
	Analytical methods used	146
8.3	Results and discussion.....	148
	8.3.1 A new approach for electrolysis experiments: Pseudo-potentiostatic operation by anode potential buffering induced by the oxygen evolution reaction.....	148
	8.3.2 Electrolysis of model organic compounds on Ti/IrO ₂	150

TABLE OF CONTENT

Formic acid (FA) oxidation using Ti/IrO ₂	150
<i>i</i> -propanol and 2-butanol oxidation using Ti/IrO ₂	153
Phenol oxidation on Ti/IrO ₂ electrodes.....	156
8.4 Conclusions	163
8.5 References	165
Chapter 9 : General Discussion	167
References.....	171
Chapter 10 : Perspectives.....	173
References.....	176
List of symbols	177
Appendix	185

Chapter 1 : Introduction

Dimensionally stable anodes (DSA®) are prepared by the deposition of a thin (1-5 μ m) active layer (usually a metal oxide) on an inert substrate (usually titanium). These electrodes were discovered 40 years ago and are still described as one of the most striking and greatest technological breakthrough of the history of electrochemistry of the last century [1]. DSA® have shown a very high catalytic activity for many reactions like O₂ evolution, Cl₂ evolution or H₂ evolution. Furthermore, these electrodes have shown to be among the most versatile of electrode materials [1]. In fact, the possibility to prepare electrodes with different compositions (RuO₂, IrO₂, Ta₂O₅, PbO₂, SnO₂, TiO₂, ZrO₂...) on different support materials in terms of nature (titanium, tantalum, niobium, zirconium, conductive silicon...) and geometry (plates, nets, meshes...) and using different methods of deposition (dipping, blading, spin coating, spray coating...) has lead to a wide variety of electrode materials, opening endless possibilities for numerous industrial applications.

Dimensionally stable anodes were first discovered and tested in the industry (Italy) and remained undisclosed for 7 years after their discovery [2] but when the first electrodes were successfully tested for chlor-alkali cells in 1968 [1], information about this new type of electrode material leaked outside the industry. Fortunately, scientists found themselves on the stream of such 'leakage' and the first paper describing their fundamental properties was published in 1971 by S.Trasatti [3]. Since then, the incredible versatility and properties of these electrodes have attracted the interest of scientists worldwide.

Moreover, apart from chlor-alkali cells, DSA® have been used since then in the domains of metal-air batteries [4], molten salt electrolysis [5], cathodic protection in concrete of bridges and other structures [6], pH measuring electrodes [7], Zn electrodeposition [8] and in the metal industry in general [9]. DSA® have also shown to be good candidates for selective oxidation of organics and treatment of waste materials [10-13] but also for oxygen evolution in acidic media because these electrodes, and the IrO₂-based anodes in particular (one of the most recent and promising DSA®), have demonstrated incredible stability under such severe conditions [14].

Despite all of the aforementioned applications, numerous mechanisms occurring on these electrodes are still a matter of active debate and it is therefore essential to acquire a better knowledge on these mechanisms through fundamental research in order to optimize the existing processes mentioned above or possibly extend the range of application possibilities.

Towards this goal, the work proposed herein is aiming at better understanding of the electrochemical behavior in aqueous acidic media of dimensionally stable anodes with IrO₂ as main active component. These IrO₂-based electrodes were prepared by thermal decomposition of a H₂IrCl₆ precursor solution on either Ti or p-Si substrate.

Several processes are studied on these IrO₂-based electrodes: the charging/discharging process, the electrochemical reactions taking place in the water stability potential domain, the oxygen evolution reaction and the oxidation of organic compounds (model aliphatic and aromatic compounds). The surface redox couples of the electrode material are suspected to be involved in all these processes.

In Chapter 3, the preparation of iridium dioxide DSA® is presented. The goal of this investigation is to control and optimize the preparation conditions (support material, deposition technique...) of these electrodes in order to produce stable coatings for

further studies. In fact, it is shown that the IrO₂ loading can be controlled by using the spin coating deposition technique together with a simple relation expressing the loading as a function of the concentration of precursor and the rotation speed of the substrate. It is shown also, that the charge measured during a cyclic voltammetry measurement in the water stability potential domain can be used as a tool in order to estimate the relative amount of active sites (and the loading) of the IrO₂-based DSA®.

In Chapter 4, the charging/discharging process of these electrodes is studied using cyclic voltammetry measurements performed at different temperatures. From these results, the electrochemical and physical processes responsible of the charging/discharging of IrO₂-based electrodes are revealed. Later in the same chapter, the electrochemical reactions occurring in the potential domain of water stability and involving the surface redox couples of the electrode material are studied using cyclic voltammetry and potential step experiments.

The mechanism of the oxygen evolution reaction (OER) on IrO₂ DSA® in acidic media is investigated in Chapter 5 using differential electrochemical mass spectrometry (DEMS) measurements. Later in the same chapter, IR drop corrected Tafel slopes related to O₂ evolution have been determined in order to consolidate the DEMS results. On the basis of these results, a new mechanism for the OER on these electrodes is proposed and the fraction of electrode material effectively participating in the process could also be determined.

In Chapter 6, the analysis performed in Chapter 5 is repeated but this time in order to study the mechanisms and active intermediates involved in the oxidation of organic compounds on these electrodes (using formic acid as model compound). Again, a mechanism is proposed and the fraction of the IrO₂ coating participating in the process is revealed.

In Chapter 7, the anodic oxidation of organic compounds is investigated on IrO₂ DSA® through cyclic voltammetry measurements. In this chapter, a new theoretical model is proposed that estimates the kinetic parameters related to the oxidation of a given organic; it is shown that these parameters are strongly dependent on the IrO₂ loading. Later in the same chapter, and using the same theoretical model together with the kinetic parameters estimated and Nernst equation, the shift of the I-V curves toward less positive potentials induced by the presence of an organic compound was evaluated. From these results, theoretical I-V curves could be plotted.

In Chapter 8, a new approach is proposed in order to perform selective organics oxidation under galvanostatic conditions with the potential 'buffered' by the oxygen evolution reaction. Based on that approach, three series of electrolysis experiments have been conducted on Ti/IrO₂ electrodes:

The oxidation of formic acid has been carried out in order to evaluate the performance of IrO₂ electrodes toward a simple anodic oxidation process. Later, the oxidation of *i*-propanol and 2-butanol were performed in order to achieve selective oxidation of these compounds using the pseudo-potentiostatic approach proposed earlier.

The experimental results obtained for formic acid, *i*-propanol and 2-butanol oxidations regarding the temporal evolutions of concentration and instantaneous current efficiency are compared with the predictions of a theoretical model based on the maximum oxidation rate. The oxidation of phenol has also been carried out in order not only to achieve selective oxidation of this aromatic compound but also to compare the specificity of hydroxylation with other methods frequently used for this reaction.

Finally, Chapter 9 and Chapter 10 summarize the main findings of this work and propose perspectives for future investigations/research.

The results presented herein provide a better understanding of the electrochemical behavior of IrO₂-based dimensionally stable anodes (DSA®) in aqueous acidic media in order to optimize existing and potential applications for these electrodes.

References

- [1] S. Trasatti, *Electrochim. Acta.*, 45 (2000) 2377
- [2] H.B. Beer, *Brit. Patent* 1 147 442 (1965)
- [3] S. Trasatti, G. Buzzanca, *J. Electroanal. Chem.* 29 (1971) App. 1
- [4] T. Hyodo, M. Hayashi, S. Mitsutake, N. Miura, N. Yamazoe, *J. Appl. Electrochem.*, 27 (1997) 745
- [5] I. Uchida, H. Urushibata, S. Toshima, *J. Electrochem. Soc.*, 128 (1981) 2351
- [6] J. Walaszkowski, *Bull. Electrochem.* 3 (1987) 535
- [7] E. Kinoshita, F. Ingman, G. Edwall, S. Glab, *Electrochim. Acta*, 31 (1986) 29

- [8] S. Kotowski, B. Busse, in : F. Hine, J.M. Fenton, B.V. Tilak, J.D. Lisius (Eds.), Performance of Electrodes for Industrial Electrochemical Processes, vol. 89, Proc. Electrochem. Soc., Pennington, NJ, 1989, p.245.
- [9] S. Nakamatsu, Electrochem. (Tokyo, Japan), 72 (2004) 187
- [10] C.A. Martinez-Huitle, M.A. Quiroz, Ch. Comninellis, S. Ferro, A. De Battisti, Electrochim. Acta, 50 (2004) 949
- [11] Ch. Comninellis, Electrochim. Acta, 39 (1994) 1857
- [12] M.R.G. Santos, M.O.F. Goulart, J. Tonholo, C.L.P.S. Zanta, Chemosphere, 64 (2006) 393
- [13] J. Zelenka, W. Gangl, P. Letonja, M. Siebenhofer, R. Marr, AIChE Annual Meeting, Conference Proceedings, Cincinnati, OH, United States, (2005)
- [14] S. Daolio, S. Barison, M. Fabrizio, A. De Battisti, S. Ferro, Dimensionally stable anodes for oxygen evolution: electrochemical properties and SIMS characterization, unpublished results

Chapter 2 : Bibliography

In the first part of this chapter, a literature review on dimensionally stable anodes (DSA®) is presented. This part focuses mainly on the composition and preparation of these electrodes as well as their practical applications in the industry. Regarding their preparation, the spin coating deposition technique, which is used for the first time for the preparation of electrodes with well-controlled thickness, is described. Furthermore, a comprehensive model for organics oxidation on 'active' and 'non-active' type electrodes is presented.

In the second part of this chapter, and for the purpose of analyzing the active intermediates involved in the oxygen evolution reaction and the oxidation of organic compounds on IrO₂ electrodes, the principles of the differential electrochemical mass spectrometry (DEMS) are presented.

Finally, a theoretical model that predicts the temporal evolutions of the instantaneous current efficiency and the concentration of an organic during its mineralization is presented. These topics were selected in order to establish a background for the experimental chapters that follow.

2.1 Dimensionally Stable Anodes (DSA®): Preparation, properties and applications

Dimensionally stable anodes (DSA®) come in various shapes and compositions and have been proven to be suited for a wide range of applications due to their versatility [1].

Initially, as described in the corresponding patents [2-4], DSA® were prepared by thermal decomposition of a metal salt solution (usually a chloride salt of the desired metal diluted in an organic volatile solvent such as *i*-propanol) on an inert substrate, which is a simple principle where the precursor solution is deposited on the substrate and then treated at high temperature so that the metal chloride salt decomposes on the substrate yielding to the corresponding metal oxide. Using different metal chloride salts in the composition of the precursor solution allows producing a wide variety of coatings; typical examples of DSA® are RuO₂, IrO₂, SnO₂ and PbO₂ based electrodes [2-10]. Typical substrates are valve metals (titanium or tantalum) because the natural oxide layer at their surface protects them against corrosion.

Since metal oxide electrodes were discovered during the 1960s in the industry and after the first fundamental study on this topic was published by S.Trasatti [11], these electrodes have been used in numerous applications (e.g. O₂ and Cl₂ evolution). In fact, these electrodes were first used in Chlor-alkali cells when industrial research discovered that their stability and lifetime were high compared to the graphite electrodes that were used a decade earlier.

Nowadays, metal oxide electrodes are commonly used as 'O₂ cathodes' in metal-air batteries or in molten salt electrolysis due to the strong resistance of these electrodes against corrosion [12,13].

The possibility of producing anodes of various shapes has led to their use for cathodic protection in concrete of bridges and other structures [14] and the sensibility of oxides toward pH have allowed to use certain DSA® (IrO₂ and PdO_x) as pH measuring electrodes [15].

Their good resistance under O₂ evolution has led to their utilization as anodes in cells for Zn electrodeposition [16] and in the metal industry in general [17]. Additionally, DSA® are used for selective oxidation of organics and the destruction of waste

materials [18-21] although further improvement is still needed for industrial applications under severe conditions, such as oxygen evolution in strongly acidic media.

Concerning the latter possibility of application, the first studies published showed that RuO_2 , IrO_2 , SnO_2 and PbO_2 based electrodes were very promising electrode materials for the oxygen evolution reaction and organics oxidation in acidic media [22-24], especially IrO_2 , which has proved to be more resistant against corrosion compared to RuO_2 and is also more environmental friendly compared to PbO_2 [22,23].

Similarly, applications in other fields are always desired: an example of such application is the use of RuO_2 in supercapacitors [25].

2.2 The spin coating deposition technique

Spin coating is a deposition technique, which allows creating thin and uniform films through centrifugal acceleration induced by the application of a rotational movement to the substrate.

In this technique, a thick layer of solution containing the active component (solid) is applied to the support ((a) on Figure 2-1). During rotation, the solution flows outward ((b) and (c) on Figure 2-1). As the precursor solution layer thins, evaporation of the solvent increases the solid concentration causing an increase in viscosity and causing the formation of the solid film ((d) on Figure 2-1). This technique allows for the creation of very uniform films of well-controlled thickness.

The schema on Figure 2-1 resumes the spin coating process:

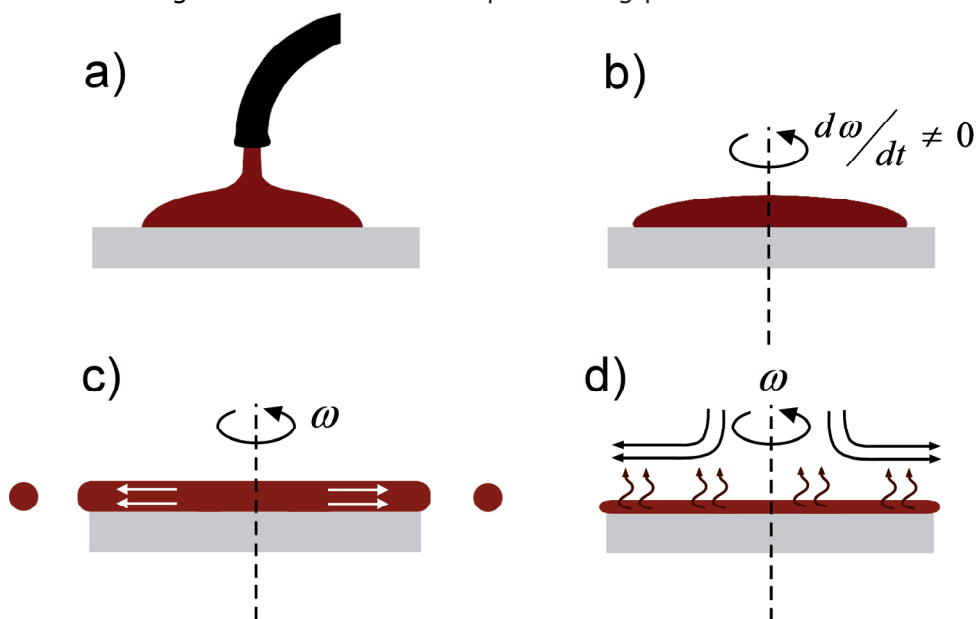


Figure 2-1: Schematic functionality of spin coating. a) Deposition of the solution containing the active component (solid), b) and c) rotation of the support, which spreads the solution homogeneously on all the surface of the substrate due to the centrifugal forces generated by the rotation. The excess of solution is ejected from the substrate and d) the volatile solvent of the solution is evaporated due to the spinning

This technique was initially used for the production of thin organic films such as photoresists or other uniform films of paint and varnish [26] but has never been used for the preparation of DSA® electrodes. In all cases, it is useful to study in detail the parameters having an influence on the final film thickness, such as the rotation speed applied to the substrate or the concentration of the active component.

Spin coating involves the acceleration of a liquid puddle on a rotating substrate. The physics behind spin coating involve a balance between centrifugal forces controlled by spin speed and viscous forces, which are determined by the viscosity of the solvent.

The formation of the film is primarily driven by two independent parameters: viscosity and spin speed. The range of film thickness easily achieved by spin coating is 1-200 μm . In order to produce thicker films, a high material viscosity, a low spin speed and a short spinning time are required. However, these parameters can affect the uniformity of the coating. Multi-layered coatings are preferred for a film thickness greater than 15 μm .

The first theoretical approaches describing the spin coating process were proposed by A.G.Emslie [27] and D.Meyerhofer [28] using several simplifications.

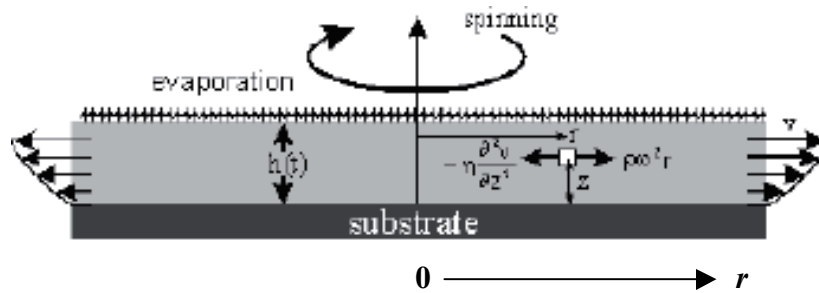


Figure 2-2: Scheme of the spin coating process [29]

The equation of force balance within a finite volume element (see Figure 2-2) can be re-written in cylindrical coordinates as:

$$-\eta \frac{\partial^2 v}{\partial z^2} = \rho \omega^2 r \quad (2-1)$$

where r is the radius pointing away from the center of rotation (m), η ($\text{kg s}^{-1} \text{m}^{-1}$) is the viscosity, v (m s^{-1}) is the velocity in radial direction, ρ (kg m^{-3}) is the density of the solution and ω is the angular velocity (rad s^{-1}) given by:

$$\omega = 2\pi f \quad (2-2)$$

Where f (s^{-1}) is the frequency. The force balance (Eq.(2-1)) can be integrated employing the following boundary conditions: $v = 0$ at the surface of the substrate ($z = 0$ on figure 2-2) and $\partial v / \partial z = 0$ at the free surface of the liquid ($z = h$ on figure 2-2), where the shearing force is set to zero.

Thus the velocity profile can be obtained (Eq.(2-3)):

$$v = \frac{1}{\eta} \left(-\frac{1}{2} \rho \omega^2 r z^2 + \rho \omega^2 r h z \right) \quad (2-3)$$

As shown in Figure 2-2, z (m) is the axis of rotation, r (m) is the radius with axisymmetry assumed and h (m) is the thickness of the film. Considering that the velocity profile is uniform, the total radial flow q ($\text{m}^2 \text{s}^{-1}$) per unit of circumference is given by Eq.(2-4):

$$q = \int_0^h v dz = \frac{\rho \omega^2 r h^3}{3\eta} = \frac{\omega^2 r h^3}{3\nu} \quad (2-4)$$

where ν ($\text{m}^2 \text{s}^{-1}$) is the kinematic viscosity.

To obtain a differential equation for h , the continuity equation is applied and can be written in cylindrical coordinates as follows:

$$\frac{\partial h}{\partial t} = -\frac{1}{r} \frac{\partial (rq)}{\partial r} \quad (2-5)$$

From the continuity equation of the flux (Eq. (2-4) and (2-5)) and using the boundary conditions at the surface of the substrate and at the free surface of the liquid cited earlier, the following first order ordinary differential equation is derived:

$$-\frac{dh}{dt} = \frac{2\rho\omega^2}{3\eta} h^3 \quad (2-6)$$

The integration of this differential equation (Eq.(2-6)) with $h = h_0$ at $t = 0$ s gives the film thickness h (m) as a function of time:

$$h(t) = \frac{l}{\left(h_0^{-2} + \frac{4\rho\omega^2}{3\eta}t\right)^{1/2}} \quad (2-7)$$

The main problem in this model is that Eq.(2-7) yields no residual film for infinite spinning time (i.e. $h \rightarrow 0$ as $t \rightarrow \infty$), which contradicts the experimental reality. This is a consequence of neglecting the solvent evaporation during the spinning process. Mayerhofer [28] takes into account evaporation using a constant evaporation rate of e (m s^{-1}).

$$-\frac{dh}{dt} = \frac{2\rho\omega^2}{3\eta}h^3 + e \quad (2-8)$$

The main goal of this derivation was the estimation of the quasi steady-state film thickness i.e. the film thickness after infinite spinning time (h_∞). Using this two-step model (spinning and evaporation), Mayerhofer [28] obtained an expression for the film thickness after infinite spinning time h_∞ (m) as a function of the initial concentration of active component c_0 (mol m^{-3}) in the applied solution.

$$h_\infty \approx \omega^{-2/3} e^{1/3} \eta^{1/3} c_0 \quad (2-9)$$

However, as the evaporation rate e itself depends on the spinning velocity, Sparrow [29] and Bornside [30] suggested a power law where the rate of evaporation is proportional to the square root of the angular velocity (Eq.(2-10)):

$$e \approx \omega^{1/2} \quad (2-10)$$

And therefore from Eq.(2-9) and Eq.(2-10), one obtains:

$$h_{\infty} \approx \omega^{-1/2} \eta^{1/3} c_0 \quad (2-11)$$

This relation describes the dependence of the final film thickness h_{∞} on the angular velocity of the substrate ω , the viscosity of the precursor solution η and the initial concentration c_0 of active component in the applied solution. This relation can be further modified if one accounts for the variation of the viscosity of the solution during the spinning [31].

2.3 General mechanism of organics oxidation on 'active' and 'non-active' type electrodes with competing side reaction of oxygen evolution

The nature of the electrode material strongly influences both the selectivity and the efficiency of the electrochemical oxidation of organic compounds [32-34]. In fact, experiments have shown that frequently oxidation of organics occurs on many electrodes without any loss in electrode activity and only at potentials in the vicinity of the on-set potential of the oxygen evolution reaction (OER) [35,36]. In order to explain these observations, a comprehensive general model for anodic oxidation of organic compounds in aqueous acidic media with competing OER has been proposed by Ch.Comninellis [32-34].

This general mechanism of heterogeneous electrochemical oxidation of organics in aqueous medium involves anodic oxygen transfer from H₂O to organics via hydroxyl radicals formed during water discharge [32-34]. The model proposed for anodic oxidation of organics in acid media, including competition with oxygen evolution allows the distinction between two limiting cases related to the behavior of the electrode: 'active' and 'non-active' anodes. IrO₂ electrodes are typical examples of 'active' type anodes whereas boron doped diamond (BDD) electrodes are typical examples of 'non-

active' type anodes. In Figure 2-3, the reaction scheme in acidic media is presented, where M represents an active site on the anode's surface.

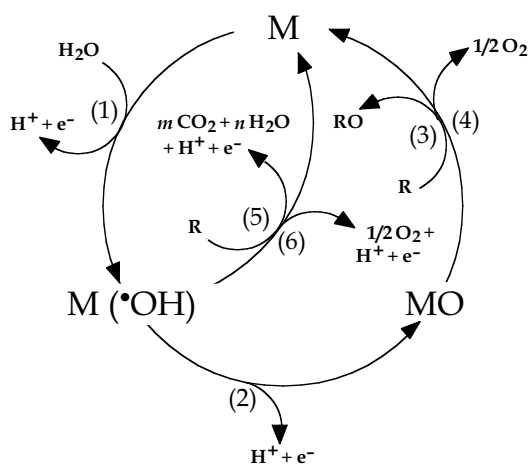


Figure 2-3: Scheme of the electrochemical oxidation of organic compounds on 'active' (reactions 1, 2, 3, 4) and 'non-active' (reactions 5, 6) anodes; M is an active site at the surface of the electrode material [32-34].

In both cases, the initial step of this model is the discharge of water molecules to form adsorbed hydroxyl radicals (Eq.(2-12)):



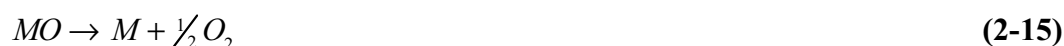
The electrochemical and chemical reactivity of the adsorbed hydroxyl radicals is highly dependent on the nature of the electrode material used. The latter can be divided into two categories, 'active' and 'non-active' electrodes, defined as followed.

2.3.1 'Active' type electrodes

For 'active' electrodes, the interaction between the active sites (M) and the hydroxyl radicals ($\bullet\text{OH}$) is strong [32-34]. In this case, the adsorbed hydroxyl radicals may interact with the anode with possible transition of oxygen from the hydroxyl radical to the anode's surface, forming the oxide MO (Eq.(2-13)):



This may be the case when higher oxidation states of the electrode's surface are available above the thermodynamic potential of oxygen evolution (1.23 V vs. SHE). The redox couple MO/M on the surface can act as mediator during the oxidation of organics (Eq.(2-14)) in competition with the side reaction of oxygen evolution due to the chemical decomposition of the higher oxide (Eq.(2-15)).

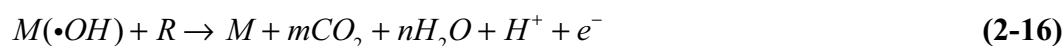


The oxidation reaction via the surface redox couple MO/M (Eq.(2-14)) results in the partial (selective) oxidation of organics. As a general rule, the closer the reversible potential of the surface redox couple is to the potential of oxygen evolution, the higher the 'active' character of the anode is [32-34]. IrO₂ based electrodes may serve as a typical example of 'active' type anodes because the standard redox potential of the IrO₃/IrO₂ couple (1.35 V vs. SHE) is close to the standard potential of O₂ evolution (1.23 V vs. SHE).

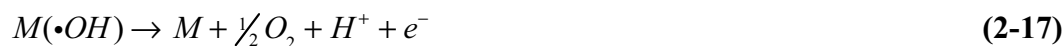
This model will be verified on IrO₂ based electrodes in chapters 5 and 6 using differential electrochemical mass spectrometry (DEMS) measurements together with isotope labeling.

2.3.2 'Non-active' type electrodes

Correspondingly, for 'non-active' type electrodes, the interaction between the active sites (M) and the hydroxyl radicals ($\bullet\text{OH}$) is weak [32-34]. In this case, the oxidation of organics is mediated by quasi-free hydroxyl radicals (Eq.(2-16)), which may result in fully oxidized reaction products such as CO_2 .



In this reaction (Eq.(2-16)), R is the fraction of an organic compound, which contains no heteroatom and needs one atom of oxygen to be transformed into fully oxidized elements. This reaction competes with the side reaction of hydroxyl radicals discharge (direct or indirect) through the formation of H_2O_2 as intermediate, which produces O_2 without any participation of the anode's surface (Eq.(2-17)).



Boron-doped diamond deposited on p-Si substrate (p-Si/BDD) is a typical example of 'non-active' anodes. This material is known to be inert and to have weak adsorption properties [37]. Hence, the latter is expected to be the ideal electrode material for electrochemical incineration of toxic and non-biocompatible pollutants. The presence of free hydroxyl radicals during organics oxidation on p-Si/BDD electrodes has been demonstrated using electron spin resonance (ESR) measurements [38].

2.4 Differential Electrochemical Mass Spectrometry (DEMS)

Electrochemical mass spectrometry (EMS) is an online analytical method that allows detecting volatile products of a given electrochemical reaction shortly after they are formed on the electrode. This process is performed by coupling an electrochemical cell with a conventional mass spectrometer (MS) in which both are connected by a porous membrane where the products formed from the electrochemical reaction in the cell are transited toward the MS.

In a typical EMS experiment, ionic currents related to the formation of given species are measured together with the faradaic current during a potential sweep (cyclic voltammetry). Both measurements (ionic and faradaic currents) are usually presented together to form the so-called mass spectrometric cyclic voltammogram (MSCV).

This set-up allowing to detect on-line the products of an electrochemical reaction using a MS was first proposed by S.Bruckenstein et al.[39]. The authors connected the working electrode to a porous membrane with non-wetting properties, which served as an interface between the electrochemical cell and the inlet of the mass spectrometer. One of the main disadvantages of this new set-up is the high delay between the formation of the products and their detection in the MS (about 20 sec.).

The set-up was, however, considerably improved a few years later by O.Wolter et al.[40]. To achieve this feat, they used a differential pumping system with turbomolecular pumps. This system allowed for a faster transfer of the products from the electrochemical cell to the ionization chamber and for a fast elimination of collected gases. Due to this improvement, the time delay between the formation of a product and its detection was reduced to 0.2 seconds. Because of that significant time delay reduction, the ionic and faradaic currents could be correlated without major distortions for scan rates up to 50 mV s^{-1} . In order to distinguish this technique from product sampling, i.e., an integral approach, O.Wolter et al.[40] named the improved method differential electrochemical mass spectrometry (DEMS).

Since the improvement of the technique, the latter has been widely used by scientists worldwide to study electrochemical kinetics.

2.4.1 DEMS setup

Interface to vacuum

In a typical DEMS experiment, it is essential to separate the volatile compounds from the electrolyte solution independently of the solvent used. This is achieved using a porous Teflon membrane introduced at the interface between the vacuum system leading to the MS and the electrochemical cell. By using this type of membrane, separation can be achieved in aqueous and also some organic electrolytes. The membrane is impermeable to liquid due to its hydrophobic properties while the dissolved gaseous and other volatile species can diffuse by evaporation through the membrane. The critical pore size depends on the solvent used for the electrolyte solution (0.8 μm for aqueous electrolyte solutions). Therefore, a typical Teflon membrane is 75 μm thick with a porosity of 50%. Because the membrane is very thin and can be damaged easily, it is supported by a glass or steel frit mounted at the interface between the vacuum and the electrochemical cell in the DEMS setup.

The DEMS cell

In the classical approach, the electrocatalyst layer, e.g., Pt, is sputtered directly onto the Teflon membrane. With this configuration, one side of the electrode is in contact with the electrolyte solution while the other side is in contact with the mass spectrometer vacuum system. The main advantage of this approach is the increase of the roughness factor of the electrocatalyst, which permits for an overall larger products formation as well as a fast transfer of the species to the MS. However, low mechanical stability and the higher thickness of the catalyst leading to depletion of the species within the electrocatalyst layer (diffusion behavior) remains a key issue. Therefore, when using this classical approach for the DEMS electrochemical cell, porous metal layer electrodes (such as IrO_2 based electrodes) were not suitable for investigation of electrode reactions that generate strong gas evolutions, because the strong bubbling caused the destruction of the electrode material.

In order to perform DEMS measurements with porous metal layer electrodes, the conventional cell (made of Teflon or glass) presented on Figure 2-4 was developed. The volume of this cell is defined by a Teflon spacer placed between the electrode and the electrochemical cell and the time delay between the formation of a product and its detection in the MS is about 0.1 seconds.

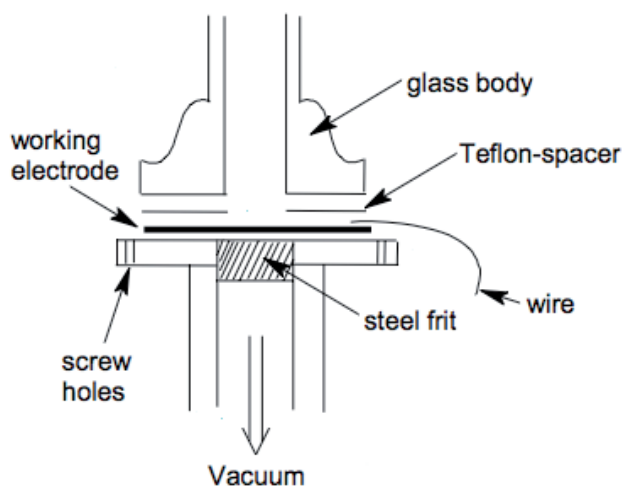


Figure 2-4: Schematic representation of the conventional electrochemical cell used for DEMS measurements [41].

However, the design of this cell only permitted using electrodes of a relatively small size. For the use of larger porous metal layer electrodes such as those prepared in the foregoing chapters, another type of electrochemical cell was developed: the thin layer DEMS cell.

In this new DEMS cell (shown on Figure 5-1 in the experimental details of Chapter 5), the electrode has a diameter of 1 cm and is separated from the porous hydrophobic Teflon membrane by a 50 to 100 μm thick electrolyte layer. The Teflon membrane is mechanically supported by a steel frit and the distance between the electrode and the Teflon membrane is ascertained by one spacer, or even two to achieve a doubled distance, made from the same material as the membrane. Due to the compression of this soft spacer, the distance is less than the nominal thickness. The cell body is made of passivated titanium because of its mechanical stability and inertness. Two capillaries positioned opposite to each other serve as electrolyte inlet and outlet and as connections to the reference and counter electrodes. Due to the large IR drop in the thin layer of electrolyte, it is advantageous to use two counter electrodes; one in the outlet and the other in the inlet. Connecting both counter electrodes to the potentiostat via different resistors ensures that the current through the capillary to the

reference electrode is less than half of the total current. With this configuration, species produced on the electrode surface diffuse to the Teflon membrane within 2 seconds.

Vacuum system

Figure 2-5 displays the experimental setup used for the DEMS measurements. The electrochemical cell is connected to the first vacuum chamber via a valve at Position (3). Another valve at Position (4) leads to the calibration volume. A shutter was placed between the ionization chamber and the analyzer section to create a pressure gradient allowing the species to flow toward the analyzer section. The evacuation is performed first mechanically by a linear drive (9) and then differentially by two molecular pumps (2); one before the ion source (5) working at a pressure of 10^{-2} bar and the other above the quadrupole rods chamber (6) working at a pressure of 10^{-5} mbar. The electrodes mounted in the electrochemical cell are connected to a potentiostat driven by a function generator.

Volatile products are ionized in the ionization chamber by electron bombardment. These ions are then accelerated through quadrupole rods (6) and analyzed using a quadrupole mass filter (m/z ratio).

The incoming signal is then amplified using a secondary electron amplifier (7) before detection. The different parameters of the entire system are controlled by an external computer, which allows data acquisition as well.

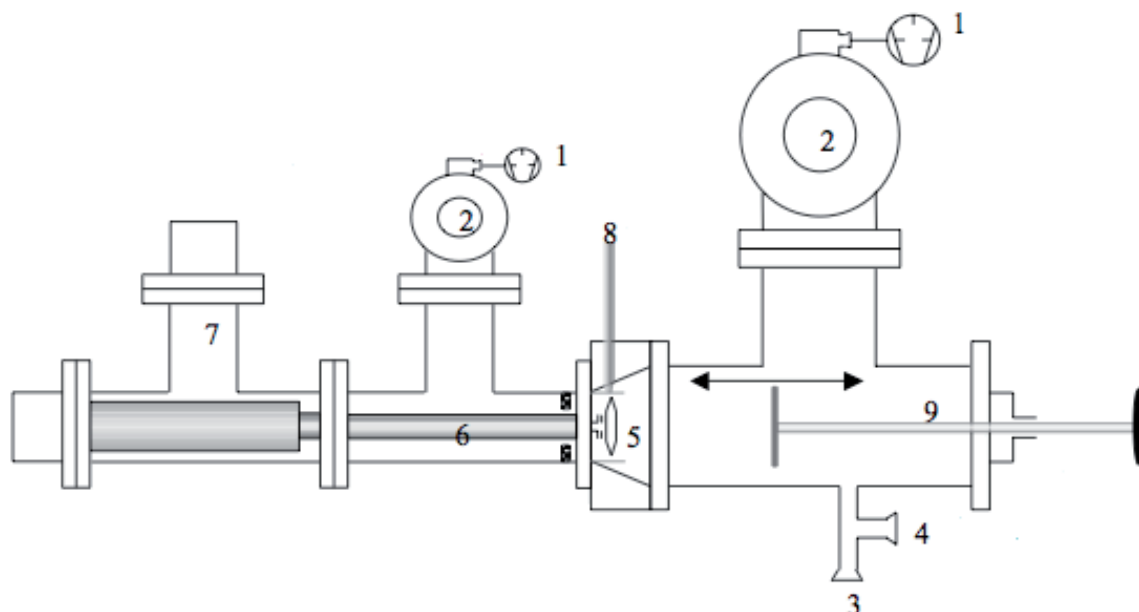


Figure 2-5: The vacuum system: (1) rotary pumps, (2) turbomolecular pumps, (3) connection to the electrochemical cell, (4) connection to the calibration leak, (5) ion source, (6) quadrupole rods, (7) secondary electron multiplier, (8) direct inlet, (9) linear drive. [41,42]

2.4.2 DEMS results analysis

The ionic current recorded during the DEMS measurements can be related to the rate of formation of the corresponding product. In fact, the ionic intensity determined by mass spectrometry is directly proportional to its incoming flux (Eq.(2-18)):

$$I_i = K^0 J_i \quad (2-18)$$

where I_i (A) is the ionic intensity of the specie i , K^0 ($C \text{ mol}^{-1}$) is a constant, which takes into account all the mass spectrometric constants/settings and the ionization probability of the corresponding species. Last, J_i (mol s^{-1}) is the molar flux of the species through the membrane into the ionization chamber.

When the species are produced electrochemically, J_i is given by the faradaic current corresponding to that process:

$$J_i = N \frac{I_f}{zF} \quad (2-19)$$

where N (-) is the collection efficiency, defined as the ratio of the amount of species detected by the MS to the total amount of species produced electrochemically. I_f (A) is the faradaic current, z is the number of electrons necessary to produce one molecule of product and F (C mol⁻¹) is the Faraday constant. By combining equations (2-18) and (2-19), one obtains:

$$I_i = NK^0 \frac{I_f}{zF} \quad (2-20)$$

It is important to note that N may be less than 1 if a fraction of the species formed diffuse away from the electrode into the electrolyte. This occurs when incomplete mixing of the electrolyte is achieved in the electrochemical cell (usually at flow rates > 2 $\mu\text{l s}^{-1}$). In this case, another more appropriate equation is used (Eq.(2-21)):

$$I_i = K^* \frac{I_f}{z} \quad (2-21)$$

with:

$$K^* = \frac{K^0 N}{F} \quad (2-22)$$

K^* (-) can be estimated using a known electrochemical reaction, such as hydrogen or oxygen evolution. The calibration of the instrument to find the value of K^* for the collection of H₂ or O₂ can be easily achieved using equation (2-22). Similarly, the oxidation of CO adsorbed on a Pt electrode is often used to calibrate the mass spectrometer for CO₂. In this case, the integrated faradaic oxidation current, as well

as the ionic current for CO_2 , are used. Alternatively, calibration of the mass spectrometer can also be achieved via a calibration leak (valve in the position (4) in Figure 2-5) and K^0 can be estimated.

In summary, differential electrochemical mass spectrometry (DEMS) is a powerful on-line method used for both the detection of products formed through an electrochemical reaction and the study of adsorbates. Using DEMS, the amounts of reaction and desorption products can be determined semi-quantitatively. Because this technique is fast (response time max 2s) and highly sensitive, concentrations of volatile reaction products below one nmol can be easily detected. Furthermore, using isotopically labeled compounds, additional information about the mechanism of the studied reaction can be obtained.

2.5 Theoretical model for the oxidation of organic compounds during electrolysis experiments based on the maximum oxidation rate

For the electrolysis experiments, a model has been developed for the electrochemical oxidation of organic compounds in a batch recirculation system under galvanostatic conditions. This model was proposed by P.-A. Michaud [43] and was first intended to predict the temporal evolutions of the concentration of an organic compound and the instantaneous current efficiency (ICE) during its electrochemical mineralization on boron-doped diamond (BDD) electrodes. Nonetheless, this model could also be adapted to 'active' type anodes such as IrO_2 -based electrodes according to the chemical reactions (2-12), (2-13), (2-14) and (2-15) presented in section 2.3.1 of this chapter.

The main assumption of this model is that the global rate of the electrochemical oxidation reaction is fast and that this oxidation reaction is controlled by current or mass transport of the organic toward the anode's surface, which depends on the difference between the applied current density j_{applied} (A m^{-2}) and the limiting current density j_{lim} (A m^{-2}). Under these conditions, the limiting current density $j_{\text{lim},t}$ (A m^{-2}) for the electrochemical oxidation reaction under given hydrodynamic conditions can be written as:

$$j_{\text{lim},t} = 4Fk_m \cdot \text{COD}_t \quad (2-23)$$

with F (C mol^{-1}) being the Faraday's constant, k_m (m s^{-1}) as the mass transport coefficient and COD_t ($\text{molO}_2 \text{ m}^{-3}$) the chemical oxygen demand at time t (s). At the beginning of the electrolysis ($t=0\text{s}$), the initial limiting current density $j_{\text{lim},0}$ is given by equation (2-24), with COD_0 ($\text{molO}_2 \text{ m}^{-3}$) as the initial chemical oxygen demand.

$$j_{\text{lim},0} = 4Fk_m \cdot \text{COD}_0 \quad (2-24)$$

2.5.1 Electrolysis under current control ($j_{\text{applied}} < j_{\text{lim}}$)

In the case of $j_{\text{applied}} < j_{\text{lim}}$ (current control), the instantaneous current efficiency ICE is 100% and the oxidation rate of the organic compound expressed as a function of COD has a constant value. Hence, the latter can be written as follows (Eq.(2-25)), with λ being the dimensionless current density (-), A the geometric anode surface area (m^2) and V_R the reaction volume (m^3).

$$r = \lambda \frac{j_{\text{lim},0}}{4F} \quad \text{with} \quad \lambda = \frac{j_{\text{applied}}}{j_{\text{lim},0}} \quad \text{and} \quad r = -\frac{V_R}{A} \frac{d(\text{COD})}{dt} \quad (\text{mol m}^{-2} \text{ s}^{-1}) \quad (2-25)$$

From Eq.(2-23), (2-24) and (2-25), the temporal evolution of COD can be evaluated (Eq.(2-26)).

$$\text{COD}_t = \text{COD}_0 \cdot \left(1 - \lambda \cdot \frac{Ak_m}{V_R} \cdot t \right) \quad (2-26)$$

The linear relation between COD and t is valid up to a critical time t_{cr} after which the applied current density is equal to the limiting one $j_{applied} = j_{lim}$. At this critical time, COD_{cr} is related to COD_0 by the following equation:

$$COD_{cr} = \lambda \cdot COD_0 \quad (2-27)$$

By combining equations (2-26) at $t = t_{cr}$ and (2-27), it is possible to calculate t_{cr} :

$$t_{cr} = \frac{1-\lambda}{\lambda} \cdot \frac{V_R}{A \cdot k_m} \quad (2-28)$$

2.5.2 Electrolysis under mass transport control ($j_{applied} > j_{lim}$)

In case of mass transport control (the applied current exceeds the limiting one $j_{applied} > j_{lim}$), the side reaction of oxygen evolution induces a decrease of the instantaneous current efficiency for organics oxidation while the chemical oxygen demand decreases exponentially with time, as described by Eq.(2-29).

$$COD_t = \lambda \cdot COD_0 \cdot \exp\left(-\frac{Ak_m}{V_R} \cdot t + \frac{1-\lambda}{\lambda}\right) \quad (2-29)$$

Figure 2-6 shows the theoretical temporal evolution of the chemical oxygen demand in the current and mass transfer controlled regimes.

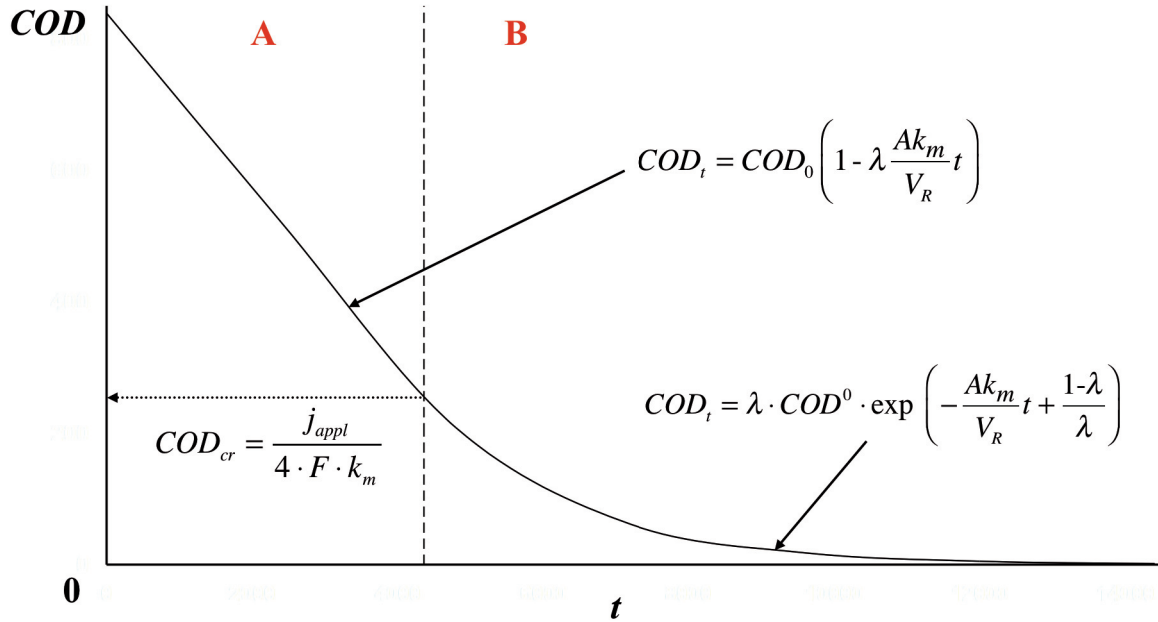


Figure 2-6: Theoretical chemical oxygen demand (COD) temporal evolution for (A) current- and (B) mass transfer controlled regimes.

COD: chemical oxygen demand ($\text{molO}_2 \text{ L}^{-1}$), **A:** geometrical surface area of the electrode (m^2), **V_R :** electrochemical reactor volume (m^3), **λ :** dimensionless current (-), **t:** time (s), **j_{applied} :** applied current density (A m^{-2}) and **k_m :** mass transfer coefficient (m s^{-1})

The instantaneous current efficiency for the oxidation of organics is defined as:

$$ICE = \frac{j_{\text{lim},t}}{j_{\text{applied}}} = \frac{COD_t}{\lambda \cdot COD_0} \quad (2-30)$$

Combining equations (2-29) and (2-30) the ICE can be expressed as follows:

$$ICE = \exp\left(-\frac{A k_m}{V_R} \cdot t + \frac{1 - \lambda}{\lambda}\right) \quad (2-31)$$

The theoretical temporal evolution of the instantaneous current efficiency calculated in the current and mass transfer controlled regimes is shown in Figure 2-7.

In order to verify the validity of this model, anodic oxidations of model organic compounds in acidic media have been performed on p-Si/BDD electrodes for different initial organic concentrations and current densities [43].

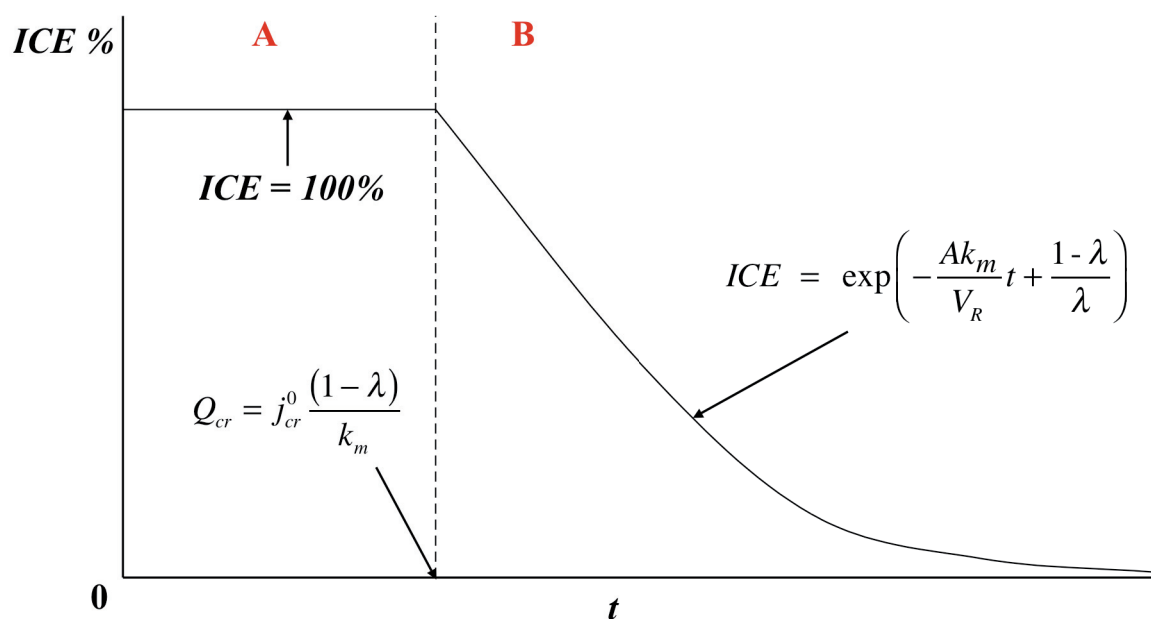


Figure 2-7: Theoretical temporal evolution of the instantaneous current efficiency (ICE) for (A) current- and (B) mass transfer controlled regimes.

ICE: instantaneous current efficiency, Q_{cr} : charge passed at the critical time, j_{cr}^0 : limiting current density at the critical time ($A\ m^{-2}$) and the rest has the same meaning as in Figure 2-6

2.6 References

- [1] S. Trasatti, *Electrochim. Acta.*, 45 (2000) 2377
- [2] H. Beer, J.M. Hinden, *EU Pat. EP 0 046 449 B1* (1985)
- [3] H. Beer, *J. Electrochem. Soc.*, 127 (1980) 303C
- [4] J.M. Hinden, H. Beer, *US pat. 4,444,642* (1984)
- [5] S. Trasatti, 'Electrodes of Conductive Metallic Oxides', Elsevier, Amsterdam (1981)
- [6] L.D. Burke, M. McCarthy, *Electrochim. Acta*, 29 (1984) 211

-
- [7] R.S. Yeo, J. Orehotzky, W. Visscher, S. Srinivasan, *J. Electrochem. Soc.*, 128 (1981) 1900
- [8] A. De Battisti, G. Lodi, M. Cappadonia, G. Battaglia, R. Kötz, *J. Electrochem. Soc.*, 136 (1989) 2596
- [9] T.V. Varlamova, I.D. Belova, R.R. Shrifina, B.Sh. Galyamov, Yu.E. Roginskaya, Yu.N. Venetsev, *Zh. Fiz. Khim.* 64 (1990) 385
- [10] J. Kolb, C.R. Franks, B.A. Schenker, *US Pat.* 3,793,164
- [11] S. Trasatti, G. Buzzanca, *J. Electroanal. Chem.* 29 (1971) App. 1
- [12] T. Hyodo, M. Hayashi, S. Mitsutake, N. Miura, N. Yamazoe, *J. Appl. Electrochem.*, 27 (1997) 745
- [13] I. Uchida, H. Urushibata, S. Toshima, *J. Electrochem. Soc.*, 128 (1981) 2351
- [14] J. Walaszowski, *Bull. Electrochem.* 3 (1987) 535
- [15] E. Kinoshita, F. Ingman, G. Edwall, S. Glab, *Electrochim. Acta*, 31 (1986) 29
- [16] S. Kotowski, B. Busse, in : F. Hine, J.M. Fenton, B.V. Tilak, J.D. Lisius (Eds.), *Performance of Electrodes for Industrial Electrochemical Processes*, vol. 89, *Proc. Electrochem. Soc.*, Pennington, NJ, 1989, p.245.
- [17] S. Nakamatsu, *Electrochem. (Tokyo, Japan)*, 72 (2004) 187
- [18] C.A. Martinez-Huitle, M.A. Quiroz, Ch. Comninellis, S. Ferro, A. De Battisti, *Electrochim. Acta*, 50 (2004) 949
- [19] Ch. Comninellis, *Electrochim. Acta*, 39 (1994) 1857
- [20] M.R.G. Santos, M.O.F. Goulart, J. Tonholo, C.L.P.S. Zanta, *Chemosphere*, 64 (2006) 393
- [21] J. Zelenka, W. Gangl, P. Letonja, M. Siebenhofer, R. Marr, *AICHE Annual Meeting, Conference Proceedings*, Cincinnati, OH, United States, (2005)
- [22] S. Daolio, S. Barison, M. Fabrizio, A. De Battisti, S. Ferro, *Dimensionally stable anodes for oxygen evolution: electrochemical properties and SIMS characterization*, unpublished results
- [23] Ch. Comninellis, G.P. Vercesi, *J. Appl. Electrochem.*, 21 (1991) 335
- [24] P. Yao, *Electrochem. and Solid-state lett.*, 11 (5) (2008) J37

CHAPITRE 2: Bibliography

- [25] B.E. Conway, *Electrochemical Supercapacitors*, Kluwer/Plenum, New York, 1999
- [26] P.H. Walker, J.G. Thompson, *Proc. Am. Soc. Testing materials*, 22, Part II, (1922) 464
- [27] A.G. Emslie, F.T. Bonner, L.G. Peck, *J. Appl. Phys.*, 29 (5) (1958) 858
- [28] D. Meyerhofer, *J. Appl. Phys.*, 49 (7) (1978) 3993
- [29] E.M. Sparrow, J.L. Gregg, *J. Heat Trans.*, 82 (1969) 94
- [30] D.E. Bornside, R.A. Brown, P.W. Ackmann, J.R. Frank, A.A. Tryba, F.T. Geyling, *J. Appl. Phys.*, 73 (1993) 585
- [31] D.W. Schubert, T. Dunkel, *Mat. Res. Innovat.*, 7 (2003) 314
- [32] G. Fóti, D. Gandini, Ch. Comninellis, A. Perret, W. Haenni, *Electrochem. Solid-State Lett.*, 2 (1999) 228
- [33] G. Fóti, Ch. Comninellis, in *Modern Aspects of Electrochemistry*, R. White, B.E Conway, C.G. Vayenas, Editors, Kluwer Academic/Plenum Publishers: New York. Vol. 37 (2004) 87
- [34] G. Fóti, D. Gandini, Ch. Comninellis, in *Current Topics in Electrochemistry*, Vol. 5, Research Trends, Trivandrum (1997) 71
- [35] Ch. Comninellis, E. Plattner, *Chimia*, 42 (1988) 250
- [36] Ch. Comninellis, C. Pulgarin, *J. Appl. Electrochem.*, 21 (1991) 703
- [37] A. Fujishima, Y. Einaga, T.N. Rao, D.A. Tryk, *Diamond Electrochemistry*, Elsevier B.V., Amsterdam, (2005)
- [38] B. Marselli, J. Garcia-Gomez, P.-A Michaud, M.A. Rodrigo, Ch. Comninellis, *J. Electrochem. Soc.*, D 79 (2003) 150
- [39] S. Bruckenstein, R.R. Gadde, *J. of. Am. Chem. Soc.*, 93 (3) (1971) 793
- [40] O. Wolter, J. Heitbaum, *Ber. Der Bunsen.Gesellschaft*, 88 (1984) 2
- [41] H. Baltruschat, *J. of the American Soc. for Mass Spec.*, 15 (12) (2004) 1693
- [42] B. Bittins-Cattaneo, E. Cattaneo, P. Koenigshoven, W. Vielstich, *Electroanal. Chem.*, 17 (1990) 181
- [43] P.-A. Michaud, PhD Thesis, Swiss Institute of Technology (EPFL), No 2595, 2002

Chapter 3 : Preparation and morphological characterization of Ti/IrO₂ and p-Si/IrO₂ electrodes

In this chapter, IrO₂ electrodes are prepared through thermal decomposition of a H₂IrCl₆ precursor solution on an inert substrate (Ti or p-Si). In a first part, these electrodes were prepared using the most common method of deposition found in literature, which consists in applying the H₂IrCl₆ precursor solution on a Ti substrate followed by solvent evaporation and thermal decomposition of the precursor. These electrodes were then characterized using voltammetric charge measurements.

In a second part, IrO₂ electrodes were prepared for the first time using the spin coating deposition technique, where centrifugal forces spread the precursor solution with simultaneous evaporation of the solvent on the rotating substrate. It was found using this technique, that it is possible to obtain thin and uniform IrO₂ coatings with controlled loadings.

The influence of the concentration of iridium salt in the precursor solution (c_0) as well as the influence of the rotation speed at which the substrate spins (ω) on the IrO₂ loading have been studied using voltammetric charge measurements. From these results, a simple relation has been proposed for the estimation of the IrO₂ loading for a given c_0 and ω .

Finally, p-Si has been used as substrate in order to avoid the problem inherent to the formation of TiO₂ at the Ti-IrO₂ interface, which occurs when titanium is used as substrate. These electrodes have been mainly used for electroanalytical measurements.

This chapter is based on the publications:

S. Fierro, L. Ouattara, E.H. Calderon, Ch. Comninellis. Influence of temperature on the charging/discharging process of IrO₂ coating deposited on p-Si substrate, *Electrochemistry Communications*, Volume 10, Issue 6, April 2008, Pages 955-959

S. Fierro, Ch. Comninellis. Kinetic study of formic acid oxidation on p-Si/IrO₂ electrodes, *Electrochim. Acta*, under preparation, February 2010

3.1 Introduction

The first iridium dioxide based electrodes, as described in the corresponding patents [1-3], were produced by thermal decomposition of the appropriate precursor solution, which was previously applied on an inert substrate such as titanium or tantalum. These electrodes belong to the family of dimensionally stable anodes (DSA®).

Because the versatility of DSA® is their main advantage [4], scientists have developed various techniques to produce these electrodes as it became obvious that every step of the preparation of these electrodes could have a direct impact on the electrochemical behaviour of the resulting coating.

The type of substrate (titanium, tantalum, niobium, zirconium etc.) and its pre-treatment (polishing, sandblasting etc.) can have a significant influence on the electrocatalytic activity and can occasionally be considered as a co-catalyst [5-9]. In fact, the chemical and electrochemical stability of the base metal used as substrate

was found to be directly related through the wear mechanism, to the service life of the electrode. One of the main problem often caused by the base metal is the formation of a non-adherent, non-conductive layer on the base metal's surface during thermal decomposition that can alter the behaviour of the electrode.

The next step is the application method where again, numerous techniques have been proposed for the application of the precursor solution on the base metal.

During the early stages of DSA® manufacture, the precursor solution was usually applied on the substrate with a paintbrush [10] or by dipping [11], in order to soak the base metal directly into the metal salt solution.

These methods were the most economical for industrial applications. However, in order to later study the intrinsic electrocatalytic properties of the electrode or purely structural effects, the scientists needed to manufacture well-defined coatings.

Those were obtained by developing new techniques such as the spray coating [12], where the precursor solution is dispersed finely on the metal, or the blading method, which consists in applying the precursor solution using a sharp blade [13] so that the excess of solution is eliminated from the substrate surface leaving a thin film of precursor solution on the support material.

However, for specific investigations, such as the study of the efficiency of DSA® as supercapacitors, the electrode is constructed such that its surface is maximized; in this respect, methods such as sol-gel have been borrowed from the field of catalyst preparation [14].

In this chapter, the manufacture and the morphological characterization of IrO₂ electrodes prepared by thermal decomposition are presented. XPS measurements have been performed on IrO₂ deposited on Ti and on p-Si so as to investigate the interference of the substrate with the IrO₂ coating. The spin coating deposition technique was used for the first time for the preparation of IrO₂ electrodes. Additionally, the influences of the concentration of H₂IrCl₆ in the precursor solution (c_0) and the rotation speed of the substrate (ω) on the final thickness of the IrO₂ coating were studied using voltammetric charge measurements.

3.2 Experimental details

Each voltammetric experiments presented herein were performed in a classical three-electrode cell (70 ml) using an Autolab PGSTAT 30. The counter electrode was a Pt wire; the reference electrode was Hg/Hg₂SO₄/K₂SO₄ (sat.) (MSE; 0.65 V vs. SHE) and the working electrode was an IrO₂ electrode prepared by thermal decomposition of H₂IrCl₆: the precursor aqueous solution (H₂IrCl₆ (99.9%, ABCR) 250mM in dry *i*-propanol (extra dry with molecular sieves, water < 50ppm, Acros Organics) was deposited using the spin coating technique on square-shaped pretreated p-Si or Ti (182.25 mm²). The oxide film was obtained by thermal decomposition in air at 500°C. Several series of IrO₂ electrodes with different loadings were prepared.

A schematic of the electrochemical cell used is shown in Figure 3-1:

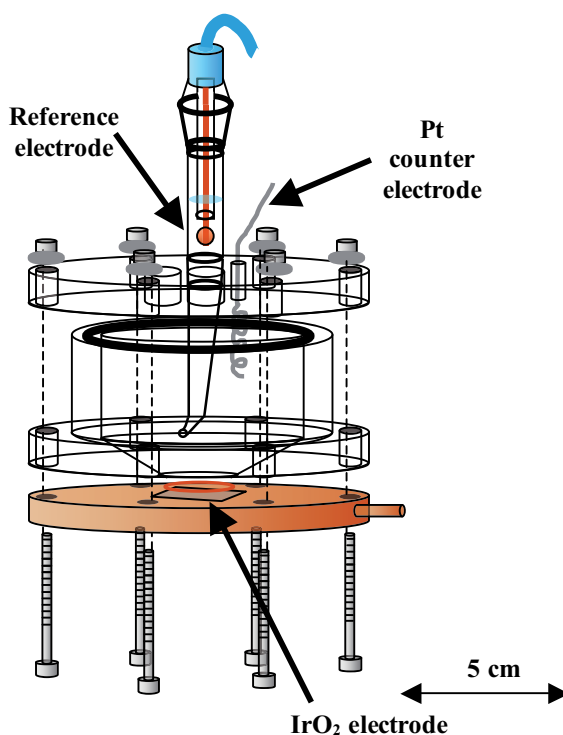


Figure 3-1: Schematic of the cell used for the voltammetric experiments

Experiments were carried out at room temperature (25°C) inside a Faraday cage using 1M HClO₄ (70% Acros organics) as support electrolyte. All potentials given in this chapter are with respect to the standard hydrogen electrode (SHE).

SEM pictures were taken using a Philips XL30 scanning electron microscope and the spincoater used for the spreading of the precursor solution for IrO₂ electrodes preparation was a SPIN150 wafer spinner from semiconductor production systems (SPS).

3.3 Results and discussion

3.3.1 Morphological and voltammetric charge studies of Ti/IrO₂ electrodes

Ti/IrO₂ electrodes are obtained after thermal decomposition of H₂IrCl₆ 0.25M in *i*-propanol solution deposited on Ti substrate. Multi-layered electrodes have been prepared by depositing several times a given volume of precursor solution (30μl) with subsequent decomposition during 10 minutes at 500°C before performing the final treatment at 500°C for 1 hour.

The titanium substrate was sandblasted, in order to increase the adherence between the substrate and the iridium oxide. The sandblasted substrate was then treated in boiling 1M oxalic acid aqueous solution for 1 hour before the IrO₂ deposition in order to increase further the roughness of the substrate and to clean all impurities coming from the sandblasting process. A SEM picture of the pretreated substrate is presented on Figure 3-2.

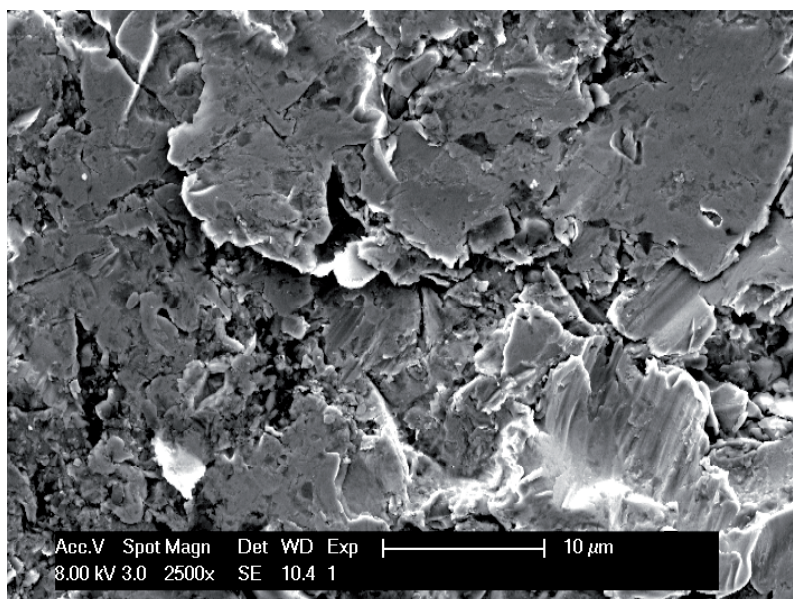


Figure 3-2: SEM micrograph of the pretreated (sandblasting + treatment in boiling 1M oxalic acid) Ti substrate

Figure 3-3 (a) and (b) show SEM images of one layer (0.96mg cm^{-2}) and eight layers (6.55mg cm^{-2}) of IrO₂ both deposited on a pretreated titanium substrate, respectively.

The deposit exhibits a cracked dried-mud structure (Figures 3-3a and 3-3b), which is the typical structure of these DSA® prepared on a Ti substrate [15-17].

Figure 3-3a shows that the titanium substrate is still visible; this is an indication that one layer (0.96mg cm^{-2}) of IrO₂ is not enough to cover entirely the substrate.

Figure 3-3b shows that when the loading is increased (6.55 mg cm^{-2}), the Ti substrate is not observed anymore.

Figure 3-3c shows a profile view of the IrO₂ coating (upper part of the picture) deposited on pretreated titanium (lower part of the picture). Furthermore, a closer enlargement in Figure 3-4 shows that the iridium dioxide coating is composed of fine nanorods-shaped crystals, which are probably formed through epitaxial growth in the defects of the pretreated titanium (resulting in the formation of nanopores). All the figures presented so far in this section clearly show that the IrO₂ coating has a highly porous structure.

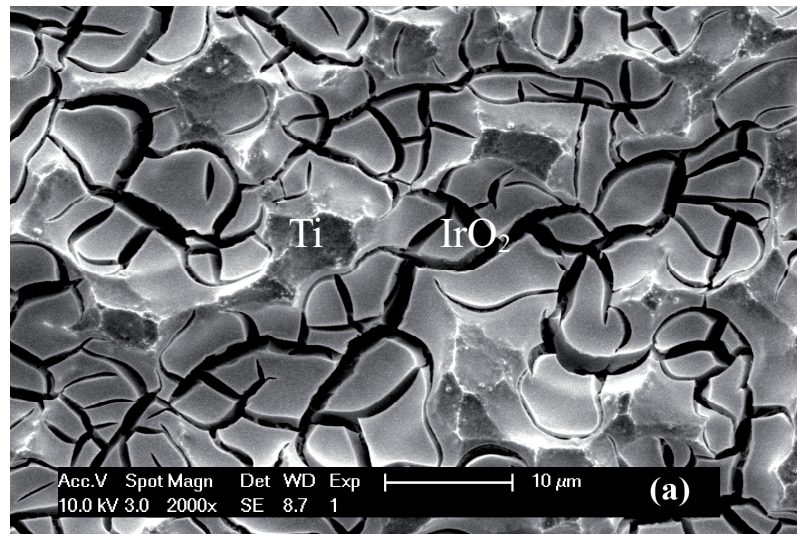


Figure 3-3a: SEM micrograph of (a) one layer (0.96 mg cm⁻²) of IrO₂ on pretreated Ti

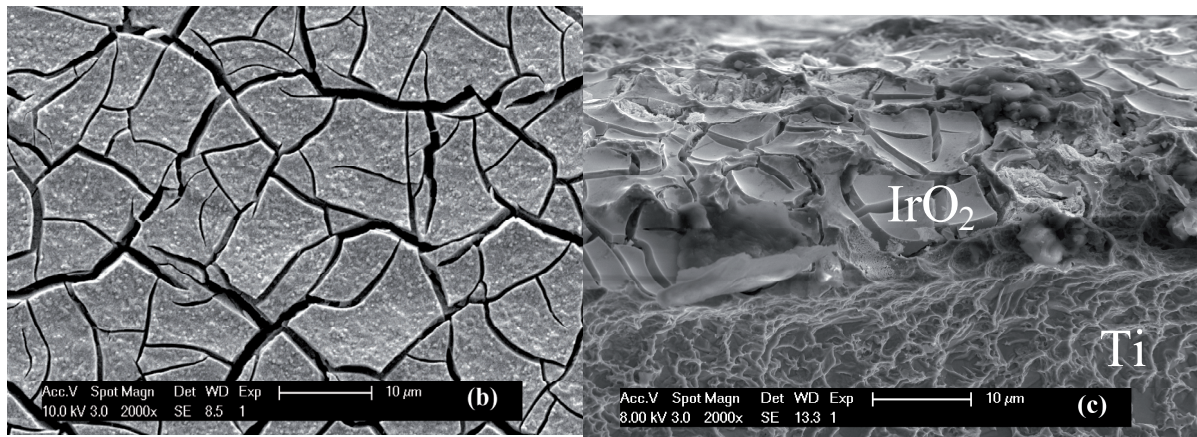


Figure 3-3 b and c: SEM micrograph of (b) eight layers (6.55 mg cm⁻²) of IrO₂ on pretreated Ti (c) profile view of one layer (0.96 mg cm⁻²) of IrO₂ on pretreated Ti

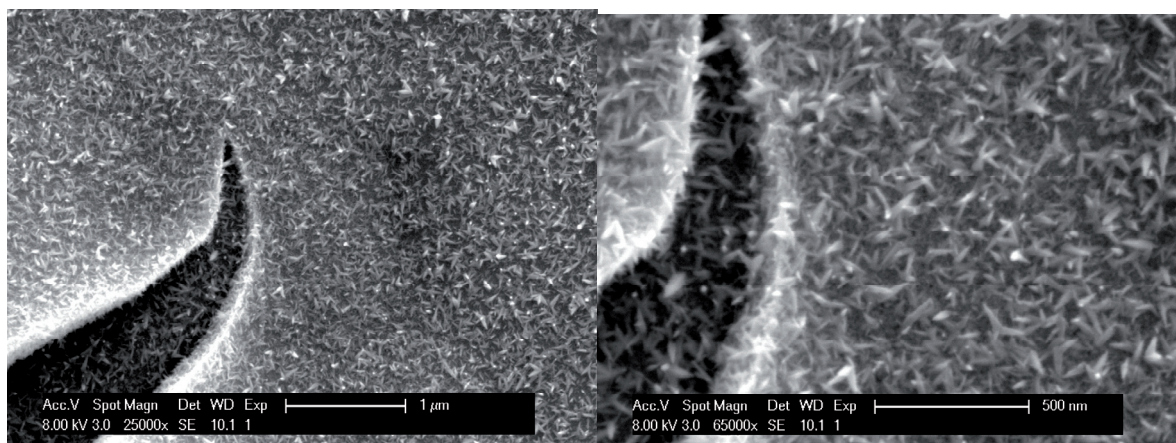


Figure 3-4 SEM micrograph at different enlargements of the IrO₂ coating deposited on pretreated Ti

Several Ti/IrO₂ electrodes with different loadings were prepared and cyclic voltammetry measurements at various scan rates were performed within the same potential window in 1M HClO₄.

Figure 3-5 shows the voltammograms for a one-layer Ti/IrO₂ (0.96 mg cm⁻²) electrode.

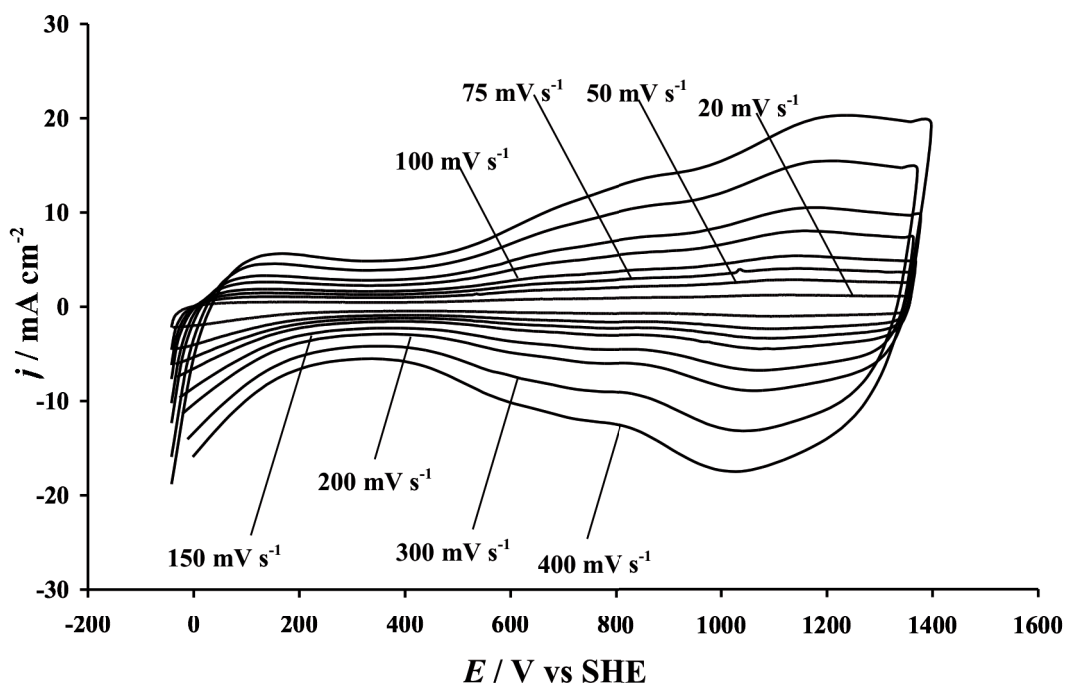


Figure 3-5: Cyclic voltammograms using Ti/IrO₂ (IrO₂ loading: 0.96 mg cm⁻²) at different scan rates. Supporting electrolyte: 1M HClO₄. T=25°C.

The corresponding voltammetric charges (q^*) were plotted as a function of scan rate for several loadings of IrO₂ (Figure 3-6).

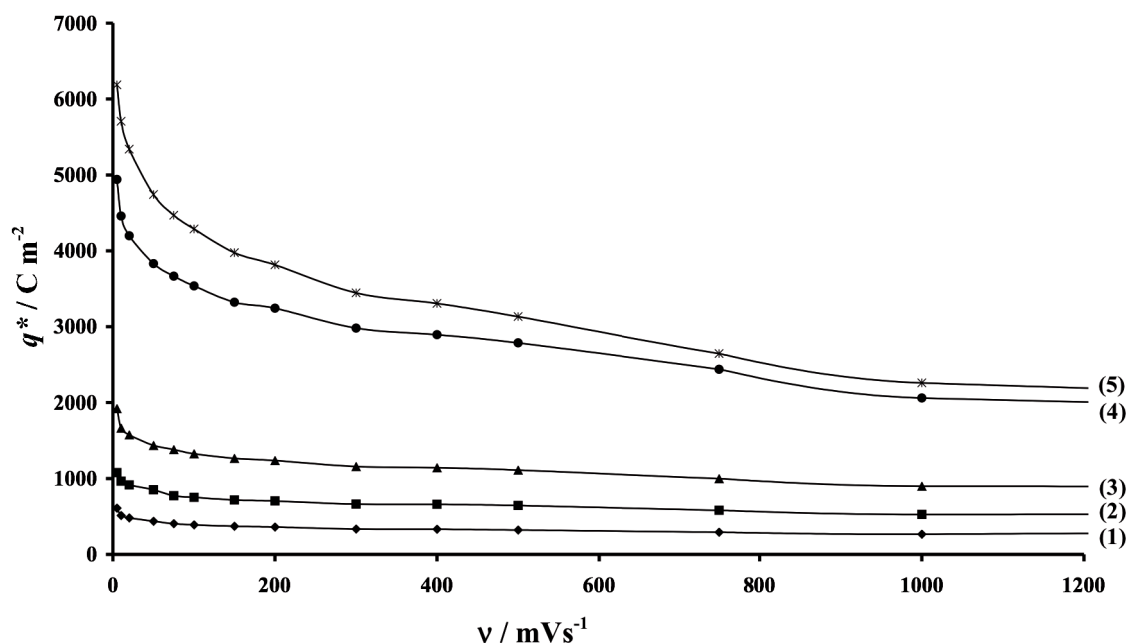


Figure 3-6: Variation of the voltammetric charge q^* with scan rate for different IrO₂ loadings: (1) 0.73 mg cm⁻², (2) 0.96 mg cm⁻², (3) 1.58 mg cm⁻², (4) 4.07 mg cm⁻² and (5) 6.55 mg cm⁻² obtained in 1M HClO₄ at 25°C.

This figure shows clearly that q^* at a given scan rate increases with the IrO₂ loading. This voltammetric charge q^* has been used as a tool to provide an estimation of the IrO₂ loading for the development of IrO₂ electrodes prepared using the spin coating deposition technique (see below).

3.3.2 Morphological and voltammetric charge study of Ti/IrO₂ electrodes prepared using the spin coating deposition method

Several Ti/IrO₂ electrodes were prepared using the spin coating deposition technique with the rotation speed of the substrate fixed at 2000rpm while the concentration of H₂IrCl₆ was varied between 5mM and 250mM. Cyclic voltammetry measurements were performed on those electrodes in the water stability potential domain at different scan rates and the corresponding voltammetric charges were measured (Figure 3-7).

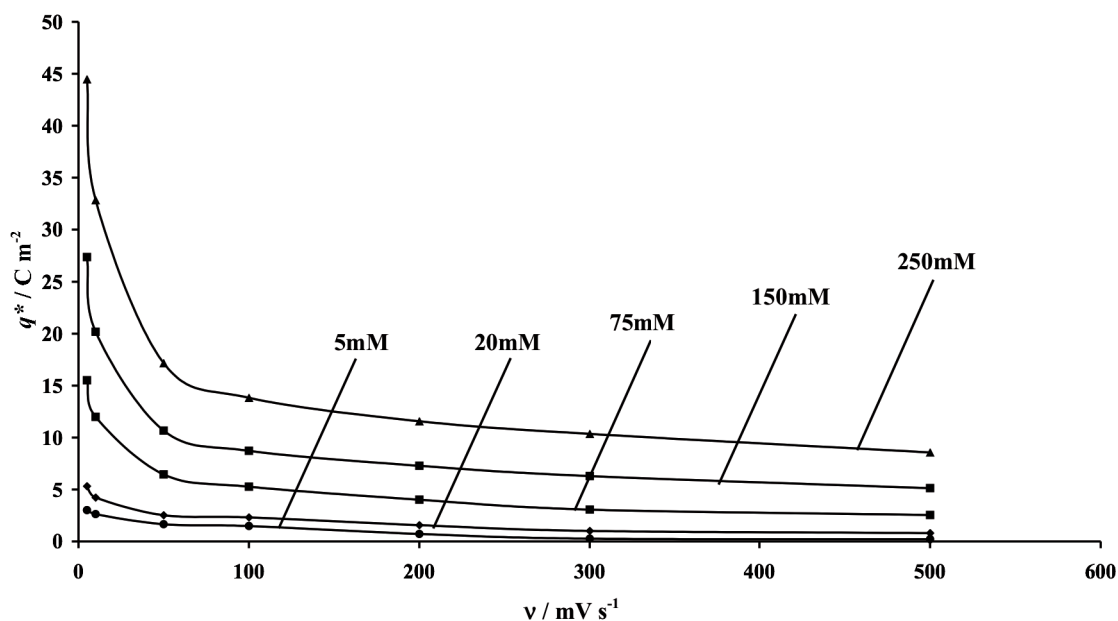


Figure 3-7: Variation of the voltammetric charge q^* with scan rate for Ti/IrO₂ electrodes prepared using the spin coating deposition technique and different concentrations of H₂IrCl₆ in the precursor solution. Rotation speed of the substrate: 2000rpm. T = 25°C

Figure 3-8 shows that for scan rates ranging between 5 and 500mVs⁻¹, q^* increases linearly with the concentration of H₂IrCl₆ in the precursor solution.

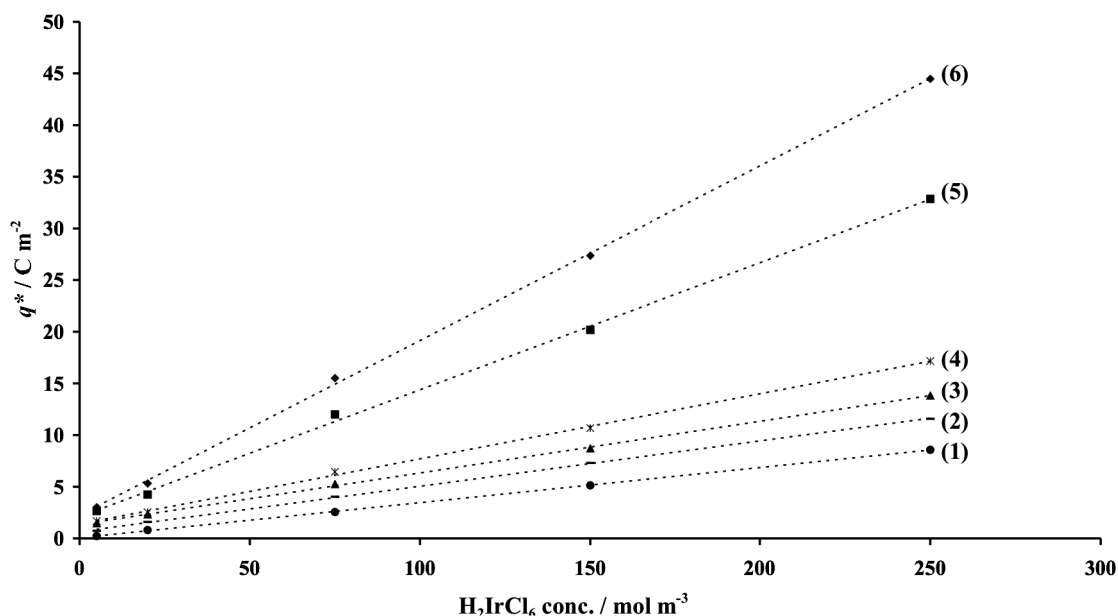


Figure 3-8: Variation of the voltammetric charge q^* with the concentration of H₂IrCl₆ in the precursor solution for Ti/IrO₂ electrodes prepared using the spin coating deposition technique (rotation speed of the substrate: 2000rpm) and for different scan rates: (1) 500mV s⁻¹, (2) 200mV s⁻¹, (3) 100mV s⁻¹, (4) 50mV s⁻¹, (5) 10mV s⁻¹ and (6) 5mV s⁻¹. T = 25°C

The other parameter of the spin coating deposition technique able to control the loading of the IrO₂ coating is the rotation speed of the substrate.

Thus several Ti/IrO₂ electrodes were prepared using a precursor solution containing 250mM of H₂IrCl₆ while the rotation speed of the substrate was varied between 500 and 3000rpm.

Again, cyclic voltammetry measurements within the water stability potential domain were performed on those electrodes at different scan rates and the voltammetric charge was measured. Figure 3-9 shows the evolution of the voltammetric charge q^* as a function of scan rate for four Ti/IrO₂ electrodes prepared using the same precursor solution except for different rotation speeds applied to the substrate.

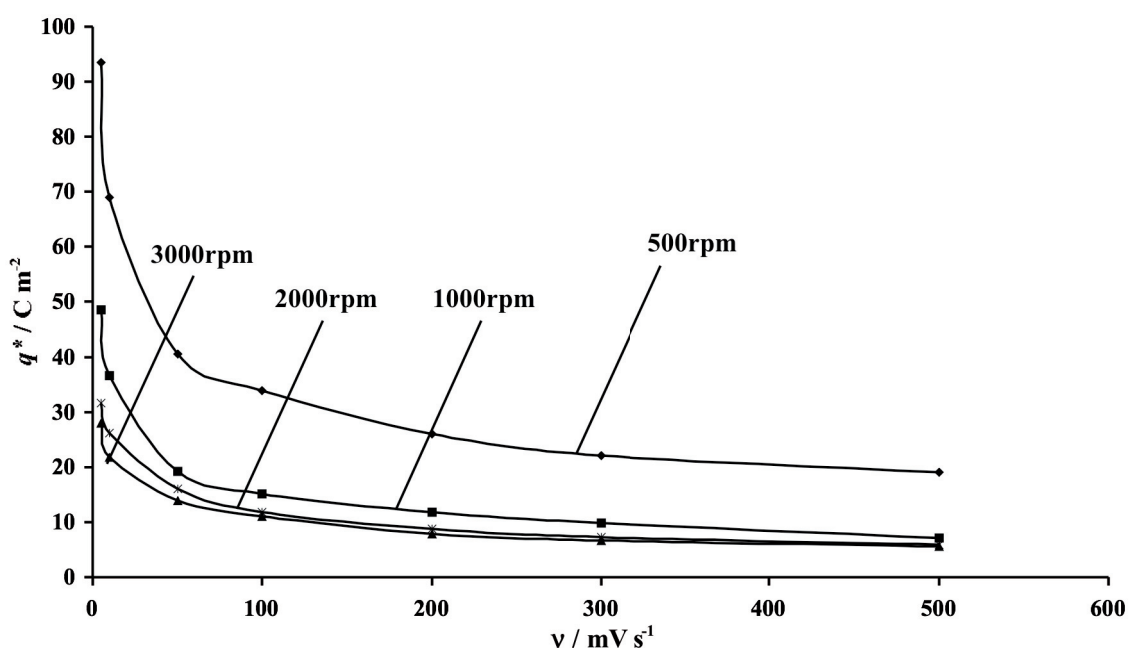


Figure 3-9: Variation of the voltammetric charge q^* as a function of scan rate for Ti/IrO₂ electrodes prepared using the spin coating deposition technique for different rotation speeds applied to the substrate. Concentration of H₂IrCl₆ in the precursor solution: 250mM. $T = 25^{\circ}\text{C}$

Considering: (a) the relation expressing the coating's thickness (h_{∞}) as a function of ω (Eq.(2-11)), (b) a constant porosity within the film and (c) the direct proportionality between the IrO₂ loading and the voltammetric charge q^* , the latter is plotted as a function of $\omega^{-0.5}$. Figure 3-9 shows that the $q^* - \omega^{-0.5}$ curves are linear for six different scan rates.

Figure 3-8 and Figure 3-10 also clearly show that it is possible to control the loading of the IrO₂ coating (from Eq.(3-3)) using the spin coating deposition technique by optimizing two parameters, which are the concentration of iridium containing salt (H₂IrCl₆) in the precursor solution (c_0) and the rotation speed of the substrate (ω).

From these results, the relation of the spin coating model (Eq.(2-11)) has been adapted to Ti/IrO₂ electrodes as follows (Eq.(3-1)):

$$q^* \approx K\omega^{-1/2}c_0 \quad (3-1)$$

Where q^* (C m⁻²) is the voltammetric charge directly related to the IrO₂ loading and K (C m rad^{0.5} s^{-0.5} mol⁻¹) is a constant, which depends on the system under investigation (precursor: H₂IrCl₆, solvent: *i*-propanol, substrate: p-Si).

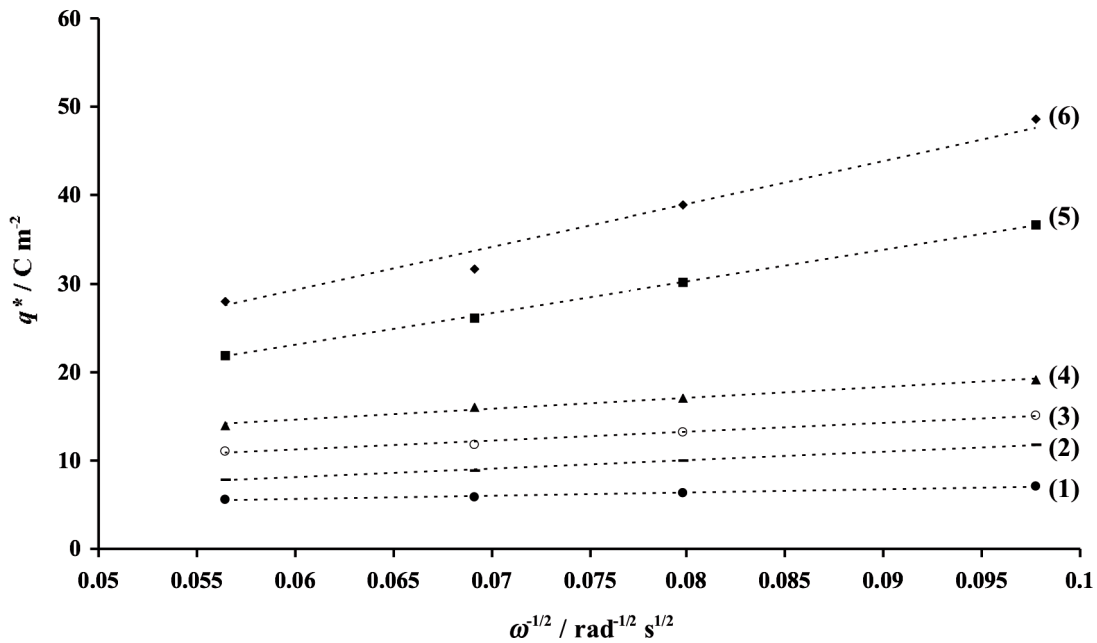


Figure 3-10: Variation of the voltammetric charge q^* as a function of $\omega^{-1/2}$ for Ti/IrO₂ electrodes prepared using the spin coating deposition technique (concentration of H₂IrCl₆ in the precursor solution: 250mM) for different scan rates: (1) 500mV s⁻¹, (2) 200mV s⁻¹, (3) 100mV s⁻¹, (4) 50mV s⁻¹, (5) 10mV s⁻¹ and (6) 5mV s⁻¹.

This new relation (Eq.(3-1)) predicts that the straight lines presented in Figures 3-8 and 3-10 should cross the origin and the results presented indicate that it is indeed the case for all the applied scan rates.

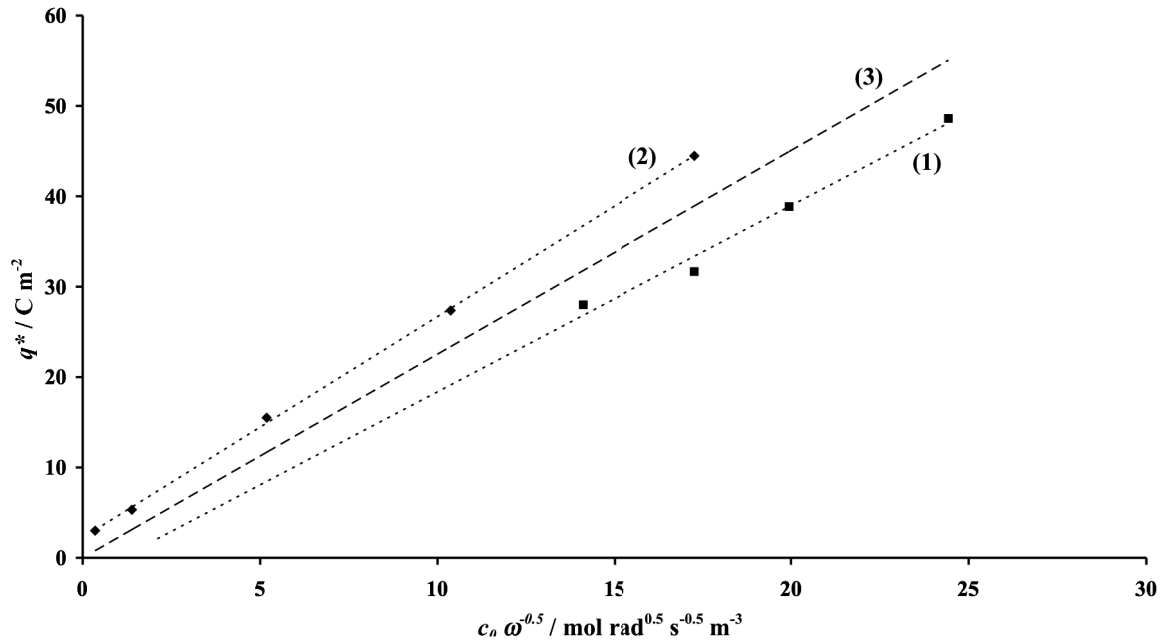


Figure 3-11: voltammetric charge q^* reported from (1) Figure 3-10 and (2) Figure 3-8 and plotted as a function of the product $c_0 \cdot \omega^{-0.5}$. (3) average plot.

From the slope obtained for the average straight line passing through the origin ((3) in Figure 3-11), the constant K in Eq.(3-1) was calculated in SI units ($\text{C m rad}^{0.5} \text{ s}^{-0.5} \text{ mol}^{-1}$). Therefore, it has been demonstrated that this model (Eq.(3-2)) can be used for the estimation of the loading of the IrO₂ coating (from Eq.(3-3)) for the system under investigation in this work (precursor: H₂IrCl₆, solvent: *i*-propanol, substrate: Ti):

$$q^* \approx 2.25(\pm 0.2)\omega^{-1/2}c_0 \quad (3-2)$$

Domain of validity: $500\text{rpm} < \omega < 3000\text{rpm}$ $5\text{mM} < c_0 < 250\text{mM}$

From voltammetric charge measurements performed on Ti/IrO₂ electrodes with different loadings, a value for the specific voltammetric charge of the IrO₂ coating (q_{sp}^*) has been determined at about 30C per gramm of IrO₂ (Chapter 4, Fig.4-10) in agreement with previous studies [18].

CHAPITRE 3: Preparation and morphological characterization of Ti/IrO₂ and p-Si/IrO₂ electrodes

Using this value, Eq.(3-2) can be rearranged to express the IrO₂ loading L_{IrO_2} (g m⁻²) as a function of ω and c_0 :

$$L_{IrO_2} \approx 0,075\omega^{-1/2}c_0 \quad (3-3)$$

This value allows the estimation of the IrO₂ loading from the voltammetric charge q^* . In order to investigate the influence of the precursor salt concentration on the homogeneity of the coating, SEM pictures of Ti/IrO₂ electrodes prepared with the rotation speed of the substrate fixed at 2000rpm but using four different H₂IrCl₆ concentrations are presented in Figure 3-12.

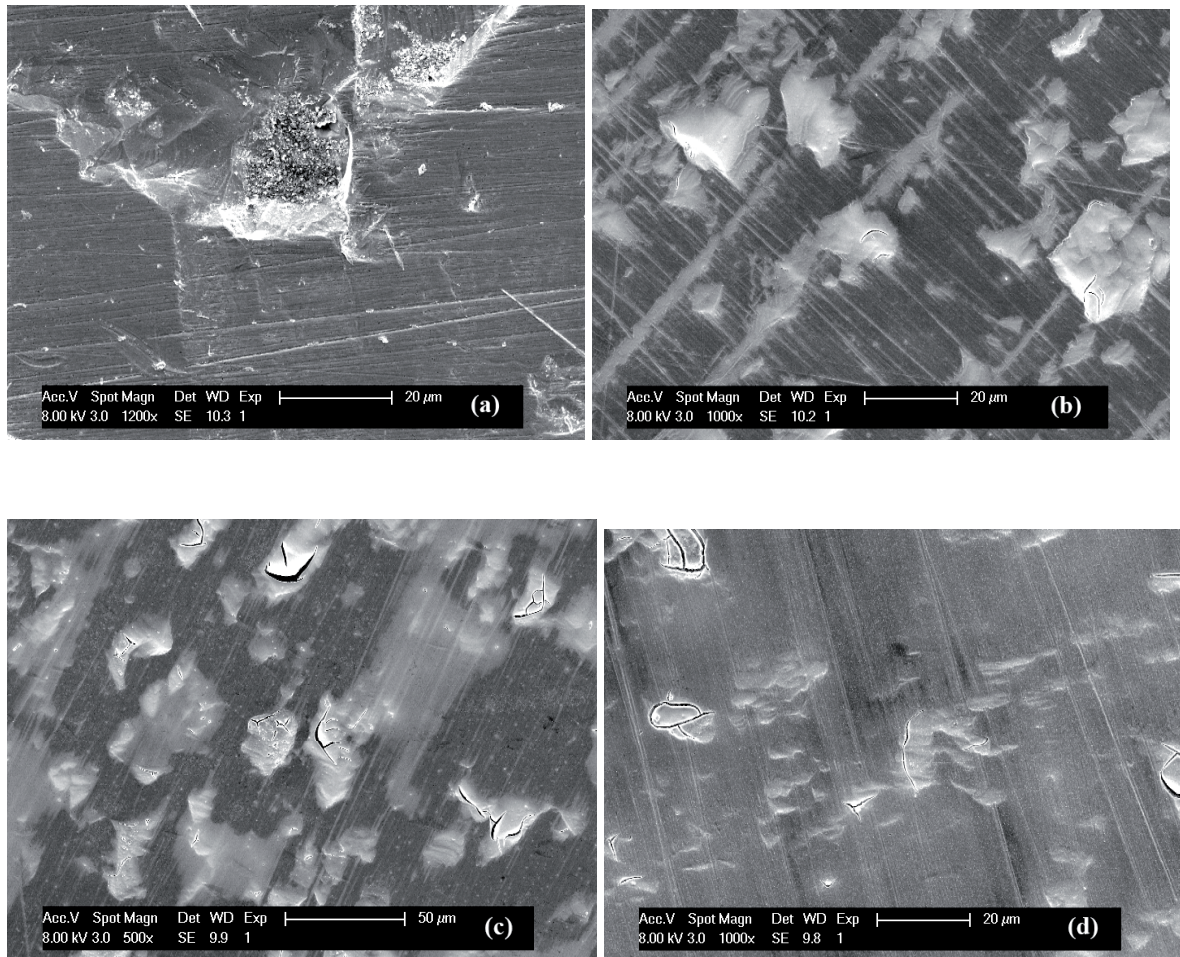


Figure 3-12: SEM micrograph of Ti/IrO₂ electrodes prepared using the spin coating deposition technique and different concentrations of H₂IrCl₆ in the precursor solution: (a) 20mM, (b) 75mM, (c) 150mM and (d) 250mM. Rotation speed of the substrate: 2000rpm. T = 25°C

These images show the presence of dark regions for small concentrations of H₂IrCl₆ (pictures (a), (b) and (c)) indicating that a significant portion of the substrate is still not covered by IrO₂. Consequently, a concentration of 250mM of iridium salt in the precursor solution has been chosen in order to ensure that the entirety of the surface is being covered.

Regarding the rotation speed of the substrate, SEM pictures of several Ti/IrO₂ electrodes prepared with different rotation speeds imposed to the substrate were taken as well. These pictures are presented in Figure 3-13.

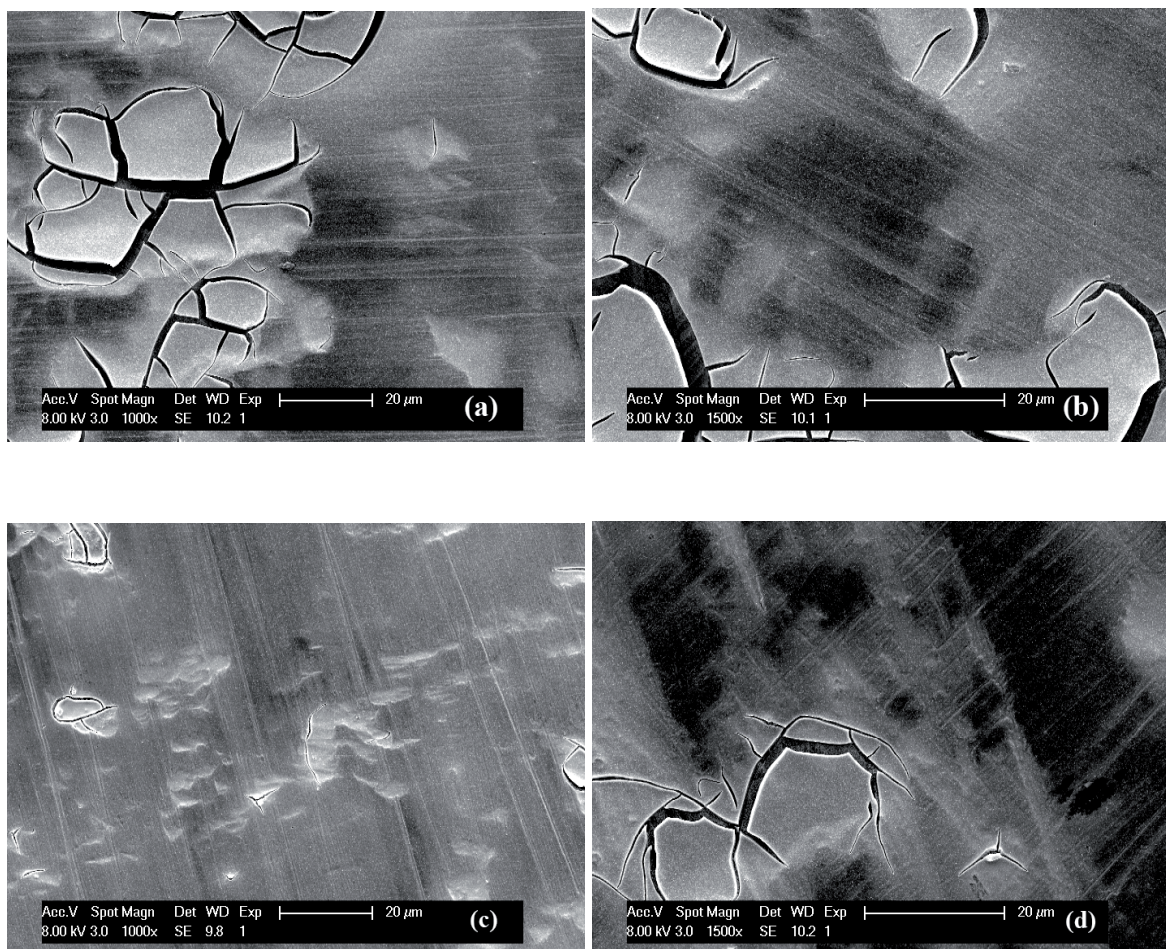


Figure 3-13: SEM micrograph of Ti/IrO₂ electrodes prepared using the spin coating deposition technique. Concentration of H₂IrCl₆ in the precursor solution: 250mM. Rotation speed of the substrate: (a) 500rpm, (b) 1000rpm, (c) 2000rpm and (d) 3000rpm

CHAPITRE 3: Preparation and morphological characterization of Ti/IrO₂ and p-Si/IrO₂ electrodes

These images show that the rotation speed has little effect on the morphology of the IrO₂ coating. However, a rotation speed of 500rpm seems to produce continuous IrO₂ films covering almost all the surface of the titanium substrate.

Therefore, the following optimal spin coating conditions for all the foregoing IrO₂-based electrodes have been chosen: 500rpm for the rotation speed of the substrate and 250mM of H₂IrCl₆ for the concentration of precursor solution.

3.3.3 p-Si as substrate

XPS measurements performed on Ti/IrO₂ electrodes have revealed the presence of Ti in the coating (Table 3-1). This is likely due to the formation of TiO₂ at the Ti/IrO₂ interface, which diffuses into the IrO₂ coating during the thermal treatment.

Table 3-1: XPS measurements performed on Ti/IrO₂ electrodes

Peaks	Position BE / eV (1)	Raw area / CPS (2)	RSF (3)	Mass conc. / %	Atomic		
					mass	Conc. / %	Theoretical conc. / %
O 1s	531.2	110996.8	0.78	24.73	15.999	78.94	66
Ti 2p	458.2	4897	2.001	1.32	47.878	1.41	-
Ir 4f	61.8	148528.1	5.021	73.95	192.193	19.65	33

(1) **Peak position (BE: binding energy)**

(2) **Raw area of the peak in count per seconds (CPS)**

(3) **Relative sensitivity factor (RSF)**

In order to avoid this interference, conductive p-Si, which is electrochemically inactive, has been used. However, as p-Si is a very slick material, the first layers of IrO₂ deposited on this new substrate were rapidly detached after the first tests as seen in Figure 3-14.

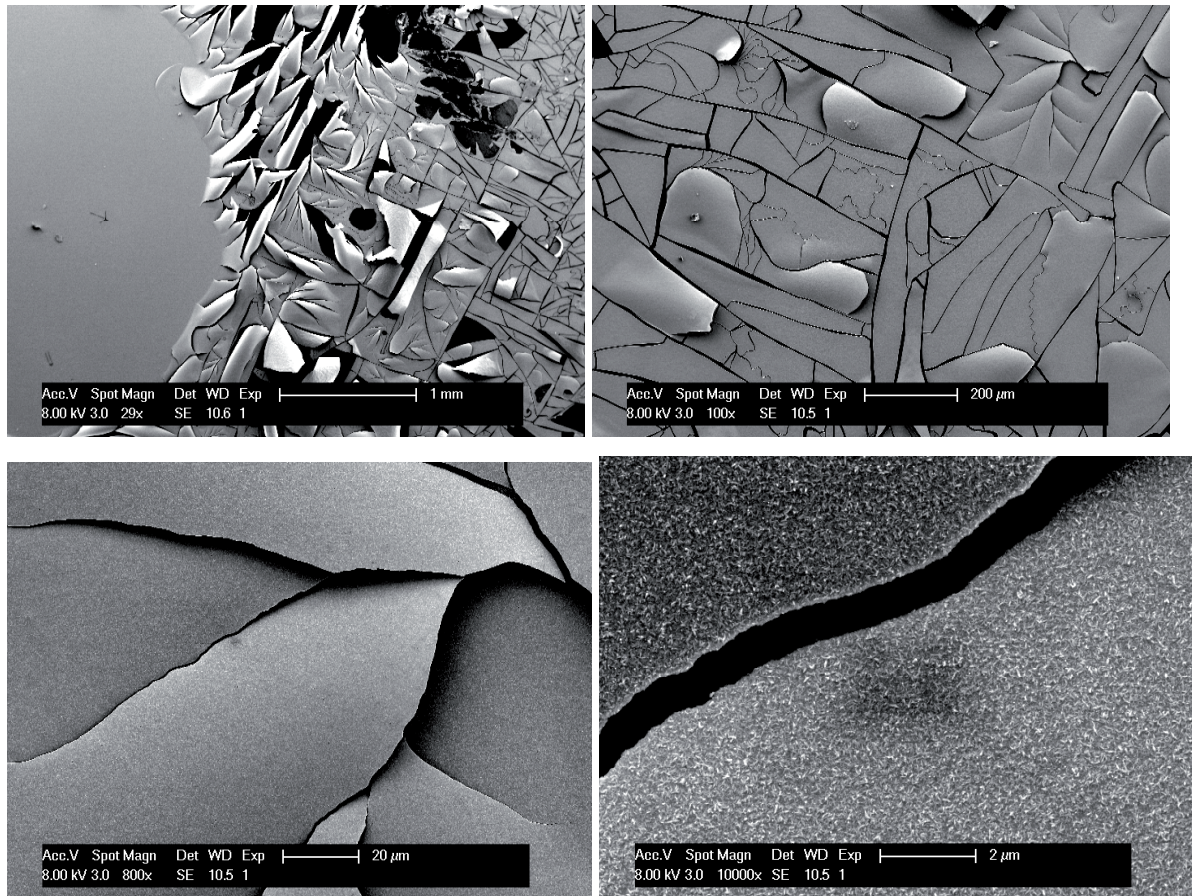


Figure 3-14: SEM micrograph at different enlargements of an IrO₂ coating deposited on untreated p-Si

Therefore, the conductive silicon was delicately sandblasted in order to improve the adherence between the IrO₂ coating and the support material; the difference between before and after sandblasting is clear (Figure 3-15a). A closer enlargement of the sandblasted p-Si is given in Figure 3-15b.

CHAPITRE 3: Preparation and morphological characterization of Ti/IrO₂ and p-Si/IrO₂ electrodes

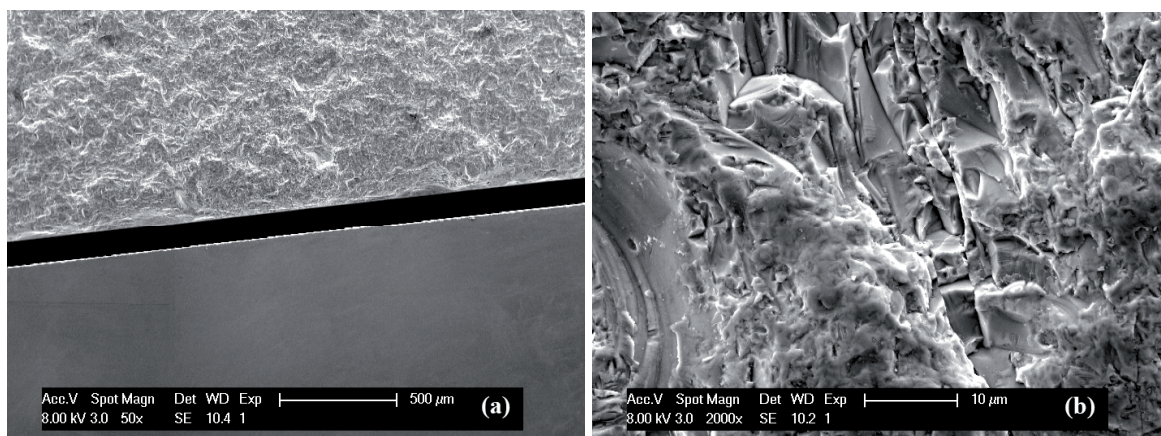


Figure 3-15: SEM micrograph of (a) the upper part is sandblasted p-Si compared with the lower part, which shows untreated p-Si and (b) a closer enlargement of sandblasted p-Si

These last images show that the sandblasting of the p-Si substrate created enough surface defects. This will certainly enhance the adherence with the coating. Figure 3-16 shows SEM images of IrO₂ deposited on sandblasted p-Si. This figure shows that parts of the sandblasted p-Si support are still visible. Furthermore, the coating exhibits the same cracked dried-mud structure previously observed on Ti substrate (Figure 3-3).

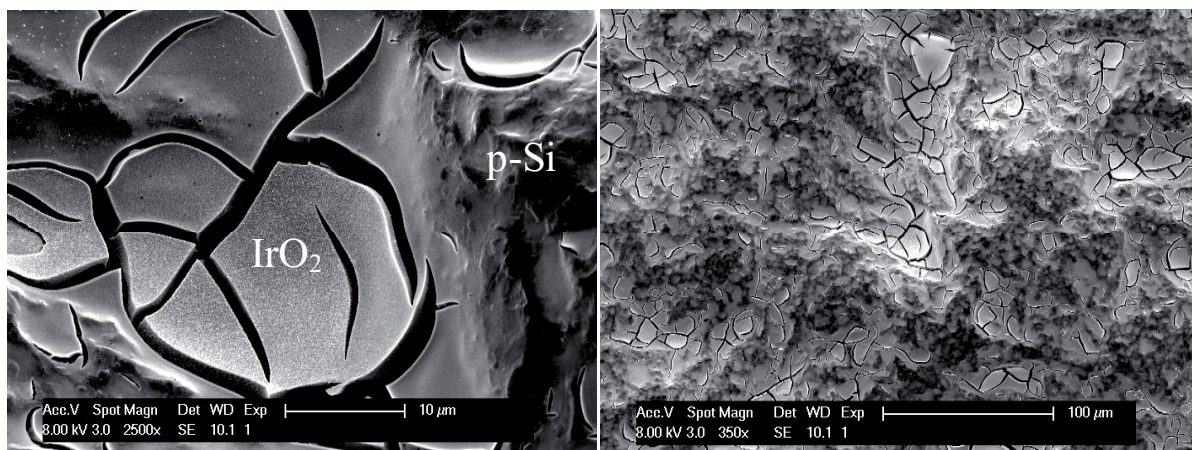


Figure 3-16: SEM micrograph at different enlargements of an IrO₂ coating deposited on sandblasted p-Si (IrO₂ loading: 0.273 mg cm⁻²)

XPS measurements were performed on these electrodes and the results are presented in Table 3-2.

Table 3-2 : XPS measurements performed on p-Si/IrO₂ DSA®

Peaks	Position BE / eV (1)	Raw area / CPS (2)	RSF (3)	Mass conc. / %	Atomic		
					mass	Conc. / %	Theoretical conc. / %
O 1s	530	93742.2	0.78	19.11	15.999	73.96	66
Si 2p	103.7	31.5	0.339	0.03	28.086	0.07	-
Ir 4f	61.8	177081.8	5.021	80.81	192.193	25.97	33

(1) **Peak position (BE: binding energy)**

(2) **Raw area of the peak in count per seconds (CPS)**

(3) **Relative sensitivity factor (RSF)**

These XPS measurements show that the coating is mainly composed of IrO₂ and only 0.03% w/w of Si is still present. From the results presented herein, it is now clear that sandblasted p-Si is the appropriate support material to adequately study the electrochemical behaviour of IrO₂-based electrodes.

3.4 Conclusions

In order to investigate the electrochemical behavior of iridium dioxide as electrode material, IrO₂ electrodes were prepared by thermal decomposition of a H₂IrCl₆ precursor solution on an inert substrate. It has been shown that the choice of sandblasted p-Si as substrate material reduces strongly undesired interactions of the substrate with the coating.

It has been shown also that the charge measured using cyclic voltammetry in the potential range of water stability is a viable tool for the estimation of the loading of the IrO₂ coating. For a better control of the loading and uniformity of the IrO₂ film, the precursor solution has been applied on the substrate using the spin coating deposition technique. The experiment revealed that the loading can be controlled via two parameters: the concentration of H₂IrCl₆ in the precursor solution and the rotation speed of the substrate. Moreover, a novel and simple relation has been proposed (Eq.(3-3)) for the estimation of the IrO₂ loading as a function of the concentration of H₂IrCl₆ in the precursor solution c_0 and the rotation speed applied to the substrate ω .

3.5 References

- [1] H. Beer, J.M. Hinden, EU Pat. EP 0 046 449 B1 (1985)
- [2] H. Beer, J. Electrochem. Soc., 127 (1980) 303C
- [3] J.M. Hinden, H. Beer, US pat. 4,444,642 (1984)
- [4] S. Trasatti, Electrochim. Acta, 45 (2000) 2377
- [5] Y. Baba, K. Nagata, S. Takahashi, N. Nakamura, N. Yoshiyasu, M. Sakurai, C. Yamada, S. Ohtani, M. Tona, Surface Science, 599 (2005) 248
- [6] M. Haruta, Catalysis Today, 36 (1997) 153
- [7] Y. Izuka, H. Fujiki, N. Yamauchi, T. Chijiiwa, S. Arai, S. Tsubota, M. Haruta, Catalysis Today, 36 (1997) 115
- [8] F. Cardarelli, P. Taxil, A. Savall, Ch. Comninellis, G. Manoli, O. Leclerc, J. Appl. Electrochem., 28 (1998) 245
- [9] G.P. Vercesi, J. Rolewicz, Ch. Comninellis, J.M. Hinden, Thermochim. Acta, 176 (1991) 31
- [10] Ch. Comninellis, G.P. Vercesi, J. Appl. Electrochem., 21 (1991) 335
- [11] Y.M. Tsou, US pat. 5,645,930 (1997)
- [12] R.A. Guidotti, H. Ye, T.D. Xiao, D.E. Reisner, D.H. Doughty, US pat. 6,926,997 (1999)
- [13] Y.-K. Lee, J.-W. Park, Han'guk Chaelyo Hakhoechi, 6(2), (1996), 166-74
- [14] Y. Takasu, S. Onone, K. Kameyama, Y. Murakami, K. Yahikosawa, Electrochim. Acta, 39 (1994) 1993
- [15] L. Ouattara, T. Diaco, I. Duo, M. Panizza, G. Foti, C. Comninellis, J. Electrochem. Soc., 150 (2003) D41
- [16] G.P. Vercesi, J.Y. Salamin, Ch. Comninellis, Electrochim. Acta 36 (1991) 991
- [17] G.P. Vercesi, J. Rolewicz, Ch. Comninellis, J. Hinder, Thermochim. Acta, 176 (1991) 31
- [18] E.Herrera Calderon, PhD Thesis, Swiss Institute of Technology (EPFL), No 4181, 2008

Chapter 4 : Surface redox activities and charging/discharging process on p-Si/IrO₂ electrodes

In this chapter, the surface redox activities of the IrO₂ coating are investigated using the electrodes prepared and described in the previous chapter.

It was found by analyzing cyclic voltammetry measurements performed at different temperatures and scan rates, that the charging/discharging process, which occur within the water stability potential domain, is related to two processes: the first one is a slow process with low activation energy (about 2.4 kJ mol⁻¹) corresponding to the diffusion of protons within the IrO₂ coating inducing surface redox activities. This charging process dominates at low scan rates and depends on the square root of the scan rate. The second contribution is a fast (instantaneous) process with near-zero activation energy, which is the charging of the electrical double layer (q_{dl}^*).

This charging process dominates at high scan rates and is scan rate independent. Moreover, from potential step experiments together with cyclic voltammetry measurements, it has been shown that the coating's surface iridium atoms valence state varies between +IV and +VI within the potential domain between the on-set potentials of H₂ and O₂ evolution.

This chapter is based on the publication:

S. Fierro, L. Ouattara, E. H. Calderon, C. Comninellis. Influence of temperature on the charging/discharging process of IrO₂ coating deposited on p-Si substrate, *Electrochemistry Communications*, Volume 10, Issue 6, April 2008, Pages 955-959

4.1 Introduction

As mentioned in the previous chapters, IrO₂ electrodes lead to significant improvements in many applications [1-7] and the electrochemical properties of the surface of these electrodes play an important role in their electrocatalytic behavior [8]. Transient techniques, like cyclic voltammetry, are usually used for the investigation of the surface reactions involved. The integration of the cyclovoltammogram provides the voltammetric charge q^* [9,10].

The majority of the publications focusing on the voltammetric charge up to date consider RuO₂ based DSA[®] deposited by thermal decomposition on a Ti substrate (Ti/RuO₂). Two main approaches have been elaborated in order to explain the dependence of q^* on scan rate on these electrodes.

The first approach proposed by Ardizzone [10] is based on the fact that the voltammetric charge q^* is related to protons diffusion within the RuO₂ coating, which is the rate determining step of the charging/discharging process. According to these authors, increasing the scan rate results in a decrease of the voltammetric charge due to the exclusion of a fraction of the available surface induced by the slow diffusion of protons within the coating.

The second approach is based on the model proposed by Sugimoto et al [11]. Here, the voltammetric charge is the result of two main contributions on top of the charging due to adsorption. The first contribution is the charging of the double layer and the

second is the charging induced by redox surface activities on the surface of the coating. At high scan rates, the slow surface charging process is excluded and only the charging of the double layer persists. This process is scan rate independent contrarily to the charging of the surface, which decreases with increasing scan rate. The following figure (Figure 4-1) summarizes this second approach.

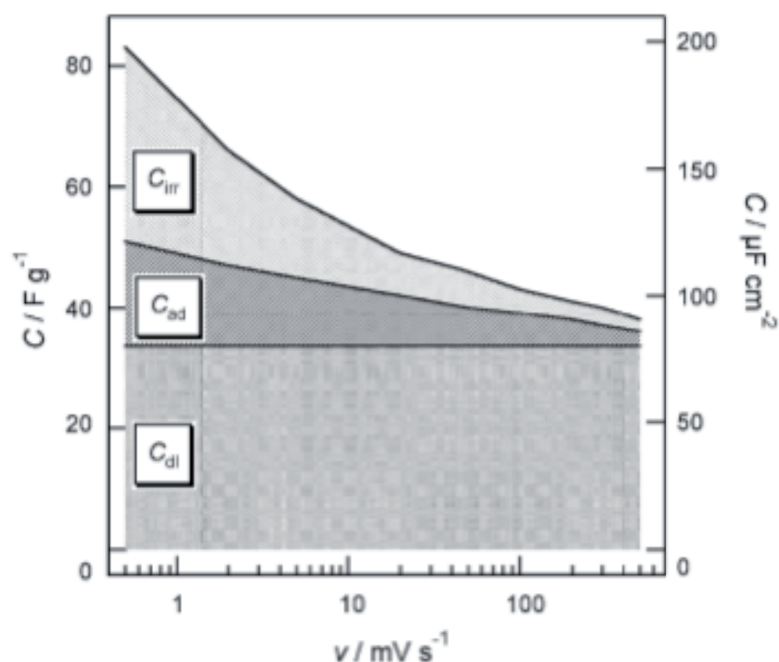


Figure 4-1: The contribution of the specific capacitance for Ti/RuO₂ electrodes as a function of scan rate where C_{dl} is the double-layer capacitance, C_{ad} is the capacitance related to cations/anions adsorption and C_{irr} is the capacitance related to an irreversible Faradaic process [11]

However, up to date, no proof on the respective accuracy of these approaches has been provided in literature for Ti/RuO₂ electrodes and even less is known for IrO₂ based electrodes.

Therefore, in this chapter, the electrochemical surface properties involved on p-Si/IrO₂ electrodes have been investigated. This chapter focuses on estimating the apparent activation energy of the charging/discharging process of p-Si/IrO₂ electrodes as a function of scan rate. Through this method, a better understanding of the charging/discharging process of these electrodes is sought.

4.2 Experimental details

Each cyclic voltammetry and potential step experiments presented in this section were performed in a thermostated three-electrode cell (70 ml) using an Autolab PGSTAT 30. The counter electrode was a Pt wire; the reference electrode was Hg/Hg₂SO₄/K₂SO₄ (sat.) (MSE; 0.65 V vs. SHE) and the working electrode was an IrO₂ electrode prepared by thermal decomposition of a precursor: the precursor aqueous solution (H₂IrCl₆ (99.9%, ABCR)) 250mM in dry *i*-propanol (extra dry with molecular sieves, water < 50ppm, Acros Organics) was deposited using the spin coating technique on square-shaped sandblasted p-Si (182.25 mm²) and then the oxide film (loading: 0.27 mg cm⁻²) was obtained by thermal decomposition in air at 500°C (p-Si/IrO₂). The presence of iridium dioxide on the substrate was verified using XPS measurements (Table 3-2).

For the potential step experiments, the decrease of the current for these electrodes is usually slow [12]. Therefore a pre-treatment had to be performed before every potential step experiment during 30 minutes at 0.4 V vs. SHE in order to stabilize the current near 0 A before applying the desired potential.

The cyclic voltammetry measurements obtained at different temperatures (from 10°C to 70°C) were conducted inside a Faraday cage and using 1M H₂SO₄ (95-97% Merck) as support electrolyte. All potentials reported in this chapter are with respect to the standard hydrogen electrode (SHE).

The cell and materials used for the cyclic voltammetry and potential step experiments are similar to the set-up used in the previous chapter (Figure 3-1 in section 3.2). The main salient feature of the cell used in this present chapter is the thermostatzation, which allows studying the influence of temperature.

4.3 Results and discussion

4.3.1 The charging/discharging process

Cyclic voltammetry in the potential window of water stability has already been used for the evaluation of the electrochemical activity of Ti/IrO₂ electrodes. In fact, we showed in section 3.3.1 that the voltammetric charge q^* obtained by integration of the voltammetric curves can be related to the IrO₂ loading.

In this section, the influences of potential window, potential scan rate and temperature on q^* are investigated in order to gain a better understanding of the charging/discharging process of p-Si/IrO₂ electrodes.

The cyclic voltammograms (CV) obtained in 1M HClO₄ on p-Si/IrO₂ for different potential windows, various scan rates and two different temperatures are shown in Figure 4-2. The current was reported relative to the IrO₂ loading (gravimetric current).

This figure shows that for both temperatures and for all the potential windows and scan rates investigated, the obtained cyclic voltammetry do not show any horizontal symmetry. Furthermore, for all the cyclovoltammograms, the ratio of the involved anodic and cathodic charge is close to 1.

Figure 4-2 shows also that for both investigated temperatures, the anodic gravimetric current (A/gIrO₂) recorded between 0.3V and 1.4V is not dependent on the fixed upper limit (1.1V or 1.4V) when the lower cut-off potential was fixed at 0.3V, while it is clearly higher when this cut-off was set at 0V. Furthermore, the cathodic gravimetric current increases strongly in absolute value in the potential window between 0.3V to 0V.

The fact that the ratio of the anodic and cathodic charges nears 1 indicates that the large cathodic gravimetric current observed between 0.3V and 0V is completely regained over the whole anodic range during the anodic sweep. This is an indication that the surface redox process involved in this potential region (0.3V to 0V) is a slow redox process.

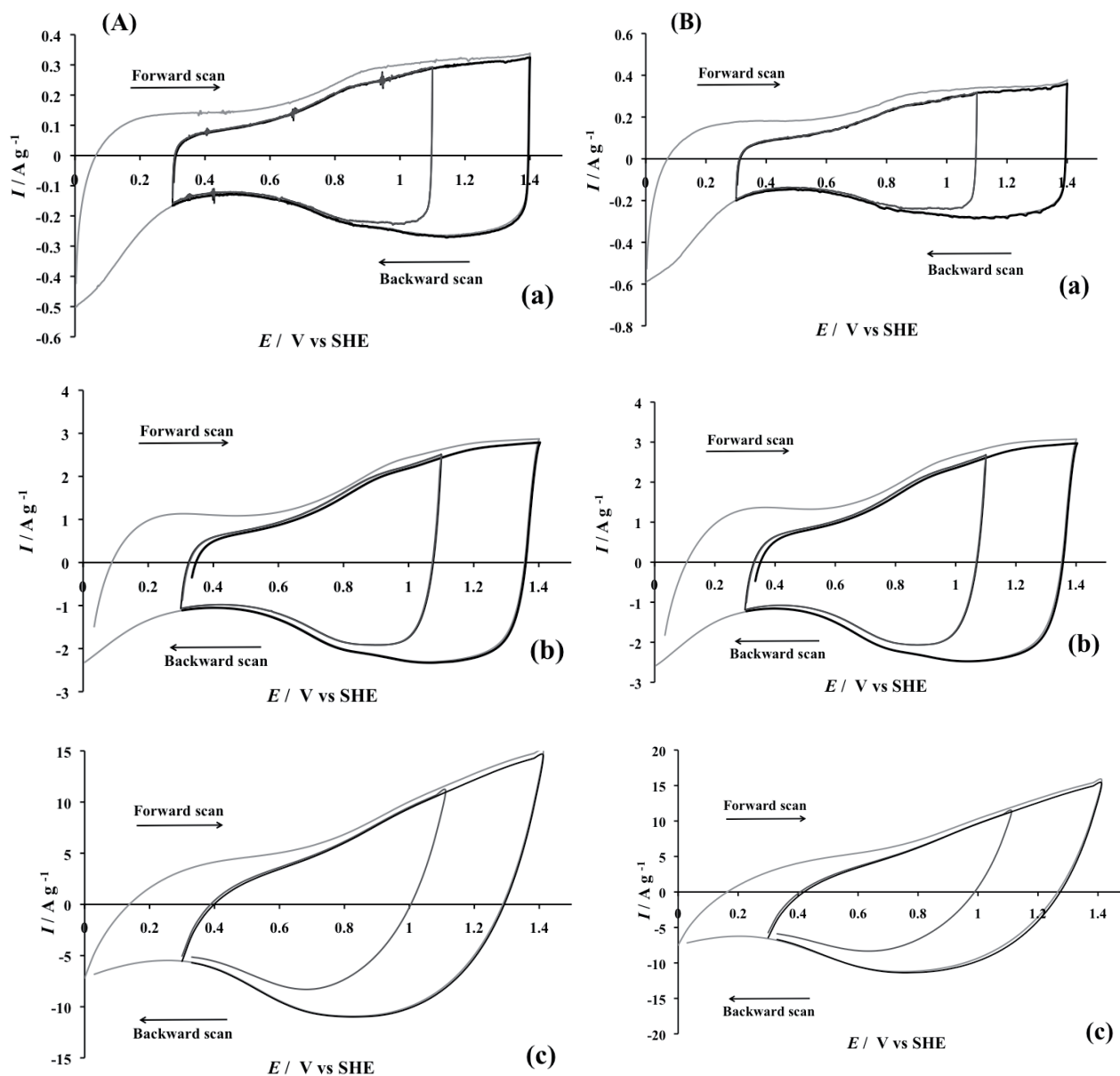


Figure 4-2: Cyclic voltammograms using three different potential windows on p-Si/IrO₂ electrode (loading: 0.27 mg cm⁻²) obtained at (A) 22°C and (B) 70°C and recorded at different scan rates (a) 5, (b) 50, (c) 300 mV s⁻¹. Electrolyte: 1M HClO₄

Figure 4-3 shows the differential gravimetric capacitance (calculated by dividing the gravimetric current by the scan rate) at (A) 22°C and (B) 70°C as a function of electrode potential obtained at different scan rates and Figure 4-4 shows the same gravimetric capacitance as a function of electrode potential obtained at different scan rates and at 22°C but for two different potential windows. Both figures (Figure 4-3 and

Figure 4-4) give once more an indication that the surface redox process involved in this potential domain is slow.

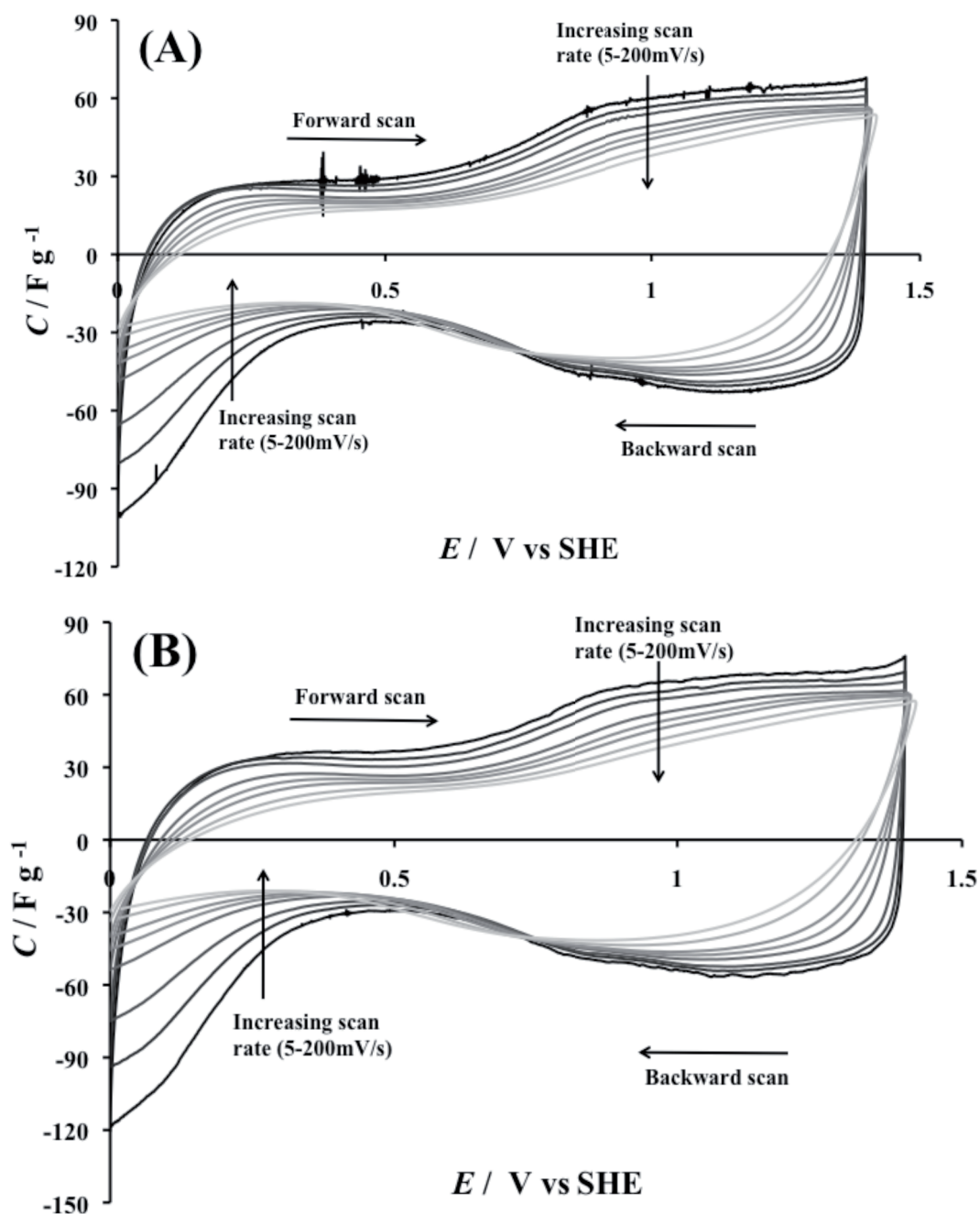


Figure 4-3 : Differential gravimetric capacitance ($F/gIrO_2$) obtained on a p-Si/IrO₂ electrode (loading: $0.27\ mg\ cm^{-2}$) as a function of the applied potential for different scan rates (5, 10, 20, 50, 75, 100 and $200\ mV\ s^{-1}$). Electrolyte: $1M\ HClO_4$. (A) $22^\circ C$ and (B) $70^\circ C$

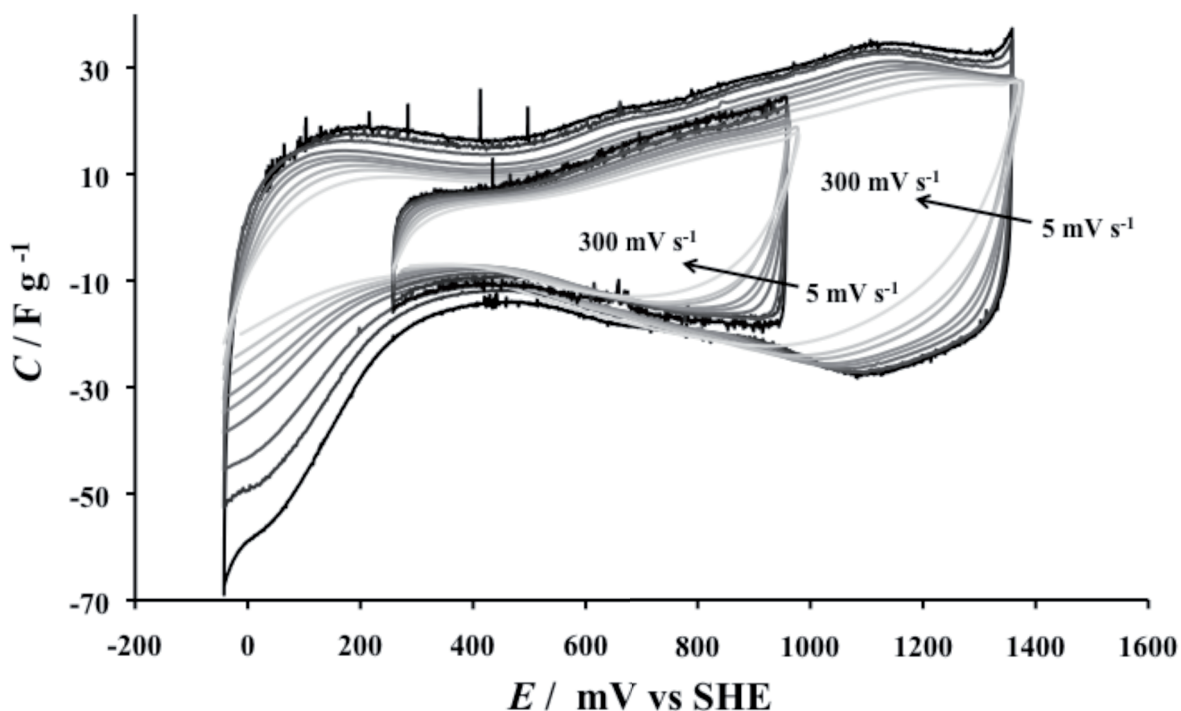


Figure 4-4: Differential gravimetric capacitance (F/gIrO₂) of a p-Si/IrO₂ electrode (loading: 0.27 mg cm⁻²) as a function of applied potential obtained at different scan rates (5, 10, 20, 50, 75, 100 and 200 mV s⁻¹) and for two potential windows: between -0.05 and 1.4 V and between 0.25 and 0.95 V). Electrolyte: 1M HClO₄. T = 22°C

The total gravimetric voltammetric charges Q (C/gIrO₂) were obtained for several operating temperatures (ranging from 8°C to 70°C) by integrating the voltammograms of Figure 4-3 in the potential window between 0 and 1.4V. The same charges were obtained for two different potential windows (at 22°C) by integrating the voltammograms of Figure 4-4.

These gravimetric charges were plotted versus scan rate. The results are presented in Figure 4-5 and Figure 4-6 respectively.

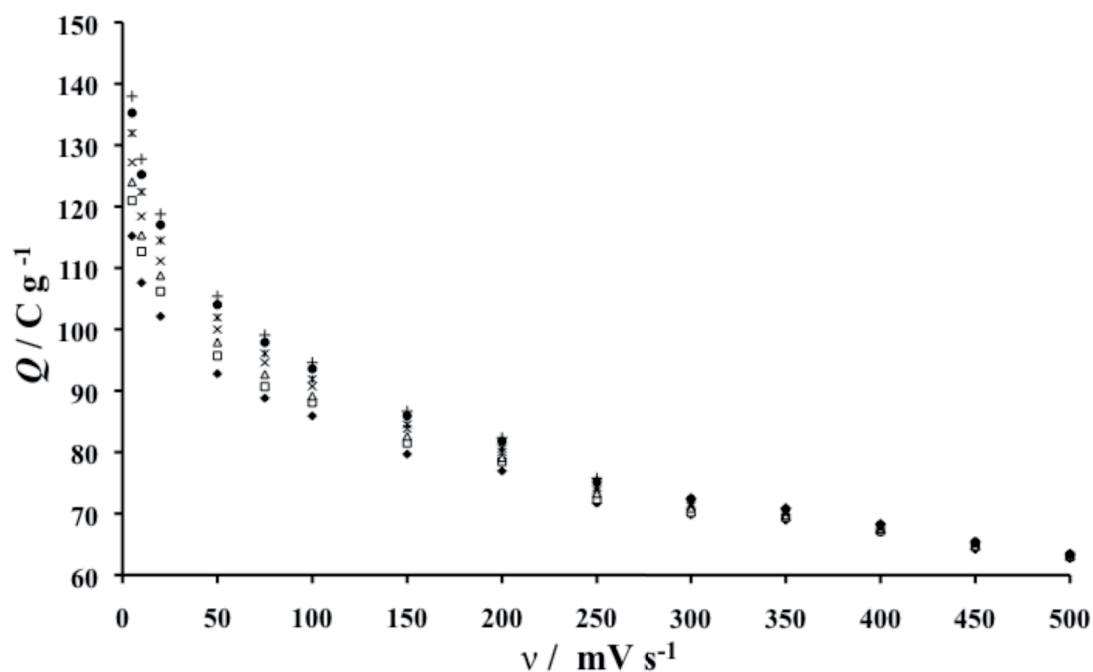


Figure 4-5: Gravimetric voltammetric charges Q (C/gIrO₂) obtained from Figure 4-3 at different temperatures and plotted versus scan rate. Electrolyte: 1M HClO₄, (+) 70°C; (•) 60°C; (*) 50°C; (x) 40°C; (Δ) 30°C; (□) 22°C and (◊) 8°C

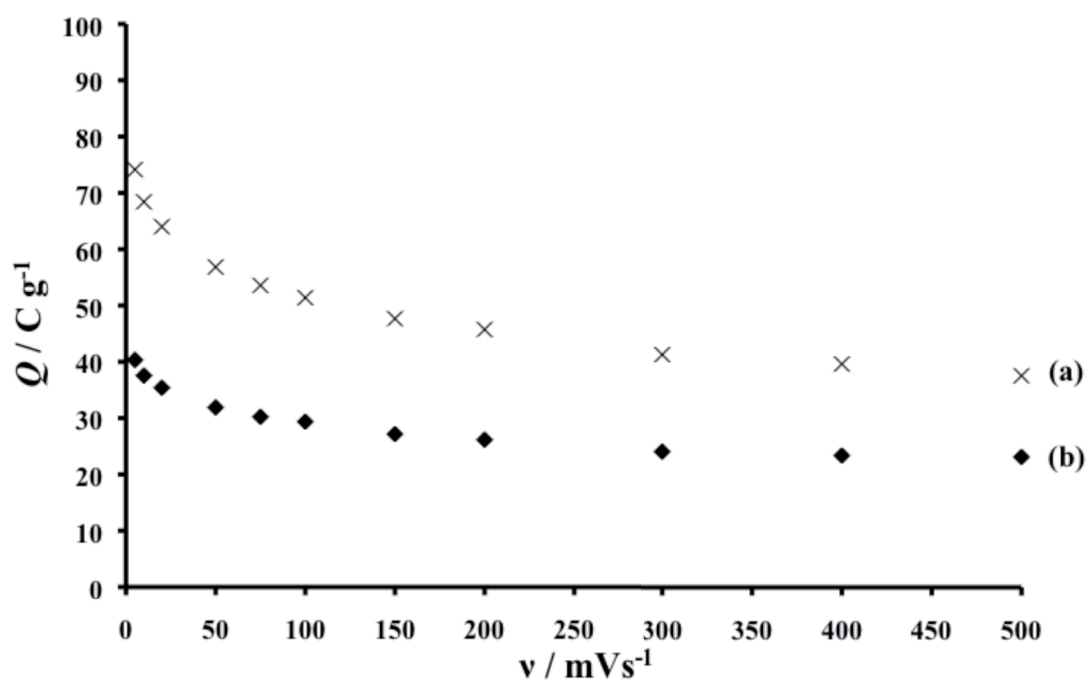
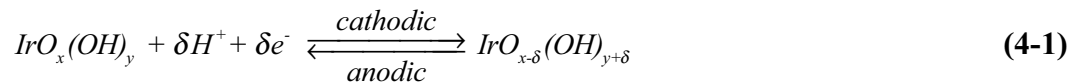


Figure 4-6: Gravimetric voltammetric charges Q (C/gIrO₂) obtained from Figure 4-4 for two potential windows and plotted versus scan rate: (a) between -0.05 and 1.4 V and (b) between 0.25 and 0.95 V. Electrolyte: 1M HClO₄, T = 22°C

CHAPITRE 4: Surface redox activities and charging/discharging process on p-Si/IrO₂ electrodes

Both figures show a fast initial decrease of the gravimetric voltammetric charge at low scan rates followed by a stabilization at high scan rates for all temperatures and potential windows investigated. Furthermore Figure 4-5 shows that the gravimetric voltammetric charge becomes temperature independent with increasing scan rates. The decrease of the charge with scan rate was explained via two main approaches already proposed in the literature.

The first approach proposed by Ardizzone et al.[10] is based on the accessibility to the active sites of the electrode. The decrease of the gravimetric voltammetric charge with scan rate has been explained by the exclusion of the inner parts of the electrode due to the slow diffusion of protons through the porous structure of the coating. The voltammetric charge has been attributed to the redox surface couples according to the Faradaic reaction (4-1).



The second approach was proposed by Sugimoto et al.[11]. This approach is based on the existence of two types of capacitances: The double layer capacitance (non-Faradaic fast process), which predominates at high scan rates and a redox surface capacitance (Faradaic slow surface process), which contributes only at low scan rates. The decrease of the voltammetric charge with scan rate is due to the slowness of the redox surface process, which is excluded at high scan rates.

In order to investigate the influence of temperature on the gravimetric voltammetric charge, the activation energy E_a (J mol⁻¹) of the charging process has been calculated for different scan rates using Arrhenius Equation (Eq. (4-2)).

$$Q = Ae^{-\frac{E_a}{RT}} \quad (4-2)$$

where A (C g⁻¹) is the pre-exponential factor, R is the ideal gas constant (J mol⁻¹ K⁻¹) and T is the temperature (K).

The resulting plot is presented on Figure 4-7.

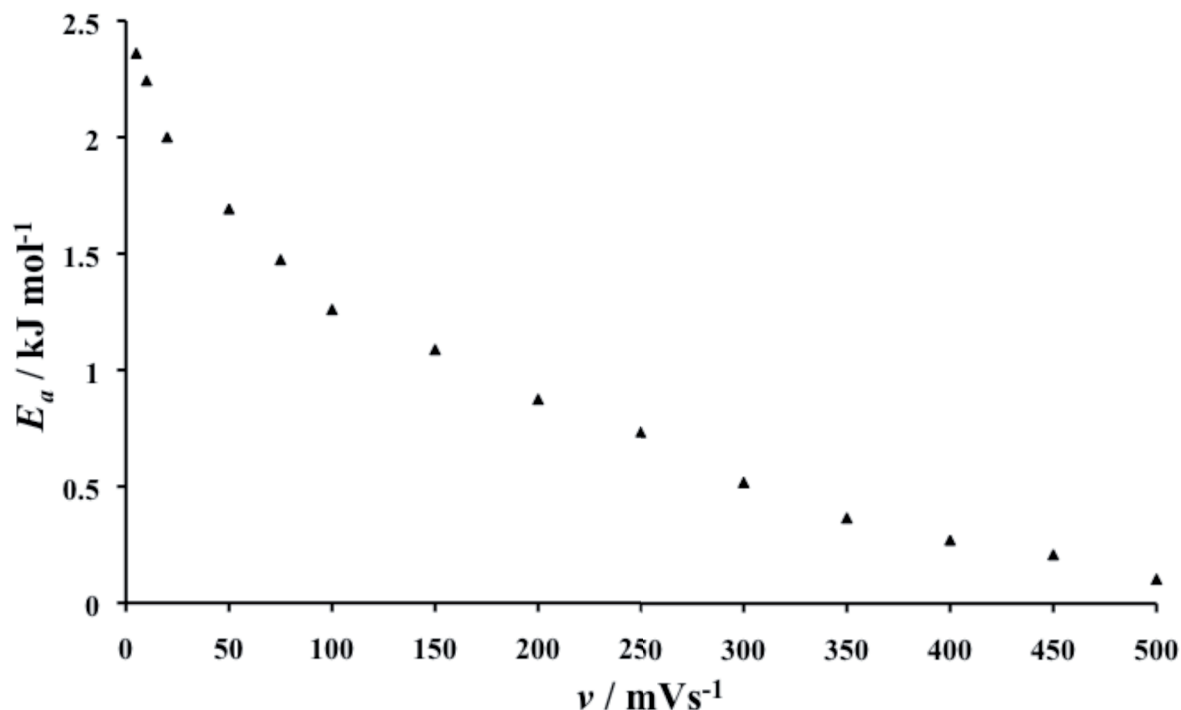


Figure 4-7: Apparent activation energy E_a of the charging/discharging process of p-Si/IrO₂ electrode (loading: 0.27 mg cm⁻²) as a function of scan rate. Electrolyte: 1M HClO₄.

This figure shows that E_a progressively decreases with increasing scan rate and ultimately tends toward zero at high scan rates (500mV s⁻¹).

From these results, we can hypothesize that two main contributions are involved in the voltammetric charge:

- A contribution related with a fast (instantaneous) process having an activation energy close to zero. This process dominates at high scan rates.
- A contribution related with a slow process with an activation energy of about 2.4 kJ mol⁻¹, which dominates at low scan rates.

In fact, the fast (instantaneous) contribution with zero activation energy corresponds probably to an electrostatic phenomenon, which is the charging of the electrical double layer (q_{dl}^*) at the electrode-electrolyte interface. The slow process with activation

CHAPITRE 4: Surface redox activities and charging/discharging process on p-Si/IrO₂ electrodes

energy of about 2.4kJ mol⁻¹ should correspond to a physical phenomenon, which is the diffusion of protons toward the active sites of the coating.

It is worthwhile to notice that q_{dl}^* can be used as a tool to estimate the relative surface area of the p-Si/IrO₂ electrodes.

In fact and as demonstrated in the previous chapter (section 3.3.1), not only the voltammetric charge decreases with the scan rate but it also increases with the loading (Figure 4-8).

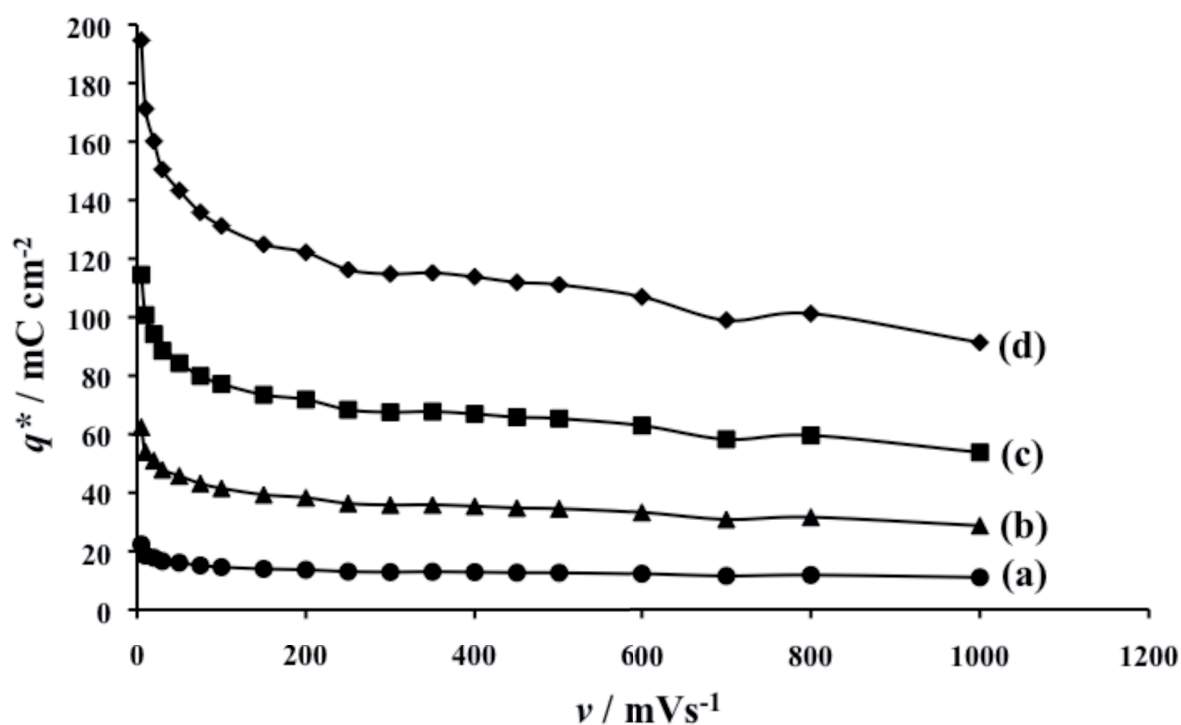


Figure 4-8: Variation of the voltammetric charge density q^* with scan rate on p-Si/IrO₂ electrodes with different IrO₂ loadings: (a) 0.35 mg cm⁻², (b) 0.87 mg cm⁻², (c) 1.75 mg cm⁻² and (d) 3.5 mg cm⁻² obtained in 1M HClO₄ at 22°C

Based on the above findings on the charging process, very high scan rates should be used for the cyclic voltammetry measurements to estimate q_{dl}^* , which is unpractical.

However, as proposed by S. Ardizzone [10], q_{dl}^* can also be obtained using the following analytical relationship Eq.(4-3).

$$q^* = q_{dl}^* + const \left(\frac{1}{v^{1/2}} \right) \quad (4-3)$$

The above equation implies that plotting q^* as a function of $v^{-1/2}$ should give straight lines; the intercepts of these straight lines with the $v^{-1/2}$ axis gives the value of q_{dl}^* for the different IrO₂ loadings investigated herein (Figure 4-9).

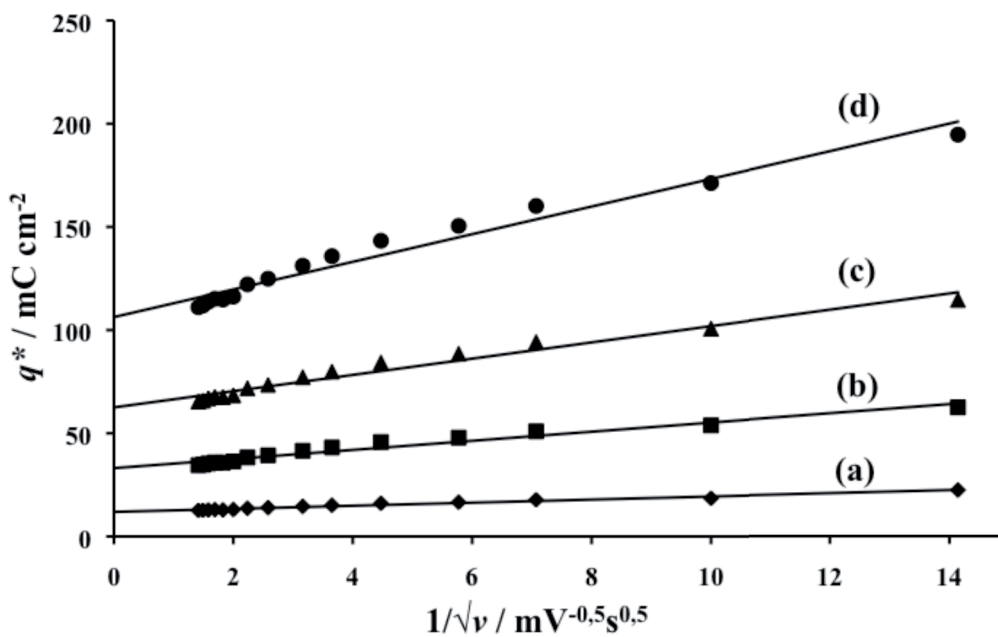


Figure 4-9: Voltammetric charge density reported as a function of $v^{-1/2}$ for the determination of q_{dl}^* by extrapolation of the straight lines to $v^{-1/2}=0$. Potential window between -0.05 and 1.35 V. Electrolyte: 1M HClO₄. T = 22°C. Conditions: idem Figure 4-8.

The variation of the values obtained for q_{dl}^* with the IrO₂ loading is given in Figure 4-10.

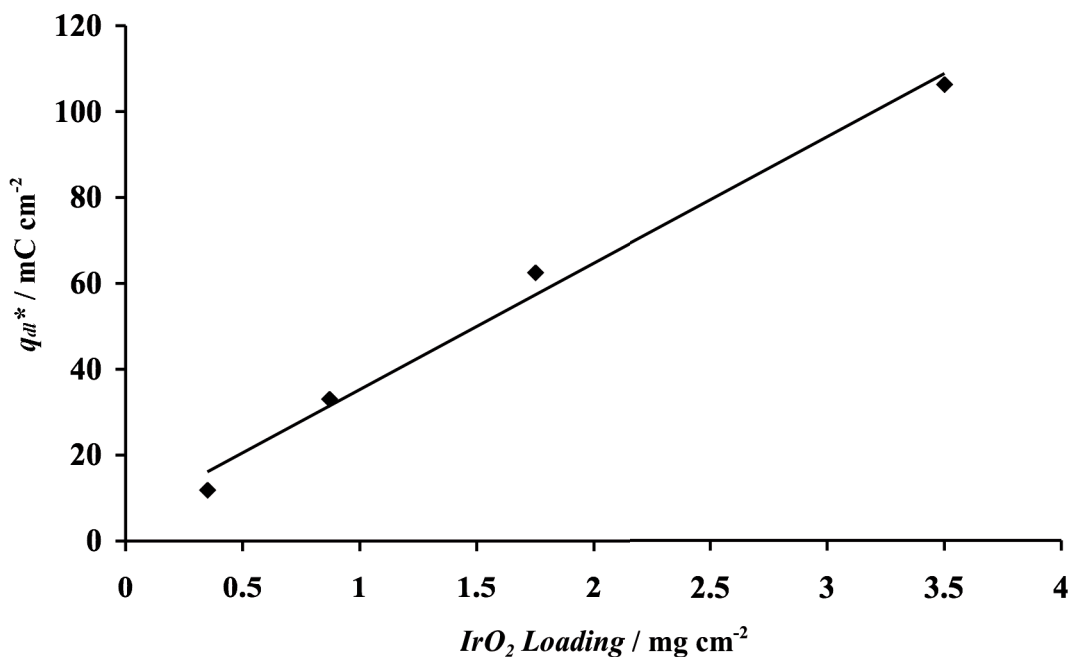


Figure 4-10: plot of q_{dl}^* as a function of IrO₂ loading. Conditions identical as given in Figure 4-9

The direct proportionality between q_{dl}^* and the IrO₂ loading demonstrates the utility of using q_{dl}^* as a mean for the estimation of the relative surface area of an IrO₂ coating and for the estimation of the loading from the voltammetric charge (~30mC/mgIrO₂) in agreement with previous studies [13].

4.3.2 Surface redox activities of p-Si/IrO₂ electrodes

Open circuit potential

The open circuit potential (OCP) of p-Si/IrO₂ electrodes in de-aerated solution was measured as a function of pH (Figure 4-11).

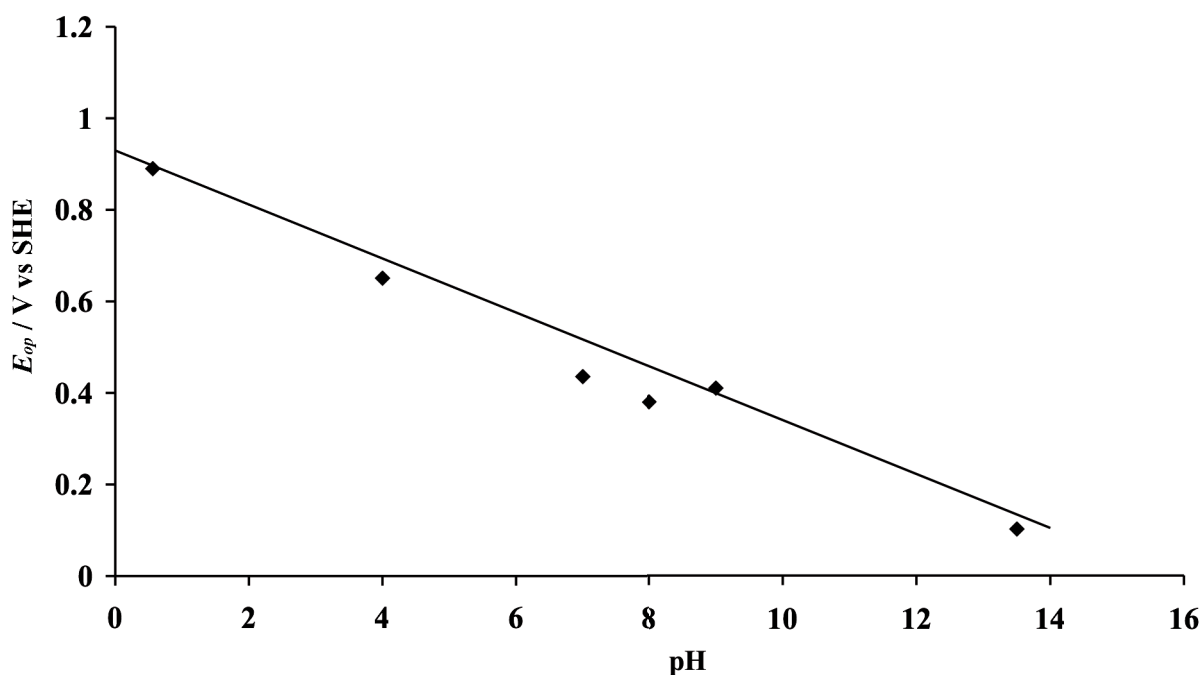
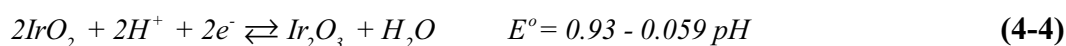


Figure 4-11: Open circuit potential (OCP) measured on p-Si/IrO₂ as a function of pH; T=25°C.

The values obtained in this experiment are in good agreement with the ones predicted by the corresponding Pourbaix diagram, which makes use of the following equilibrium reaction (Eq.(4-4)) [14].



This is an indication that, at the open circuit potential, p-Si/IrO₂ electrodes in de-aerated solution are essentially in the Ir(IV)/Ir(III) state, in agreement with estimations from many previous studies [15].

Cyclic voltammetry measurements on p-Si/IrO₂

Figure 4-12 shows cyclic voltammetry (CV) measurements performed at different scan rates on a p-Si/IrO₂ electrode.

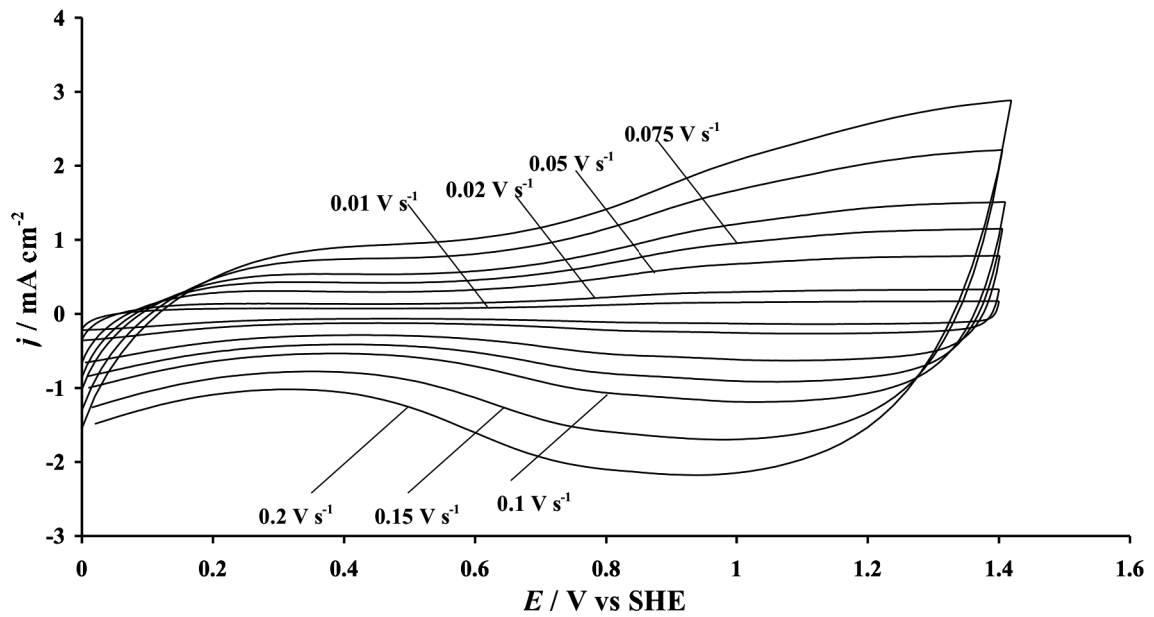


Figure 4-12: Cyclic voltammograms at different scan rates obtained on p-Si/IrO₂ in 1M HClO₄; T=25°C.

From these CV measurements, the current density (j) at a given potential has been plotted as a function of scan rate (ν) (Figure 4-13).

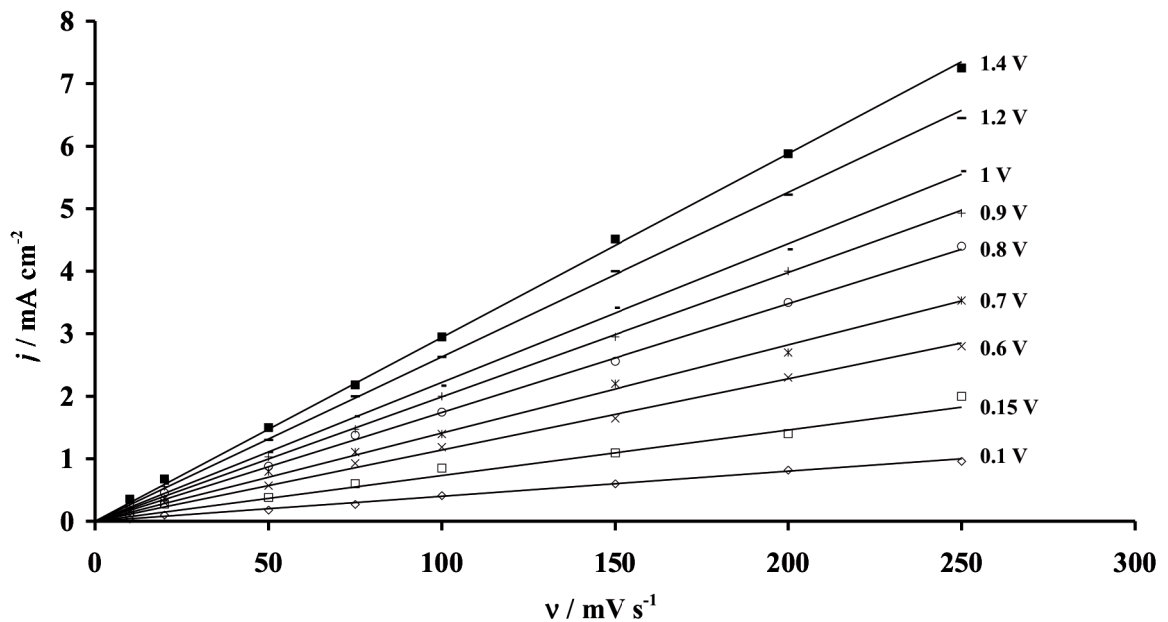


Figure 4-13: Current densities at different potentials on p-Si/IrO₂ obtained from the CV curves of Figure 4-12 plotted as a function of scan rate; T=25°C. Potentials given with respect to the SHE.

From the slopes of the straight lines given in Figure 4-13 the 'apparent capacitance' (C_{app}) can be determined as a function of applied potential using equation (4-5). The values obtained are reported in Figure 4-17:

$$j = C_{app} \cdot v \quad (4-5)$$

Figure 4-14 shows the chronoamperometric experiments realized on p-Si/IrO₂ for different potential steps included in the water stability potential domain.

Figure 4-15 shows $j \cdot t^{-1/2}$ plots obtained on p-Si/IrO₂ for $t > 1.5$ s (in order to avoid issues related with the charging of the double layer).

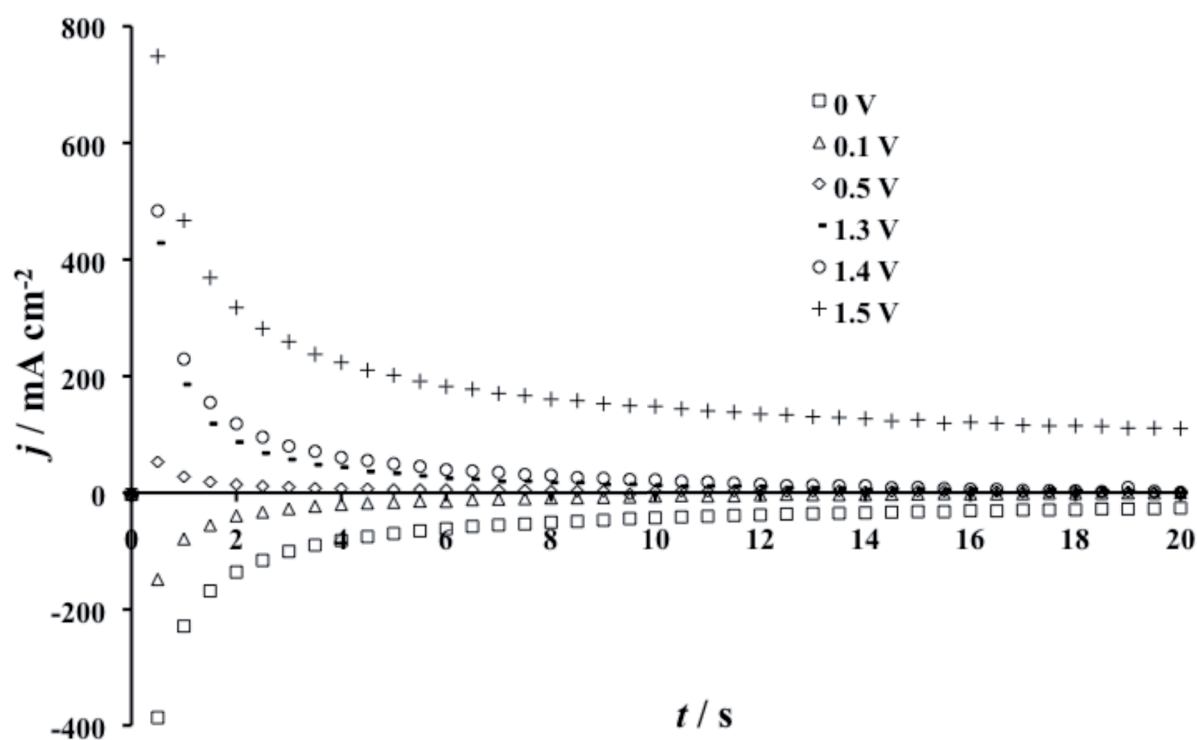


Figure 4-14: Chronoamperometric measurements at different applied potentials obtained on p-Si/IrO₂ in 1M HClO₄. T = 25°C. Potentials given with respect to the SHE.

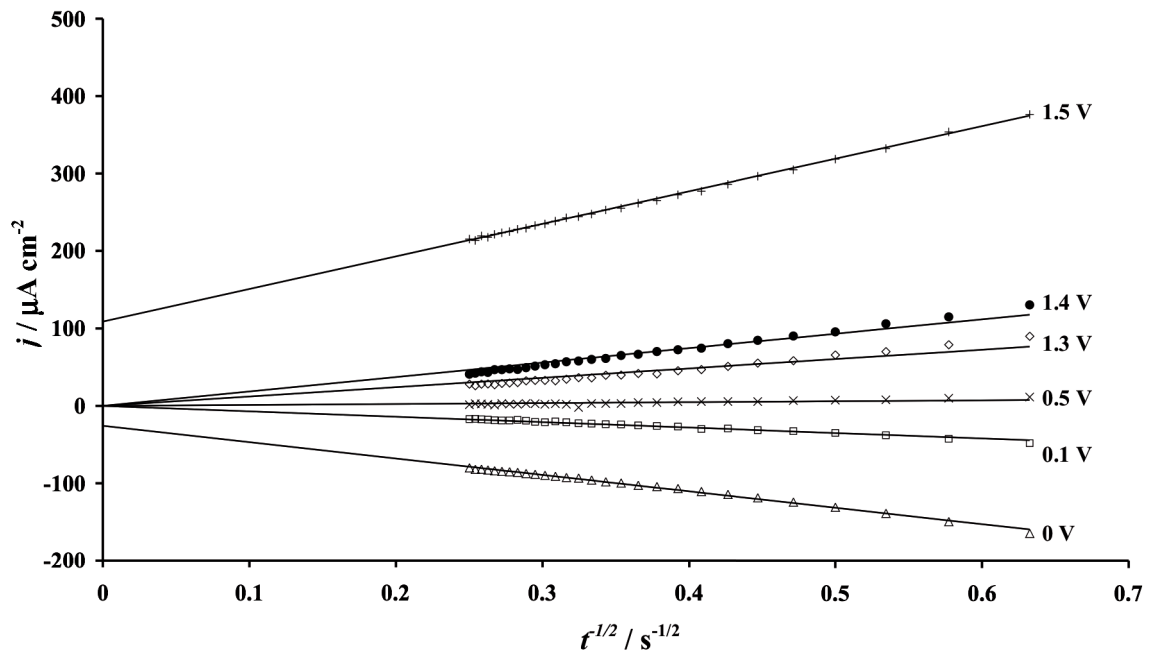


Figure 4-15: $j - t^{1/2}$ curves obtained from the chronoamperometric measurements for p-Si/IrO₂ in 1M HClO₄ presented in Figure 4-14 at different applied potentials; T=25°C. Potentials given with respect to the SHE.

The linearity of these plots indicates that semi-infinite linear diffusion is involved in the discharging process. It is worthwhile to notice that the straight lines corresponding to potentials situated in the vicinity of the hydrogen (0 V) and the oxygen (1,4 V) evolution reactions do not cross the origin due to the background current related to those reactions.

In order to explain this behaviour, a model has been proposed according to which the current decay observed during the potential step experiments is due to redox activities of the coating in which protons diffusion is the rate determining step (Eq.(4-1)) [12,16].

Under these conditions, Cottrell's equation can be applied (Eq.(4-6)):

$$i = \frac{z \cdot F \cdot A \cdot \Delta C \cdot D^{1/2}}{\pi^{1/2} \cdot t^{1/2}} \quad (4-6)$$

Where i is the current (A), z is the number of exchanged electrons, F is the Faraday constant (96485 C mol⁻¹), A is the electrode's geometric surface area (m²), D is the diffusion coefficient of protons within the coating (m² s⁻¹), t is the time (s) and ΔC is

the concentration change of protons (mol m⁻³) generated by the applied potential step.

The integral form of Cottrell's equation from $t=0$ s to a given time t gives the total (cumulative) charge (q_t) that passed during a given potential step experiment as a function of time (Eq.(4-7)):

$$q_t = \int_0^t i dt = \frac{2 \cdot z \cdot F \cdot A \cdot \Delta C \cdot D^{1/2}}{\pi^{1/2}} t^{1/2} \quad (4-7)$$

This new equation (Eq.(4-7)) predicts a proportionality between q_t and $t^{1/2}$.

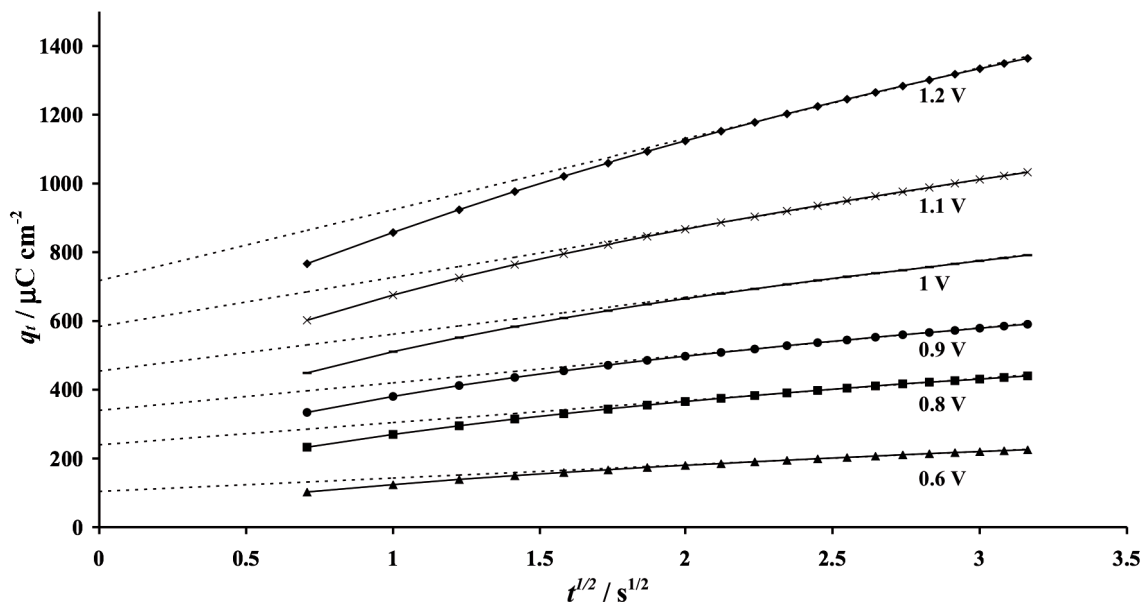


Figure 4-16: Total charge q_t (Eq.(4-7)) as a function of $t^{1/2}$ obtained in 1M HClO₄ on p-Si/IrO₂ from chronocoulometric measurements performed at different applied potentials; T= 25°C. Potentials given with respect to the SHE.

The results presented on Figure 4-16 show that this is indeed the case, however the straight lines obtained with this relationship do not cross the origin. The extrapolation of these lines to $t=0$ s for each applied potential yields to the corresponding surface charge q_s as demonstrated by K.Doblhofer and al.[12]. This charge is certainly related to the surface iridium atoms, which are the most accessible to the electrolyte, Γ_o (mol cm⁻²).

The amount of these surface atoms can be estimated from the following relation (Eq.(4-8)).

$$\Gamma_o = \frac{q_s}{zFA} \quad (4-8)$$

This surface charge q_s can be included in the integral form of Cottrell's equation (Eq.(4-9)):

$$q_t = \frac{2 \cdot z \cdot F \cdot A \cdot \Delta C \cdot D^{1/2}}{\pi^{1/2}} t^{1/2} + q_s \quad (4-9)$$

Figure 4-17 shows the total surface charge obtained by extrapolation of the $q_t \cdot t^{1/2}$ plots given in Figure 4-16 to $t=0$ s together with the apparent capacitance C_{app} obtained from the slopes of the straight lines given in Figure 4-13 as a function of potential for p-Si/IrO₂ electrode. It is worthwhile to notice that the values of q_s for potentials involving oxygen or hydrogen evolution have been estimated by subtracting the charge related to these reactions from the total charge.

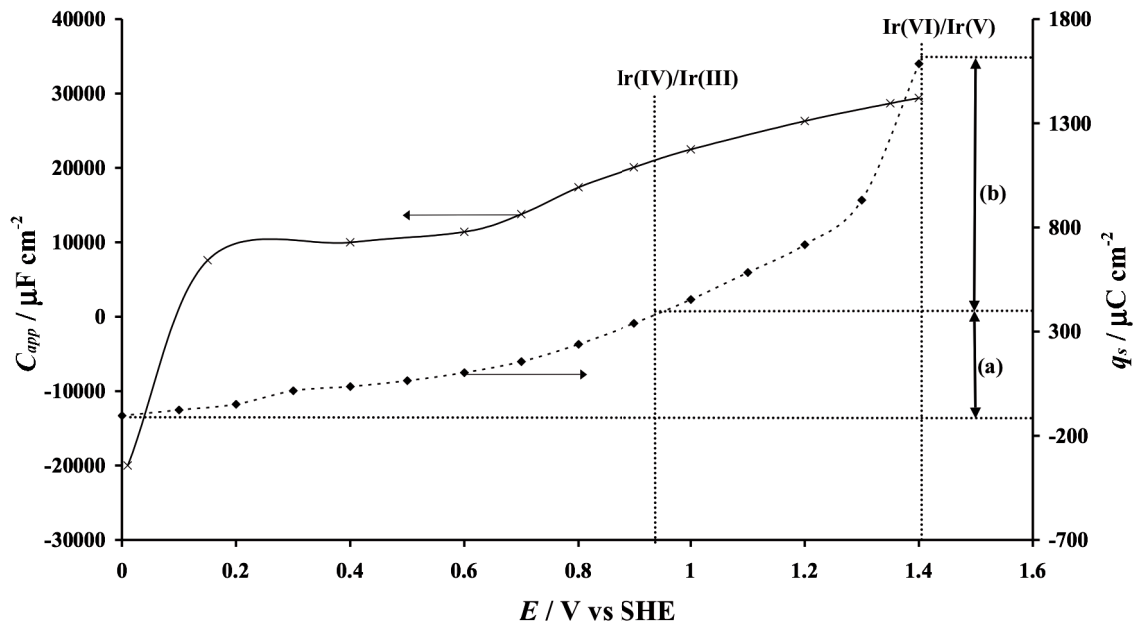


Figure 4-17: (♦) Surface charges- potential plots (q_s - E , right axis), obtained from the $q_t \cdot t^{1/2}$ plots (Figure 4-16) by extrapolation to $t=0$ (Eq.(4-9)). (x) Apparent capacitance - potential plots (C_{app} - E , left axis) obtained from the slope of the j - v plots (Figure 4-13) using Eq.(4-5). Conditions: Idem Figure 4-16.

Proposed surface reactions for p-Si/IrO₂ electrodes

As there is no capacitance maximum, the charge passed between the open circuit potential OCP (0.93 V), at which the Ir is in the Ir(IV)/Ir(III) state, and the onset potential of the oxygen evolution reaction OER (1.4 V), at which the Ir is in the Ir(VI)/Ir(V) state [17], has been taken as a reference. In fact approximately 1200 mC cm⁻² are passed between the OCP (Ir(IV)/Ir(III) state) at 0.9 V and the onset potential of OER (Ir(VI)/Ir(V) state) at 1.4 V (interval (b) in Figure 4-17). In other words, the charge needed for a one-electron exchange of the surface Ir atoms is 1200/2 = 600 mC cm⁻² (geometric surface area).

Using the value of 600 mC cm⁻² for 1e⁻ change of the surface Ir atoms, it is possible to derive the surface oxidation state of the p-Si/IrO₂ electrode at the onset potential of the hydrogen evolution reaction HER. In fact the charge q_s passed between the OCP and the onset potentials of HER (0 V) is about 480 mC cm⁻² (interval (a) in Figure 4-17). This is not enough charge for another 1e⁻ change of all the surface Ir atoms, therefore these results are a proof that the surface remains mainly in the Ir(IV)/Ir(III) state (even at potentials close to the HER).

4.4 Conclusions

In this chapter, the electrochemical activity of p-Si/IrO₂ electrodes within the water stability potential domain has been studied. The main findings are:

The apparent activation energy (E_a) measured for the charging/discharging process depends strongly on the scan rate used for the cyclic voltammetry measurements. In fact, at low scan rates (5 mV s⁻¹), E_a for the charging/discharging process has a value of about 2.4 kJ mol⁻¹ and at high scan rates (500 mV s⁻¹), E_a reaches values close to zero. This has allowed to consider two contributions in the charging/discharging process of the p-Si/IrO₂ electrode. The first contribution corresponds to a fast (instantaneous) process with zero activation energy, which is the charging of the electrical double layer at the electrode-electrolyte interface. The second contribution is related with the slow diffusion of protons within the IrO₂ coating with an activation energy of about 2.4 kJ mol⁻¹.

Furthermore, the measured surface charges corresponding to the surface redox activities of p-Si/IrO₂ electrodes show clearly that the oxidation state of the surface iridium atoms varies from +IV to +VI in the potential domain between the on-set potentials of H₂ and O₂ evolution (from 0 V to 1.5 V).

4.5 References

- [1] Y. Kiros, M. Pirjamali, M. Bursell, *Electrochim. Acta*, 51 (2006) 3346
- [2] N. Furuya, H. Aikawa, *Electrochim. Acta*, 45 (2000) 4251
- [3] S. Trasatti, W.E. O'Grady, in: H. Gerisher, C.W. Tobias (Eds.), *Advances in Electrochemistry and Electrochemical Engineering*, John Wiley and Sons, New York, USA, 1981, p. 177
- [4] J.E. Bennett, *Int. J. Hydrogen Energy*, 5 (1980) 401
- [5] Ch. Comninellis, G. Foti, D. Gandini, *Curr. Top. Electrochem.*, 5 (1997) 1
- [6] J. Rolewicz, Ch. Comninellis, E. Plattner, J. Hinden, *Electrochim. Acta*, 33 (1988) 573
- [7] J.-P. Gueneau de Mussy, J.V. Macpherson, J.-L. Delplancke, *Electrochim. Acta*, 48 (2003) 1131
- [8] S. Fierro, T. Nagel, H. Baltruschat, Ch. Comninellis, *Electrochem. Commun.*, 9 (2007) 1969
- [9] C. Angelinetta, S. Trasatti, L.D. Atanososka, R.T. Atanasoski, *J. Electroanal. Chem.*, 214 (1986) 535
- [10] S. Ardizzone, G. Fregonara, S. Trasatti, *Electrochim. Acta* 35 (1990) 263.
- [11] W. Sugimoto, T. Kizaki, K. Yokoshima, Y. Murakami, Y. Takasu, *Electrochim Acta*, 49 (2004) 313
- [12] K. Doblhofer, M. Metikos, Z. Ogumi, H. Gerischer, *Ber. Bunsenges. Phys. Chem.*, 82 (1978) 1046
- [13] E.Herrera Calderon, PhD Thesis, Swiss Institute of Technology (EPFL), No 4181, 2008

- [14] M. Pourbaix, Atlas d'Equilibres Electrochimiques, Gauthier-Villars et G., Paris 1963
- [15] S. Trasatti, in Studies in Physical and Theoretical Chemistry: Electrodes of Conductive Metal Oxides Part A, S. Trasatti, Editors, Elsevier Scientific Publishing Company: Amsterdam. (1980) 155
- [16] S. Fierro, L. Ouattara, E. Herrera Calderon, Ch. Comninellis, Electrochem. Comm., 10 (2008) 955
- [17] L.M. Da Silva, M. Leoneardo, V. Franco, V. Debora, L.A. Faria, J.F.C. Boodts, Electrochim. Acta, 49 (2004) 3977

Chapter 5 : Active intermediates involved in the oxygen evolution reaction (OER) on IrO₂ electrodes: Voltammetric and DEMS study

In this chapter, the surface redox activities involved in the oxygen evolution (OER) reaction in acidic aqueous media are investigated for IrO₂ electrodes.

This was performed using ¹⁸O labeling together with differential electrochemical mass spectrometry (DEMS) measurements. DEMS is a powerful technique, where ionic currents corresponding to the formation of given volatile species are recorded in parallel to the faradaic current during a cyclic voltammetry measurement.

The DEMS measurements have shown, that during successive cyclic voltammetric measurements in H₂¹⁸O containing electrolyte the amount of ¹⁶O₂ ($m/z=32$) decreases, with a concomitant increase of ¹⁸O¹⁶O ($m/z=34$) with each successive cycle before reaching a steady state after four cycles. The ¹⁶O₂ concentration in the evolved oxygen obtained is higher during the first scans because ¹⁶O from the IrO₂ coating contributes in the oxygen evolution reaction.

Analysis of the experimental data has shown that the amount of lattice oxygen, which is involved in the oxygen exchange reaction, is in the order of 1% of the total IrO₂ loading. This is an indication that only the outer surface of the oxide electrode participates in the OER. Similar results have been obtained for higher IrO₂ loadings.

In a second series of experiments, it has been demonstrated that oxygen evolution on IrO₂ marked with ¹⁸O in regular water results in an isotope exchange reaction, which forms Ir¹⁶O₂ and marked oxygen (¹⁸O¹⁶O) thus proving again that the IrO₂ coating participates actively in the OER.

Consequently, we can conclude that the IrO₂ layers of the electrode participate in the OER in acidic media to an extent of several monolayers at least. This mechanism was confirmed from Tafel slope measurements for the OER on IrO₂ electrodes.

This chapter is based on the publications:

S. Fierro, T. Nagel, H. Baltruschat, Ch. Comninellis. Investigation of the oxygen evolution reaction on Ti/IrO₂ electrodes using isotope labelling and online mass spectrometry, *Electrochemistry Communications*, Volume 9, Issue 8, May 2007, pages 1969-1974

L.Ouattara, S. Fierro, O. Frey, M. Koudelka, Ch. Comninellis. Electrochemical comparison between IrO₂ prepared by anodic oxidation of pure iridium and IrO₂ prepared by thermal decomposition of H₂IrCl₆ precursor solution, *Journal of Applied Electrochemistry*, Volume 39, February 2009, pages 1361-1367

5.1 Introduction

Oxygen evolution is one of the most important technological reactions in electrochemistry taking place at many industrial processes namely water electrolysis, metal electro-winning and cathodic protection. IrO₂ electrodes are among the most frequently used for the oxygen evolution reaction (OER) in acidic media [1].

Despite the large number of existing publications for these electrodes, the mechanism of oxygen evolution on these anodes is still an area of active debate.

CHAPITRE 5: Active intermediates involved in the oxygen evolution reaction (OER) on IrO₂ electrodes: Voltammetric and DEMS study

During the last decade, a generalized phenomenological model has been proposed for the oxygen evolution reaction in acidic media [2-4]. This model is shown in Figure 2-3 of the bibliography (Chapter 2, section 2.3) and can be adapted to IrO₂-based electrodes, where IrO₂ becomes the active site M from Figure 2-3. The mechanism is composed of two steps.

The first step is the discharge of water molecules at the electrode's surface to form hydroxyl radicals (Eq.(5-1)).



In the second step, the chemisorbed hydroxyl radicals interact with the electrode surface forming the higher oxide (Eq.(5-2)).



The final step is the decomposition of the higher oxide to yield the lower oxidation state oxide and oxygen (Eq.(5-3)).



Oxides for which a higher oxidation state is available close to the thermodynamic potential of oxygen evolution (1.23 V vs. SHE in acid media) are excellent candidates for the electrocatalytic evolution of O₂.

This mechanism in which the oxide participates in the oxygen evolution reaction has been also reported by others [5,6]. However there are only a few direct experimental evidences, which support this mechanism. In fact, only the work of Wohlfahrt-Mehrens [7] has demonstrated, using DEMS measurements that the RuO₂ layers participate in the oxygen evolution process. To the author's knowledge, there are no such measurements for IrO₂ electrodes in the literature up to date.

In order to prove the participation of the IrO₂ coating in the oxygen evolution reaction, differential electrochemical mass spectrometry (DEMS) measurements in a thin layer flow cell have been carried out using marked water (H₂¹⁸O). During the measurements, cyclovoltammograms (CV) were recorded together with the ionic currents from the mass spectrometer responses for ions for which $m/z=32$, 34 and 36 (corresponding to ¹⁶O¹⁶O, ¹⁶O¹⁸O and ¹⁸O¹⁸O molecules). Finally, in order to confirm the mechanism of the OER on IrO₂ electrodes, polarization curves have been performed in order to estimate the corresponding Tafel slope.

5.2 Experimental details

5.2.1 Differential electrochemical mass spectrometry (DEMS)

The DEMS measurements are conducted in two separate compartments: the electrochemical compartment with the electrolyte inlet, where the faradaic reactions take place, and the mass spectrometric compartment with the electrolyte outlet, where the ion detection takes place. In a typical DEMS experiment, the ion current corresponding to the formation of a given volatile specie is recorded in parallel to the faradaic current during the voltammetric sweep.

Because the Ti/IrO₂ electrode is prepared by thermal decomposition, deposition on the Teflon membrane as in [8] was not possible. Instead a thin layer flow through cell [9], which is schematized in Figure 5-1, was used:

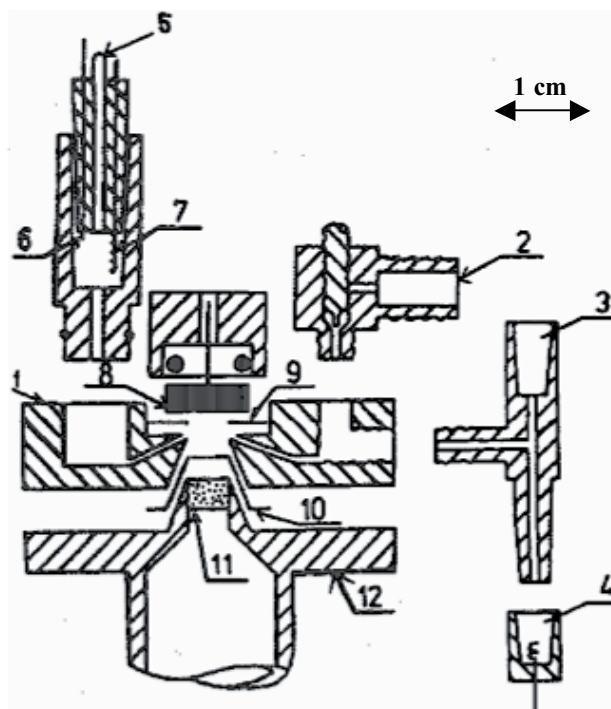


Figure 5-1: Thin layer cell: (1) cell body made from titanium, (2) connection to electrolyte supply, (3) T-connection, (4) counter electrode, (5) electrolyte outlet, (6) capillary to reference electrode, (7) second counter electrode, (8) Ti/IrO₂, (9) Teflon spacer, 50 – 100 μm thickness; inner diameter 6mm, (10) micro-porous Teflon foil, interface between electrochemical cell and vacuum, (11) steel frit, (12) stainless steel support [9]

The cell is connected to a quadrupole mass spectrometer (Pfeiffer Vacuum QMG 422). The electrolyte volume and the geometric surface area (0.28 cm²) of the working electrode are defined by a thin (50-100 μm) porous Teflon ring placed on the disc-shaped electrode.

The Ti/IrO₂ working electrodes (two different loadings: 0.64mg cm⁻² (2840 nMol cm⁻²) and 5.25mg cm⁻² (23280 nMol cm⁻²)) were prepared by thermal decomposition at 500°C of a precursor aqueous solution of H₂IrCl₆ (99.9%, ABCR) deposited on disc-shaped titanium supports (0.64 cm²), which were previously sandblasted and then treated in boiling 1 M oxalic acid (≥97%, Fluka) solution for 1 hour. All solutions were deaerated with argon during measurements.

The reference electrode used for the DEMS experiments was a standard hydrogen electrode (SHE) so the potentials in this chapter are given with respect to this electrode. Two Au wires were used as counter electrodes.

The electrolyte used was 1M HClO₄ prepared from HClO₄ (ultrapure from Merck), millipore water and marked water (H₂O¹⁸, 66-70%, Cambridge Isotope Laboratories). The solutions were ventilated with argon (5.0 from Praxair). All measurements were conducted at room temperature and with flowing electrolyte (5 μl s⁻¹).

Selected values of *m/z* ions signals (*m/z* = 32, 34 and 36) are measured as ionic currents allowing the simultaneous recording of the faradaic current versus electrode potential (CV) and the selected ionic currents versus electrode potential (MSCV).

5.2.2 Voltammetric experiments

All the voltammetric experiments presented in this chapter were performed in a classical three-electrode cell (70 ml) using an Autolab PGSTAT 30. The counter electrode was a Pt wire; the reference electrode was Hg/Hg₂SO₄/K₂SO₄ (sat.) (MSE; 0,65 V vs. SHE) and the working electrodes was an IrO₂ electrode prepared by thermal decomposition of a precursor: the IrO₂ film (0,27 mg cm⁻²) was deposited on square-shaped sandblasted p-Si (100 mm²) by the thermal decomposition of a H₂IrCl₆ (99,9%, ABCR) precursor aqueous solution in air at 500°C.

The cell and materials used for the cyclic voltammetry experiments on IrO₂ electrodes are identical to the set-up used for the measurements presented in the previous chapter (Figure 3-1 in section 3.2).

All potentials given in this chapter are with respect to the standard hydrogen electrode (SHE).

5.2.3 Ohmic drop correction

The ohmic drop correction of polarization curves has been performed according to the method given in the literature [10-12]. The overpotential η (V) observed during an experiment is given by equation (5-4):

$$\eta = a + b \ln j + jR \quad (5-4)$$

where a (V) is the Tafel constant, b (V dec⁻¹) is the Tafel slope, j (A cm⁻²) is the current density and R (Ω cm⁻²) is the total area-specific uncompensated resistance of the system, which is assumed to be constant. The derivative of Eq. (5-4) with respect to current density gives Eq. (5-5) from which b and R can be easily obtained by plotting $d\eta/dj$ as a function of $1/j$.

$$\frac{d\eta}{dj} = \frac{b}{j} + R \quad (5-5)$$

The estimation of R allows correcting the experimental overpotential by subtracting the ohmic drop jR according to equation (5-6):

$$\eta_{corr} = \eta - jR \quad (5-6)$$

During the calculations, the derivative $d\eta/dj$ was replaced by their finite elements $\Delta\eta/\Delta j$ estimated from each pair of consecutive experimental points.

5.3 Results and discussion

5.3.1 DEMS measurements

In order to determine to what extent the iridium dioxide coating participates in the oxygen evolution reaction, two series of experiments (series A and B) have been carried out.

Series A: In the first series of experiments, the DEMS cell containing the Ti/IrO₂ (2840 nMol IrO₂/cm²) electrode was filled with a 1 M HClO₄ solution containing 10% (w/w) of marked water (H₂¹⁸O); then, several successive cyclic scans (10 mV s⁻¹) were applied between 0 and 1.6 V. The faradaic current obtained from the cyclovoltammetric

CHAPITRE 5: Active intermediates involved in the oxygen evolution reaction (OER) on IrO₂ electrodes: Voltammetric and DEMS study

measurements (CV) together with the ionic currents obtained from the mass spectrometer responses for ions with $m/z = 32, 34$ and 36 (corresponding to $^{16}\text{O}^{16}\text{O}$, $^{16}\text{O}^{18}\text{O}$ and $^{18}\text{O}^{18}\text{O}$ molecules) were recorded during several successive potential scans.

Figure 5-2 shows a typical example of ionic and faradaic currents obtained during the first cyclic scan. From the ionic currents, we note that mainly $^{16}\text{O}_2$, $^{16}\text{O}^{18}\text{O}$ are formed together with a small amount of $^{18}\text{O}_2$.

The CV shows (A on Figure 5-2) that the onset potential of oxygen evolution reaction is about 1.5 V, which is identical to the onset potential obtained from the ionic currents. The hysteresis observed in the cathodic sweep is due to the slow diffusion through the thin layer of electrolyte.

Concerning the cyclovoltammogram, the current observed at low potentials (<1.4 V) is not related to oxygen evolution (no ionic current is measured in this potential region) but to the reversible oxidation (forward scan)-reduction (reverse scan) of the surface through a mechanism involving protons exchanges with the solution according to the reaction proposed in section 4.3.1 (Eq.(4-1)).

Figure 5-3 shows the gas phase concentrations of $^{16}\text{O}_2$ and $^{16}\text{O}^{18}\text{O}$ measured during the five successive scans as well as those predicted from the concentration of marked water (H_2^{18}O) in the electrolyte.

CHAPITRE 5: Active intermediates involved in the oxygen evolution reaction (OER) on IrO₂ electrodes: Voltammetric and DEMS study

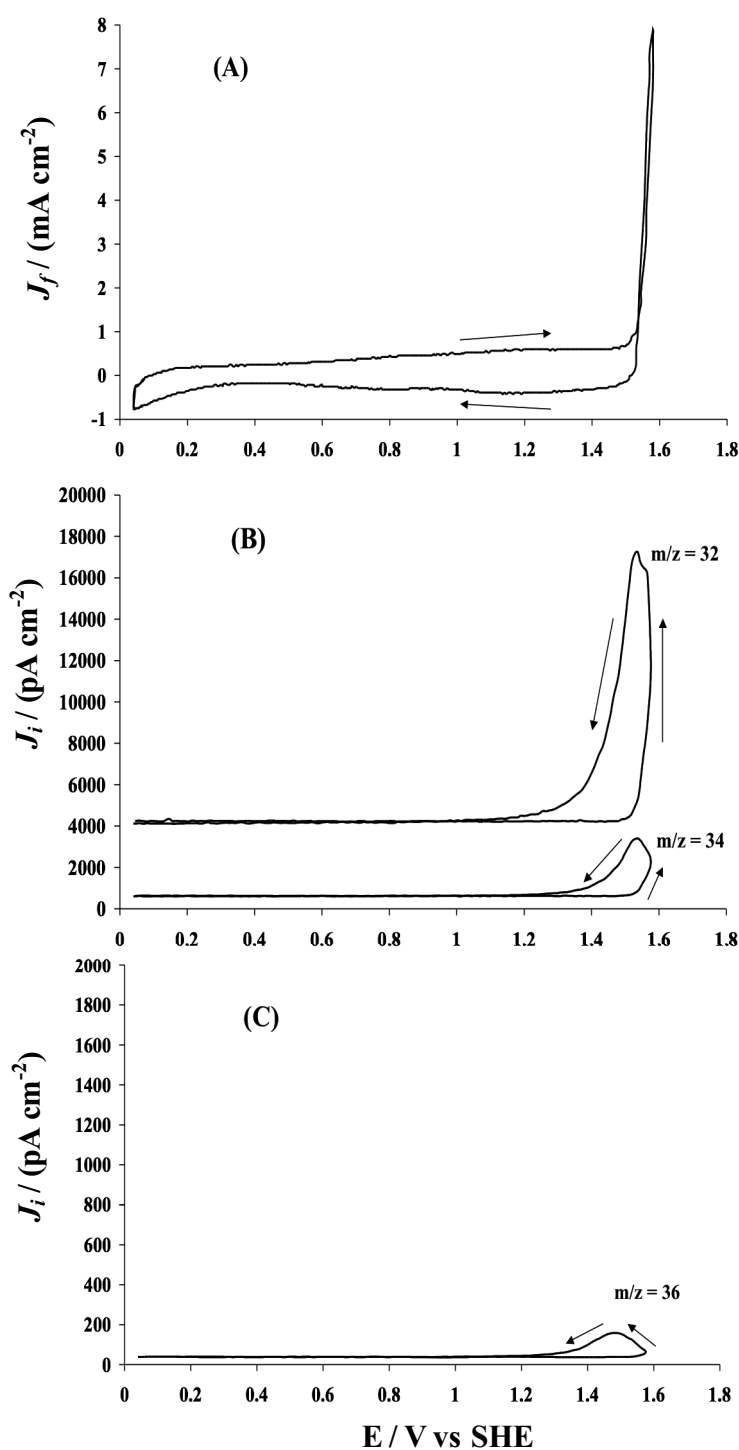


Figure 5-2: DEMS measurements using Ir¹⁶O₂ (2840 nMol/cm²) in 1 M HClO₄ solution containing 10% (w/w) of marked water (H₂¹⁸O), Potential scan rate: 10 mV s⁻¹, T: 25°C. (A) shows the Faradaic current density (J_f) obtained from the cyclic voltammetric measurements, (B) shows the ionic current densities (J_i) obtained from the mass spectrometer responses for ions with $m/z = 32$ (¹⁶O₂), 34 (¹⁸O¹⁶O) and (C) shows the ionic current density (J_i) obtained from the mass spectrometer response for ion with $m/z = 36$ (¹⁸O₂)

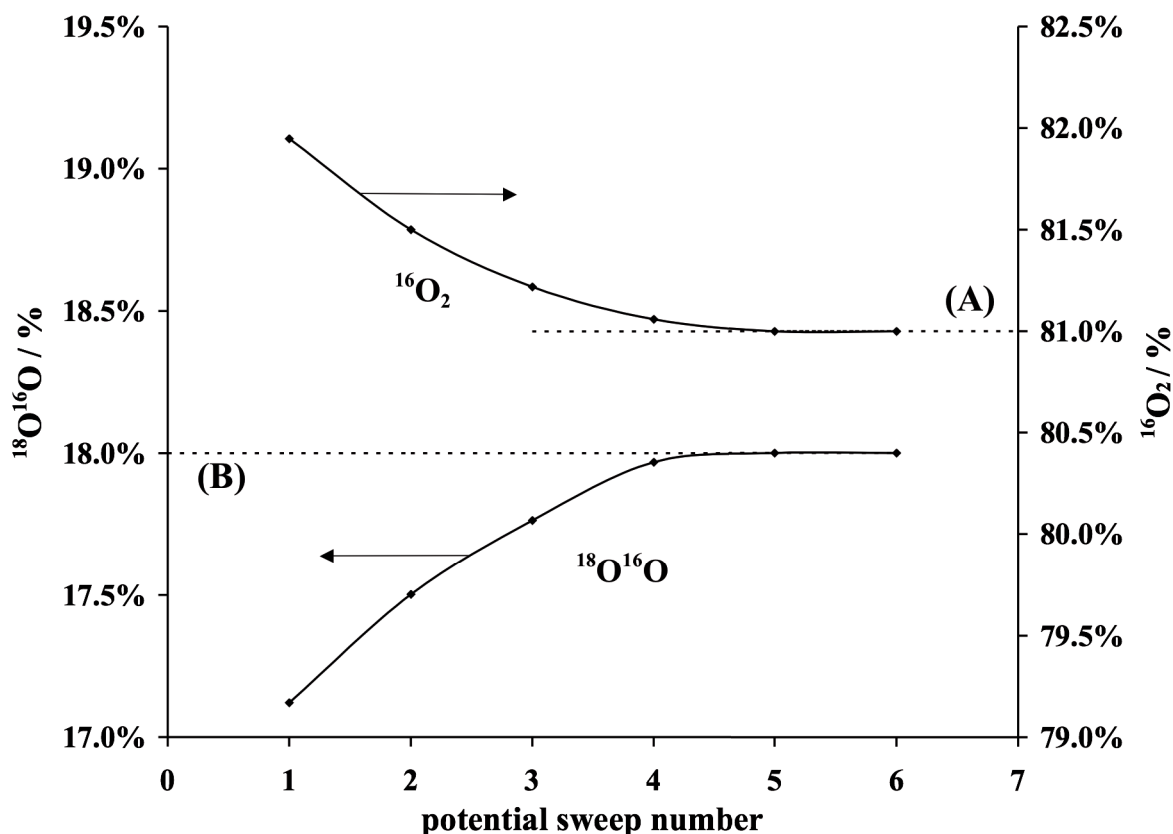
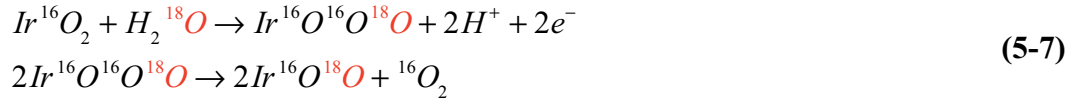


Figure 5-3: DEMS measurements for oxygen evolution on Ir¹⁶O₂ (2840 nMol/cm²) in 1 M HClO₄ solution containing 10% (w/w) of marked water (H₂¹⁸O). Potential scan rate: 10 mV s⁻¹, T: 25°C. Evolution of ¹⁶O₂ and ¹⁸O¹⁶O concentrations with each consecutive potential scan. (A) and (B) are respectively the concentrations of ¹⁸O¹⁶O and ¹⁶O₂ predicted from the concentration of H₂¹⁸O in the electrolyte.

This figure shows clearly that the concentration of ¹⁶O₂ decreases, with a concomitant increase of ¹⁶O¹⁸O with each successive cycle before reaching a steady state (which corresponds to the predicted value) after four cycles. The flowing electrolyte conditions assure the constant value of the concentration of marked water in the cell; therefore, the increase of ¹⁶O¹⁸O (*m/z*=34) or/and the concomitant decrease of ¹⁶O₂ (*m/z*=32) with each successive scan proves directly that the oxide layer takes part in the O₂ evolution reaction.

CHAPITRE 5: Active intermediates involved in the oxygen evolution reaction (OER) on IrO₂ electrodes: Voltammetric and DEMS study

In fact, considering that the composition at the ionic current steady state (i.e. the composition obtained at the 5th scan) corresponds to the composition of the bulk electrolyte [81% ¹⁶O₂ ($m/z=32$) and 18% ¹⁶O¹⁸O ($m/z=34$)], the concentration of ¹⁶O₂ ($m/z=32$) obtained during the first scans is higher because ¹⁶O from the IrO₂ coating contributes in the oxygen evolution reaction (Eq.(5-7)).



Using Faraday's law, the amount of Mol (m) and the corresponding number (n) of ¹⁶O lattice oxygen atoms, which are transformed to ¹⁸O per unit of electrode geometric surface area for each scan until no further exchange is occurring (in our case the first three scans) can be calculated using the following relations (Eq. (5-8) and (5-9)).

$$m = \frac{1}{2} \cdot 10 \cdot \frac{\Delta Q_{34}}{\sum Q_i} \cdot \frac{Q_f}{zF} = \frac{1}{2} \cdot 10 \cdot \gamma \cdot \frac{Q_f}{zF} \quad (5-8)$$

$$n = N_A \cdot m \quad (5-9)$$

Where m is the number of Mol of ¹⁶O lattice oxygen atoms, which are exchanged to ¹⁸O per unit of electrode geometric surface area (Mol cm⁻²), n is the number of ¹⁶O lattice oxygen atoms, which are exchanged to ¹⁸O per unit of electrode geometric surface area (atoms cm⁻²), N_A is Avogadro's constant (6.022·10²³ atoms·mol⁻¹), ΔQ_{34} is the excess of ionic charge for each scan (with respect to the steady state value of the 5th scan) related to the formation of ¹⁶O¹⁸O and to the incorporation of ¹⁸O into the oxide lattice (pC cm⁻²).

$\Sigma Q_i = Q_{32} + Q_{34} + Q_{36}$ is the total ionic charge related with the formation of oxygen (¹⁶O₂ + ¹⁶O¹⁸O + ¹⁸O₂) (pC cm⁻²) and $\gamma = \frac{\Delta Q_{34}}{\sum Q_i}$ is the excess ratio (with respect to the

CHAPITRE 5: Active intermediates involved in the oxygen evolution reaction (OER) on IrO₂ electrodes: Voltammetric and DEMS study

steady state value of the 5th scan) related with the incorporation of ¹⁸O into the oxide lattice (-).

Finally, Q_f is the Faradaic charge related with the formation of oxygen (C cm⁻²), F is Faraday's constant (96485 C mol⁻¹) and z is the number of electrons involved in the oxygen evolution reaction ($z=2$).

In this formula, the factor of 1/2 originates from the fact that the concentration of ¹⁸O¹⁶O in dioxygen is two times higher than the atomic concentration of ¹⁸O referred to the total number of oxygen atoms. Concerning the factor 10, it originates from the fact that in our experiments, a concentration of 10% of H₂¹⁸O has been used and consequently, the effective number of exchanged atoms (which would have been obtained if we had used a concentration of 100% of H₂¹⁸O) is higher by a factor of 10.

For the experiment presented in Figure 5-3, the excess ratio (γ) of ¹⁶O¹⁸O for each scan has been calculated.

Furthermore, from the cyclovoltammetric measurements (Figure 5-2A), the faradaic charge density related to the oxygen evolution reaction can be estimated ($Q_f = 2.6 \times 10^7$ nC cm⁻²). From these values and using Eq. (5-9), the amount of ¹⁸O atoms formed at each scan can be calculated. The values obtained together with the total amount of ¹⁸O atoms formed during the three successive scans are given in Table 5-1.

Table 5-1: Estimation of the amount of ¹⁶O lattice oxygen atoms (m), which are transformed to ¹⁸O per unit of electrode geometrical surface area (atoms cm⁻²) for a Ti/IrO₂ electrode (loading: 2840 nMol cm⁻²) and for three successive scans (see Eq.(5-9))

IrO ₂ loading: 2840 nMol cm ⁻²			
scan	γ (-)	Q_f (nC cm ⁻²)	m (nMol cm ⁻²)
1	8.8×10^{-3}	2.6×10^7	5.9
2	5.0×10^{-3}	2.6×10^7	3.4
3	2.4×10^{-3}	2.6×10^7	1.7
Σ			11

CHAPITRE 5: Active intermediates involved in the oxygen evolution reaction (OER) on IrO₂ electrodes: Voltammetric and DEMS study

This table shows that the value obtained for the total amount of exchanged oxygen is 11 nMol cm⁻² for 1 cm² of electrode geometric surface area, which corresponds to 6.5×10¹⁵ of oxygen atoms per cm² exchanged i.e. about 5 monolayers.

Comparison of these values with the IrO₂ loading (2840 nMol cm⁻²) indicates that the amount of lattice oxygen, which is involved in the oxygen exchange reaction represents 1% of the total IrO₂ loading. This is an indication that only the outer surface of the oxide electrode participates in the oxygen evolution reaction.

Deeper layers are certainly excluded by the oxygen gas evolved, which blocks the inert parts of the oxide coating.

Similar results have been obtained with higher IrO₂ loadings (23280 nMol cm⁻²) as shown in Figure 5-4 and Table 5-2. The experiment revealed that even if the total amount of oxygen exchanged is higher (277 nMol cm⁻² or 75×10¹⁵ oxygen atoms cm⁻²), the fraction of the IrO₂ coating participating in the oxygen evolution remains close to 1%.

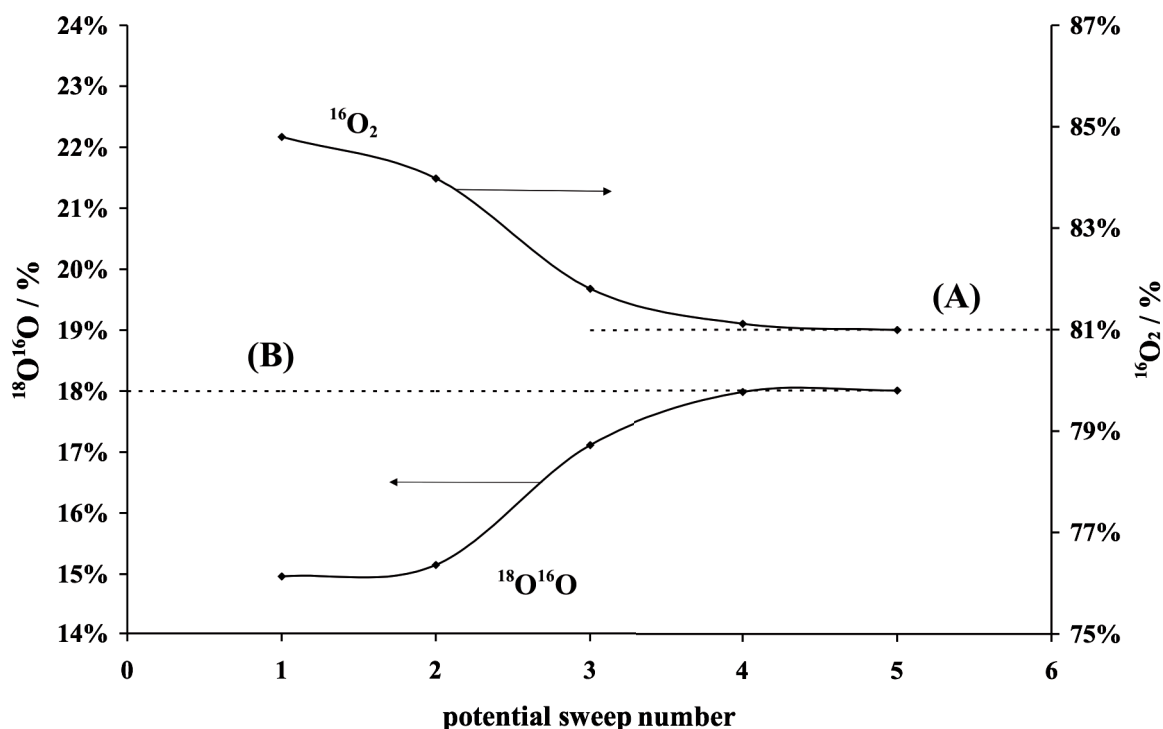


Figure 5-4: DEMS measurements for oxygen evolution on Ti/IrO₂ (Ir¹⁶O₂) (23280 nMol cm⁻²) in 1 M HClO₄ solution containing 10% (w/w) of marked water (H₂¹⁸O). Potential scan rate: 10 mV s⁻¹, T: 25°C. Evolution of ¹⁶O₂ and ¹⁸O¹⁶O concentrations with each consecutive potential scan. (A) and (B) are respectively the concentrations of ¹⁶O₂ and ¹⁸O¹⁶O predicted from the concentration of H₂¹⁸O in the electrolyte.

Table 5-2: Estimation of the amount of ¹⁶O lattice oxygen atoms (*m*), which are transformed to ¹⁸O per unit of electrode geometrical surface area (atoms cm⁻²) for a Ti/IrO₂ electrode (loading: 23280 nMol cm⁻²) and for three successive scans (see Eq.(5-9))

IrO ₂ loading: 23280 nMol cm ⁻²			
scan	γ (-)	Q_f (nC cm ⁻²)	m (nMol cm ⁻²)
1	3.00×10^{-2}	1.6×10^8	124.6
2	2.83×10^{-2}	1.6×10^8	116.8
3	0.86×10^{-2}	1.6×10^8	35.5
Σ			276.9

Series B: In this series of experiments, the Ti/IrO₂ electrode (2840 nMol IrO₂ cm⁻²) was treated firsthand by continuous potential cycling between 0 and 1.6 V (five cycles at 10 mV s⁻¹) in 1 M HClO₄ solution containing approximately 10% H₂¹⁸O. During these scans (as expected from the experiments of Series A), ¹⁸O containing oxide is formed while oxygen constituted mainly of ¹⁶O₂ and ¹⁶O¹⁸O is evolved.

After this treatment, the ¹⁸O containing electrolyte was withdrawn from the cell, which was washed several times with H₂¹⁶O and later filled with 1 M HClO₄/H₂¹⁶O while keeping the anode potential constant at 0.34 V (vs. SHE). In this new electrolyte, several successive CV cycles (10 mV s⁻¹) were performed from 0 up to 1,6 V. The faradaic current obtained from the cyclovoltammograms (CV) together with the ionic currents obtained from the mass spectrometer responses for ions with $m/z=32$, 34 and 36 were recorded for several successive scans.

Figure 5-5 shows the concentrations of ¹⁶O₂ and ¹⁶O¹⁸O obtained during five successive scans.

This figure highlights that the concentration of ¹⁶O¹⁸O in the gas phase decreases with a concomitant increase of ¹⁶O₂ after each cycle before reaching a steady state after four cycles. The concentration of ¹⁸O¹⁶O in the last sweep (0.47%) corresponds to an atomic concentration of ¹⁸O of 0.23 %, which is close to the natural abundance of 0.2%.

In these measurements, the decrease of ¹⁶O¹⁸O or/and the simultaneous increase of ¹⁶O₂ with each successive scan indicates that the ¹⁸O containing oxide layer was

CHAPITRE 5: Active intermediates involved in the oxygen evolution reaction (OER) on IrO₂ electrodes: Voltammetric and DEMS study

replaced by its ¹⁶O analogue via an isotope exchange reaction, which occurred when the electrolyte was substituted by H₂¹⁶O. This demonstrates again that the oxide layer plays an important role in the O₂ evolution reaction. Using Faraday's law, the amount of ¹⁸O in the oxide layer, which was replaced by ¹⁶O during treatment in 1 M HClO₄/H₂¹⁶O solution was estimated to be about 4 nMol cm⁻² or 2.4 × 10¹⁵ molecules of ¹⁸O for 1 cm² of the electrode's geometric surface area. This is only about one third of the exchange obtained in the first series of experiments (series A); the difference might be attributed to a slow exchange during the rinsing procedure (loss of ¹⁸O) or by interdiffusion of the IrO₂ lattice into the bulk.

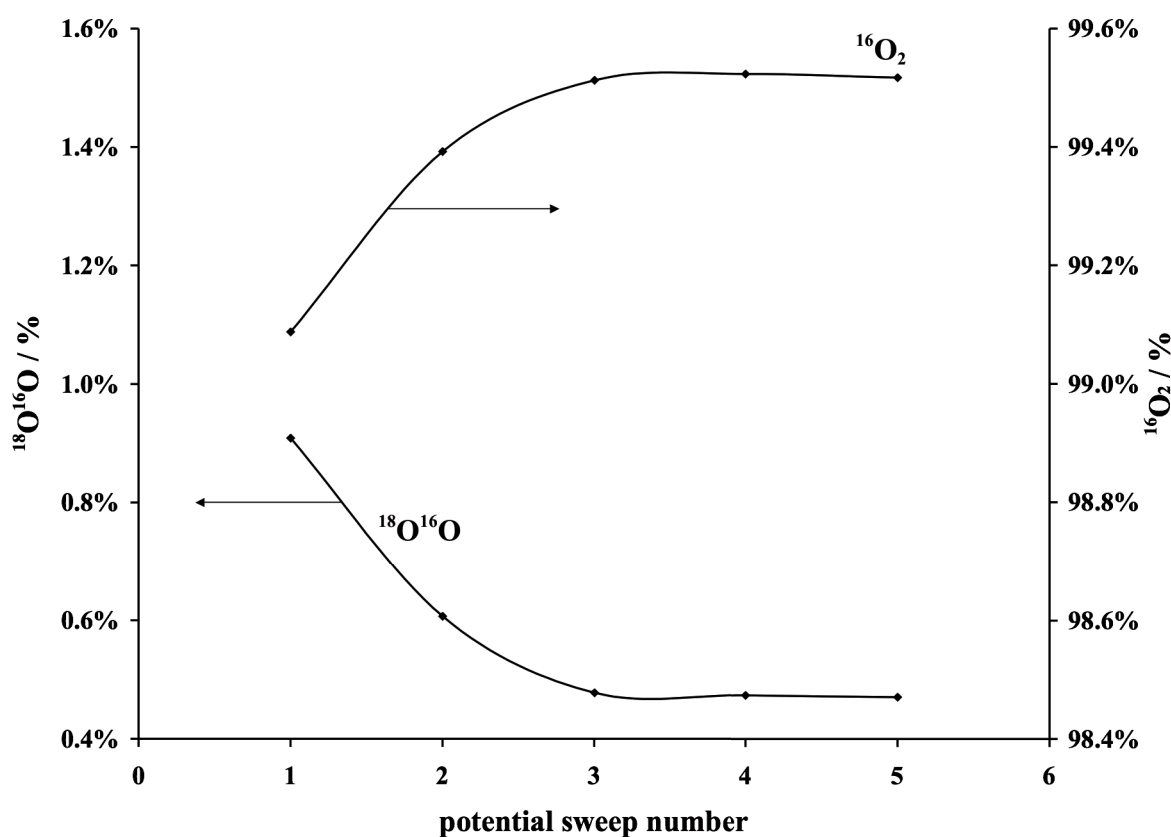


Figure 5-5: DEMS measurements for oxygen evolution on IrO₂ (2840 nMol cm⁻²) in 1 M HClO₄/H₂¹⁶O. Potential scan rate: 10 mV s⁻¹, T: 25°C. The IrO₂ electrode has been pre-treated in HClO₄/H₂¹⁸O electrolyte (see text). Evolution of ¹⁶O₂ and ¹⁸O¹⁶O concentrations with each consecutive potential scan.

5.3.2 Tafel slope measurement for the oxygen evolution reaction on p-Si/IrO₂ electrodes

Figure 5-6 shows a typical steady state polarization curve of the OER on p-Si/IrO₂ electrodes in 1 M HClO₄. In the same figure, the corresponding Tafel plot obtained before (a) and after (b) ohmic drop correction (inset of Figure 5-6) is also shown. The graphical determination of the uncompensated resistance used for the IR drop correction is given on Figure 5-7:

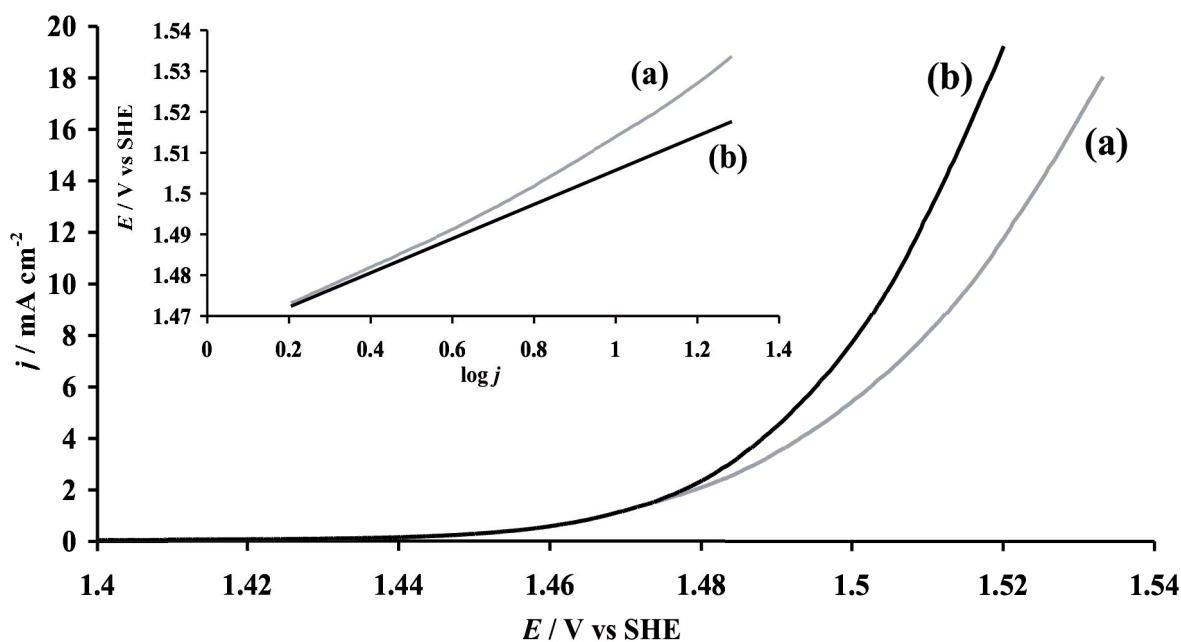


Figure 5-6: Steady state polarization curves (a) before and (b) after ohmic drop correction recorded between 1.4 V and 1.52 V using p-Si/IrO₂ (IrO₂ loading: 0.35 mg cm⁻²). Inset: Corresponding Tafel plots. Supporting electrolyte: 1M HClO₄. T=25°C.

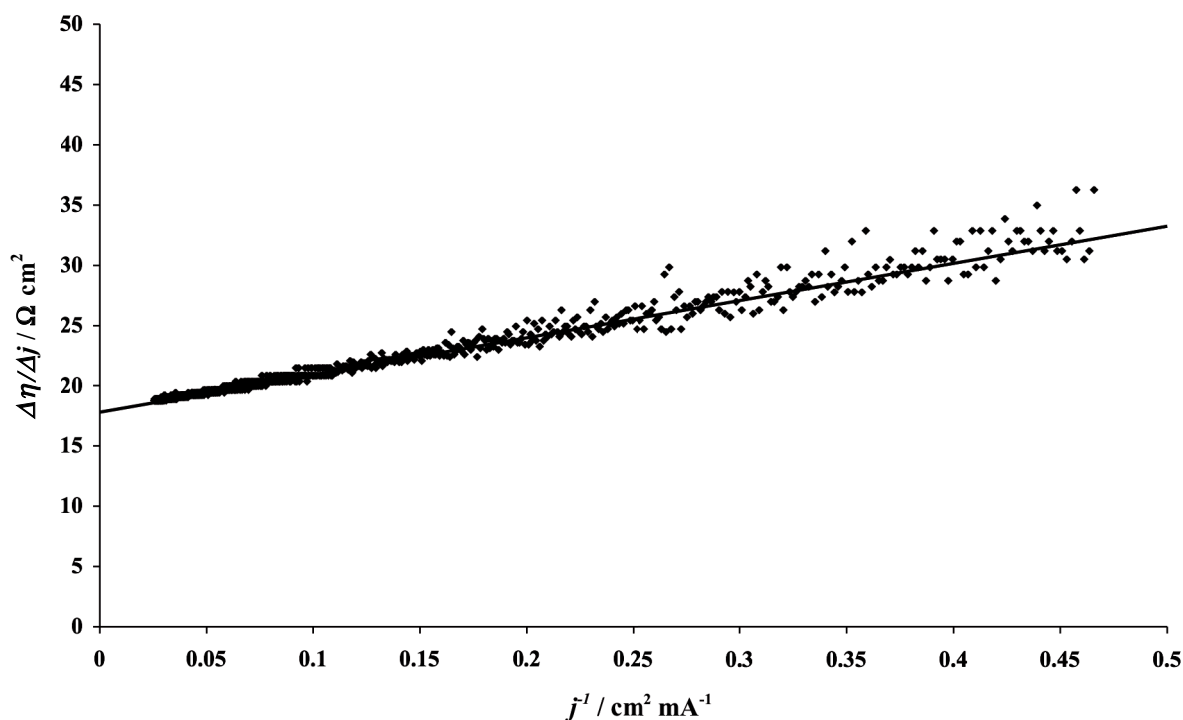


Figure 5-7: Graphical determination of the uncompensated resistance (according to equation (5-6)) from anodic polarization curves recorded on p-Si/IrO₂ (IrO₂ loading: 0.35 mg cm⁻²)

The above figures strongly suggest that even at high overpotentials, the IR drop corrected Tafel plot exhibits a linear relation with a slope of about 40 mV decade⁻¹, while the uncorrected Tafel plot displays a quasi-linear allure with a slope of about 60 mV decade⁻¹. The area-specific uncompensated resistance, equal to 18 Ω cm², was determined from the y-intercept of the plot given in Figure 5-7 for current densities exceeding 1 mA cm⁻² (>1.46 V).

These figures show the importance of the ohmic drop correction procedure because the resistance estimated was non negligible. This correction resulted in a Tafel slope deviation of about 50%.

It is worthwhile to notice that these polarization measurements are reproducible even after treatment of the electrode for a long period of time (several hours) at high anodic potentials (>1.5 V). This is an indication of the high anodic stability of IrO₂ electrodes prepared by thermal decomposition.

In acidic media, the following reaction path (Eq. (5-10), (5-11) and (5-12)) was proposed for the oxygen evolution (OER) on active oxide electrodes [12]:



where S stands for active sites and OH_{ads} , O_{ads} are adsorption intermediates.

This mechanism predicts the following Tafel slopes: 120mV decade⁻¹ if Eq. (5-10) is the rate determining step (rds), 40mV decade⁻¹ for Eq. (5-11) and 30mV decade⁻¹ for Eq.(5-12).

In this chapter, a mechanism was proposed for the OER on IrO₂ electrodes (from Eq. (5-1) to Eq.(5-3)). The adsorption of hydroxyl radicals produced from water discharge on the IrO₂ surface (Eq.(5-1)) corresponds to Eq.(5-10) of the general mechanism given above. The formation of IrO₃ (Eq.(5-2)) corresponds to Eq.(5-11) whereas the formation of oxygen via decomposition of IrO₃ (Eq.(5-3)) corresponds to Eq.(5-12).

The Tafel slopes measured on p-Si/IrO₂ electrodes indicate that formation of a higher oxide (Eq.(5-11)) is the rds. Therefore, the formation of IrO₃ (Eq.(5-2)) seems to be the rds of the OER on these electrodes.

Nonetheless, it should be mentioned that the slopes of the Tafel plots constructed for the OER using p-Si/IrO₂ in this work (40 mV decade⁻¹) differ from those reported by others, which were near 60mV decade⁻¹ for the OER in acidic media. A very intriguing reaction path involving $M-OH_{ads}$ intermediates with different energy states has been proposed by these authors to explain this abnormally high Tafel slope [12,13]. Problems related with uncompensated IR drop correction and partial blockage of the electrode's surface by the evolved oxygen are certainly the main culprit of this discrepancy. In the present study, the experiments have been carefully conducted in order to avoid these problems.

5.4 Conclusions

In this chapter, the surface redox activities involved in the oxygen evolution reaction on Ti/IrO₂ have been studied using differential electrochemical mass spectrometry (DEMS) measurements together with ¹⁸O labeling.

The DEMS measurements have shown that during successive cyclic voltammetric measurements in H₂¹⁸O containing electrolyte, the amount of ¹⁶O₂ (*m/z*=32) decreases with a concomitant increase of ¹⁸O¹⁶O (*m/z*=34) with each successive cycle before reaching a steady state. The amount of lattice oxygen, which is involved in the oxygen exchange reaction, has been found to be in the order of 1% of the total IrO₂ loading. This fraction was found to be loading independent. In a second experiment, it was demonstrated that oxygen evolution on an IrO₂ coating marked with ¹⁸O in H₂¹⁶O containing electrolyte resulted in the formation of Ir¹⁶O₂ and marked oxygen (¹⁸O¹⁶O).

Consequently, the DEMS measurements have shown that only the outer surface of the IrO₂ layer of Ti/IrO₂ participates in the oxygen evolution reaction.

The Tafel slope obtained on p-Si/IrO₂ during oxygen evolution was estimated at 40mV decade⁻¹ from IR drop corrected polarization curves. This result gives a strong evidence that the formation of IrO₃ (Eq.(5-2)) is the rate-determining step of the OER.

5.5 References

- [1] S. Daolio, S. Barison, M. Fabrizio, A. De Battisti, S. Ferro, Dimensionally stable anodes for oxygen evolution: electrochemical properties and SIMS characterization, unpublished results
- [2] G. Fóti, D. Gandini, Ch. Comninellis, A. Perret, W. Haenni, *Electrochem. Solid-State Lett.*, 2 (1999) 228
- [3] G. Fóti, Ch. Comninellis, in: R. White, B.E. Conway, C.G. Vayenas (Eds.), *Modern Aspects of Electrochemistry*, vol. 37, Kluwer Academic/Plenum Publishers, New York, 2004, p. 87
- [4] G. Fóti, D. Gandini, Ch. Comninellis, in *Current Topics in Electrochemistry, Research Trends (Trivandrum)*, 5 (1997) 71

CHAPITRE 5: Active intermediates involved in the oxygen evolution reaction (OER) on IrO₂ electrodes: Voltammetric and DEMS study

- [5] L.I. Krishtalik, *Electrochim. Acta*, 26 (1981) 329
- [6] F. Beck, H. Schulz, *Electrochim. Acta*, 31 (1986) 943
- [7] M. Wohlfahrt-Mehrens, J. Heitbaum, *J. Electroanal. Chem.*, 237 (1987) 251
- [8] J. Willsau, J. Heitbaum, *Electrochim. Acta*, 26 (1981) 329
- [9] Z. Jusys, H. Massong, H. Baltruschat, *J. Electrochem. Soc.*, 146 (1999) 1093
- [10] D.M. Schub, M.F. Reznik, *Elektrokhimiya*, 21 (1985) 937
- [11] N. Krstajic, S. Trasatti, *J. of Applied Chem.*, 28 (1998) 1291
- [12] L.A. De Faria, J.F.C. Boodts, S. Trasatti, *J. Of Applied Chem.*, 26 (1996) 1195
- [13] S. Gottesfeld , S. Srinivasan, *J. Electroanal. Chem.*, 86 (1978) 89

Chapter 6 : Active intermediates involved in the oxidation of organic compounds on Ti/IrO₂ electrodes: DEMS study

In this chapter, the active intermediates involved in the oxidation of organic compounds on IrO₂ electrodes in acidic aqueous media are investigated.

DEMS measurements were used together with ¹⁸O labeling because the experiments in the precedent chapter showed that this method was effective in identifying accurately the active intermediates involved in the oxygen evolution reaction (section 5.3.1).

In a first series of experiments, a Ti/IrO₂ electrode was labeled with ¹⁸O (formation of Ir¹⁶O¹⁸O) by treatment in H₂¹⁸O as similar to the experiments presented in the previous chapter. Later, in a second series of experiments, this labeled electrode was used for the electrochemical oxidation of formic acid using cyclic voltammetry. The amounts of C¹⁶O₂ and C¹⁶O¹⁸O formed during several successive potential scans were followed by on-line mass spectrometry.

The presence of C¹⁸O¹⁶O ($m/z=46$) shown by the DEMS results during the anodic scan demonstrated that the IrO₂ coating participated in the oxidation of formic acid. This is because formic acid was the only source of carbon in the electrolyte, which reacted with the marked oxygen atom present in the labeled IrO₂ lattice.

Analysis of the experimental data has shown that no more than 3.7% of the surface IrO₂ participated in the exchange of oxygen between electro-generated labeled IrO₃ (Ir¹⁶O¹⁶O¹⁸O) and adsorbed formic acid (HC¹⁶O¹⁶OH) producing marked carbon dioxide (C¹⁶O¹⁸O) and Ir¹⁶O₂.

From these results, we can conclude that the IrO₂ layers of Ti/IrO₂ participate in the oxidation of organic compounds in acidic media across at least several monolayers.

This chapter is based on the publication:

S. Fierro, T. Nagel, H. Baltruschat, Ch. Comninellis. Investigation of formic acid oxidation on Ti/IrO₂ electrodes using isotope labelling and online mass spectrometry, *Electrochemical and Solid-State Letters*, Volume 11, Issue 7, April 2008, pages E20-E23

6.1 Introduction

IrO₂-based dimensionally stable anodes (DSA®) are principally used for water electrolysis, metal electro-winning and cathodic protection due to their high stability and high activity during the oxygen evolution reaction [1-4].

These anodes have also been used for the oxidation of organic compounds for applications in both electro-organic synthesis and incineration of organic pollutants present in wastewater [2,3,5].

Until present, many studies have been conducted on the active intermediates involved in the oxidation of organics on IrO₂ based electrodes [6-8]; however, the exact mechanism implicated in this reaction is still a topic of active debate.

In the precedent chapter, it was shown that the IrO₂ coating participates (via formation/decomposition of IrO₃) in the oxygen evolution reaction on Ti/IrO₂ electrodes. The participation of the higher valent state oxide IrO₃ during the OER was

first hypothesized when the phenomenological model for the oxidation of organics with competing OER (presented in the bibliography on Figure 2-3) on 'active' and 'non-active' type anodes in acidic media was proposed.

This model was also discussed (from Eq.(5-1) to Eq.(5-3)) in the previous chapter. The first step is the discharge of water, which yields to the formation of hydroxyl radicals (Eq.(5-1)); later, these radicals are chemisorbed to the electrode material to form the higher valent state oxide (IrO₃) (Eq.(5-2)). Finally, this model suggested that IrO₃ was directly involved in the oxygen evolution reaction on Ti/IrO₂ electrodes, which was verified in the precedent chapter using DEMS measurements (see previous chapter, section 5.3.1).

Moreover, the same model suggests (Figure 2-3) that the oxidation of organic compounds (*R*) (Eq.(6-1)) compete with the OER involving also IrO₃ as intermediate:



However, there exists no direct experimental evidence showing that the IrO₂ coating participates in the oxidation of organic compounds.

In this chapter and in order to determine whether the IrO₂ coating is involved or not in the oxidation of organics, formic acid (FA) has been used as model compound and differential electrochemical mass spectrometry (DEMS) measurements were performed using pre-labeled IrO₂ electrodes (Ir¹⁶O¹⁸O).

6.2 Experimental details

Differential electrochemical mass spectrometry (DEMS)

For the DEMS experiments conducted in this chapter, we make use of a set-up that is identical to the one presented in the previous chapter during the study of the OER (Figure 5-1).

Also, the same Ti/IrO₂ working electrode was used (loading: 0.67 mg cm⁻² or 2840 nMol cm⁻²) and the DEMS experiments were carried out under the same conditions (see section 5.2.1).

The only difference here is that the selected values of m/z ions signals measured as ionic currents ($m/z = 32, 34, 36, 44, 46$) allowed not only to verify that the Ti/IrO₂ electrode has been successfully marked with ¹⁸O ($m/z = 32, 34, 36$) but also to target the mass signals in the MSCV corresponding to the marked or unmarked carbon dioxide ($m/z = 44, 46$) that will be formed from the oxidation of FA.

Consequently, the electrolyte used for the second series of experiment contained no marked water but was 2mM HCOOH (98% from Sigma-Aldrich) in 1M HClO₄.

All potentials given in this chapter are with respect to the standard hydrogen electrode (SHE).

6.3 Results and discussion

DEMS measurements using Ti/IrO₂

In order to answer the question as to what extent the IrO₂ coating participates in the oxidation of formic acid, two series of experiments (series A and B) have been conducted. The goal of the first series of experiments (series A) was to label the IrO₂ coating with ¹⁸O (formation of Ir¹⁶O¹⁸O), by treatment in H₂¹⁸O as already shown in the previous chapter (section 5.3.1). Later, in a second series of experiments (series B), this labeled electrode was used for the electrochemical oxidation of formic acid. The m/z ions signals 44 and 46 corresponding to C¹⁶O₂ and C¹⁶O¹⁸O respectively were rigorously monitored in order to ensure that ¹⁸O was transferred from the IrO₂ coating to the formic acid oxidation product.

Series A: In this first series of experiments, the DEMS cell containing the Ti/IrO₂ electrode (2840 nMol IrO₂/cm²) was firstly filled with a 1 M HClO₄ solution containing 10% (w/w) of marked water (H₂¹⁸O). Later, several successive cyclic scans (10 mV s⁻¹) were applied between 0 and 1.6 V. The faradaic current obtained from the cyclovoltammetric measurements (CV) together with the ionic currents obtained from

the mass spectrometer responses for ions with $m/z = 32, 34$ and 36 (corresponding to $^{16}\text{O}^{16}\text{O}$, $^{16}\text{O}^{18}\text{O}$ and $^{18}\text{O}^{18}\text{O}$ molecules) were recorded for several successive potential scans.

Figure 5-2 (presented in the previous chapter) shows a typical example of the ionic and faradaic currents obtained during the first cyclic scan. From the ionic currents, we can notice that mainly $^{16}\text{O}_2$, $^{16}\text{O}^{18}\text{O}$ are formed in conjunction with a small amount of $^{18}\text{O}_2$. The hysteresis is due to the time lag between O_2 formation and detection in the two compartments.

Figure 6-1 shows the gas phase concentrations of $^{16}\text{O}_2$ and $^{16}\text{O}^{18}\text{O}$ measured during five successive scans as well as those predicted from the concentration of marked water (H_2^{18}O) in the electrolyte.

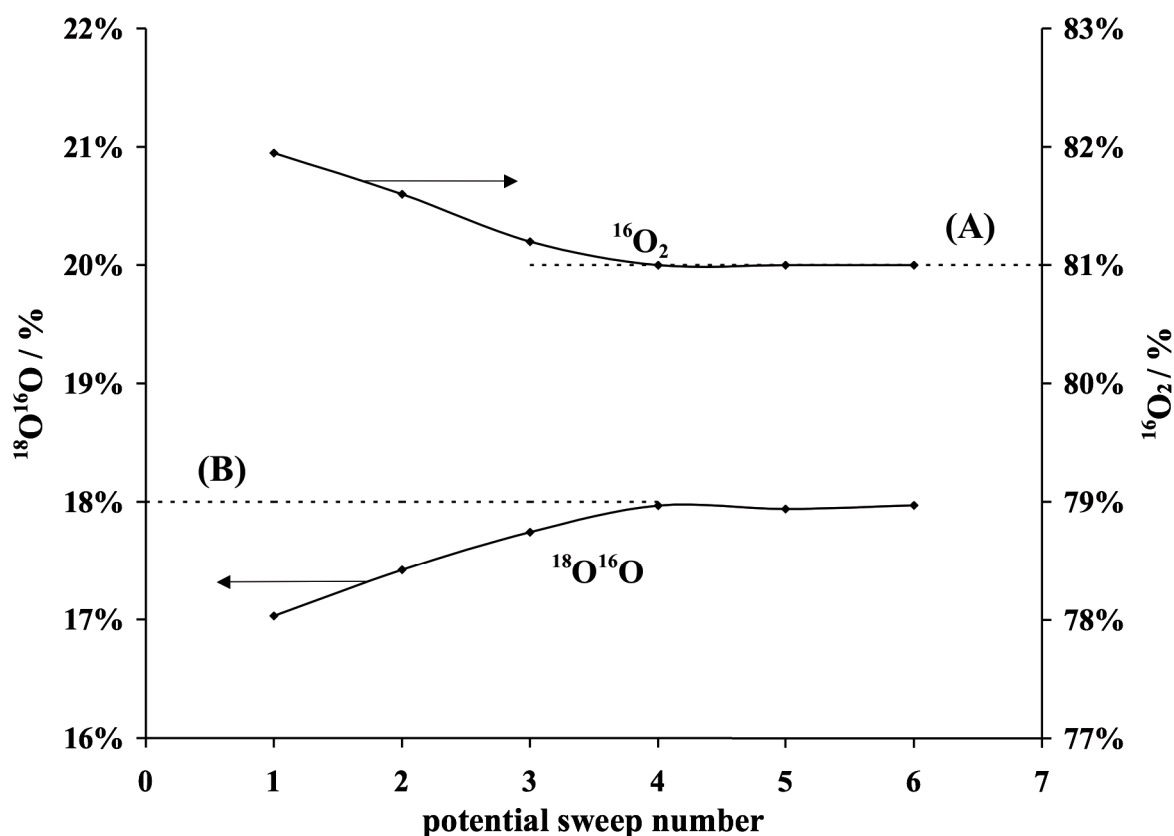


Figure 6-1: DEMS measurements for oxygen evolution on Ir¹⁶O₂ (2840 nMol cm⁻²) in 1 M HClO₄ solution containing 10% (w/w) of marked water (H₂¹⁸O). Potential scan rate: 10 mV s⁻¹, T: 25°C. Evolution of ¹⁶O₂ and ¹⁸O¹⁶O concentrations with each consecutive potential scan. (A) and (B) are respectively the concentrations of ¹⁶O₂ and ¹⁸O¹⁶O predicted from the concentration of H₂¹⁸O in the electrolyte.

This figure clearly shows that during each successive cycle the concentration of ¹⁶O₂ decreases while the concentration of ¹⁶O¹⁸O increase before reaching a steady state after four cycles (which corresponds to the values predicted by the concentration of marked water in the electrolyte). The flowing electrolyte conditions guarantee the constant value of the concentration of marked water in the cell; therefore, the increase of ¹⁶O¹⁸O ($m/z=34$) and/or the concomitant decrease of ¹⁶O₂ ($m/z=32$) with each consecutive scan proves that the marking of the IrO₂ coating with ¹⁸O was successful (see previous chapter, section 5.3.1). In fact, considering that the gas phase composition at the ionic current steady state (i.e. the composition obtained at the 5th scan) corresponds to the bulk electrolyte composition (81% ¹⁶O₂ ($m/z=32$) and 18% ¹⁶O¹⁸O ($m/z=34$)), the concentration of ¹⁶O₂ ($m/z=32$) measured during the first few scans was higher because ¹⁶O from the IrO₂ coating contributed in the oxygen evolution reaction and therefore, during this treatment, a small fraction of the marked oxygen was inserted into the oxide lattice according to Eq.(5-7).

Later, using the same relation based on the Faraday law that was developed in the precedent chapter (Eq.(5-8) and (5-9)), the amount of moles (m) and the corresponding number (n) of ¹⁶O lattice oxygen, which are exchanged to ¹⁸O per unit of electrode geometrical surface area for each consecutive scan until no further exchange is occurring, can be calculated.

The values obtained together with the total amount of ¹⁸O atoms formed during the three successive scans are given in Table 6.1.

Table 6-1: Estimation of the amount of ¹⁶O lattice oxygen atoms (m), which are transformed to ¹⁸O per unit of electrode geometrical surface area (atoms cm⁻²) on a Ti/IrO₂ electrode (loading: 2840 nMol cm⁻²) for three successive scans (see Eq.(5-8))

IrO ₂ loading: 2840 nMol cm ⁻²			
scan	γ (-)	Q_f (nC cm ⁻²)	m (nMol cm ⁻²)
1	9.1×10^{-3}	2.6×10^7	6.1
2	5.2×10^{-3}	2.6×10^7	3.5
3	0.2×10^{-3}	2.6×10^7	1.3
Σ			10.9

CHAPITRE 6: Active intermediates involved in the oxidation of organic compounds on Ti/IrO₂ electrodes: DEMS study

This table shows that the value obtained for the total amount of exchanged oxygen is about 11 nMol cm⁻² for 1 cm² of the electrode's geometric surface area, which corresponds to 6.5×10¹⁵ of oxygen atoms exchanged per cm².

It is worthwhile to notice that the amount of oxygen exchanged is practically identical to the result obtained for the same experiment presented in the previous chapter (Table 5-1). This proves that the DEMS experiments have the desired attributes of being accurate and reproducible.

Knowing this value (11 nMol cm⁻²) and the IrO₂ loading (2840 nMol cm⁻²), it was estimated that the amount of lattice oxygen, which is involved in the oxygen exchange reaction, represents 11/2840=0.38% of the total IrO₂ loading.

This value should be compared to the amount of IrO₂, which composes the electrode's surface, i.e. which is in contact with the solution. From the integration of the voltammogram (A) given in Figure 5-2 between 0 V and 1.5V, a charge density of 0.056 C cm⁻² was obtained. Assuming that this charge is entirely related to the oxidation of the surface IrO₂ to IrO₃ we get a number of 290 nMol cm⁻² of iridium dioxide in contact with the solution.

This represents 10.2% of all the IrO₂ contained in the electrode; if only a fraction of the IrO₂ from the electrode's surface is oxidized or if the charge is partly related to the charging of the double layer (which seems likely in the present experiment), the number of iridium atoms present at the surface is even larger, which means that less than 3,7% of the surface iridium atoms participate in the oxygen exchange.

Series B: In this series of experiments, the labeled IrO₂ electrode (2840 nMol IrO₂ cm⁻²), prepared in series A, was first carefully rinsed with H₂¹⁶O before being introduced into a clean DEMS cell in order to eliminate any presence of marked water within the system. Finally, the cell was filled with 1 M HClO₄/H₂¹⁶O containing 2mM of HCOOH.

In this new electrolyte, several successive CV sweeps (10 mV s⁻¹) were performed from 0 up to 1.6 V (vs. SHE). The faradaic current obtained from the cyclovoltammograms (CV) together with the ionic currents computed from the mass spectrometer responses for ions with *m/z*=44 and 46 (corresponding to C¹⁶O¹⁶O and C¹⁶O¹⁸O molecules respectively) were recorded for several successive potential scans.

Figure 6-2 shows a typical example of the ionic currents corresponding to C¹⁶O₂ and C¹⁶O¹⁸O as well as the faradaic current obtained during the first cyclic scan.

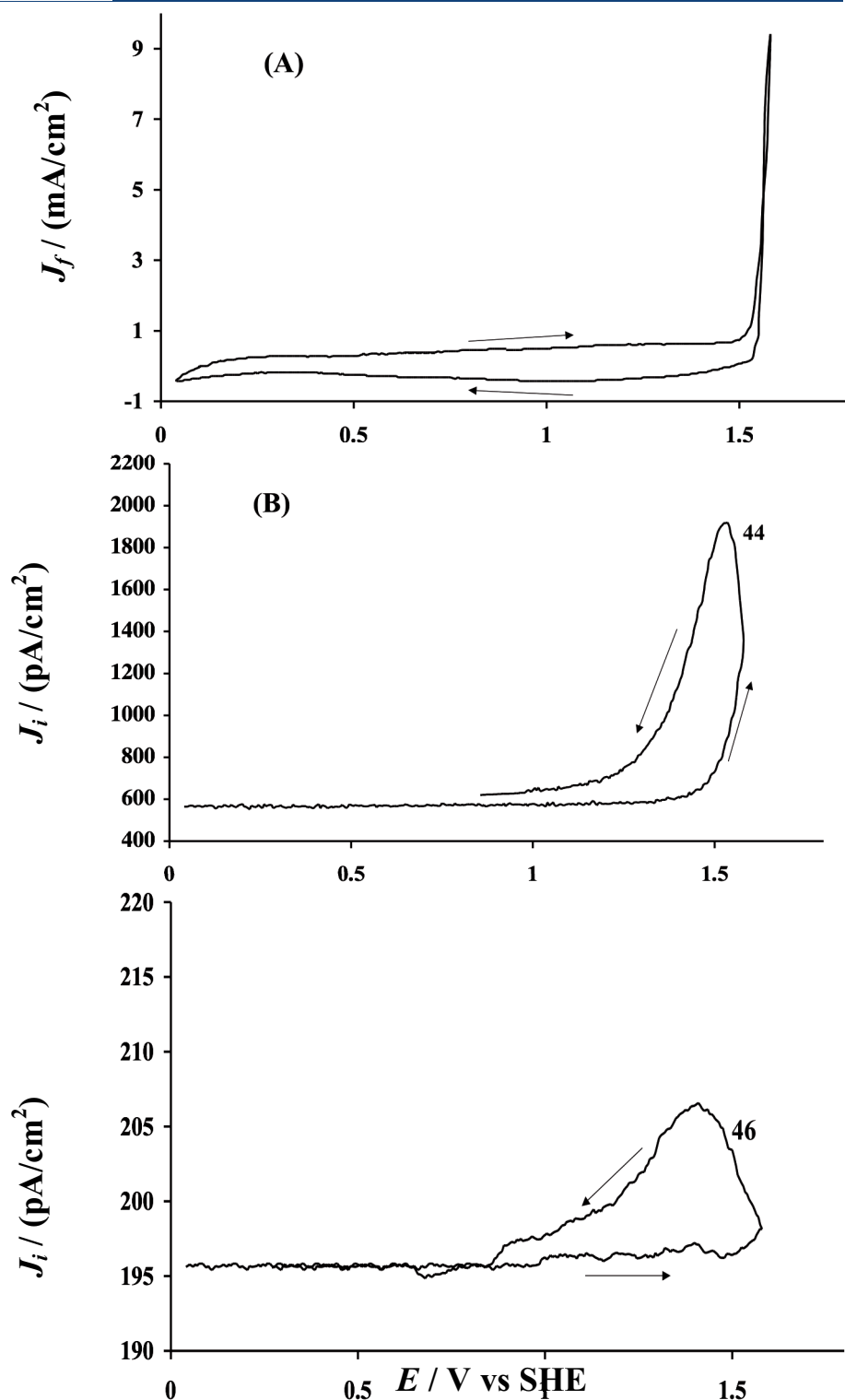


Figure 6-2: DEMS measurements using a labeled iridium oxide electrode ($\text{Ir}^{16}\text{O}^{18}$) in 2mM $\text{HCOOH}/1\text{M}$ HClO_4 solution containing regular water (H_2^{16}O). Potential scan rate: 10 mV s^{-1} , T : 25°C . (A) Faradaic current density (J_f) obtained from the cyclic voltammetric measurements. (B) Ionic current densities (J_i) obtained from the mass spectrometer responses for ions with m/z : 44 (C^{16}O_2), 46 ($\text{C}^{18}\text{O}^{16}\text{O}$).

This figure shows that C¹⁶O¹⁸O was formed during the experiment. This result is a clear proof that the IrO₂ coating participated in the oxidation of formic acid (Eq.(6-2)) because the latter was the only source of carbon in the bulk allowing it to react with the marked oxygen atoms inserted in the lattice during the experimental procedure of series A (Eq.(5-7)).

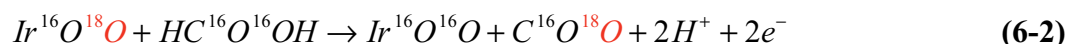


Figure 6-3 shows the relative amounts of C¹⁶O₂ and C¹⁶O¹⁸O obtained during six successive scans.

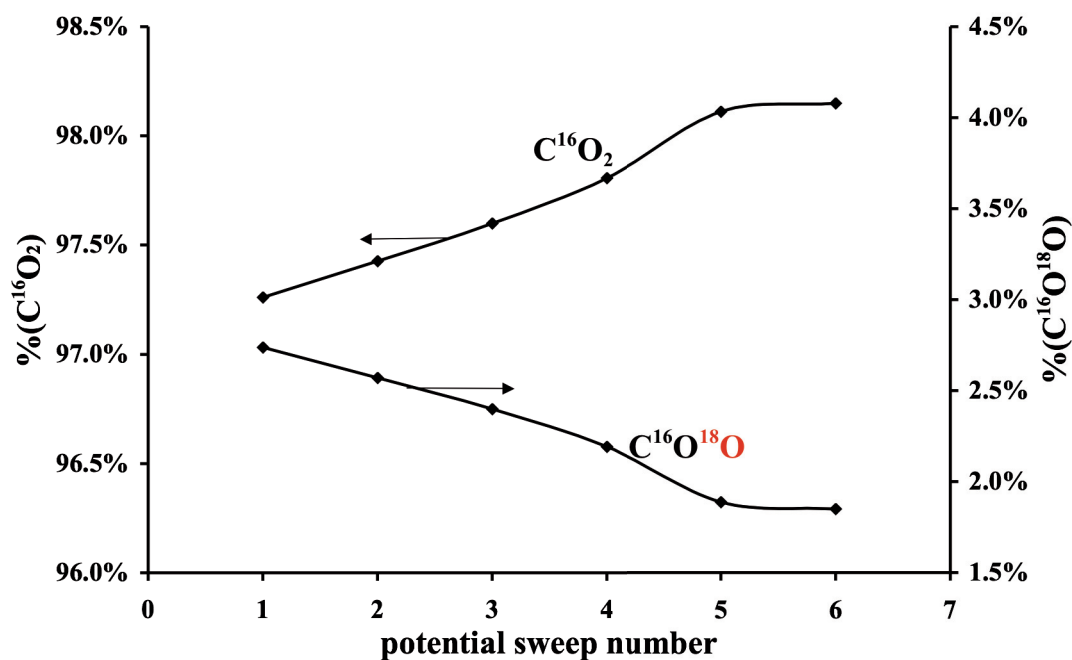


Figure 6-3: DEMS measurements for formic acid oxidation on a labeled iridium dioxide electrode (Ir¹⁶O¹⁸O) (2840 nMol cm⁻²). Electrolyte: 2mM formic acid in aqueous (H₂¹⁶O) 1M HClO₄. Potential scan rate: 10 mV s⁻¹, T: 25°C. Evolution of C¹⁶O₂ and C¹⁸O¹⁶O concentrations with each consecutive potential scan.

The figure shows that during each successive cycle the concentration of C¹⁶O¹⁸O in the gas phase decreases while the concentration C¹⁶O₂ increases before reaching a steady state after five cycles.

In these measurements, the decrease of C¹⁶O¹⁸O and/or the simultaneous increase of C¹⁶O₂ after each scan indicates that the ¹⁸O inserted in the IrO₂ coating in the

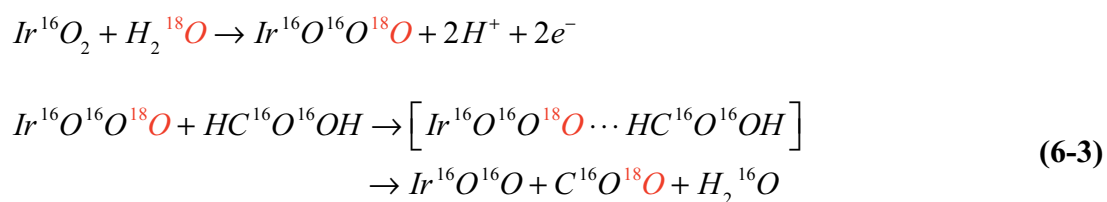
experiments of series A (Eq.(5-7)) was present in the CO₂ formed from the oxidation of formic acid (Eq.(6-2)) in the experiments of series B. This, again, demonstrates that the iridium oxide layer plays a role in the oxidation of formic acid. Using Faraday's law, the amount of ¹⁸O in the oxide layer, which was consumed during the oxidation of formic acid and replaced by ¹⁶O was estimated to be about 10.6 nMol cm⁻² or 6.4 ×10¹⁵ molecules of ¹⁸O for 1 cm² of the electrode's geometric surface area (see Table 6-2).

Table 6-2: Estimation of the amount of ¹⁸O lattice oxygen atoms (m), which are transformed to ¹⁶O per unit of electrode geometrical surface area (atoms cm⁻²) during formic acid oxidation in regular water (H₂¹⁶O), for four successive scans in series B experiments (see Eq.(5-8))

IrO ₂ loading: 2840 nMol/cm ²			
scan	γ (-)	Q_f (nC/cm ²)	m (nMol/cm ²)
1	8.4×10^{-3}	1.8×10^7	3.9
2	6.7×10^{-3}	1.8×10^7	3.1
3	5.0×10^{-3}	1.8×10^7	2.3
4	2.9×10^{-3}	1.8×10^7	1.3
Σ			10.6

This quantity represents almost the totality of the amount of ¹⁸O exchanged during the first series of experiments (series A); however, the steady state was reached after 6 scans instead of 5. This small difference between the two amounts of ¹⁸O exchanged during series A and B of the experimental procedure might be attributed to the co-evolution of oxygen during formic acid oxidation.

The exact mechanism of formic acid oxidation via the IrO₃/IrO₂ redox couple is certainly complex; however, because ¹⁸O from the IrO₂ lattice was exchanged with the ¹⁶O of formic acid to produce C¹⁶O¹⁸O (Eq.(6-2)), we can speculate that the formed higher oxide IrO₃ acts as mediator during the oxidation of adsorbed formic acid. This can lead to oxygen exchange between Ir¹⁶O₂¹⁸O and adsorbed formic acid producing C¹⁶O¹⁸O and Ir¹⁶O₂ (Eq.(6-3)).



This reaction occurs via the same intermediate (IrO₃) participating in the oxygen evolution reaction on Ti/IrO₂ electrodes. Therefore, the OER and the oxidation of organic compounds compete on the same active intermediate (IrO₃).

6.4 Conclusions

In this chapter, the surface redox activities involved in the oxidation of organics (using formic acid as model compound) have been studied for Ti/IrO₂ using DEMS experiments together with ¹⁸O labeling.

Successive cyclic voltammetric measurements on Ir¹⁶O₂ electrodes in H₂¹⁸O containing electrolyte have successfully shown that after each successive cycle, the amount of ¹⁶O₂ (*m/z*=32) decreases, while the concentration of ¹⁸O¹⁶O (*m/z*=34) increase before reaching a steady state. This proved that marked oxygen was inserted inside the coating. In a second series of experiment, formic acid in H₂¹⁶O was oxidized on this labeled electrode and the results revealed the presence of C¹⁶O¹⁸O (*m/z*=46). In fact, the concentration of C¹⁶O¹⁸O decreased, while the concentration of C¹⁶O₂ increased, which proves that the IrO₂ coating did actively participate in the oxidation of organics.

The analysis of the experimental data has shown that almost the totality of the ¹⁸O inserted in the coating was exchanged with the adsorbed formic acid (0.38% of the total IrO₂ loading). Since the oxygen exchange proved to be highly reproducible (different loadings (Chapter 5, section 5.3.1), same value for oxygen evolution and formic acid oxidation), we assume that these sites (at maximum 3.7% of the surface atoms) represent the catalytically active sites for oxygen evolution and formic acid oxidation.

6.5 References

- [1] S. Trasatti, W.E. O'Grady (1981) In: Gerisher H, Tobias CW (eds) *Advances in electrochemistry and electrochemical engineering*, Wiley, New York, p 177
- [2] Ch. Comninellis, A. Nerini, *J. Appl. Electrochem.*, 25 (1995) 23
- [3] F. Beck, H. Schulz, *Electrochim. Acta*, 29 (1984) 1569
- [4] S. Trasatti, *Electrochim. Acta*, 45 (2000) 2377
- [5] F. Beck, E. Lodowicks, *Chem. Eng. Technol.*, 17, (1994) 338
- [6] Ch. Comninellis, *Electrochim. Acta*, 39 (1994) 1857
- [7] Ch. Comninellis, G. Fòti, D. Gandini, A. Perret, W. Haenni, *Electrochem. Solid-State Lett.*, 2, (1999) 228
- [8] Ch. Comninellis, V. Schaller, O. Simond, *Electrochim. Acta*, 42 (1997) 2009

Chapter 7 : Voltammetric study of the oxidation of model organic compounds on p- Si/IrO₂ electrodes

In this chapter, the electrochemical oxidation of model aliphatic (formic acid, *i*-propanol and 2-butanol) and aromatic (phenol) compounds is investigated on p-Si/IrO₂ electrodes in aqueous acidic media using linear potential sweep voltammetry measurements.

From measurements performed using different IrO₂ loadings and organic concentrations, the kinetic parameters of the oxidation of organic compounds (formic acid, *i*-propanol, 2-butanol and phenol) have been quantitatively determined using a model that involves the redox couple IrO₃/IrO₂ as mediator of these reactions. These experiments revealed that these kinetic parameters are strongly dependent on the IrO₂ loading.

Furthermore, using the kinetic parameters obtained together with the Nernst equation and the I-V curves of the supporting electrolyte (1M HClO₄), theoretical I-V curves could be constructed for different concentrations of formic acid (model organic compound) and different IrO₂ loadings.

This chapter is based on the publications:

S. Fierro, L. Ouattara, E. H. Calderon, E. Passas-Lagos, H. Baltruschat, Ch. Comninellis. Investigation of formic acid oxidation on Ti/IrO₂ electrodes, *Electrochimica Acta*, Volume 54, Issue 7, July 2008, Pages 2053-2061

S. Fierro, Ch. Comninellis. Kinetic study of formic acid oxidation on p-Si/IrO₂ electrodes, *Electrochim. Acta*, submitted manuscript, February 2010

7.1 Introduction

In the previous chapters (Chapter 5 and Chapter 6), it has been demonstrated using differential electrochemical mass spectrometry (DEMS) measurements together with isotope labeling that the oxidation of organic compounds on IrO₂ electrodes is mediated by the surface IrO₃/IrO₂ redox couple (redox catalysis) and proceeds in parallel with the side reaction of oxygen evolution (OER) due to IrO₃ decomposition [1,2].

The goal of the experiments presented in this chapter is to develop a phenomenological kinetic model for the oxidation of organic compounds on IrO₂ electrodes for applications in electrosynthesis processes (electrolysis).

Our model is mainly based on the work of F.Beck [3], where the electrode potential can be expressed by Nernst equation, which is dictated by the surface redox couple responsible of the electron transfer. This model was validated using the oxidation of different aliphatic alcohols and ethers on Ti/Cr₂O₃+TiO₂ electrodes as example [3]. Unfortunately, these electrodes were anodically corroded resulting in the contamination of the electrolyte solution with chromium. An alternative solution to this problem is proposed in this chapter: we used IrO₂ electrodes, because they are stable under organic oxidation conditions even in highly acidic media. In the first part of this chapter, the kinetic parameters of the oxidation of model organic compounds have been estimated from

voltammetric measurements recorded using different IrO₂ loadings and organic concentrations. In the second part of this chapter, the shift of the I-V curve toward less positive potentials in the presence of an organic compound is investigated.

7.2 Experimental details

Voltammetric experiments using p-Si/IrO₂

The voltammetric experiments presented in this chapter were performed in a three-electrode cell (70 ml) using an Autolab PGSTAT 30. The counter electrode was a Pt wire; the reference electrode was Hg/Hg₂SO₄/K₂SO₄ (sat.) (MSE; 0.65 V vs. SHE) and the working electrodes were several IrO₂ based electrodes (with different IrO₂ loadings) prepared by thermal decomposition of a precursor: the precursor aqueous solution (H₂IrCl₆ (99.9%, ABCR) 250mM in dry *i*-propanol (extra dry with molecular sieves, water < 50ppm, Acros Organics) was deposited using the spin coating technique (described in Chapter 3) on square-shaped sandblasted p-Si (100 mm²) substrate and then the oxide film was obtained through thermal decomposition in air at 500°C.

The deposition and thermal decomposition processes were repeated in order to produce multi-layered p-Si/IrO₂ electrodes having different loadings (Table 7-1).

The presence of iridium dioxide on the substrate was confirmed using XPS measurements (Table 3-1).

Table 7-1: IrO₂ loadings of the p-Si/IrO₂ electrodes prepared using the spin coating deposition technique.

Number of layers	1	2	3	5	6	10	13	20
IrO ₂ loading [mg cm ⁻²]	0.23	0.35	0.69	0.87	1.63	1.75	2.99	3.5

All the above experiments were carried out at room temperature inside a Faraday cage and using 1M HClO₄ (95-97% Merck) as support electrolyte. All potentials in this chapter are with respect to the standard hydrogen electrode (SHE).

The cell and materials used for the voltammetric experiments on p-Si/IrO₂ are similar to the set-up used in the precedent chapters (Figure 3-1 in section 3.2).

7.3 Results and discussion

During organics oxidation on IrO₂ electrodes, the oxidation competes with the oxygen evolution reaction (OER). The I-V curves show that there is a shift toward less positive potentials in the presence of an organic compound.

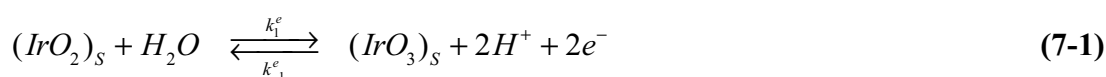
In this chapter, a conceptual model is proposed. The first part of the model is used to determine the kinetic parameters of the main reaction (oxidation of the organic compound) whereas the second part of the model is put forth to evaluate the potential shift toward less positive values of the OER current response in the presence of an organic compound. Finally, the results obtained together with the I-V curves recorded using only the support electrolyte were used to construct theoretical I-V curves for the reaction under investigation under a given organic concentration and IrO₂ loading.

Therefore, several p-Si/IrO₂ electrodes with different loadings (0.23; 0.35; 0.87; 1.63; 1.75 and 3.50 mg·cm⁻²) were used to investigate the oxidation of organic compounds. Linear voltammetry measurements were performed at 10mV s⁻¹ and at room temperature on these electrodes using various organics (formic acid, *i*-propanol, 2-butanol and phenol) having different concentrations in 1M HClO₄.

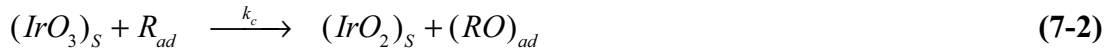
Model for organics oxidation on p-Si/IrO₂ electrodes

Three main reactions are involved in the following phenomenological model:

a) Electrochemical oxidation of IrO₂ active species (Eq.(7-1)):



b) Chemical oxidation of the adsorbed organic matter *R* by the electrogenerated IrO₃ (Eq.(7-2)):



c) Oxygen evolution reaction via decomposition of IrO₃ (Eq.(7-3)):



In this simplified model, the oxidation of organics (main reaction) and the evolution of O₂ (side reaction) compete on electrogenerated IrO₃.

The main assumptions behind this model are:

- The formation of IrO₃ (Eq.(7-1)) is a fast reaction compared to the oxidation of organics (Eq.(7-2)).
- Transport and adsorption of the organics in solution are fast processes.
- The surface redox couple IrO₃/IrO₂ follows Nernst law.

The rate of electrogeneration of IrO₃ (Eq.(7-1)) can be given by the following equation (Eq.(7-4)).

$$r_{IrO_3} = \frac{j}{zF} = \gamma_{3D} k_1^e \Gamma_0 (1 - \Theta) - \gamma_{3D} k_{-1}^e \Gamma_0 \Theta \quad \text{with} \quad \gamma_{3D} = \frac{A_{real}}{A_g} \quad (7-4)$$

with γ_{3D} being the three dimensional roughness factor (-) defined as the ratio between the real and geometrical surface areas of the electrode surface, Γ_0 the density of IrO₂ surface sites available for IrO₃ formation (mol m⁻²), Θ (-) the fractional electrode surface transformed from IrO₂ to IrO₃, k_1^e and k_{-1}^e (s⁻¹) the electrochemical rate constants for the forward and reverse reaction (Eq.(7-1)) and finally z the number of electrons involved in the process ($z = 2$ in this case).

Thus the current density j (A m⁻²) for the electrogeneration of IrO₃ can be evaluated using the following relation (Eq.(7-5)).

$$j = \gamma_{3D} z F \Gamma_0 \left[k_1^e (1 - \Theta) - k_{-1}^e \Theta \right] \quad (7-5)$$

CHAPITRE 7: Voltammetric study of the oxidation of model organic compounds on p-Si/IrO₂ electrodes

The rate of chemical oxidation of the organic by IrO₃ (Eq. (7-2)) is given by Eq.(7-6):

$$r_{oxid.} = \gamma_{3D} k_c \Gamma_0 \Theta \cdot C_R^{ad} \quad (7-6)$$

with k_c being the chemical rate constant ($\text{m}^3\text{mol}^{-1}\text{s}^{-1}$) and C_R^{ad} the concentration of adsorbed organic compounds at the electrode's surface (mol m^{-3}). The decomposition rate of IrO₃ on the electrode's surface is given by the following equation (Eq.(7-7)), with k_d standing for the decomposition rate constant (s^{-1}).

$$r_{dec.} = \gamma_{3D} k_d \Gamma_0 \Theta \quad (7-7)$$

Assuming steady-state conditions, the rate of IrO₃ electrogeneration is given by the sum of the organic oxidation rate and the IrO₃ decomposition rate (Eq.(7-8)):

$$r_{IrO_3} = r_{oxid.} + r_{dec.} \quad (7-8)$$

Insertion of equations (7-5), (7-6) and (7-7) into equation (7-8) gives Eq.(7-9):

$$k_1^e(1 - \Theta) - k_{-1}^e\Theta = k_c\Theta \cdot C_R^{ad} + k_d\Theta \quad (7-9)$$

Finally by substitution, the fractional surface coverage of the active species Θ can be estimated using Eq.(7-10):

$$\Theta = \frac{k_1^e}{k_1^e + k_{-1}^e + k_c C_R^{ad} + k_d} \quad (7-10)$$

CHAPITRE 7: Voltammetric study of the oxidation of model organic
compounds on p-Si/IrO₂ electrodes

Assuming that $C_R^{ad} = C_R^{bulk} = C_{Rf}$, the insertion of Eq.(7-10) into Eq.(7-5), yields to:

$$j = \gamma_{3D} z F k_1^e \Gamma_0 \left[\frac{k_c C_R + k_d}{k_1^e + k_{-1}^e + k_c C_R + k_d} \right] \quad (7-11)$$

Because of the inherent difficulty in determining the kinetic parameters from Eq. (7-11), we considered the inverse of equation (7-11) instead:

$$\frac{1}{j} = \frac{1}{\gamma_{3D} z F k_1^e \Gamma_0} + \frac{k_1^e + k_{-1}^e}{\gamma_{3D} z F k_1^e \Gamma_0 (k_c C_R + k_d)} \quad (7-12)$$

According to this equation (Eq.(7-12)), the inverse of the current density $1/j$ plotted versus the inverse of the organic bulk concentration $1/C_R$ should give a straight line with a y-intercept of $1/(z\gamma_{3D}Fk_1^e\Gamma_0)$. Furthermore and in order to calculate the charge transfer coefficient α and the apparent standard rate constant $(k_1^{e,0})_{ap}$ (Eq. (7-13)) of the electrochemical reaction ($\text{mol m}^{-2} \text{s}^{-1}$), it is necessary to plot the logarithm of the y-intercepts obtained versus the corresponding overpotential, considering that $E_0 = 1.3 \text{ V}$ for reaction (7-3).

$$(k_1^{e,0})_{ap} = \gamma_{3D} k_1^{e,0} \Gamma_0 \quad (7-13)$$

Using the slopes of the resulting straight lines, it is possible to calculate α using the following relations (Eq.(7-14)).

$$k_1^e = k_1^{e,0} \exp\left(\frac{\alpha z F}{RT} \cdot \eta\right) \quad \text{or} \quad \ln k_1^e = \ln k_1^{e,0} + \left(\frac{\alpha z F}{RT}\right) \cdot \eta \quad (7-14)$$

where z , F , R and T have their usual meaning and η is the overpotential (V).

CHAPITRE 7: Voltammetric study of the oxidation of model organic compounds on p-Si/IrO₂ electrodes

Finally the apparent standard rate constants $(k_1^{e,0})_{ap}$ obtained have been plotted as a function of the IrO₂ loading and as a function of the values found for the electrical double layer capacitance q_{dl}^* . This capacitance has been determined in the same manner than in Chapter 4, section 4.3.1.

By working at high overpotentials (> 1.45 V) and subtracting the background current from the obtained current-potential curves, Eq. (7-12) can be transformed to (assuming $k_d = 0$ and $k_{-1}^e = 0$):

$$\frac{1}{j} = \frac{1}{\gamma_{3D} z F k_1^e \Gamma_0} + \frac{1}{z F (k_c)_{ap}} \cdot \frac{1}{C_R} \quad \text{with} \quad (k_c)_{ap} = \gamma_{3D} \Gamma_0 k_c \quad (7-15)$$

with $(k_c)_{ap}$ being the apparent rate constant (m s^{-1}) for reaction (7-2), which can be estimated from the slope of the resulting $(1/j)$ vs. $(1/C_R)$ plot.

The second part of this model is based mainly on the work of Beck [3], who studied the oxidation of organics on Ti/Cr₂O₃ based anodes. However, for this part of the model, the side reaction of O₂ evolution (Eq.(7-3)) has been neglected.

Furthermore, because the IrO₂ coating is stable under the investigated conditions, the sum of the higher and the lower oxide (IrO₃ and IrO₂) concentrations remains constant in the coating:

$$[IrO_2] + [IrO_3] = \gamma_{3D} [\Gamma_0 (1 - \Theta) + \Gamma_0 \Theta] = \gamma_{3D} \Gamma_0 \quad (7-16)$$

Considering these assumptions, the anode potential can be given by Nernst equation.

$$U_B = U_{B,0} + \frac{RT}{zF} \ln \frac{[IrO_3]}{[IrO_2]} = U_{B,0} + \frac{RT}{zF} \ln \frac{\Theta}{(1 - \Theta)} \quad (7-17)$$

with $U_{B,0}$ (V) standing for the standard potential of the surface redox couple.

Assuming that the transport and adsorption of dissolved R is fast and in equilibrium with the previously adsorbed R :

$$C_R^{ad} = K \cdot C_R \quad (7-18)$$

And knowing that the rate of chemical oxidation of FA by IrO₃ is given by Eq.(7-6); combining expressions (7-15), (7-17) and (7-18) gives:

$$j = zFk_c \frac{C_R \cdot K \cdot \gamma_{3D} \cdot \Gamma_0}{1 + \exp\left(-\frac{zF}{RT}(U_B - U_{B,0})\right)} = zF \frac{C_R^{ad} \cdot (k_c)_{ap}}{1 + \exp\left(-\frac{zF}{RT}(U_B - U_{B,0})\right)} \quad (7-19)$$

Considering again that $C_R^{ad} = C_R^{bulk} = C_R$ (i.e. $K = 1$), one obtains:

$$j = zFk_c \frac{C_R \cdot K \cdot \gamma_{3D} \cdot \Gamma_0}{1 + \exp\left(-\frac{zF}{RT}(U_B - U_{B,0})\right)} = zF \frac{C_R \cdot (k_c)_{ap}}{1 + \exp\left(-\frac{zF}{RT}(U_B - U_{B,0})\right)} \quad (7-20)$$

This relation (Eq.(7-20)) predicts that the current density increases linearly with the organic concentration and also induces a negative potential shift of the I-V curves.

Estimation of the kinetic parameters of organic oxidation on p-Si/IrO₂ electrodes using formic acid, *i*-propanol, 2-butanol and phenol as model compounds

Figure 7-1 displays the linear voltammetry measurements for different concentrations of formic acid in 1M HClO₄ and for four p-Si/IrO₂ electrodes with different loadings. A negative potential shift of the oxidation current is observed in the domain of water discharge with increasing FA concentrations as predicted by Eq.(7-19) of the model.

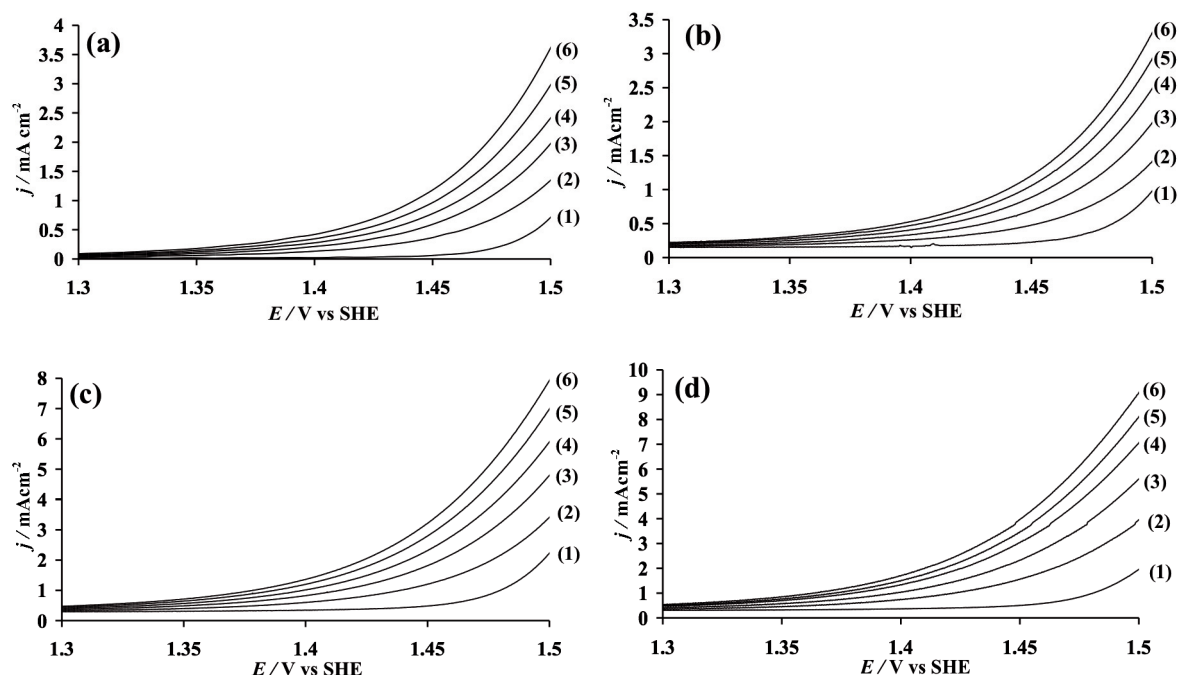


Figure 7-1: Linear voltammograms recorded using p-Si/IrO₂ anodes with different loadings ((a) 0.35 mg cm⁻², (b) 0.87 mg cm⁻², (c) 1.75 mg cm⁻², (d) 3.5 mg cm⁻²) for different concentrations of formic acid in 1M HClO₄: (1) 0M, (2) 0.2M, (3) 0.4M, (4) 0.6M, (5) 0.8M, (6) 1M. $v = 10 \text{ mV s}^{-1}$, $T = 25 \text{ }^\circ\text{C}$ (5th scan).

The I-V curves in the presence of formic acid presented in Figure 7-1 have been corrected by subtraction of the I-V curves obtained in 1M HClO₄ (background I-V curves related to the side reaction of O₂ evolution). Figure 7-2 shows an example of the resulting background subtracted curves. Using these curves and at the following fixed anodic potentials: 1.348, 1.392, 1.402, 1.451 and 1.5 V, the current density was plotted against the concentration of formic acid for several IrO₂ loadings (Figure 7-3). The linearity observed between the current density and the concentration of FA for all IrO₂ loadings is in agreement with the current-overpotential relation derived earlier (Eq. (7-19)).

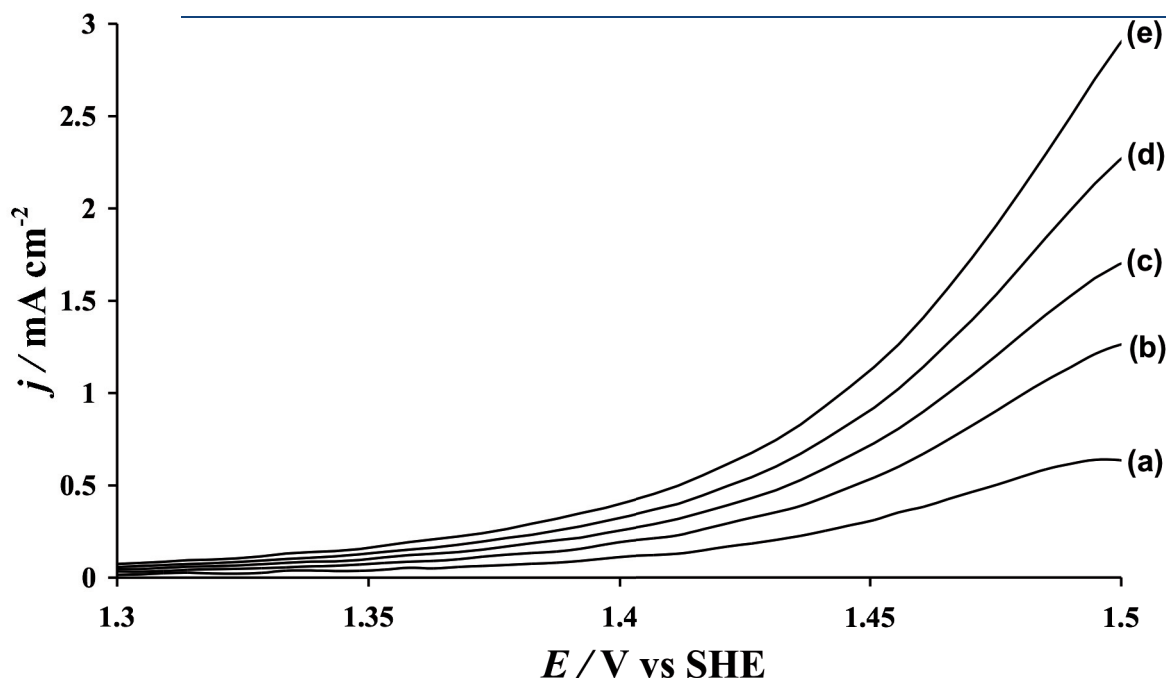


Figure 7-2: Linear voltammograms presented in Figure 7-1(a) after subtraction of the background current (related to OER) using a p-Si/IrO₂ anode (IrO₂ loading: 0.35 mg cm⁻²) for different concentrations of formic acid in 1M HClO₄: (a) 0.2M, (b) 0.4M, (c) 0.6M, (d) 0.8M, (e) 1M. $\nu = 10 \text{ mV s}^{-1}$, $T = 25 \text{ }^\circ\text{C}$ (5th scan).

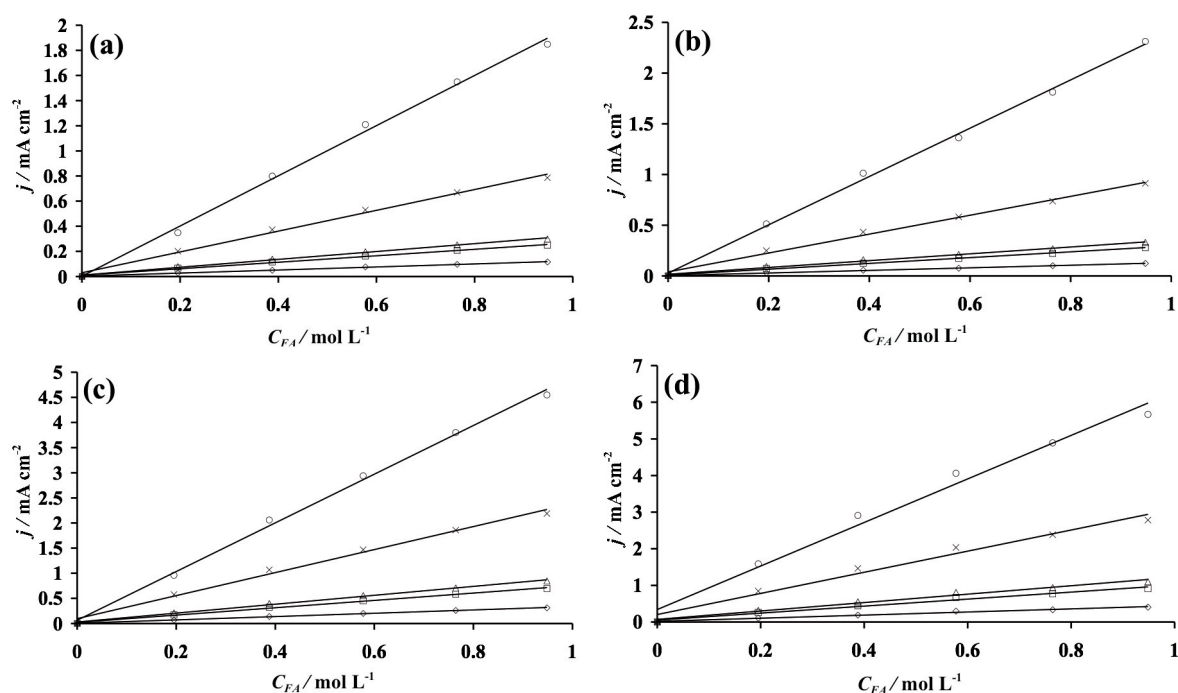


Figure 7-3: Current densities of the background-subtracted linear voltammograms (given in Figure 7-2) plotted vs. the concentration of formic acid for p-Si/IrO₂ anodes with different loadings ((a) 0.35 mg cm⁻², (b) 0.87 mg cm⁻², (c) 1.75 mg cm⁻², (d) 3.5 mg cm⁻²), at fixed anodic potentials (vs. SHE) of: (○) 1.348 V, (x) 1.392 V, (△) 1.402 V, (□) 1.451 V and (◇) 1.5 V.

As a next step, the inverse of the current densities ($1/j$) were plotted against the inverse of the concentration of formic acid ($1/C_{FA}$) at fixed potentials for several IrO₂ loadings (Figure 7-4). This figure validates the linearity predicted by Eq. (7-15) of the model. The apparent rate constant of the oxidation reaction (k_c)_{ap} can, again, be estimated accurately using the slopes of these straight lines.

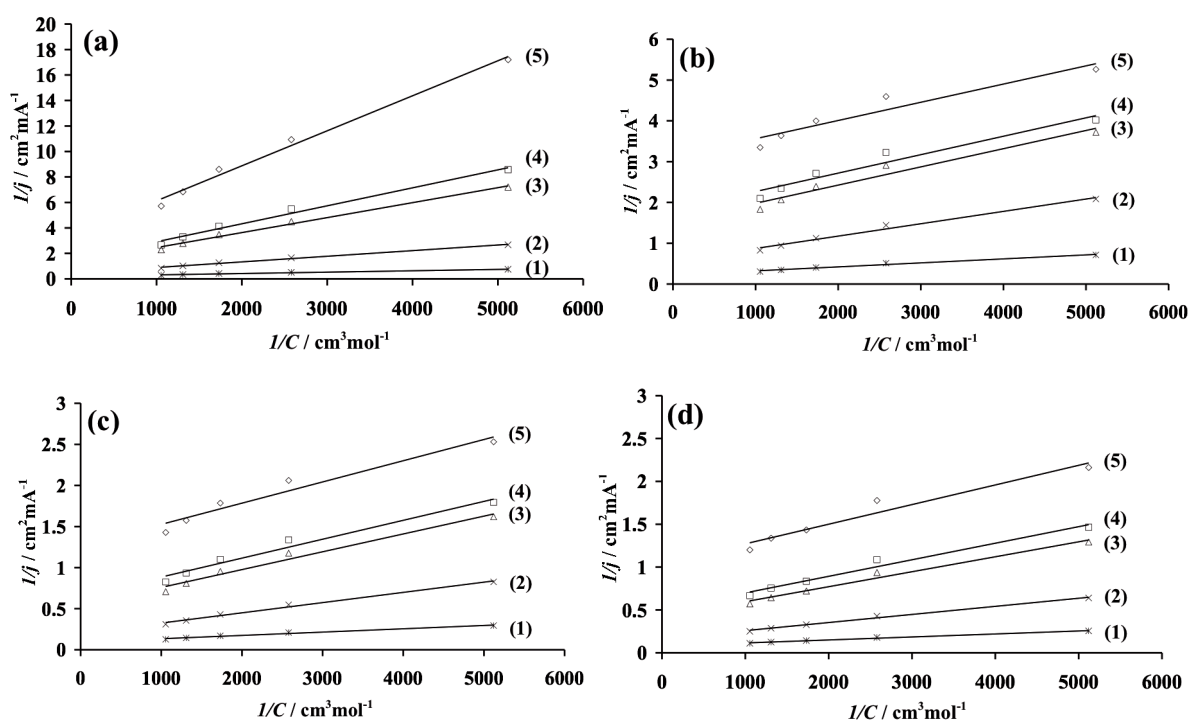


Figure 7-4: Inverse of the current density plotted vs. the inverse of the concentration of formic acid in solution for p-Si/IrO₂ anodes with different loadings ((a) 0.35 mg cm⁻², (b) 0.87 mg cm⁻², (c) 1.75 mg cm⁻², (d) 3.5 mg cm⁻²), at fixed anodic potentials (vs. SHE) of: (○) 1.348 V, (x) 1.392 V, (Δ) 1.402 V, (□) 1.451 V and (◇) 1.5 V.

By plotting the logarithm of the y-intercepts obtained from Figure 7-4 versus the corresponding overpotentials (considering that $E_0 = 1.3$ V [3]), it is possible to estimate the charge transfer coefficient α and the apparent standard rate constant ($k_I^{e,0}$)_{ap} for all IrO₂ loadings using the slopes and y-intercepts of the resulting straight lines (Figure 7-5) together with Eq.(7-14).

The kinetic parameters calculated for all IrO₂ loadings are summarized in Table 7-2. Furthermore, as shown in Figure 7-6, the apparent standard rate constant of the electrochemical reaction of IrO₃ formation ($k_I^{e,0}$)_{ap} and the apparent rate constant of the chemical reaction of formic acid oxidation (k_c)_{ap} both increase with the IrO₂ loading.

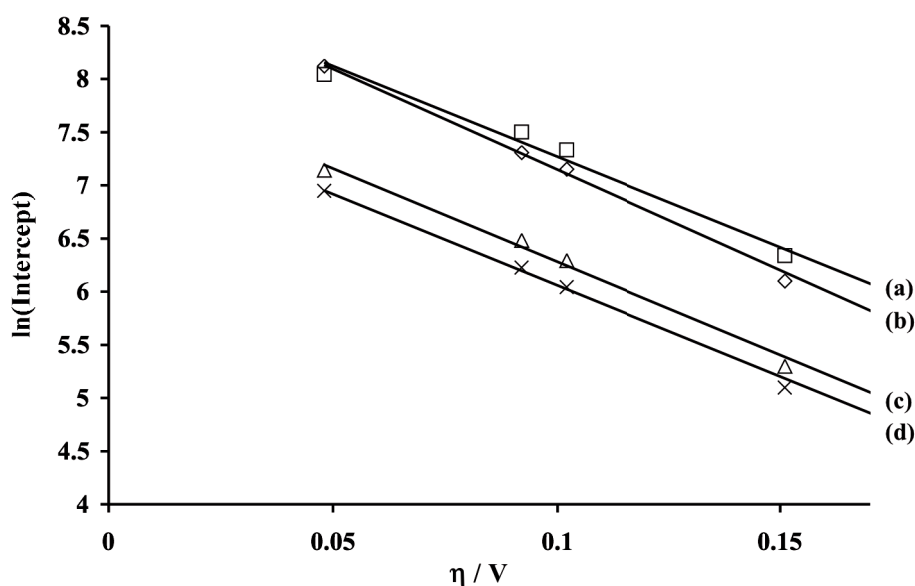


Figure 7-5: Plots of the logarithm of the y-intercepts obtained for different IrO₂ loadings ((a) 0.35 mg cm⁻², (b) 0.87 mg cm⁻², (c) 1.75 mg cm⁻², (d) 3.5 mg cm⁻²) from figure 7-4 versus the corresponding overpotentials η (E₀ = 1.3 V vs. SHE [3]) for formic acid oxidation on p-Si/IrO₂ anodes. T = 25°C.

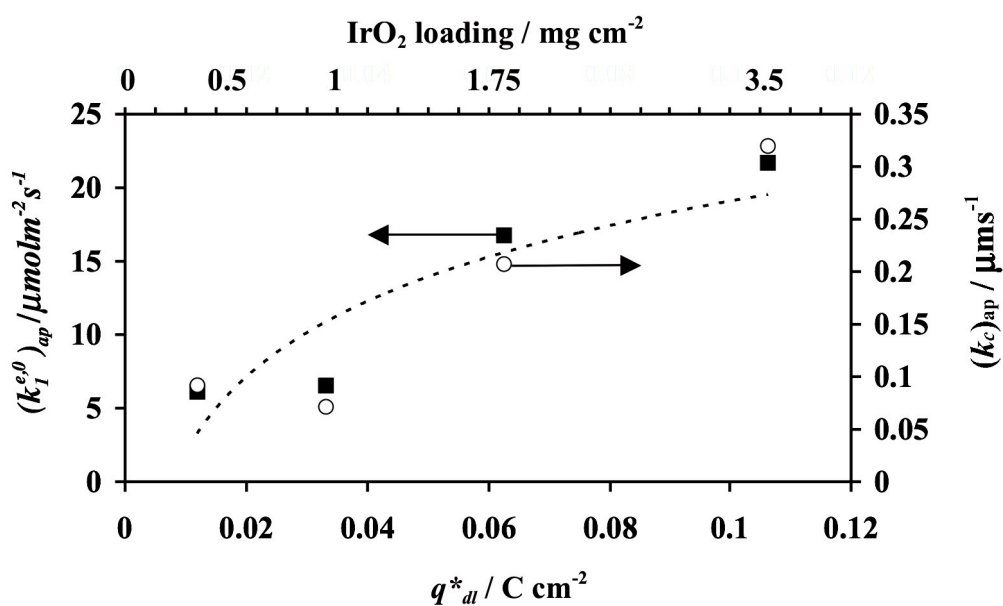


Figure 7-6: Apparent rate constants (k₁^{e,0})_{ap} and (k_c)_{ap} as a function of the double layer capacitance q*_{dl} and the IrO₂ loading. Formic acid oxidation on p-Si/IrO₂. T = 25°C.

For a more accurate comparison, two more aliphatic model compounds (*i*-propanol and 2-butanol) and one model aromatic compound (phenol) were investigated and analyzed consistently using the aforementioned model. These compounds follow similar trends (Table 7-2).

Table 7-2: Kinetic parameters of the oxidation of model organic compounds for different IrO₂ loadings at 25 °C.

Compound	IrO ₂ loading [mg cm ⁻²]	$(k_1^{e,0})_{ap}$ [μmol m ⁻² s ⁻¹]	$(k_c)_{ap}$ [μm s ⁻¹]	α [-]
Formic acid	0.35	6.129	0.092	0.245
	0.87	6.539	0.071	0.221
	1.75	16.761	0.207	0.227
	3.5	21.7	0.32	0.222
<i>i</i> -propanol	0.23	4.39	0.063	0.482
2-butanol	1.63	8.55	0.104	0.374
phenol	2.99	17.488	0.244	0.416

As seen in Table 7-2, the charge transfer coefficient for formic acid oxidation is almost independent of the IrO₂ loading, in contrast to $(k_1^{e,0})_{ap}$, which increases with increasing IrO₂ loadings (further measurements performed using *i*-propanol, 2-butanol and phenol on different IrO₂ loadings have shown the same trend).

This is due to the fact that α is an intensive parameter related with the intrinsic electrocatalytic properties of IrO₂ whereas $(k_1^{e,0})_{ap}$ is an extensive parameter depending on geometric factors. This feature is characteristic of 'active-type' anodes.

Theoretical I-V curves of formic acid oxidation on p-Si/IrO₂ electrodes

In this section, the values obtained for $(k_c)_{ap}$ of FA oxidation for different IrO₂ loadings (Table 7-2) have been used together with Eq.(7-20) of the model proposed in this chapter to provide an estimation of the shift of electrode potential for a given concentration of FA and a given IrO₂ loading. From these calculations and knowing only the I-V curves of the supporting electrolyte, theoretical I-V curves of FA oxidation for different FA concentrations and IrO₂ loadings have been constructed.

Figure 7-7A shows these curves for different concentrations of formic acid using a p-Si/IrO₂ electrode (3,5 mg cm⁻²). For the sake of comparison, Figure 7-7B shows the experimental I-V curves.

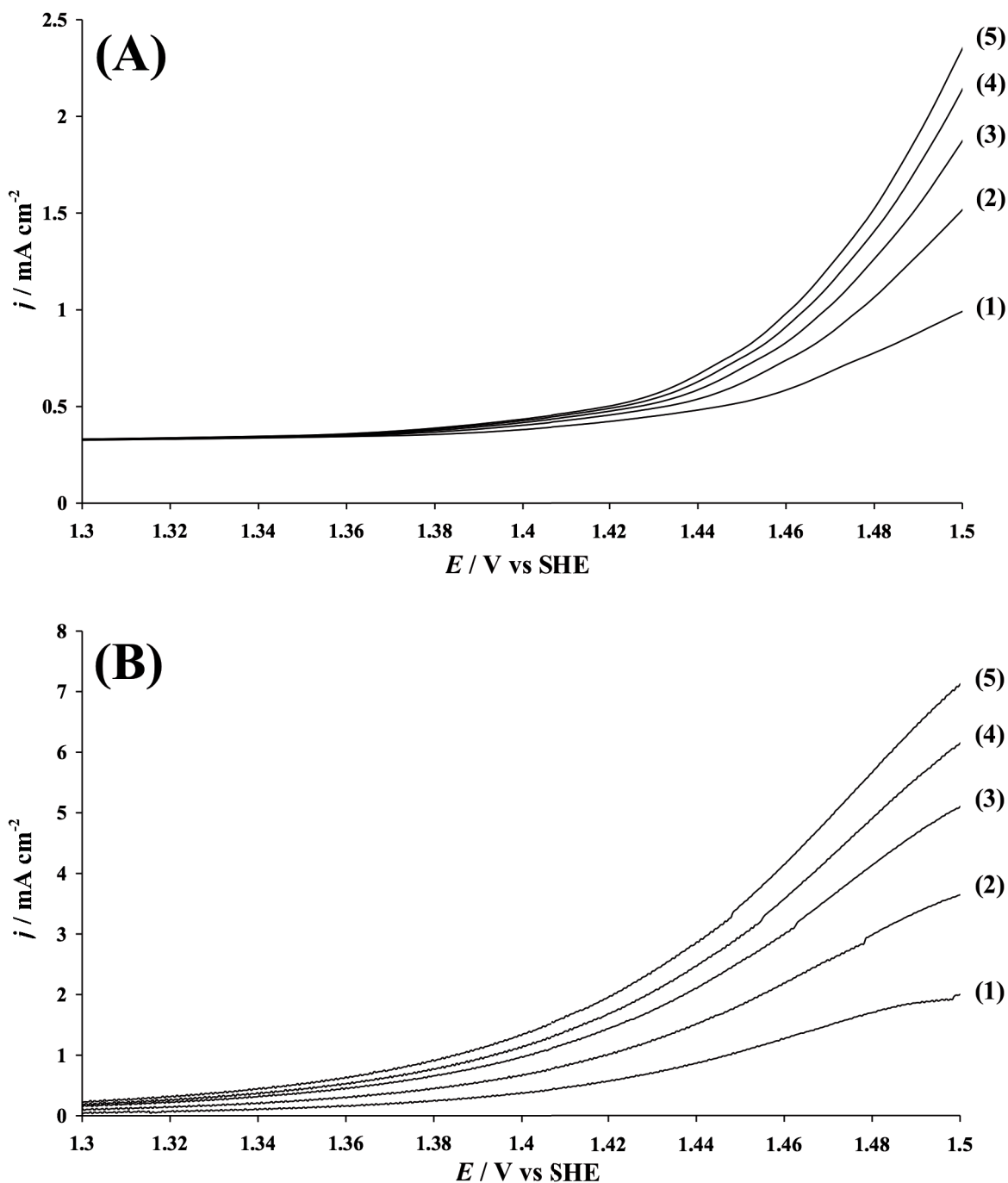


Figure 7-7: (A) Theoretical I-V curves obtained from Eq.(7-20) and (B) Experimental I-V curves of the linear voltammograms presented in Figure 7-1(d) using a p-Si/IrO₂ anode (IrO₂ loading: 3.5 mg cm⁻²) for different formic acid concentrations in 1M HClO₄: (1) 0.2M, (2) 0.4M, (3) 0.6M, (4) 0.8M, (5) 1M. $v = 10 \text{ mV s}^{-1}$, $T = 25 \text{ }^\circ\text{C}$ (5th scan). In both cases the side reaction of oxygen evolution has been neglected.

These figures provide a proof that the theoretical curves follow the same trend as the experimental results. However, the current density measured experimentally for a given potential is higher than the values predicted by the model. The same case was observed for all the other IrO₂ electrodes with different loadings. This is probably due to the fact that in Eq.(7-20) of the model proposed in this chapter, it is assumed that the adsorption constant (K) is equal to 1, which is likely inaccurate. It is possible, however, using the results presented in Figure 7-7, to estimate the expected values of K with a good degree of accuracy. Considering now an average value of $K = 2,5(\pm 0,5)$, we found a very good agreement between the experiments and the theoretical I-V curves for all FA concentrations and IrO₂ loadings.

7.4 Conclusions

The electrochemical oxidation of model aliphatic and aromatic organic compounds on p-Si/IrO₂ electrodes has been investigated using linear potential sweep voltammetry measurements.

From the I-V curves recorded using different IrO₂ loadings and organic concentrations and using a new theoretical model developed in this chapter, the kinetic parameters of the oxidation of various model organic compounds have been estimated. It was found that these kinetic parameters are strongly dependent on the IrO₂ loading.

Furthermore, using the same model together with the above newly estimated kinetic parameters and Nernst equation, it became feasible to evaluate the shift of the I-V curves toward less positive potentials in the presence of an organic compound. Using these results, theoretical I-V curves could be plotted. Small deviations were observed between the experimental and theoretical I-V curves due to the difference between the value of the adsorption constant K assumed for the model ($K = 1$) and the experimental reality. Considering a value of $K = 2,5(\pm 0,5)$, a good agreement between the experimental and theoretical results was observed.

7.5 References

- [1] S. Fierro, T. Nagel, H. Baltruschat, Ch. Comninellis, *Electrochem. Comm.*, 9 (2007) 1969
- [2] S. Fierro, T. Nagel, H. Baltruschat, Ch. Comninellis, *Electrochem. And Solid-State Lett.*, 11 (7) (2008) E20
- [3] F. Beck, H. Schulz, *Electrochim Acta* 29 (1984) 1569

Chapter 8 : Selective oxidation of organic compounds on IrO₂ electrodes

In this chapter, the selective anodic oxidation of model aliphatic (*i*-propanol and 2-butanol) and aromatic (phenol) compounds is investigated on Ti/IrO₂ electrodes in aqueous acidic media using electrolysis experiments.

In the first part of this chapter, a new approach is proposed in order to perform electrochemical oxidation of organic compounds on anode materials by working under galvanostatic conditions with the potential 'buffered' by the competing side reaction of oxygen evolution. According to this procedure, the working potential is fixed by the nature of the electrode material and is 'buffered' during organics oxidation by the side reaction of OER. Using this approach, selective oxidation of *i*-propanol, 2-butanol and phenol has been achieved on IrO₂ electrodes. This behavior was attributed to the low oxidation power of this electrode material (Table 8-1). However, the current efficiency of the oxidation remains low due to the side reaction of O₂ evolution.

The comparison between the chemical and electrochemical hydroxylation of phenol has shown that in the electrochemical process, the formation of *p*-benzoquinone and hydroquinone predominates, in contrast to chemical oxidation, where pyrocatechol is the dominant product. It was found that this high selectivity of the electrochemical hydroxylation towards para-substituted products (benzoquinone and hydroquinone) formation was caused by specific adsorption of phenol molecules on the anode's surface.

This chapter is based on the publications:

S. Fierro, L. Ouattara, E. H. Calderon, E. Passas-Lagos, H. Baltruschat, Ch. Comninellis. Investigation of formic acid oxidation on Ti/IrO₂ electrodes, *Electrochimica Acta*, Volume 54, Issue 7, July 2008, Pages 2053-2061

S. Fierro, E. Passas-Lagos, E. Chatzisyneon, D. Mantzavinos, Ch. Comninellis. Pseudo-potentiostatic electrolysis by potential buffering induced by the oxygen evolution reaction, *Electrochemistry Communications*, Volume 11, Issue 7, May 2009, Pages 1358-1361

E. Chatzisyneon, S. Fierro, I. Karafyllis, D. Mantzavinos, A. Katsaounis. Anodic oxidation of phenol on Ti/IrO₂ electrode: Experimental studies, *Catalysis Today*, accepted manuscript, January 2010

S. Fierro, G. Fòti, Ch. Comninellis in: *Electrolysis: Theory, Types and Applications*, Nova Publishers, New York, 2010

8.1 Introduction

Evidence is mounting for growing interest in oxidative electrochemical processes because of their promising versatility, environmental compatibility and cost effectiveness in selective organic synthesis and electrochemical incineration of organic pollutants (ECI) in aqueous medium. In the case of organic electrosynthesis, the goal is to enhance the reaction selectivity and, in case of the ECI process, to achieve the mineralization of toxic and non-biocompatible pollutants with high current efficiencies [1]. A typical example is the oxidation of organic compounds on platinum-based anodes, for both electrosynthesis and fuel cell applications. The main problem using these electrocatalytic anodes is the reduction of catalytic activity during organics oxidation. The reason behind this reduction

can be explained by the adsorption of reaction intermediates (carbon monoxide) or/and the formation of polymeric material at the anode surface, leading to poisoning or/and fouling.

The anodic oxidation of organics arises from several mechanisms including direct and indirect oxidation. In the direct process, an electron exchange occurs between the organic compound and the electrocatalytic surface of the electrode. In the indirect electrochemical process, the oxidation of organics is mediated by an active redox couple. This process can be homogenous or heterogeneous in nature (see Figure 8-1). In the first case, the mediators (e.g. Ag²⁺/Ag⁺, Mn³⁺/Mn²⁺) dissolved in the electrolyte are reacting with the organic compounds through a homogenous reaction and then are regenerated at the electrode's surface. The main disadvantage of this process is the necessity to separate these mediators from the reaction products after reaction. Heterogeneous mediators are fixed at the surface of the electrode, where the reaction with the organic compounds and their regeneration take place, without contamination of the reaction mixture.

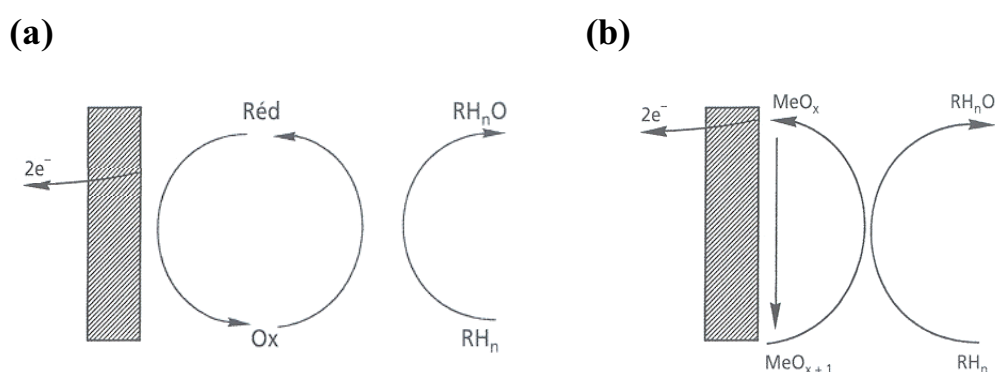


Figure 8-1: Schematic presentation of the indirect electrochemical process for organics oxidation (RH_n to RH_nO) via the redox couple (Ox/Red). (a) Homogeneous (redox couple in solution) (b) Heterogeneous (redox couple fixed at the anode surface)

As far as the IrO₂-based electrodes (prepared by thermal decomposition) are concerned, they were suspected to be good candidates for partial electrochemical oxidation of organics. Furthermore, it was found that when using these electrodes, electrochemical oxidation of organics in aqueous media was occurring with competing side reaction of oxygen evolution without any loss of electrode activity [2,3].

Based on these observations, a general mechanism for anodic oxidation of organics in acidic media (Figure 2-3), including the competition with oxygen evolution, has been

proposed by Comninellis [1,4,5]. This mechanism was validated in the previous chapters (sections 5.3.1 and 0) using differential electrochemical mass spectrometry (DEMS) measurements [6,7].

In the first part of this chapter, a new electrolysis operation mode for organics oxidation under pseudo-potentiostatic conditions induced by the side reaction of oxygen evolution is presented. It is hypothesized that selective oxidation of organic compounds can be achieved on IrO₂ anodes using the latter approach.

Therefore, three series of electrolysis on Ti/IrO₂ electrodes have been carried out. In the first series, the oxidation of formic acid has been investigated to evaluate the performance of these electrodes toward a simple anodic oxidation process. In the second series of experiments, the oxidations of *i*-propanol and 2-butanol were investigated so as to achieve selective oxidation of these compounds using the approach of pseudo-potentiostatic conditions proposed in the first part of the chapter. In the last series, the oxidation of phenol was investigated in order not only to achieve selective oxidation of this aromatic compound using the aforementioned approach but also to compare the specificity of hydroxylation with the classical methods.

8.2 Experimental details

Preparative electrolysis experiments

For the investigation of the anodic oxidation of aliphatic compounds (formic acid, *i*-propanol and 2-butanol), a single compartment electrochemical cell was used.

Due to the complexity of the phenol oxidation process, (the oxidation product of phenol formed at the anode can be reduced at the cathode), a two-compartments cell was used as it is necessary to separate the anodic compartment from the cathodic one using a cationic Nafion® membrane.

Electrolysis using a single compartment electrochemical cell

The cell build-up contains two plastic caps, both 165 mm in diameter. The cathodic cap has a thickness of 10 mm with an aluminum plate integrated as electrical supporter. The anodic cap has a thickness of 50 mm and a depth of 40 mm (including the aluminum plate) including in- and outlet ports for the circulation of the electrolyte.

The Ti/IrO₂-anode (1-4 mg IrO₂ per cm²) and Zr-cathode have a diameter of 100 mm and are 1 mm thick with an effective surface area of 63.62 cm². The inter-electrode gap is 10 mm. Both the Ti/IrO₂ anode and Zr cathode are glued with silverpaste on the aluminum supporting plate, which are equipped with current feeders, as shown in Figure 8-2. The electrodes are separated by two o-rings made of rubber.

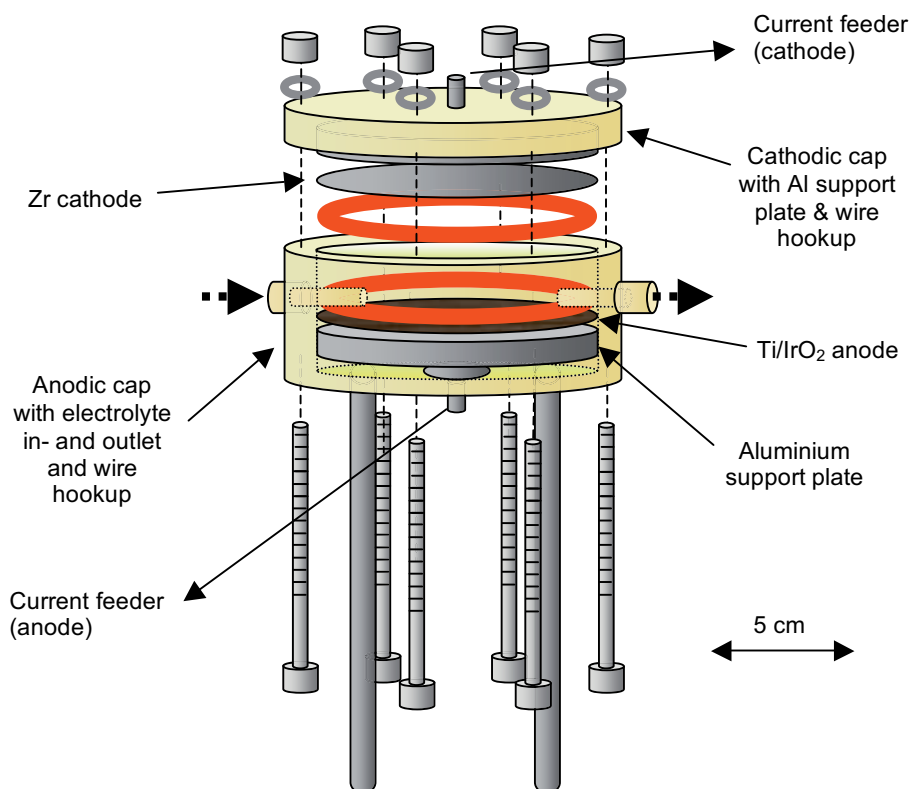


Figure 8-2: Scheme of the one compartment electrochemical cell.

The experimental set-up used is given in Figure 8-3. The electrolyte is recirculated using a pump through the cell and the tank, (volume of 250 mL).

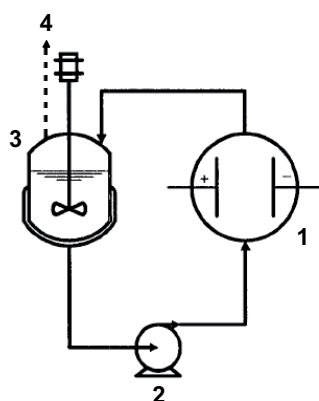


Figure 8-3: Set-up of the single compartment electrolysis experiment: (1) single compartment cell; (2) pump; (3) tank; (4) reflux condenser.

Electrolysis was carried out under galvanostatic conditions and at controlled temperatures (25°C and 50°C) using 250mL of 1M HClO₄ containing the organic compound under investigation.

During electrolysis, several samples were collected at constant intervals for analysis while monitoring the cell potential.

Electrolysis using a two-compartments electrochemical cell separated by a Nafion® membrane

The build-up of this cell is similar to the single compartment cell, the only difference being that this cell contains two symmetrical compartments: one for the anolyte and one for the catholyte as shown in Figure 8-4.

The characteristics of this cell are:

Anode-cathode distance: 10mm

Anode effective surface (Ti/IrO₂): 63.6 cm² (IrO₂ loading: 2.6 mg cm⁻²)

Cathode surface (Zr): 63.6 cm²

Separator (anode/cathode): Nafion® 117

The Nafion® N117 / H⁺ (Du Pont Polymers, Fayetteville, North Carolina) has been treated during 2h in a 2M HNO₃ solution at 80 °C and was subsequently washed with

Millipore water, treated again in nitric acid for 2h at 80 °C and finally washed several times with Millipore water. The membrane was kept under water before use.

The experimental set up used is shown in Figure 8-5. The anodic and cathodic compartments of the electrolytic cell, which are separated by a Nafion® membrane, are both thermostated electrolyte tanks, each with a volume of 500 mL. Using two pumps, the catholyte/anolyte solutions are circulating inside the cell through the electrode chambers. The flow rates of the hydrogen and oxygen gases generated by the electrolysis were measured with gas analyzers.

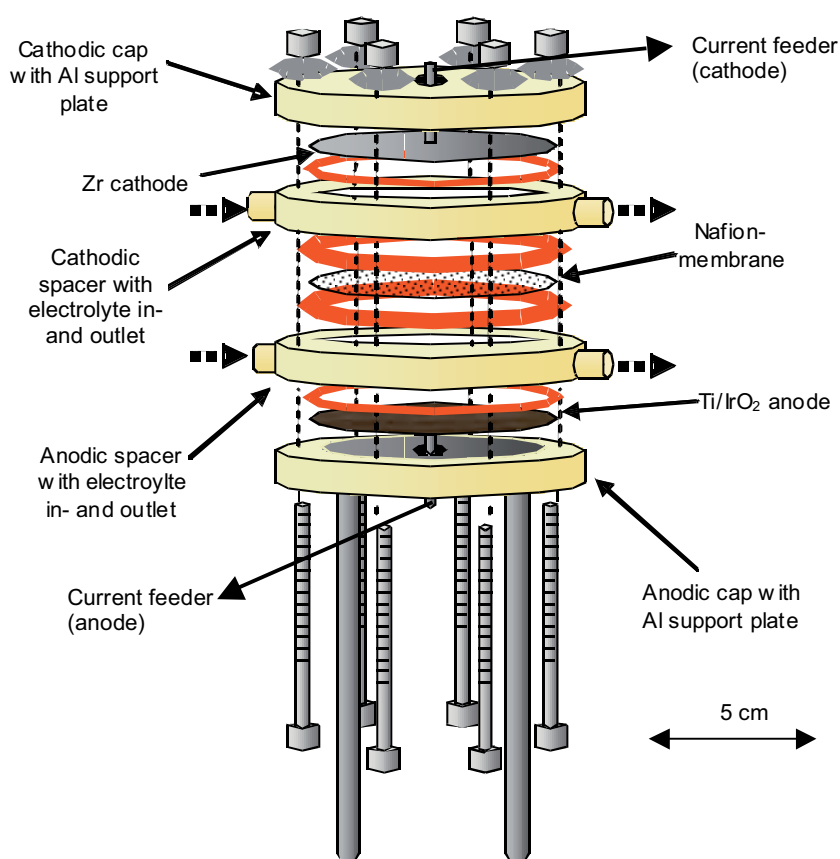


Figure 8-4: Scheme of the electrochemical cell separated by a Nafion® membrane.

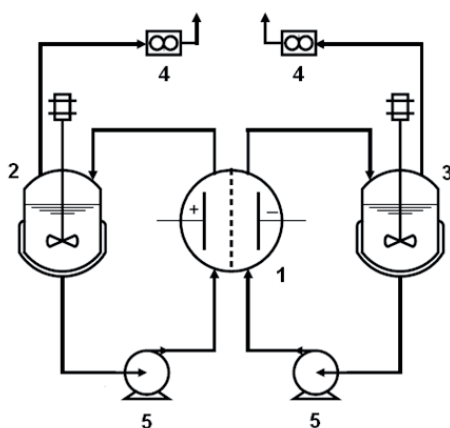


Figure 8-5: Experimental set-up of the electrolysis using the two-compartment cell: (1) Nafion® separated two compartments cell; (2) anodic electrolyte tank; (3) cathodic electrolyte tank; (4) gas analyzers; (5) pumps.

To check our electrolysis system, bulk electrolysis under galvanostatic conditions was carried out in the two-compartment cell using a 1M HClO₄ solution. The volumetric flow rates of hydrogen and oxygen formed at the cathode and at the anode respectively were also measured.

The molar flow rates measured experimentally for both H₂ and O₂ were then plotted against the applied current. If the plots of the experimental data are in agreement with the theoretical plots predicted by Faraday's law (as is shown in Figure 8-6), we can confidently ascertain that the cell is working properly and that it is possible to start the electrolysis experiments.

This check should be done on a regular basis in order to guarantee the functionality of the electrolysis system.

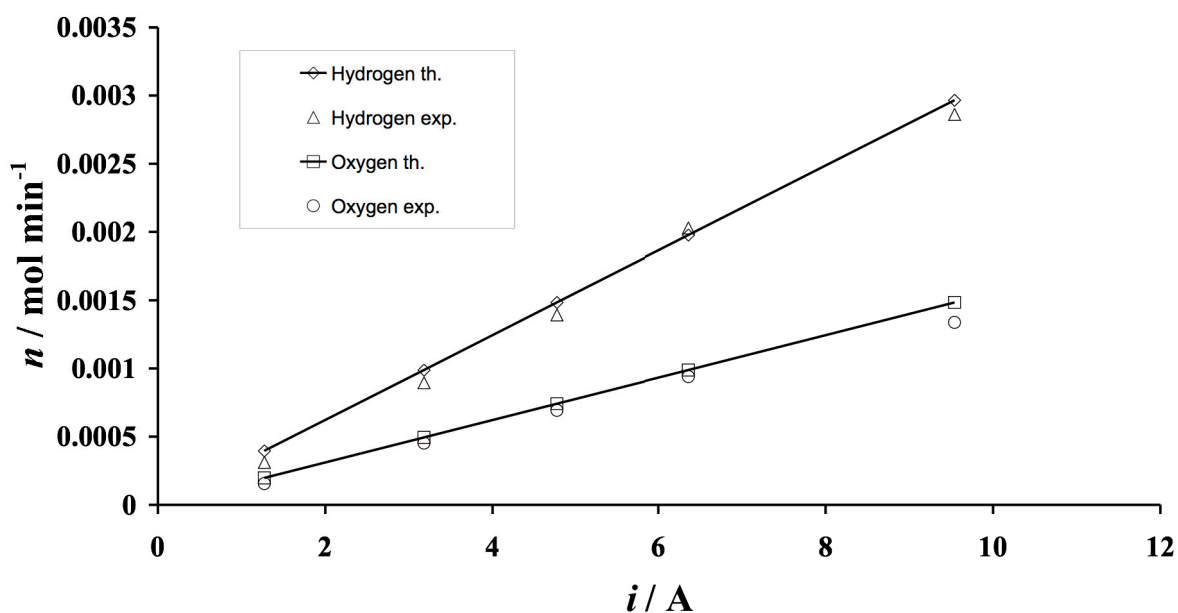


Figure 8-6: Comparison between the H₂ and O₂ flow rates predicted by Faraday's law and the same flow rates measured experimentally during electrolysis of a 1M HClO₄ solution (separated cell).

For the preparative electrolysis experiment, the anodic tank is filled up with 500 mL of phenol solution in 1M HClO₄ and to avoid an overpressure on the Nafion® membrane, the cathodic tank is filled simultaneously with 500 mL of the supporting electrolyte (1M HClO₄). Once the pumps are turned on, all necessary measures were taken to eliminate the presence of air bubbles that could disturb the circulation of the electrolyte while the thermostat keeps the solutions at a constant temperature (25°C and 50°C).

During electrolysis, samples have been taken from the anolyte compartment at constant time intervals for analysis. The cell potential was also monitored during electrolysis.

Determination of the average mass transfer coefficient for both reactors

The average mass transfer coefficient (k_m) for the oxidation of $[\text{Fe}(\text{CN})_6]^{3-}$ (Eq.(8-1)) in the electrochemical reactor was determined by measuring the anodic limiting current density (j_{lim}) using a solution of 10mM $[\text{Fe}(\text{CN})_6]^{3-}$ in 0.5M Na₂SO₄. Using the previously estimated values for the limiting current j_{lim} , the mass transfer coefficient k_m was determined according to Eq.(8-2):



$$k_m = \frac{j_{lim}}{F \cdot C} \quad (8-2)$$

where F is the Faraday's constant and C is the concentration of $[Fe(CN)_6]^{3-}$ in the solution (10mM). The limiting current was estimated to be about 3.86 mA·cm⁻² and so the mass transfer coefficient k_m could be evaluated to be in the order of 2·10⁻⁵m s⁻¹ for a flow rate of 200 L h⁻¹.

It is worthwhile to mention that the mass transfer coefficient measured above, which corresponds to reaction (8-1), is most likely different from the mass transfer coefficient associated with the oxidation of a given organic compound ($k_{m,Org}$).

Despite this difference, the mass transfer coefficient for organics oxidation ($k_{m,Org}$) under the same hydrodynamic conditions can be estimated using the following relation (Eq.(8-3)).

$$k_{m,Org} = \frac{D_{Org}}{D_{[Fe(CN)_6]^{3-}}} k_{m,[Fe(CN)_6]^{3-}} \quad (8-3)$$

where D (m² s⁻¹) is the diffusion coefficient.

Analytical methods used

The methods used are the analysis of the Chemical Oxygen Demand (*COD*) and the Total Organic Carbon (*TOC*), High Performance Liquid Chromatography (*HPLC*) and Gas Chromatography (*GC*).

Chemical oxygen demand (COD)

The chemical oxygen demand is measured by the Hach *COD* method. It is a commercial adaptation of the work of Jirka and Carter [8], where an oxidation takes place in a tube

containing a reagent made up of potassium dichromate, sulfuric acid, a silver salt and mercuric sulfate. The silver salt acts as a catalyst for the oxidation of the organic compounds and the mercuric(II)-sulfate reduces the interferences caused by the presence of chlorides.

Two milliliters of the solution to be analyzed are introduced into the reaction tube, which is heated 2h at 150 °C. After the tube has been cooled down to room temperature, the value of the chemical oxygen demand (in mgL⁻¹) can be read directly on the spectrophotometer's screen (DR 2010, Hach Company, Loveland, Colorado). This is done after calibration of the device using the pure electrolyte (1M HClO₄). The error depended on the sample and was generally lower than 10%.

Total organic carbon (TOC)

The principle of total organic carbon analysis is based on the complete combustion of organics in a pure oxygen flow. It takes place in a furnace at 680 °C, containing platinum/aluminum-based catalysts. The carbon dioxide formed is quantified by infrared spectrometry and the TOC of the acidified sample (in order to eliminate the inorganic carbon) is directly estimated (in mg carbon per litre) using a Shimadzu TOC-5050 device (Shimadzu Corporation, Tokyo, Japan).

Each measurement was repeated three times, in order to guarantee a high degree of accuracy in the computed values ($\approx 98\%$). The accuracy of the measurements depended on the calibration and the nature of the compounds to be analyzed; the error was generally lower than 10%.

High performance liquid chromatography (HPLC)

The global parameters COD and TOC mentioned previously do not allow for a direct quantitative determination of the products formed during electrolysis. The technique used to analyze these products is named high performance liquid chromatography (HPLC). The separation of the products formed is based on the principle of ionic exclusion. The analyses are carried out using a solvent mixture. The mobile phase contains 55% of acetonitrile and 45% of 10% glacial acetic acid in our case flowing at 0,8 cm³·min⁻¹. For our HPLC analysis, a Shimadzu LC-2010 device (Shimadzu Corporation, Tokyo, Japan) with a Nucleosil 100-5 C₁₈ column was used.

Gas chromatography (GC)

Aliphatic compounds such as *i*-propanol or 2-butanol, as well as their oxidation products, are not appropriate to be analyzed with HPLC. In GC analysis used here, the mobile phase is composed of the vaporized sample (at 250 °C) and an inert carrier gas (N₂), which flows through a narrow column filled with a polar layer of polyethyleneglycol (stationary phase, J&W DB-WAX) at 0,7 mL min⁻¹. At the column's exit, the separated compounds are detected electronically based on their specific retention time by a flame ionization detector (FID). For our GC analysis, an Agilent 6850-Series GC device (Agilent Technologies, Santa Clara, USA) was used.

8.3 Results and discussion

8.3.1 A new approach for electrolysis experiments: Pseudo-potentiostatic operation by anode potential buffering induced by the oxygen evolution reaction

Oxidative electrochemical processes have been recently the subject of active research. In these studies it is common practice to perform these oxidations under potentiostatic conditions so as to guarantee a high selectivity for a given product (in electrosynthesis). However, operating under potentiostatic conditions requires a reference electrode as well as a powerful potentiostat, which are unavoidable limiting factors.

In this chapter, a new approach is proposed to perform electrochemical oxidation of organics by working under galvanostatic conditions with the anode potential 'buffered' by the competing side reaction of oxygen evolution (OER). In fact, the anode potential is governed by the overpotential of oxygen evolution on the selected anode material. Table 8-1 shows different anode materials with their oxidation potential, which is fixed by the overpotential of oxygen evolution. Furthermore this table shows that the higher the oxygen evolution overpotential is, the higher the oxidation power of the anode becomes.


As a general rule, the oxidation power of the anode increases with the overpotential of oxygen evolution of a given material (Table 8-1). In fact, 'active' type anodes such as IrO₂ electrodes have a low oxidation power while 'non-active' type anodes such as BDD have a high oxidation power.

The principle of the anode potential buffering induced by the oxygen evolution reaction can be investigated by observing the polarization curves obtained using *i*-propanol as organic compound on iridium dioxide and BDD electrodes (Figure 8-7).

This figure shows that a large increase in current results into a small change of the anode potential due to potential 'buffering' induced by the side reaction of oxygen evolution. As a matter of fact, a change of one decade in current (Δj on Figure 8-7) will induce a shift of 40mV of the IrO₂ electrode's potential and a shift of 120mV for the boron doped diamond electrode. These potential shifts are related to the respective Tafel slopes for the oxygen evolution reaction of IrO₂ and BDD electrodes [9,10].

Therefore, and because the oxidation power of IrO₂ electrodes is low (low overpotential of oxygen evolution), selective electro-organic synthesis is expected to proceed efficiently on IrO₂ electrodes using this approach. This will be verified in this chapter through electrolysis experiments of model organic compounds using Ti/IrO₂ anodes.

Table 8-1: Oxidation power of different anode materials

Electrode	Oxidation potential / V	Overpotential of O ₂ evolution / V	Oxidation power of the anode
RuO ₂	1.4-1.7	0.18	
IrO ₂	1.5-1.8	0.25	
Ti/PtO _x	1.7-1.9	0.3	
Ti/PbO ₂	1.8-2.0	0.5	
Ti/SnO ₂ -Sb ₂ O ₅	1.9-2.2	0.7	
p-Si/BDD	2.2-2.6	1.3	

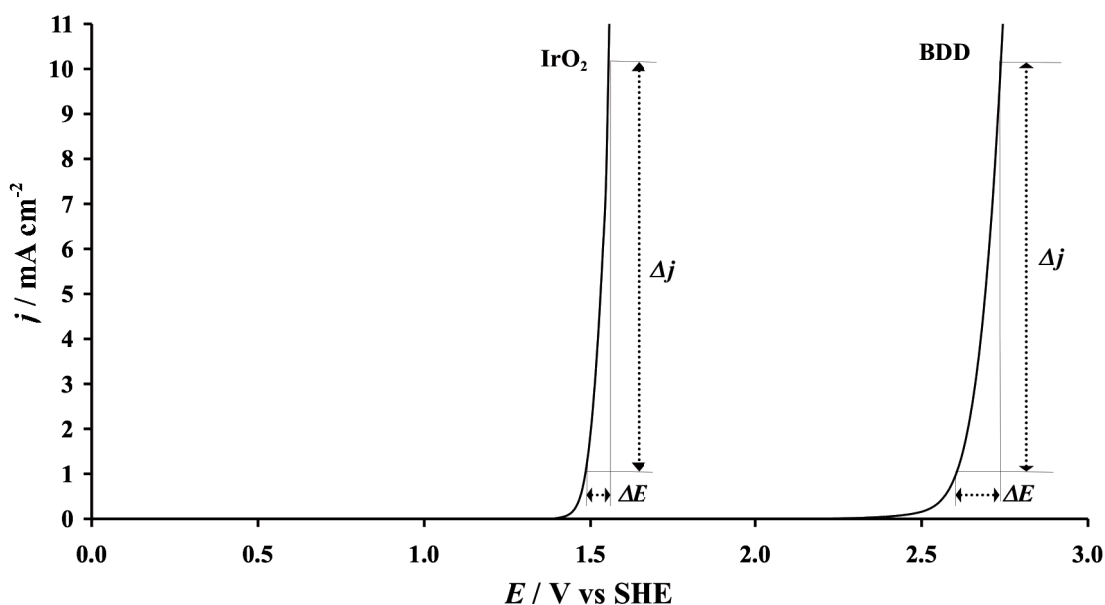


Figure 8-7: Principle of the anode potential buffering induced by the oxygen evolution reaction using a steady state polarization curve obtained in 1M HClO₄ + 100mM *i*-propanol on Ti/IrO₂ and boron doped diamond anodes. A change of one decade in current induces a shift of 40mV of the anode's potential for the Ti/IrO₂ anode and a shift of 120mV for the BDD anode.

8.3.2 Electrolysis of model organic compounds on Ti/IrO₂

Formic acid (FA) oxidation using Ti/IrO₂

The oxidation of FA on Ti/IrO₂ anodes is investigated in order to evaluate the performance of these electrodes during a simple anodic oxidation process. In fact, FA is oxidized to CO₂ without formation of intermediates (Eq.(8-4)).



Electrolysis has been carried out using a 0.75 M formic acid solution in 1M HClO₄ under galvanostatic conditions (85 mA cm⁻²). During electrolysis, the concentration of FA in the supporting electrolyte has been analyzed and displayed as a function of time. The temporal evolution of FA concentration obtained experimentally was then compared with

the predictions of the theoretical model proposed by P.-A. Michaud [11], which is based on the maximum rate of oxidation and is given in the bibliography (Chapter 2 section 2.5). This comparison is presented in Figure 8-8. In this model, the COD has been replaced by the concentration of formic acid because it is directly oxidized to CO₂ without formation of any intermediates in solution (Eq.(8-4)).

The limiting current for the oxidation of formic acid at a given time was estimated via the following relation (Eq.(8-5)):

$$j_{\text{lim},t} = 2Fk_{m,FA} \cdot [FA]_t \quad (8-5)$$

with $[FA]_t$ being the concentration of formic acid (mol L⁻¹) at a given time and $k_{m,FA}$ the mass transfer coefficient (m s⁻¹) of FA oxidation calculated using Eq.(8-3) with $D_{HCOOH} = 1.8 \cdot 10^{-7}$ cm² s⁻¹.

Figure 8-8 suggests a very good agreement between the experimental results and the theoretical predictions.

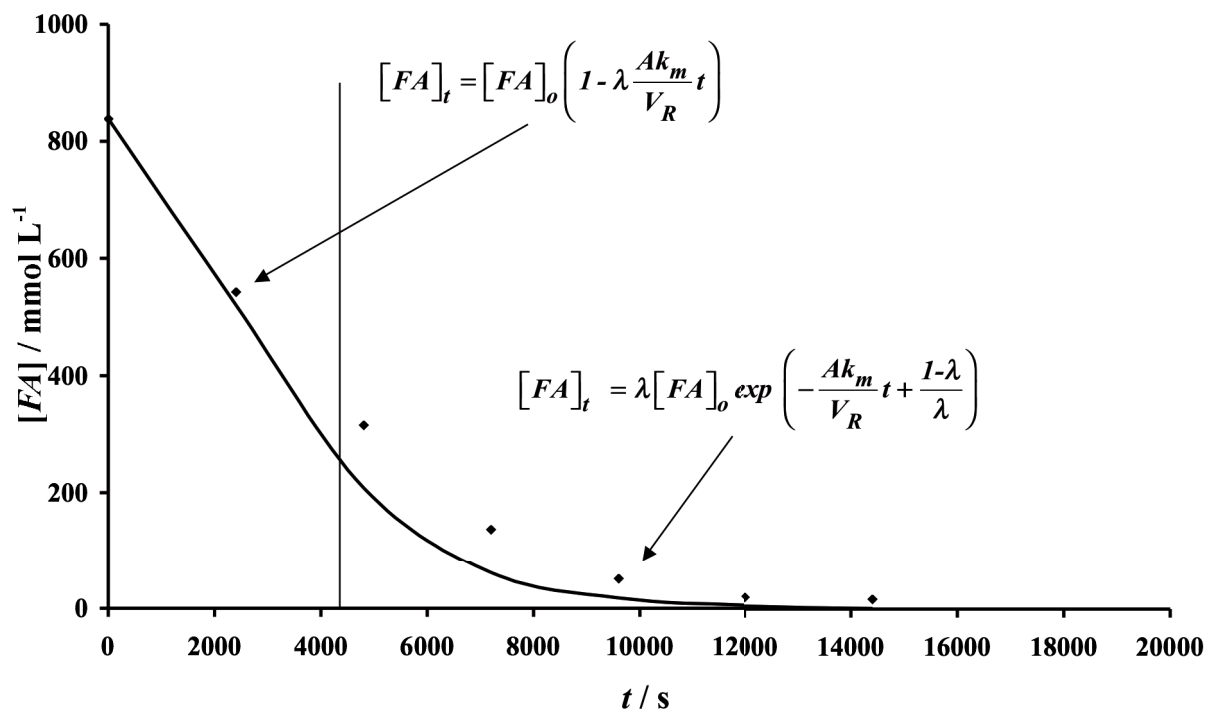


Figure 8-8: Experimental (dots) and theoretical (continuous line) temporal evolution of formic acid (FA) concentration during electrolysis of a 0.75 M formic acid solution in 1M HClO₄ on a Ti/IrO₂ anode (2.3 mg·cm⁻²) at 50 °C (one compartment cell, $j_{\text{applied}} = 85$ mA·cm⁻²). Estimated anode potential: 1.7±0.05 V vs. SHE.

In fact, in agreement with the model, the concentration of formic acid measured experimentally decreases linearly until a critical time t_{cr} of 4357 s after which it decreases exponentially with time. Furthermore, the instantaneous current efficiencies (ICE) determined experimentally are in good agreement with the values predicted by the model (Figure 8-9). In fact, for both the experimental and theoretical evolutions, the ICE has a value of 100% up to the aforementioned critical time, after which the latter decreases exponentially to zero.

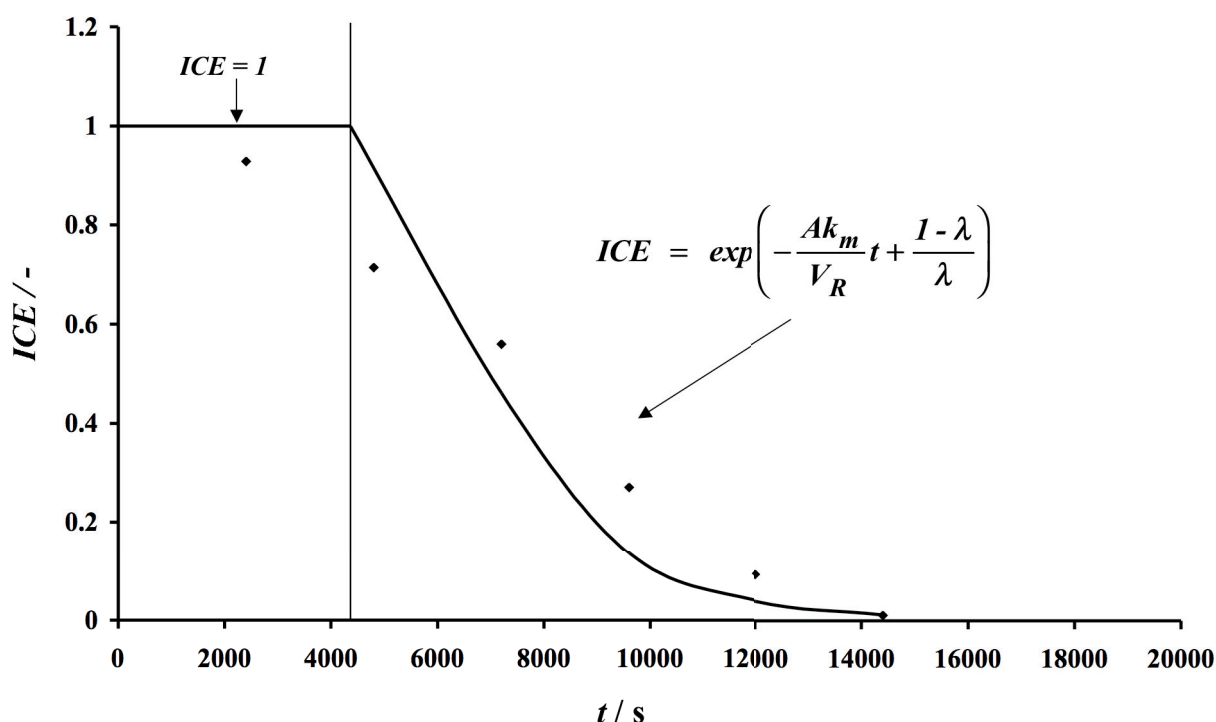
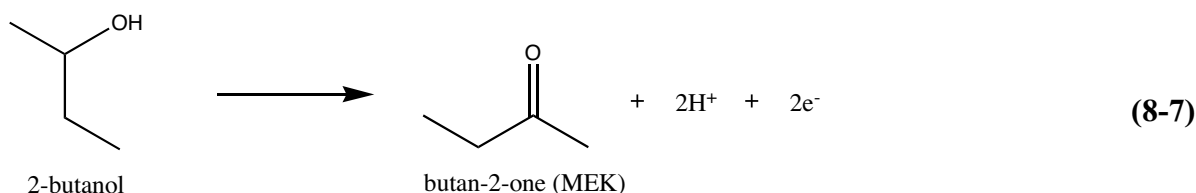
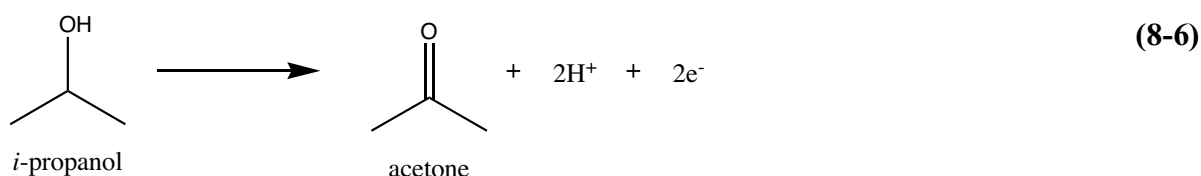


Figure 8-9: Experimental (dots) and theoretical (continuous line) temporal evolutions of the instantaneous current efficiency (ICE) during electrolysis of a 0.75 M formic acid solution in 1M HClO₄ on a Ti/IrO₂ anode (2.3 mg·cm⁻²) at 50 °C (one compartment cell, $j_{applied} = 85 \text{ mA}\cdot\text{cm}^{-2}$). Estimated anode potential: $1.7 \pm 0.05 \text{ V vs. SHE}$.

The good agreement observed between the experimental results and the predictions of the model provides a strong evidence that the key assumptions behind this model remain valid (see section 2.5) i.e. that the reaction of formic acid with electrogenerated IrO₃ (Eq. (7-5)) is a fast reaction and that the process is controlled by mass transport.

***i*-propanol and 2-butanol oxidation using Ti/IrO₂**

The principle of pseudo potentiostatic oxidation (described in the previous paragraph) has been applied for the selective oxidation of *i*-propanol and 2-butanol on Ti/IrO₂ anodes. In fact, *i*-propanol is oxidized to acetone according to Eq.(8-6) and 2-butanol is oxidized to butan-2-one or methyl ethyl ketone (MEK) according to Eq.(8-7):



The selectivity for the targeted oxidation product (acetone and MEK respectively in this case) S_p (-) has been calculated using the following relation (Eq.(8-8)):

$$S_p = \frac{C_p(q)}{C_R^0 - C_R(q)} \tag{8-8}$$

Where $C_p(q)$ is the concentration of the targeted product after the passage of a specific electrical charge q (Ah L⁻¹) while C_R^0 and C_R (mol L⁻¹) are the concentrations of starting material at the beginning of the electrolysis and after the passage of a specific electrical charge q respectively.

Electrolysis have been carried out using a 0,77 M *i*-Pr in 1M HClO₄ solution for *i*-propanol oxidation and a 0,73 M 2-butanol solution in 1M HClO₄ for 2-butanol oxidation under galvanostatic conditions (85 mA cm⁻²). During electrolysis, the concentration of starting material (*i*-propanol and acetone respectively) and the concentration of the oxidation products (2-butanol and MEK respectively) in the supporting electrolyte have been

analyzed and displayed as a function of the specific charge passed. Using these measurements and Eq.(8-8), the selectivity for the formation of the corresponding ketone was determined and plotted as a function of the specific charge passed together with the total mass balance, which is the sum of the concentrations of *i*-propanol and acetone (respectively the sum of the concentrations of 2-butanol and MEK). The results are shown in Figure 8-10 for the oxidation of *i*-Pr and in Figure 8-11 for the oxidation of 2-butanol.

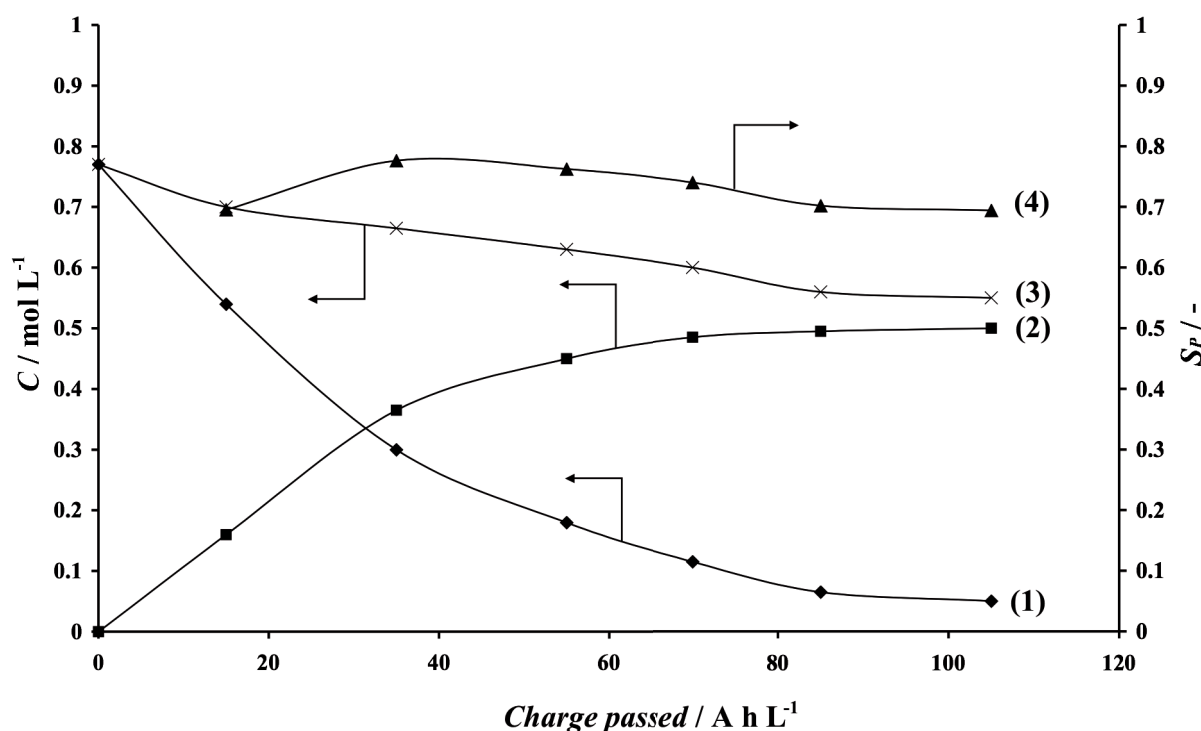


Figure 8-10: Evolution of *i*-propanol concentration (1), acetone concentration (2), total mass balance (3) and acetone selectivity (4) (Eq.(8-8)) during the oxidation of *i*-propanol (0,77M in 1M HClO₄) on Ti/IrO₂ anode at 50°C under galvanostatic conditions (85 mA cm⁻²). Estimated anode potential: 1,7±0.05 V vs. SHE.

These figures show similar results i.e., a high selectivity (70-80%) for the formation of the corresponding ketone even for high conversions of the starting material (80-90%) and under non-optimized conditions.

A decrease in the total mass balance, which is the sum of the concentrations of the starting materials and the oxidation products, was observed for both oxidations suggesting in turn that a fraction of the starting material was mineralized. During the electrolysis, the cell potential remained constant (4.3±0.1 V) and the anode potential was

estimated at 1.7 ± 0.05 V using I-V curves recorded in 1M HClO₄ + *i*-propanol ($j = 85$ mA cm⁻²).

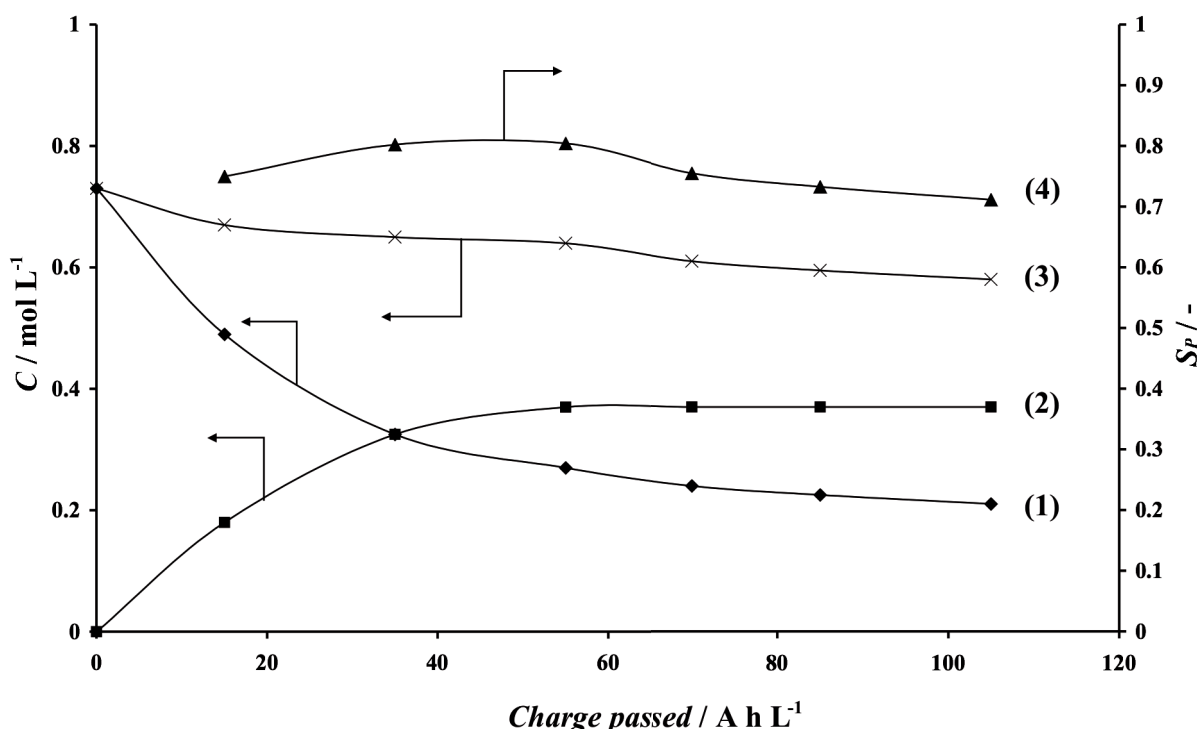


Figure 8-11: Evolution of 2-butanol concentration (1), methyl ethyl ketone (MEK) concentration (2), total mass balance (3) and MEK selectivity (4) (Eq.(8-8)) during the oxidation of 2-butanol (0,73M in 1M HClO₄) on Ti/IrO₂ anode at 50°C under galvanostatic conditions (85 mA cm⁻²). Estimated anode potential: $1,7 \pm 0.05$ V vs. SHE.

Moreover, the current efficiency of ketone formation does not exceed 2% during electrolysis (not shown), which is due to the side reaction of O₂ evolution. In fact, this side reaction allows working under pseudo-potentiostatic conditions by inducing potential buffering.

Furthermore, the temporal evolutions of instantaneous current efficiency (ICE) and COD determined experimentally (not shown) deviate strongly from the values predicted by the model based on the maximum rate presented in the bibliography (section 2.5). On the opposite, a good agreement was found between the experimental and predicted values for the case of FA oxidation. This is likely related to the slow oxidation rate of both *i*-propanol and 2-butanol oxidations and to the anodic stability (toward further oxidation) of the ketones formed due to the buffering of the anode potential at 1.7 ± 0.05 V, which is induced by the side reaction of O₂ evolution.

Phenol oxidation on Ti/IrO₂ electrodes

The first step of phenol oxidation involves the formation of hydroxylated products both ortho (pyrocatechol, reaction (2) in Figure 8-12) and para (hydroquinone, reaction (1) in Figure 8-12) substituted, which are further oxidized into the corresponding quinones (reactions (3) and (5) in Figure 8-12). The goal of this study is not only to investigate the possibility of selective oxidation under pseudo potentiostatic conditions but also to compare the specificity of the hydroxylation of phenol (reactions (1), (2), (3) and (5) in Figure 8-12) with the classical methods.

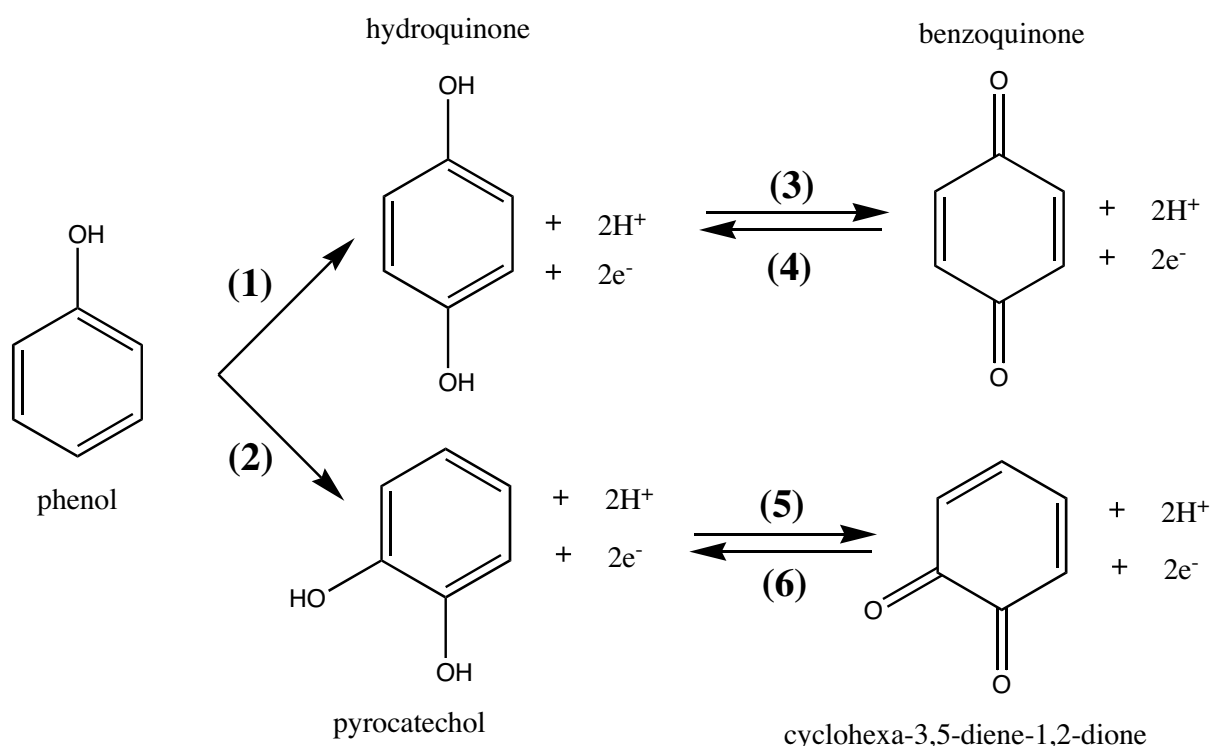


Figure 8-12: Mechanism of phenol oxidation

In order to prevent the cathodic reduction of the quinones formed (reactions (4) and (6) on Figure 8-12), it is necessary to separate the anodic from the cathodic chamber with a cationic membrane (Nafion®).

The electrolysis of a 10mM phenol solution on Ti/IrO₂ anode in 1M HClO₄ has been carried out under galvanostatic conditions (55 mA cm⁻²) at 25 and 50 °C in both the single and the two-compartments cell described in paragraph 0 of this chapter. During electrolysis, the concentrations of phenol and its oxidation products (hydroquinone, *p*-benzoquinone and pyrocatechol) have been analyzed and reported as a function of the

specific charge passed. Furthermore, the selectivities of hydroquinone (S_{hydro}), *p*-benzoquinone (S_{benzo}), pyrocatechol (S_{pyro}) together with the total aromatic selectivity ($S_{arom} = S_{hydro} + S_{benzo} + S_{pyro}$) were determined using Eq.(8-8) and plotted as a function of the specific passed charge as well.

Electrolysis in a two-compartments cell (Figure 8-4)

In Figure 8-13 presents the results obtained for the electrolysis experiment conducted in the two-compartment cell at 50°C. This figure shows that about 90% of the phenol in solution was converted into intermediates (hydroquinone, benzoquinone and pyrocatechol through reactions (1), (3) and (2) of Figure 8-12 respectively) after the passage of 50 Ah L⁻¹ of specific charge. The total mass balance remained stable during the entire experiment, which suggests that no starting material or oxidation products were mineralized during the process. Benzoquinone is the favored oxidation product (reaction (3) in Figure 8-12), reaching a selectivity of more than 70% (≈ 6.5 mmol L⁻¹). The cell potential remained constant during electrolysis (4.5±0.2 V).

The values obtained for η_{Total} during the electrolysis carried out at 50°C (Figure 8-14) show that most of the current is used for the side reaction of oxygen evolution. In fact, this side reaction allows working under pseudo-potentiostatic conditions.

At 25°C the same trend was observed but with slightly lower phenol conversion and slightly lower selectivities for the formation of intermediates.

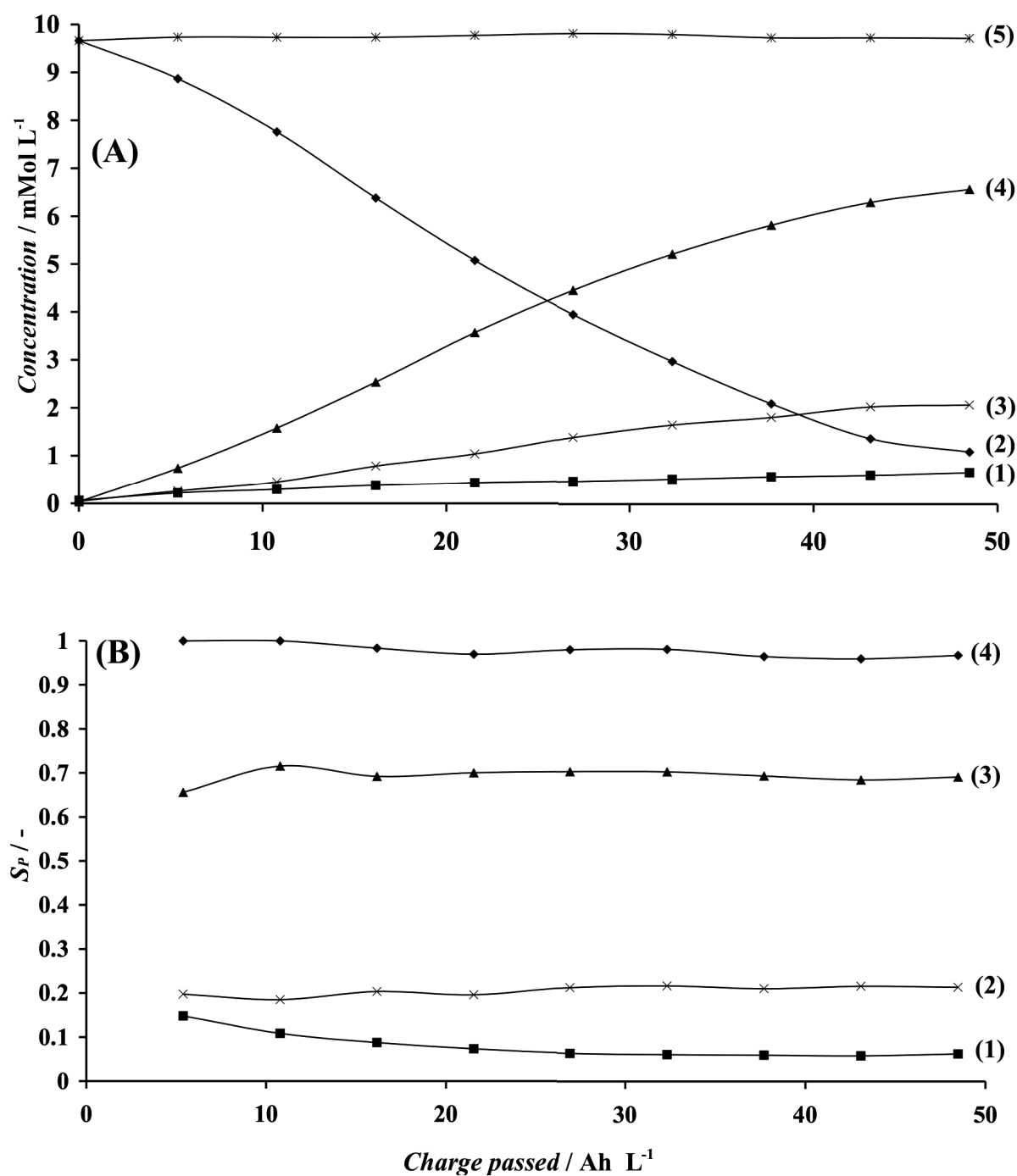


Figure 8-13: (A) Hydroquinone (1), phenol (2), pyrocatechol (3), benzoquinone (4) and the total mass balance (5) concentrations. (B) Hydroquinone (1), pyrocatechol (2) and benzoquinone (3) selectivities (Eq.(8-8)) and total aromatic selectivity (4) as a function of the specific charge passed during electrolysis of phenol (10mM phenol in 1M HClO₄) on Ti/IrO₂ anode at 50 °C under galvanostatic operation (55 mA·cm⁻²) in the two-compartment cell.

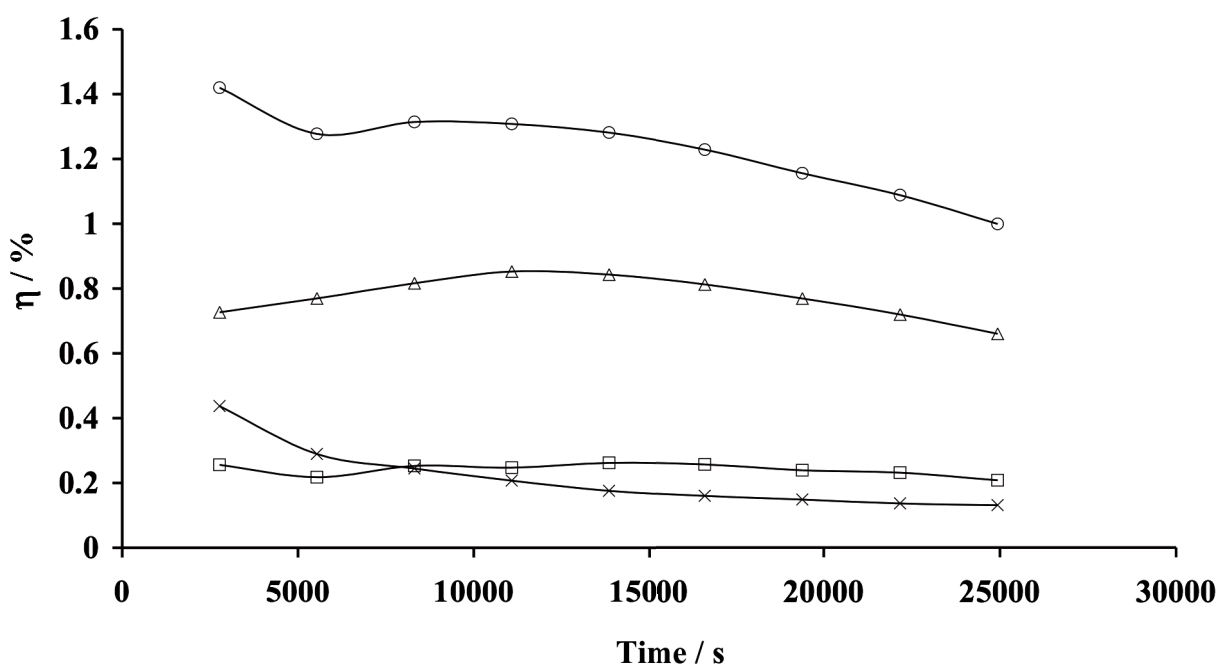


Figure 8-14: Partial current efficiency for the oxidation of phenol into (Δ) benzoquinone, (x) pyrocatechol and (□) hydroquinone. (○) total current efficiency for phenol oxidation into benzoquinone + catechol + hydroquinone. Conditions: idem Figure 8-13.

Electrolysis in a single-compartment cell (Figure 8-2)

Electrolysis of phenol was performed at 50°C under the same galvanostatic conditions described in the precedent paragraph but this time using a single-compartment cell. The results (Figure 8-15) indicate that the main product formed was hydroquinone with similar regioselectivity after the same time of electrolysis.

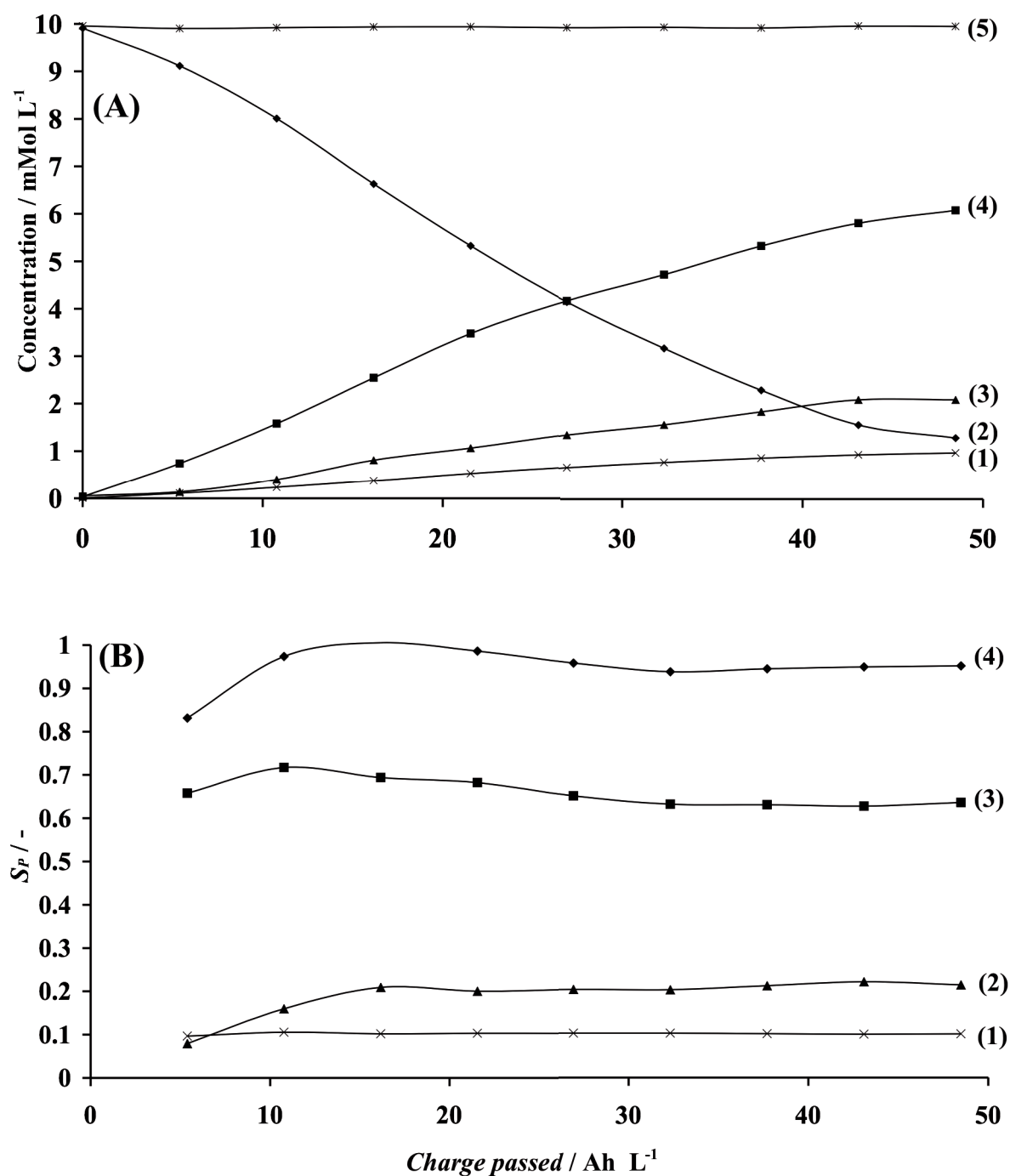


Figure 8-15: (A) Benzoquinone (1), phenol (2), pyrocatechol (3), hydroquinone (4) and the total mass balance (5) concentrations and (B) pyrocatechol (1), benzoquinone (2) and hydroquinone (3) selectivities (Eq.(8-8)) and total aromatic selectivity (4) as a function of the specific charge passed during electrolysis of phenol (10mM phenol in 1M HClO₄) on Ti/IrO₂ anode at 50 °C under galvanostatic operation (55 mA·cm⁻²) in the single-compartment cell.

Hence, it is now clear that under those conditions, the *p*-benzoquinone formed at the anode was mostly reduced at the cathode yielding to the formation of hydroquinone (reaction (4) in Figure 8-12).

Specificity of the electrochemical oxidation of phenol on IrO₂ electrodes

Regarding the specificity of hydroxylation, the para-selectivity S_{para} (defined as the ratio of the concentrations of *p*-oriented products obtained for hydroquinone and *p*-benzoquinone ([HQ] and [*p*-BQ] respectively (mol L⁻¹) over the sum of the concentrations of all reaction products) has been used in order to perform a comparative study between the anodic oxidation of phenol on IrO₂ electrodes and other electrochemical/chemical methods (Eq.(8-9)):

$$S_{para} = \frac{[HQ] + [p\text{-BQ}]}{[HQ] + [p\text{-BQ}] + [CAT]} \quad (8-9)$$

where [CAT] stands for pyrocatechol concentration (mol L⁻¹).

Using the results presented in Figure 8-13, it was found that the value of S_{para} Eq.(8-9) calculated for the anodic oxidation of phenol on Ti/IrO₂ anodes in a two-compartments-cell is close to 0.8 independently of phenol conversion. This *p*-selectivity is compared with the values reported in the literature using other techniques in Table 8-2.

Table 8-2: Selectivities S_{para} obtained from Eq.(8-9) and phenol conversion for the oxidation of phenol performed through different techniques

Method	Chemical			Electrochemical
	Hydroxylation (with H ₂ O ₂)	Homogeneous catalysis	Heterogeneous catalysis	Direct oxidation
Catalyst	-	Fenton's reagent	Zeolith TS1	Ti/IrO ₂
S_{para} [-]	0.33	0.25	0.73	0.8
Phenol Conversion [%]	100	24.7	37	90
Reference	[12]	[13]	[14]	-

This table shows that without using any catalyst and for the catalytic hydroxylation of phenol using Fenton's reagent as catalyst the para-selectivity (S_{para}) obtained is low (<0.33) for the chemical oxidation of phenol with hydrogen peroxide. This is likely attributed to the fact that both processes take place in solution (homogeneous media); where the hydroxyl radicals involved in the reaction have a high accessibility to ortho-positions forming pyrocatechol; resulting into a small p -selectivity ($S_{para} = 0.33$).

As far as the heterogeneous processes are concerned, it has been reported that steric effects within the zeolite pores are related to the high para-selectivity [14,15]. In fact, in a recent work published by Yokoi [14], porous zeolites (TS-1) were used for the selective oxidation of phenol and the values obtained for S_{para} were similar to ones reported here (see Table 8-2).

According to the authors, it is speculated that phenol molecules get trapped inside the zeolite's pores through adsorption, which disables sterically the ortho position of the phenol molecule (Figure 8-16).

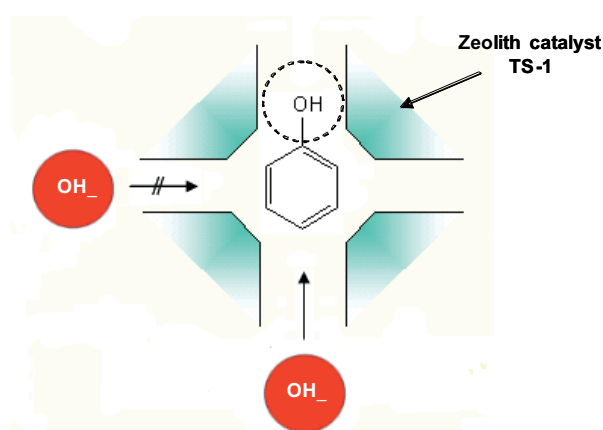


Figure 8-16: Speculated mechanism of hydroxylation of adsorbed phenol in TS-1 (zeolite catalyst) [14].

The fact that a decrease of the p -selectivity occurred after blockage of the zeolite's pores proved that steric effects are an important factor, which influence the specificity of this reaction [14].

The electrochemical methods seem to be good alternatives to enhance the para-selectivity of the reaction as well.

In fact, a high p -selectivity has been obtained for the anodic oxidation of phenol on various electrode materials [3,16-18]; however, what really sets apart IrO₂ compared to other electrode materials is the absence of combustion of the starting material or the

intermediates formed as well as the high para-selectivity obtained even for a high conversion of phenol.

Furthermore, the higher selectivity of para-hydroxylation products obtained after the electrochemical oxidation on Ti/IrO₂ and other electrodes compared to other methods is likely related to steric effects similar to those observed on zeolith. In fact, SEM micrographs of Ti/IrO₂ electrodes (see Chapter 3) showed that this material is also porous, possibly resulting in a similar adsorption mechanism than observed with zeolithes.

Due to steric effects of the phenol molecules, the phenoxy radicals formed are adsorbed in the pores of the IrO₂ coating mostly with the para-position facing towards the active species IrO₃, leading to a higher *p*-selectivity.

Furthermore, the high *p*-selectivities observed during both heterogeneous processes could be attributed to similar mechanism involving phenol adsorption through the pores of the zeolith and the Ti/IrO₂, respectively. However, iridium dioxide is slightly favored as there exists no blockage mechanism that could lower the *p*-selectivity contrary to the zeolith; furthermore, chemicals such as H₂O₂ are not used during the electrochemical process and thus it is more environmental friendly.

8.4 Conclusions

The electrochemical oxidation of model aliphatic and aromatic organic compounds on IrO₂ electrodes has been investigated through electrolysis experiments.

In the first part of this chapter, a new approach was proposed for electrolysis experiments, which consists in working under galvanostatic conditions with the potential 'buffered' by the competing side reaction of oxygen evolution. This approach allows working under pseudo-potentiostatic conditions. Therefore, when using this method the working potential is fixed by the oxidation power (O₂ overpotential) of the electrode material. Using this approach, three series of electrolysis have been carried out in this chapter.

In the first series, the oxidation of formic acid on Ti/IrO₂ electrodes was investigated to evaluate the performance of these electrodes toward a simple anodic oxidation process. The results revealed an instantaneous current efficiency of 100% for FA oxidation in the domain of current control, because it is transformed directly into CO₂. Consequently, a

good agreement was found between the experimental results and the results obtained using the model based on the maximum oxidation rate presented in the bibliography (section 2.5), which predicts the temporal evolutions of concentration and instantaneous current efficiency. This shows that the reaction between formic acid and electrogenerated IrO₃ is indeed a fast reaction and is controlled by mass transfer. In the second series of experiments, electrolysis of *i*-propanol and 2-butanol on Ti/IrO₂ were carried out in order to achieve selective oxidation of these compounds using the principle of pseudo-potentiostatic oxidation described in the first part of the chapter. The results of these experiments have shown a high selectivity towards acetone and MEK respectively because these oxidation products are stabilized due to the buffering of the anode potential around 1.7 V, which is induced by the competing side reaction of O₂ evolution. Consequently, the experimental results obtained in the case of *i*-propanol and 2-butanol electrolysis deviated strongly from the predictions of the model as a contrary to the case of formic acid oxidation.

In the last series of experiments, phenol electrolysis was carried out on Ti/IrO₂ not only to achieve selective oxidation but also in order to compare the specificity of hydroxylation with the classical methods. It is shown that the intermediates benzoquinone, pyrocatechol and hydroquinone are formed with a high selectivity (even at low temperature) for benzoquinone when using the two-compartment cell and for hydroquinone when using the single-compartment cell. The fact that the total aromatic selectivity (S_{arom}) was close to 1 indicates that the oxidation products of phenol are stable toward further oxidation similar to what others have already reported [19,20]. This is due to the buffering of the anode potential induced by the side reaction of O₂ evolution.

The comparison between the electrochemical oxidation of phenol on IrO₂ electrodes with other chemical and electrochemical techniques has shown that the values of the selectivity for the para substituted products and the conversion of starting material obtained on IrO₂ electrodes are similar to those reported for other electrochemical methods but higher than those reported for chemical methods used for the same oxidation. The high para selectivity obtained on IrO₂ electrodes could be due to steric effects similar to those observed during the oxidation of phenol on TS1 zeolithes. However, one unique feature of direct anodic oxidation on IrO₂ electrodes compared to other electrochemical techniques is the absence of combustion of phenol or its oxidation products and the high para-selectivity obtained even after quasi-complete conversion of phenol.

8.5 References

- [1] G. Fóti, Ch. Comninellis, in *Modern Aspects of Electrochemistry*, R. White, B.E Conway, C.G. Vayenas, Editors, Kluwer Academic/Plenum Publishers: New York. Vol. 37 (2004) 87
- [2] Ch. Comninellis, E. Plattner, *Chimia*, 42 (1988) 250
- [3] Ch. Comninellis, C. Pulgarin, *J. Appl. Electrochem.*, 21 (1991) 703
- [4] G. Fóti, D. Gandini, Ch. Comninellis, A. Perret, W. Haenni, *Electrochem. Solid-State Lett.*, 2 (1999) 228
- [5] G. Fóti, D. Gandini, Ch. Comninellis, in *Current Topics in Electrochemistry*, Vol. 5, Research Trends, Trivandrum (1997) 71
- [6] S. Fierro, T. Nagel, H. Baltruschat, Ch. Comninellis, *Electrochem. Comm.*, 9 (2007) 1969
- [7] S. Fierro, T. Nagel, H. Baltruschat, Ch. Comninellis, *Electrochem. And Solid-State Lett.*, 11 (7) (2008) E20
- [8] A.M. Jirka, M.J. Carter, *Anal. Chem.*, 47 (1975) 1397
- [9] L. Ouattara, S. Fierro, O. Frey, M. Koudelka, Ch. Comninellis, *J. Appl. Chem.*, 39 (2009) 1361
- [10] A. Kapałka, G. Fóti, Ch. Comninellis, *Electrochem. Comm.*, 10 (2008) 607
- [11] P.-A. Michaud, PhD Thesis, Swiss Institute of Technology (EPFL), No 2595, 2002
- [12] J. McMurry in: *Organic Chemistry*, 4th ed., Brooks/Cole Publishing Company, New York, 1996
- [13] J.A. Zazo, J.A. Casas, A.F. Mohedano, M.A. Gilarranz, J.J. Rodriguez, *Environ. Sci. Technol.*, 39 (2005) 9295
- [14] T. Yokoi, P. Wu, T. Tatsumi, *Catalysis Communications*, 4 (2003) 11
- [15] U. Wilkenhöner, G. Langhendries, F. Van Laar, G.V. Baron, D.W. Gammon, P.A. Jacobs, E. Van Steen, *J. Catal.*, 203 (2001) 201
- [16] J. Iniesta, P.-A. Michaud, M. Panizza, G. Cerisola, A. Aldaz, Ch. Comninellis, *Electrochim. Acta*, 46 (23) (2001) 3573

- [17] J. Hoare, *Standard Potentials in Aqueous Solutions*, Marcel Dekker INC., 1985
- [18] B. Fleszar, J. Plozynska, *Electrochim. Acta*, 30 (1985) 31
- [19] K. Waterson, J.W. Wang, D. Bejan, N.J. Bunce, *J. Appl. Electrochem.*, 36 (2006) 227
- [20] C. Bock, B. McDougall, *J. Electrochem. Soc.*, 146 (1999) 2925

Chapter 9 : General Discussion

This chapter summarizes the most important findings obtained in this thesis regarding the electrochemical behaviour in aqueous acidic media of IrO₂-based electrodes prepared by thermal decomposition of H₂IrCl₆ precursor solution. This brief summary focuses on the preparation of these electrodes and the mechanisms taking place during; (i) the charging/discharging process within the water stability potential domain, (ii) the oxygen evolution reaction, and (iii) the oxidation of organic compounds. Those reactions emphasize the key role of the active surface redox couple IrO₃/IrO₂ of this particular electrode material.

This work focused on the IrO₂-based electrode prepared by thermal decomposition of H₂IrCl₆ precursor solution on an inert substrate (Ti or p-Si).

As a first step we concentrated our efforts on the preparation and morphological characterization of IrO₂ electrodes. It was found that the charge measured during a cyclic voltammetry measurement recorded in the water stability potential domain could be used as a tool in order to estimate the loading of the IrO₂ coating. Furthermore, it was shown that it is possible to control the loading of the coating using the spin coating deposition technique together with voltammetric charge measurements. In fact, a new and simple relation has been proposed (Eq.(3-2)) for the estimation of the IrO₂ coating's loading as a function of the concentration of H₂IrCl₆ in the precursor solution and the rotation speed of the substrate (Chapter 3).

Cyclic voltammetry measurements performed at different temperatures and scan rates have shown that the charging/discharging process on IrO₂ electrodes is due to two key mechanisms. The first one is a slow process due to diffusion of protons within the IrO₂ coating (reaction (4-1)); this process has an apparent activation energy of about 2.4 kJ mol⁻¹ and dominates at low scan rates (5mV s⁻¹). The second contribution is an instantaneous electrostatic process related to the double layer capacitance, which was found to dominate at high scan rates (500mV s⁻¹).

Moreover, using potential step experiments, the surface redox activities occurring on p-Si/IrO₂ electrodes in the water stability potential domain were further investigated by measuring the surface charge (the charge related to the surface and/or the most accessible iridium atoms of the IrO₂ coating) as a function of the potential applied. The surface charge was estimated by extrapolating the obtained total charges to $t = 0$ s assuming that within the time range selected (long time decay i.e. $t > 1.5$ s), the current decay is caused solely by a semi-infinite linear diffusion process, which is the diffusion of protons within the IrO₂ coating (reaction (4-1)). This method had already been used by Gerischer et al.[1] for the same study but on RuO₂-based electrodes.

The results obtained using p-Si/IrO₂ electrodes have shown that the valence state of the iridium surface atoms of these electrodes varies from +IV (IrO₂) to +VI (IrO₃) between the on-set potentials of H₂ and O₂ evolution through two consecutive slow processes occurring between 0.9 V and 1.5 V vs. SHE.

As far as the study of the oxygen evolution reaction (OER) on IrO₂ based electrodes is concerned, the mechanisms involved in this process were a subject of active debate [2,3]. The OER on IrO₂ electrodes was studied using differential electrochemical mass spectrometry (DEMS) measurements together with isotope labeling and Tafel slopes estimations (Chapter 5).

DEMS measurements were carried out using Ti/IrO₂ electrodes in 1M HClO₄ containing 10% of marked water (H¹⁸O₂) as electrolyte. The monitoring of the ionic currents related to the formation of different electro-generated oxygen species (¹⁶O₂, ¹⁸O¹⁶O and ¹⁸O₂) have shown that the relative amount of marked oxygen (¹⁸O¹⁶O) formed on the IrO₂ electrode increased with a concomitant decrease of the relative amount of 'regular' oxygen (¹⁶O₂) with each successive voltammetric scan until reaching constant values, which could be predicted by the bulk concentrations of 'regular' (H₂¹⁶O) and marked (H₂¹⁸O) water in the electrolyte. This is a direct evidence that the higher valent-state oxide of iridium (IrO₃) is directly involved in the oxygen evolution reaction. Moreover, using Faraday law (Eq.(5-8)), it was shown that about 1% of the IrO₂ loading is effectively participating during the process. Similar results were obtained for higher IrO₂ loadings. Furthermore, a Tafel slope of 40mV decade⁻¹ (IR drop corrected) was estimated for the OER on IrO₂ electrodes. This value for the Tafel slope suggests that the rate-determining step (rds) of the OER on IrO₂ electrodes is the formation of a higher valence state oxide (IrO₃), which is in good agreement with the DEMS results.

As for the electrochemical oxidation of organic compounds, the investigation of the mechanisms involved was carried out on Ti/IrO₂ electrodes using again DEMS measurements (Chapter 6). In the first part of the experiment, the IrO₂ coating was 'labeled' with marked oxygen similar than for the investigation of the OER presented in Chapter 5. During the second part of the experiment, the cell containing the marked electrode was rinsed carefully and subsequent DEMS measurements using a 'regular' electrolyte solution of 1M HClO₄ containing 2mM of formic acid were performed. During the course of these experiments, the ionic currents corresponding to the formation of different species of electro-generated carbon dioxide (C¹⁶O₂ and C¹⁶O¹⁸O) were monitored. The presence of C¹⁶O¹⁸O observed during these DEMS measurements is a direct evidence that the higher valent state oxide of iridium (IrO₃) is directly involved in the oxidation of organic compounds because formic acid was the only source of carbon in the bulk and the latter reacted with the marked IrO₂ coating (Ir¹⁶O¹⁸O) to form marked carbon dioxide (C¹⁶O¹⁸O). Therefore, both the oxygen evolution reaction and the oxidation of organics compete on the same intermediate (IrO₃) on IrO₂ electrodes.

As a next step, we focused on the oxidation of organic compounds on Ti/IrO₂ electrodes. Using voltammetric measurements recorded on different IrO₂ loadings for different organic concentrations and using a new theoretical model, it was shown in Chapter 7 that the apparent kinetic parameters of organics oxidation via the surface redox couple IrO₃/IrO₂ are strongly dependent on the IrO₂ loading. Furthermore, and using still the same model, the potential shift toward less positive values induced by the presence of an

organic compound was investigated and quantified. The I-V curves in the presence of different concentrations of formic acid (model compound) were constructed for different IrO₂ loadings using the I-V curves of the supporting electrolyte (1M HClO₄) and the kinetic parameters calculated earlier. Small differences were observed between the predicted and experimental I-V curves due to limitations associated with the appropriate estimation of the adsorption constant K in the model.

In Chapter 8, a new approach was proposed in order to perform electrochemical oxidation of organics by working under galvanostatic conditions with the anode potential 'buffered' by the competing side reaction of oxygen evolution. According to this mode of operation, the working potential is fixed by the nature of the electrode material and is buffered during organics oxidation by the side reaction of OER. This approach has been used for electrolysis experiments on Ti/IrO₂ electrodes using aliphatic and aromatic model compounds (formic acid, *i*-propanol, 2-butanol and phenol).

The oxidation of formic acid on Ti/IrO₂ electrodes was carried out in order to evaluate the performance of these electrodes toward a simple anodic oxidation process. The results have shown that formic acid is rapidly mineralized with an instantaneous current efficiency (*ICE*) of 100% in the domain of current control through a simple oxidation mechanism involving no intermediates. In fact, a good agreement was found between the experimental results and the results predicted by the model based on the maximum oxidation rate, which predicts the temporal evolutions of concentration and *ICE* (bibliography, section 2.5).

Next, the oxidation of *i*-propanol and 2-butanol were carried out in order to achieve selective oxidation of these compounds using the approach of pseudo-potentiostatic oxidation proposed earlier. It was found that the relatively high selectivity towards acetone and MEK respectively, is related to the buffering of the working potential.

Consequently, the experimental results obtained in the case of *i*-propanol and 2-butanol electrolysis deviated significantly from the predictions of the model based on the maximum oxidation rate (bibliography, section 2.5) in contrast to the case of formic acid oxidation. Finally, electrolysis of phenol on Ti/IrO₂ electrodes was carried out in order to achieve selective oxidation of this compound and then compare the specificity of the hydroxylation reaction with classical methods.

This comparison has shown that on Ti/IrO₂ electrodes, a high selectivity for the para-substituted products can be obtained after quasi-complete conversion of phenol. The high para selectivity obtained on IrO₂ electrodes has been related to steric effects similar to those observed during the oxidation of phenol on TS1 zeolithes [4].

References

- [1] K. Doblhofer, M. Metikos, Z. Ogumi, H. Gerischer, *Ber. Bunsenges. Phys. Chem.*, 82 (1978) 1046
- [2] L.I. Krishtalik, *Electrochim. Acta*, 26 (1981) 329
- [3] F. Beck, H. Schulz, *Electrochim. Acta*, 31 (1986) 943
- [4] T. Yokoi, P. Wu, T. Tatsumi, *Catalysis Communications*, 4 (2003) 11

Chapter 10 : Perspectives

The research perspectives of this work were focused on two distinct topics.

The first perspective of research concerning IrO₂-based electrodes was focused on their method of preparation. The main goal was to study the electrochemical behaviour of an IrO₂ electrode prepared by thermal treatment of iridium metal (TOIROF) and of an IrO₂ electrode prepared by anodic oxidation of pure Ir (AIROF) and then compare them with the behaviour of IrO₂ electrodes prepared by thermal decomposition (TDIROF) studied in this work. Later, the method of preparation of TOIROF was used in order to produce and characterize a stable IrO₂ ultra micro-electrode array (MEA) for analytical applications.

Preliminary studies have shown that the surface redox activities involved are similar for TDIROF and TOIROF [1]. This similarity is inherent to the preparation conditions of both oxide films (thermal treatment in air at 500°C). However, the surface activities involved on AIROF seem to be much faster than those involved on the other IrO₂-based films. The investigation of the oxygen evolution reaction in acidic media has shown that all IrO₂-based films exhibited similar mechanism (same Tafel slope of 40mV decade⁻¹) involving the same intermediate (IrO₃) and similar specific electrocatalytic activity [2].

The surface redox couple involved in the anodic oxidation of formic acid (FA) highly depends on the preparation technique of the IrO₂ anodes. In fact, on TDIROF and TOIROF, the oxidation of FA and the OER compete via the same surface redox couple Ir(VI)/Ir(IV). However, this is not the case on AIROF, where the oxidation of FA involves the Ir(V)/Ir(IV) surface redox couple and is not competing with the OER [1,2].

Electrode stability measurements have shown that no corrosion was observed on TDIROF and TOIROF under strong OER and organic oxidation conditions. In contrast, the AIROF are rapidly corroded under anodic treatment and this corrosion is further enhanced by the presence of formic acid [1,2].

Finally, the mode of preparation of TOIROF was used to produce an IrO₂-based ultra micro-electrode array (MEA) [3]. The limit between the planar and spherical diffusion profile domains has been established as a function of scan rate and using that criteria, a diffusion coefficient of 1,03·10⁻⁵ cm² s⁻¹ was estimated for [Fe(CN)₆]³⁻, which is in agreement with values reported in the literature. One advantage of the miniaturization of the IrO₂-based electrode lies in the ability to detect very low concentrations of a given specie for analytical applications. In fact, in our case, steady-state currents could still be recorded on the TOIROF MEA for concentrations of Fe(CN)₆^{4-/3-} of 0,5mM L⁻¹.

The second core research topic of this thesis focused on the electrochemical behavior of ammonia (NH₄⁺/NH₃) on IrO₂-based electrodes (TDIROF and AIROF) for applications in ammonia removal (alkaline media) from wastewaters [4,5].

The preliminary investigation of ammonia oxidation on IrO₂ based electrodes has shown that the electrochemical oxidation of ammonia on IrO₂ electrodes occurs in the potential region related to surface activities involving the redox couple Ir(V)/Ir(IV), which results in the formation of two anodic peaks: one during the forward scan and the second during the backward scan. The anodic peak in the backward scan results from the oxidation of ammonia on freshly reduced Ir(VI) to Ir(V).

During ammonia oxidation, TDIROF is deactivated by adsorbed products of ammonia oxidation. In contrast, AIROF seems not to be blocked during ammonia oxidation.

The difference between both electrodes may be attributed to the difference between the activities of the iridium oxide's surface redox couples. In fact, on AIROF, the surface redox couple Ir(IV)/Ir(III) exhibits a large separation (750mV) of the oxidation/reduction peaks, which is due to local pH changes within the film induced by the release/consumption of protons during the activity of this surface redox couple. This, in turn, indicates that the surface as well as the inner parts of the AIROF are electrochemically active under these conditions. This result allowed to determine that this separation between both peaks can be reduced to 100mV in the presence of ammonia, which acts as a buffer. In contrast, on TDIROF, it seems that, under similar conditions, only the surface of the electrode material is active, because the voltammetric response of these electrodes is not influenced by local pH changes. Consequently, the separation between the oxidation and reduction peaks of the surface redox couple Ir(IV)/Ir(III) is more reasonable (100mV).

These results summarized above were published in the following articles (given in appendix):

S. Fierro, A. Kapałka, Ch. Comninellis. Ultra Micro electrode array of IrO₂ prepared by thermal treatment of pure Ir, *Electrochemistry Communications*, accepted manuscript, January 2010, doi:10.1016/j.elecom.2010.02.006

S. Fierro, A. Kapałka, Ch. Comninellis. Electrochemical comparison between IrO₂ prepared by thermal treatment of iridium metal and IrO₂ prepared by thermal decomposition of H₂IrCl₆, *Electrochemistry Communications*, 12 (2010) 172-174

A. Kapałka, S. Fierro, Z. Frontistis, A. Katsaounis, O. Frey, M. Koudelka, Ch. Comninellis, K.M. Udert. Electrochemical oxidation of ammonia (NH₄⁺/NH₃) on thermally and electrochemically prepared IrO₂ electrodes. Submitted manuscript, *Journal of Applied Electrochemistry*, August 2009

A. Kapałka, S. Fierro, Z. Frontistis, A. Katsaounis, O. Frey, M. Koudelka, Ch. Comninellis, K.M. Udert. Electrochemical behaviour of ammonia ($\text{NH}_4^+/\text{NH}_3$) on electrochemically grown anodic iridium oxide film (AIROF) electrode. *Electrochemical Communications*, 11 (2009) 1590-1592

L.Ouattara, S. Fierro, O. Frey, M. Koudelka, Ch. Comninellis. Electrochemical comparison between IrO_2 prepared by anodic oxidation of pure iridium and IrO_2 prepared by thermal decomposition of H_2IrCl_6 precursor solution, *Journal of Applied Electrochemistry*, Volume 39, February 2009, pages 1361-1367

References

- [1] S. Fierro, A. Kapałka, Ch. Comninellis, *Electrochem. Commun.*, 12 (2010) 172
- [2] L. Ouattara, S. Fierro, O. Frey, M. Koudelka, Ch. Comninellis, *J. Appl. Chem.*, 39 (2009) 1361
- [3] S. Fierro, A. Kapałka, Ch. Comninellis. Ultra Micro electrode array of IrO_2 prepared by thermal treatment of pure Ir, *Electrochem. Comm.*, accepted manuscript, January 2010, doi:10.1016/j.elecom.2010.02.006
- [4] A. Kapałka, S. Fierro, Z. Frontistis, A. Katsaounis, O. Frey, M. Koudelka, Ch. Comninellis, K.M. Udert, Electrochemical oxidation of ammonia ($\text{NH}_4^+/\text{NH}_3$) on thermally and electrochemically prepared IrO_2 electrodes. Submitted manuscript, *Journal of Applied Electrochemistry*, August 2009
- [5] A. Kapałka, S. Fierro, Z. Frontistis, A. Katsaounis, O. Frey, M. Koudelka, Ch. Comninellis, K.M. Udert, *Electrochemical Communications*, 11 (2009) 1590-1592

ELECTROCATALYSIS INDUCED BY SURFACE REDOX ACTIVITIES ON CONDUCTIVE METAL OXIDE ELECTRODES

List of symbols

Roman symbols

<i>Symbol</i>	<i>Meaning</i>	<i>Units</i>
A	(a) area	m^2
	(b) pre-exponential factor in Eq.(4-2)	C g^{-1}
A_g	geometrical surface area	m^2
A_{real}	real surface area	m^2
a	Tafel constant	V
b	Tafel slope	V dec^{-1}
C	(a) concentration	mol m^{-3}
	(b) gravimetric capacitance	F g^{-1}
C_{ad}	capacitance related to cations/anions adsorption	F g^{-1}
C_{app}	apparent capacitance	F m^{-2}
C_{dl}	double-layer capacitance	F g^{-1}
C_{irr}	capacitance related to an irreversible faradaic process	F g^{-1}
C_p	bulk concentration of reaction product p	mol m^{-3}
C_R^{ad}	concentration of adsorbed R	mol m^{-3}
$C_R^{bulk} (= C_R)$	bulk concentration of R	mol m^{-3}
C_R^0	initial bulk concentration of R	mol m^{-3}

LIST OF SYMBOLS

<i>Symbol</i>	<i>Meaning</i>	<i>Units</i>
ΔC	concentration change	mol m^{-3}
c_0	initial concentration of active component	mol m^{-3}
COD	chemical oxygen demand	$\text{molO}_2 \text{ m}^{-3}$
COD_{cr}	chemical oxygen demand at the critical time	$\text{molO}_2 \text{ m}^{-3}$
COD_t	chemical oxygen demand at time t	$\text{molO}_2 \text{ m}^{-3}$
COD_0	initial chemical oxygen demand	$\text{molO}_2 \text{ m}^{-3}$
D	diffusion coefficient	$\text{m}^2 \text{ s}^{-1}$
E	potential	V
E_a	activation energy	J mol^{-1}
E_{op}	open circuit potential	V
E_0	standard thermodynamic potential	V
e	evaporation rate	m s^{-1}
F	Faraday constant	C mol^{-1}
f	frequency	s^{-1}
h	thickness	m
h_∞	thickness after infinite spinning time	m
h_0	initial thickness	m
I	gravimetric current	A g^{-1}
I_f	faradaic current	A
I_i	ionic intensity	A
i	current	A
ICE	instantaneous current efficiency	
J_f	faradaic current density	A m^{-2}
J_i	(a) molar flux of i	mol s^{-1}
	(b) ionic current density	A m^{-2}
j	current density	A m^{-2}

Symbol	Meaning	Units
$j_{applied}$	applied current density	$A\ m^{-2}$
j_{lim}	limiting current density	$A\ m^{-2}$
$j_{lim,0}$	initial limiting current density	$A\ m^{-2}$
Δj	current density difference	$A\ m^{-2}$
j_{cr}^0	limiting current density at the critical time	$A\ m^{-2}$
K	(a) constant in Eq.(3-1) (b) adsorption constant in Eq.(7-18)	$C\ m\ rad^{0,5}\ s^{-0,5}\ mol^{-1}$
K^*	calibration constant in Eq.(2-21)	
K^0	calibration constant in Eq.(2-18)	$C\ mol^{-1}$
k_c	chemical rate constant of reaction (7-2)	$m^3\ mol^{-1}\ s^{-1}$
k_d	decomposition rate constant of reaction (7-3)	s^{-1}
k_m	mass transport coefficient	$m\ s^{-1}$
$(k_c)_{ap}$	apparent rate constant of chemical reaction (7-3)	$m\ s^{-1}$
k_1^e	electrochemical rate constant of reaction (7-1)	s^{-1}
k_{-1}^e	electrochemical rate constant of the reverse reaction (7-1)	s^{-1}
$k_1^{e,0}$	standard rate constant for electrochemical reaction (7-1)	s^{-1}
$(k_1^{e,0})_{ap}$	apparent standard rate constant of reaction (7-1)	$mol\ m^{-2}\ s^{-1}$
L_{IrO_2}	IrO_2 loading	$mg\ cm^{-2}$
m	amount of ^{16}O exchanged to ^{18}O	$mol\ m^{-2}$
N	collection efficiency	
N_A	Avogadro's constant	$atoms\ mol^{-1}$
n	number of ^{16}O atoms exchanged to ^{18}O	$atoms\ m^{-2}$
Q	gravimetric voltammetric charge	$C\ g^{-1}$

LIST OF SYMBOLS

<i>Symbol</i>	<i>Meaning</i>	<i>Units</i>
Q_{cr}	specific charge passed at the critical time	C
Q_f	faradaic charge	C m ⁻²
Q_i	ionic charge	C m ⁻²
ΔQ	excess of ionic charge	C m ⁻²
q	(a) total radial flow per unit of circumference	m ² s ⁻¹
	(b) specific electrical charge passed	A s m ⁻³
q_s	surface charge density	C m ⁻²
q_t	total (cumulative) charge density	C m ⁻²
q^*	voltammetric charge density	C m ⁻²
q_{dl}^*	fraction of q^* corresponding to double-layer charging	C m ⁻²
q_{sp}^*	specific voltammetric charge	C g ⁻¹
R	(a) ideal gas constant	J mol ⁻¹ K ⁻¹
	(b) resistance	Ω m ⁻²
r	(a) radius	m
	(b) reaction rate	mol m ⁻² s ⁻¹
S_p	selectivity for product p	
S_{para}	para selectivity	
T	temperature	K
t	time	s
t_{cr}	critical time	s
U_B	anode potential	V
$U_{B,0}$	standard surface redox potential	V
V_R	reaction volume	m ³
z	(a) distance on the rotation axis	m
	(b) number of electrons	

Greek symbols

<i>Symbol</i>	<i>Meaning</i>	<i>Units</i>
α	charge transfer coefficient	
Γ_0	density of surface atoms	mol m ⁻²
γ	excess ratio	
γ_{3D}	three dimensional roughness factor	
η	(a) viscosity	kg s ⁻¹ m ⁻¹
	(b) overpotential	V
	(c) average current efficiency	
η_{corr}	IR drop corrected overpotential	V
θ	fractional surface coverage	
λ	dimensionless current density	
ν	(a) kinematic viscosity	m ² s ⁻¹
	(b) scan rate	V s ⁻¹
ρ	density	kg m ⁻³
v	velocity in radial direction	m s ⁻¹
ω	angular velocity	rad s ⁻¹

ELECTROCATALYSIS INDUCED BY SURFACE REDOX ACTIVITIES ON CONDUCTIVE METAL OXIDE ELECTRODES

Publications related to this work

S. Fierro, Ch. Comninellis. Kinetic study of formic acid oxidation on p-Si/IrO₂ electrodes, *Electrochim. Acta*, submitted manuscript, February 2010

S. Fierro, A. Kapałka, Ch. Comninellis. Ultra Micro electrode array of IrO₂ prepared by thermal treatment of pure Ir, *Electrochem. Comm.*, accepted manuscript, January 2010, doi:10.1016/j.elecom.2010.02.006

S. Fierro, A. Kapałka, Ch. Comninellis. Electrochemical comparison between IrO₂ prepared by thermal treatment of pure iridium and IrO₂ prepared by thermal decomposition of H₂IrCl₆ precursor solution, *Electrochem. Comm.*, 12 (2010) 172

S. Fierro, G. Fòti, Ch. Comninellis in: *Electrolysis: Theory, Types and Applications*, Nova Publishers, New York, 2010

E. Chatzisyneon, S. Fierro, I. Karafyllis, D. Mantzavinos, A. Katsaounis. Anodic oxidation of phenol on Ti/IrO₂ electrode: Experimental studies, *Catalysis today*, accepted manuscript, January 2010

A. Kapałka, S. Fierro, Z. Frontistis, A. Katsaounis, O. Frey, M. Koudelka, Ch. Comninellis, K.M. Udert. Electrochemical oxidation of ammonia (NH₄⁺/NH₃) on thermally and electrochemically prepared IrO₂ electrodes. Submitted manuscript *J. Appl. Electrochem.*, August 2009

A. Kapałka, S. Fierro, Z. Frontistis, A. Katsaounis, O. Frey, M. Koudelka, Ch. Comninellis, K.M. Udert. Electrochemical behaviour of ammonia (NH₄⁺/NH₃) on electrochemically grown anodic iridium oxide film (AIROF) electrode. *Electrochem. Comm.*, 11 (2009) 1590-1592

S. Fierro, E. Passas-Lagos, E. Chatzisyneon, D. Mantzavinos, Ch. Comninellis. Pseudo-potentiostatic electrolysis by potential buffering induced by the oxygen evolution reaction, *Electrochem. Comm.*, 11 (2009) 1358-1361

L.Ouattara, S. Fierro, O. Frey, M. Koudelka, Ch. Comninellis. Electrochemical comparison between IrO₂ prepared by anodic oxidation of pure iridium and IrO₂ prepared by thermal decomposition of H₂IrCl₆ precursor solution, *J. of Appl. Electrochem.*, 39 (2009) 1361-1367

ELECTROCATALYSIS INDUCED BY SURFACE REDOX ACTIVITIES ON CONDUCTIVE METAL OXIDE ELECTRODES

S. Fierro, L. Ouattara, E. H. Calderon, E. Passas-Lagos, H. Baltruschat, Ch. Comninellis. Investigation of formic acid oxidation on Ti/IrO₂ electrodes, *Electrochim. Acta*, 54 (2008) 2053-2061

S. Fierro, L. Ouattara, E. H. Calderon, Ch. Comninellis. Influence of temperature on the charging/discharging process of IrO₂ coating deposited on p-Si substrate, *Electrochem. Comm.*, 10 (2008) 955-959

S. Fierro, T. Nagel, H. Baltruschat, Ch. Comninellis. Investigation of formic acid oxidation on Ti/IrO₂ electrodes using isotope labelling and online mass spectrometry, *Electrochem. Solid-State Lett.*, 11 (2008) E20-E23

S. Fierro, T. Nagel, H. Baltruschat, Ch. Comninellis. Investigation of the oxygen evolution reaction on Ti/IrO₂ electrodes using isotope labelling and online mass spectrometry, *Electrochem. Comm.*, 9 (2007) 1969-1974

Oral presentations

S. Fierro, T. Nagel, H. Baltruschat, Ch. Comninellis. Investigation of oxygen evolution and formic acid oxidation on Ti/IrO₂ electrodes using isotope labelling and on-line mass spectrometry. 6th spring meeting of the International Society of Electrochemistry (ISE), Foz do Iguacu (Brazil), March 16th-March 19th, 2008.

S. Fierro, A. Kapałka, Ch. Comninellis. Electrochemical oxidation of organic compounds on IrO₂ and on Boron Doped Diamond (BDD) electrodes. Zing Electrochemistry 2009 conference, Playa del Carmen (Mexico), February 8th-February 11th, 2009.

S. Fierro, A. Kapałka, Ch. Comninellis. Electrochemical oxidation of organic compounds on IrO₂ and on Boron Doped Diamond (BDD) electrodes. 2nd European conference on environmental applications of advanced oxidation processes (EAAOP-2), Nicosia (Cyprus), September 9th-September 11th, 2009.

Appendix

Publications related to the research perspectives

ELECTROCATALYSIS INDUCED BY SURFACE REDOX ACTIVITIES
ON CONDUCTIVE METAL OXIDE ELECTRODES

Electrochemical comparison of IrO₂ prepared by anodic oxidation of pure iridium and IrO₂ prepared by thermal decomposition of H₂IrCl₆ precursor solution

Lassiné Ouattara · Stéphane Fierro ·
Olivier Frey · Milena Koudelka · Christos Comninellis

Received: 10 October 2008 / Accepted: 26 January 2009 / Published online: 18 February 2009
© Springer Science+Business Media B.V. 2009

Abstract Surface redox activities, oxygen evolution reaction (OER), oxidation of formic acid (FA), and anodic stability were investigated and compared for IrO₂ electrodes prepared by two techniques: the thermal decomposition of H₂IrCl₆ precursor (TDIROF) and the anodic oxidation of metallic iridium (AIROF). Surface redox activities involved on the AIROF were found to be much faster than those involved on the TDIROF. Concerning the oxygen evolution reaction, both films show a similar mechanism and specific electrocatalytic activities. The situation seems to be different for FA oxidation. In fact, on TDIROF, the oxidation of FA and the OER compete involving the same surface redox couple Ir(VI)/Ir(IV) contrary to FA oxidation on AIROF, where the Ir(V)/Ir(IV) surface redox couple is involved. Finally, electrode stability measurements have shown that contrary to TDIROF, which are very stable under anodic polarization, the AIROF are rapidly corroded under anodic treatment. This corrosion is enhanced even further in the presence of formic acid.

Keywords TDIROF · AIROF · Surface redox activity · Oxygen evolution · Formic acid oxidation · Anodic stability

1 Introduction

Iridium dioxide electrodes form part of the dimensionally stable anodes (DSA[®]), which are widely used in industry for metal electro-winning, cathodic protection, and electro-organic synthesis [1–4].

The first iridium dioxide electrodes, as described in the corresponding patents [5, 6], were thermally decomposed iridium oxide films (TDIROF) produced by thermal decomposition of the appropriate precursor solution on an inert substrate such as titanium or tantalum.

Later, other techniques of conductive IrO₂ film formation such as the anodic oxidation of metallic iridium were considered. In fact, it has been shown that pure iridium and mostly the corresponding anodic iridium oxide film (AIROF) formed through potential cycling exhibit some interesting electrochemical properties and especially toward the oxygen evolution reaction (OER) [7–9].

Although the activity and stability of AIROF and TDIROF toward OER have been widely studied [1–4, 10–12], the mechanisms involved in the process are still a matter of discussion.

More recently, the electro-catalytic activity of TDIROF toward the oxidation of organics has been described. However, little is known about the surface redox activity and stability during the oxidation of organics on AIROF.

However, as the participation of the TDIROF coating via the IrO₃/IrO₂ redox couple during OER and the oxidation of formic acid in acidic media has been proved

L. Ouattara
Laboratoire de Chimie Physique, UFR SSMT, Université
de Cocody, 22 BP 582, Abidjan 22, Ivory Coast

S. Fierro (✉) · C. Comninellis (✉)
Institute of Chemical Sciences and Engineering,
Swiss Federal Institute of Technology, ISIC-EPFL,
CH-1015 Lausanne, Switzerland
e-mail: stephane.fierro@epfl.ch

C. Comninellis
e-mail: christos.comninellis@epfl.ch

O. Frey · M. Koudelka
The Sensors, Actuators and Microsystems Laboratory, Institute
of Microtechnology, University of Neuchâtel, SAMLAB-
UNINE, Jaquet-Droz 1, 2007 Neuchâtel, Switzerland

recently using DEMS [13, 14], the aim of the present study is to compare an IrO₂ electrode prepared by anodic oxidation of pure Ir (AIROF) with an IrO₂ electrode prepared by thermal decomposition of a precursor solution (TDIROF) by investigating the surface redox activities in the water stability potential region as well as during the OER and the oxidation of formic acid as model organic compound.

2 Experimental

All electrochemical experiments were performed in a classical three-electrode cell (70 mL) using an Autolab PGSTAT 30. The counter electrode was a Pt wire; the reference electrode was Hg/Hg₂SO₄/K₂SO₄ (sat.) (MSE; 0.65 V vs. SHE) and two different working electrodes were used:

- Anodic iridium oxide film electrode (AIROF): An iridium film (0.1 μm) was deposited by sputtering on p-Si (0.0054 mm²) using a thin (0.02 μm) tantalum interlayer (p-Si/Ir). The anodic iridium oxide film (AIROF) was formed through potential cycling of this electrode between -0.05 and 1.45 V.
- An IrO₂ electrode prepared by thermal decomposition of a precursor (TDIROF): the IrO₂ film (0.35 mg cm⁻²) was deposited on disc-shaped sandblasted p-Si (182.25 mm²) by the thermal decomposition of a H₂IrCl₆ (99.9%, ABCR) precursor solution in air at 500° (TDIROF). The presence of iridium dioxide on the substrate was verified using XPS measurements (not presented).

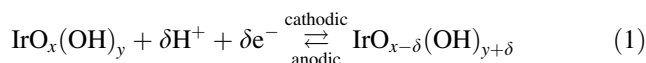
All potentials in this work are with respect to the standard hydrogen electrode (SHE).

3 Results and discussion

3.1 Surface redox activities

The cyclic voltammetry measurements of IrO₂ films prepared by the thermal decomposition technique (TDIROF), recorded for three potential windows in the potential range between 0.0 and 1.4 V and presented in Fig. 1, show two main features:

- The charge involved in the anodic scan is completely recovered during the cathodic scan ($q_+ = q_-$) for all the scan rates investigated (10–500 mV s⁻¹). However, the CV shows an axial symmetry (around the potential axis) only if the lower potential limit is higher than 0.4 V. In fact, at lower potential limits, a strong distortion of the CV around the potential axis is observed. This is an indication that the surface processes involved at low potentials (<0.4 V) are slow.
- The TDIROF are completely inactive toward the electrochemical reduction of dissolved oxygen (aerated and de-aerated solutions give the same CV).
- Furthermore, from measurements of the apparent activation energy (E_a) for the charging/discharging process using TDIROF reported in a previous paper [15], we have to consider two contributions. The first contribution is due to a fast (instantaneous) process with zero activation energy related to the charging of the electrical double-layer at the electrode–electrolyte interface and the second is related with the slow diffusion of protons within the IrO₂ coating inducing surface redox activities (Eq. 1) with an activation energy around 2.4 kJ mol⁻¹ [15].



The cyclic voltammetry measurements of IrO₂ films prepared by the anodic oxidation of metallic iridium

Fig. 1 Cyclic voltammograms using TDIROF (IrO₂ loading: 0.273 mg cm⁻²) at 100 mV s⁻¹ for different potential windows *a* between 0.3 and 1.1 V, *b* between 0.3 and 1.4 V, *c* between 0 and 1.4 V. Supporting electrolyte: 1 M HClO₄. *T* = 25 °C

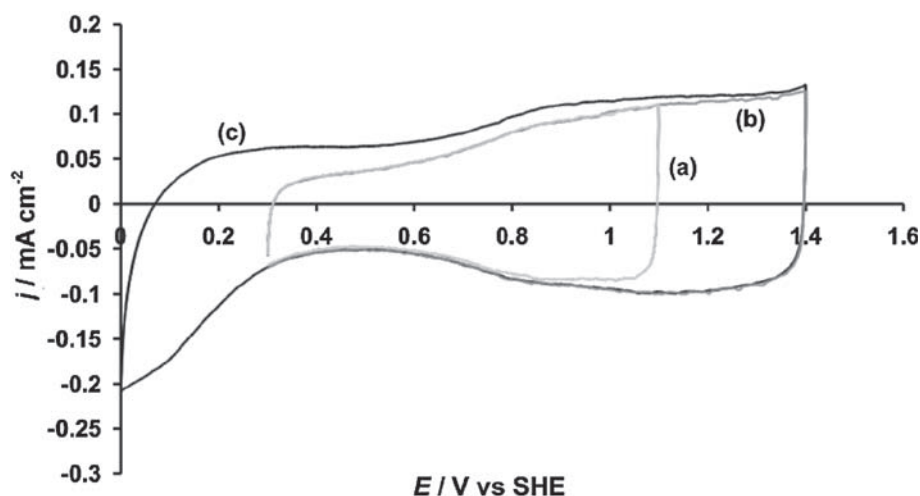
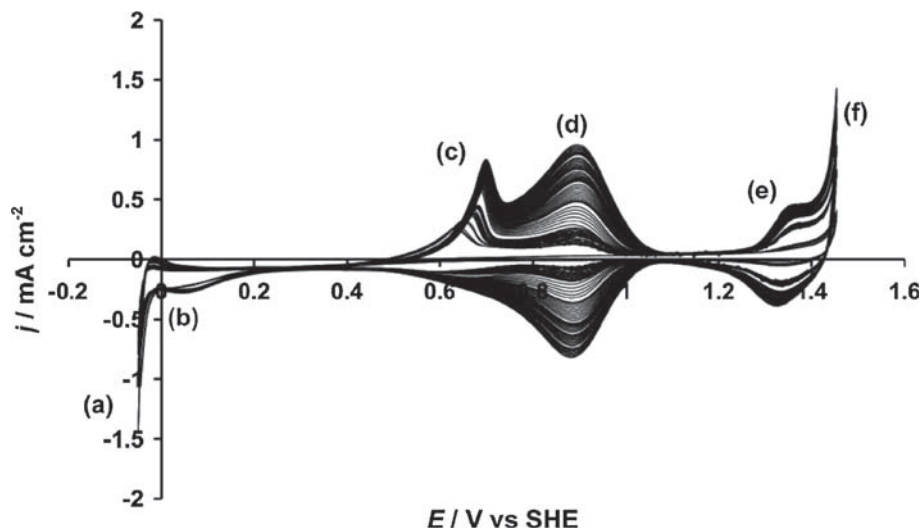


Fig. 2 Successive cyclic voltammograms (three scan number intervals: from scan 1 to scan 40; from scan 90 to scan 130 and from scan 150 to scan 350) using a p-Si/Ir electrode at 50 mV s^{-1} between -0.05 and 1.45 V . Supporting electrolyte: $1 \text{ M H}_2\text{SO}_4$. $T = 25 \text{ }^\circ\text{C}$. *a* hydrogen evolution domain, *b* reduction of dissolved O_2 domain, *c* pre-peak, *d* redox couple Ir(IV)/Ir(III), *e* redox couple Ir(V)/Ir(IV) and *f* oxygen evolution reaction domain



(AIROF) are very different from those obtained using TDIROF. These anodic films are obtained by cycling the potential in the range between -0.05 and 1.45 V . Figure 2 shows three series of consecutive CV scans (from scan 1 to scan 40, from scan 90 to scan 130 and from scan 150 to scan 350) recorded at 50 mV s^{-1} in $1 \text{ M H}_2\text{SO}_4$ using a metallic iridium electrode. The results are in very good accordance with similar CV curves found in literature [11, 12]. The first voltammograms show almost no surface activity between hydrogen evolution at -0.05 V (Region (a) in Fig. 2) and oxygen evolution at 1.45 V (Region (f) in Fig. 2), which are the first signals to appear together with dissolved O_2 reduction at 0.2 V (Region (b) in Fig. 2) in aerated solution. This last reaction has been clearly identified as no activity was observed in that potential region when using de-aerated solutions.

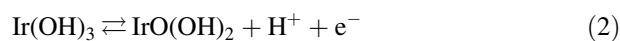
After approximately 50 scans, three anodic peaks appear at 0.65 V (peak (c) in Fig. 2), 0.9 V (peak (d) in Fig. 2) and 1.2 V (peak (e) in Fig. 2). The irreversible peak (c) (reported as pre-peak) is the first to appear followed by the reversible peaks (d) and (e) before oxygen evolution.

The pre-peak is progressively shifted toward more positive potentials with increasing scan number (from 0.65 V for scan number 50 to 0.7 V for scan number 350); however, the position of peaks (d) and (e) are only slightly shifted with increasing scan number. These shifts are certainly related to the reversibility of the surface processes involved.

Figure 3 shows CV measurements of AIROF obtained in the potential range between -0.05 and 1.25 V then moving toward the upper potential limit with increments of 20 mV up to 1.49 V . This figure shows clearly that the reduction of dissolved oxygen at 0.2 V is strongly related with the oxygen evolution reaction, which has an onset potential of about 1.36 V .

The surface reactions related to redox couples (d) and (e) have been discussed in literature [11, 12] and are believed to be the following:

At 0.9 V , peak (d) on fig. 2:



At 1.35 V , peak (e) on fig. 2:



These cyclic voltammetry measurements show that TDIROF and AIROF have different kinetics for the involved surface redox activity. In fact, on iridium dioxide prepared through thermal decomposition (TDIROF), the surface process is slow while on the oxide film prepared anodically (AIROF), numerous fast surface redox reactions are involved. Furthermore, AIROF are active toward the reduction of dissolved oxygen contrary to TDIROF, which is inactive toward the same process.

These differences are mainly due to the preparation technique of the electrode. In fact, AIROF are produced under mild conditions involving the anodic oxidation at room temperature through potential cycling of pure iridium metal. It has been shown that this method yields much more hydrated IrO_2 with higher bulk defect densities compared to TDIROF [16]. Furthermore, it has been shown that treating the AIROF at high temperature, which implies the loss of water molecules, yields to an electrode whose behavior tend to approach the one of TDIROF [8]. It is therefore clear that the observed differences in the surface processes between TDIROF and AIROF are related to the hydration of the obtained oxide.

3.2 The oxygen evolution reaction

Figure 4 shows a typical steady polarization curve for the OER on TDIROF electrodes in 1 M HClO_4 . In the same

Fig. 3 Cyclic voltammograms recorded at 50 mV s^{-1} using AIROF for different potential windows: the lower cut-off was fixed at -0.05 V while the higher cut-off varies from 1.25 to 1.49 V with increments of 20 mV . Supporting electrolyte: $1 \text{ M H}_2\text{SO}_4$. $T = 25 \text{ }^\circ\text{C}$

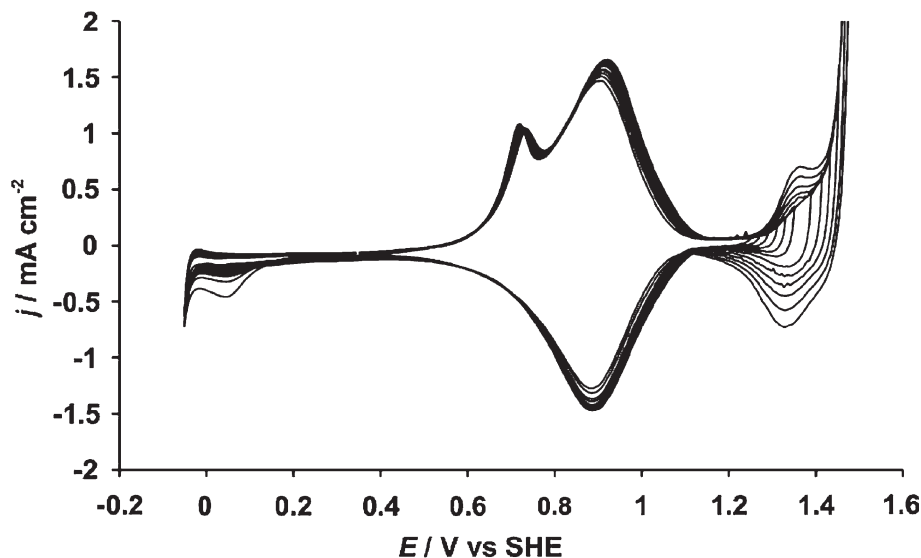
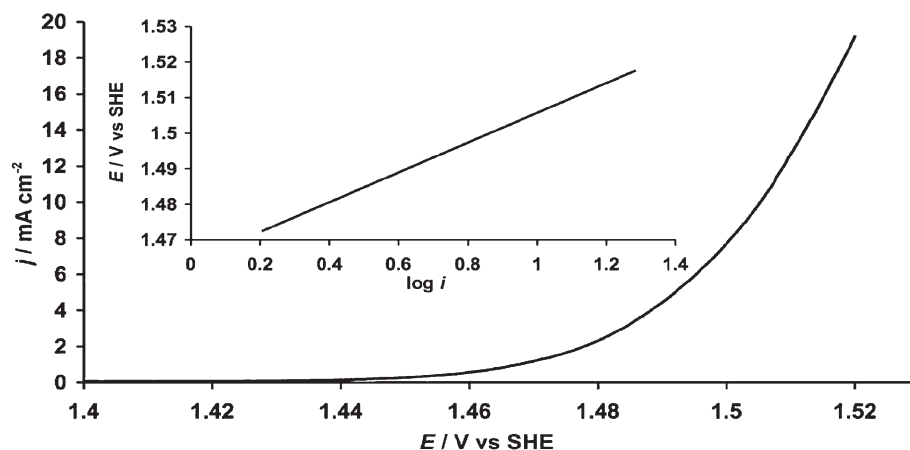


Fig. 4 Steady-state polarization curves recorded between 1.4 and 1.52 V using TDIROF (IrO_2 loading: 0.35 mg cm^{-2}). Inset Corresponding IR drop-corrected Tafel plot. Supporting electrolyte: 1 M HClO_4 . $T = 25 \text{ }^\circ\text{C}$



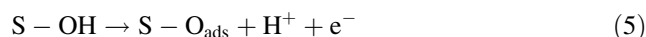
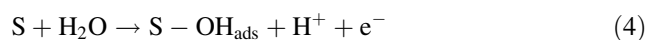
figure, the corresponding Tafel plot obtained after IR drop correction (inset of Fig. 4) is also given. It can be seen that even at high overpotentials, the IR drop-corrected Tafel plot gives a linear relation with a slope of about 40 mV/decade .

It is worthwhile to notice that these polarization measurements are reproducible even after treatment of the electrode for a long period of time (several hours) at high anodic potentials ($>1.5 \text{ V}$). This is an indication of the high anodic stability of the TDIROF.

Figure 5 shows IR drop corrected Tafel plots obtained for a fresh iridium electrode (p-Si/Ir) ((a) on Fig. 5) and for AIROF ((b) on Fig. 5) formed by potential cycling (50 cycles at 50 mV s^{-1} between -0.05 and 1.45 V).

This figure shows clearly that the Tafel slope for the OER changes from 120 mV/decade for the Ir metal to 40 mV/decade for the AIROF indicating that the rate determining step of the OER on pure iridium differs from the one occurring on AIROF.

In acid medium, the following reaction path (Eqs. 4, 5 and 6) was proposed for the oxygen evolution reaction (OER) on active oxide electrodes [17].



where S stands for active sites and OH_{ads} , O_{ads} are adsorption intermediates.

This mechanism predicts the following Tafel slopes: 120 mV/decade if step 4 is the rate-determining step (rds), 40 mV/decade for step 5 and 30 mV/decade for step 6.

The measured Tafel slopes indicate that water discharge (step 4) is the rds for the OER on metallic iridium (Tafel slope 120 mV/decade) and formation of a higher oxide (step 5) is the rds in case of IrO_2 formed either by the anodic oxidation of metallic Ir (AIROF) or by the thermal

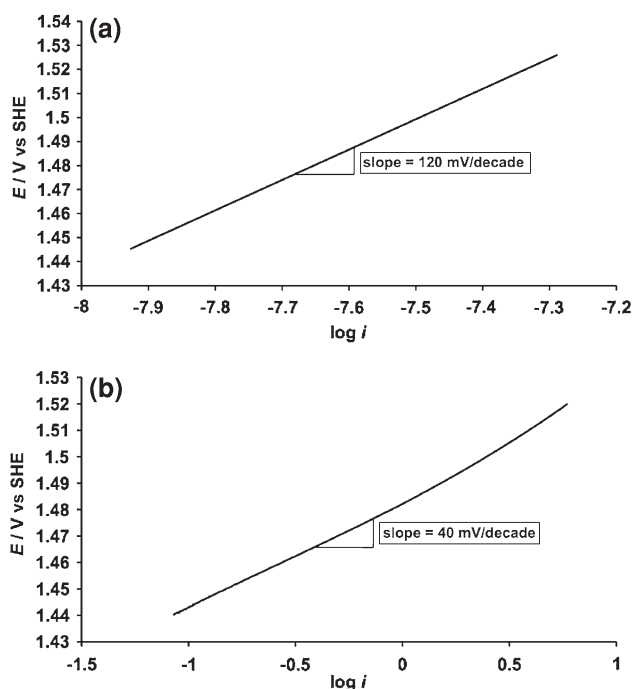


Fig. 5 IR drop-corrected Tafel slopes recorded between 1.44 and 1.52 V corresponding to: **a** fresh p-Si/Ir electrode, **b** AIROF. Supporting electrolyte: 1 M H₂SO₄. *T* = 25 °C

decomposition of a precursor solution (TDIROF). This is an indication that the same mechanism of OER is involved on both AIROF and TDIROF. The participation of the higher oxide in the OER on TDIROF via the IrO₃/IrO₂ redox couple has been recently demonstrated using ¹⁸O labelling together with differential electrochemical mass spectrometry (DEMS) measurements [13].

It is worthwhile to notice that the treatment of the AIROF at high potentials (>1.6 V) for a few minutes results in an increase of Tafel slope from 40 to 120 mV/decade. This is an indication that at these potentials, the anodically formed film is corroded as already reported by others [10, 18].

Figure 6 shows that the normalized polarization curves (the current is reported relative to the voltammetric charge measured from the CV curves between −0.05 and 1.45 V at 50 mV s^{−1}) for the OER are almost the same for both TDIROF and AIROF electrodes. This is an indication that both electrodes have almost the same specific electrocatalytic activity.

However, it is worthwhile to mention that the obtained Tafel plots for the OER using TDIROF in this work (40 mV/decade) are different from those reported by others. In fact, a Tafel slope of 60 mV/decade for the OER in acidic media has been usually reported [17, 19]. A very intriguing reaction path involving S–OH_{ads} intermediates with different energy states has been proposed by these authors in order to explain this abnormal Tafel slope

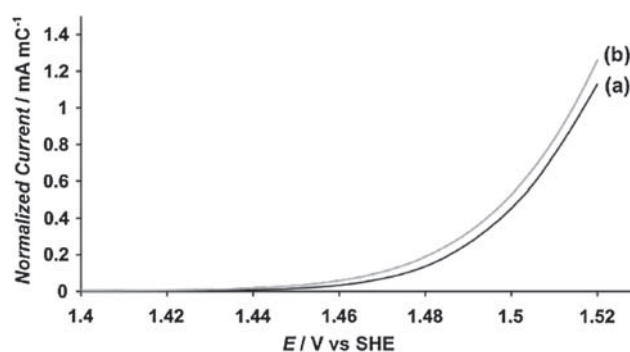


Fig. 6 Normalized steady-state polarization curves using: *a* the AIROF, *b* the TDIROF (IrO₂ loading: 0.35 mg cm^{−2}). The current has been normalized relative to the voltammetric charge measured between −0.05 and 1.45 V at 50 mV s^{−1}. *T* = 25 °C

[17, 19]. Problems related with uncompensated IR drop correction and partial blockage of the electrode surface by the evolved oxygen are certainly related with the reported abnormal Tafel slopes. In the present study, the experiments have been carefully conducted in order to avoid these problems.

3.3 Oxidation of organics using formic acid as a model compound

Figure 7 shows steady-state polarization curves obtained on TDIROF in 1 M HClO₄ containing different concentration of Formic Acid (FA). The shift of these I–V curves toward less positive potentials in presence of FA is related with the involvement of the same redox couple IrO₃/IrO₂ in both the oxygen evolution reaction (Eq. 9) and FA oxidation (Eq. 10) competing during the process according to the reaction path given in Eq. 7–10.

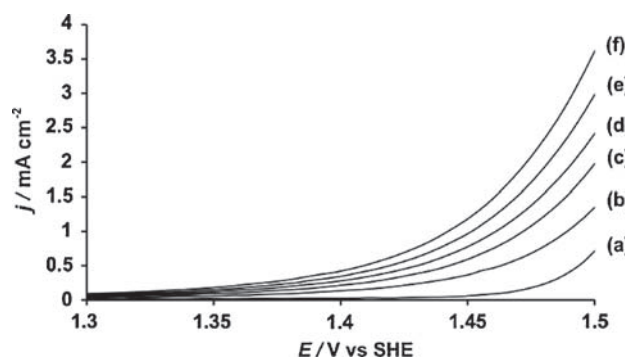
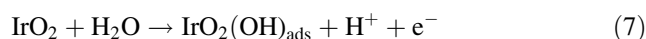
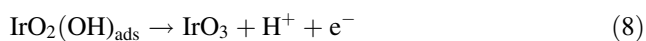
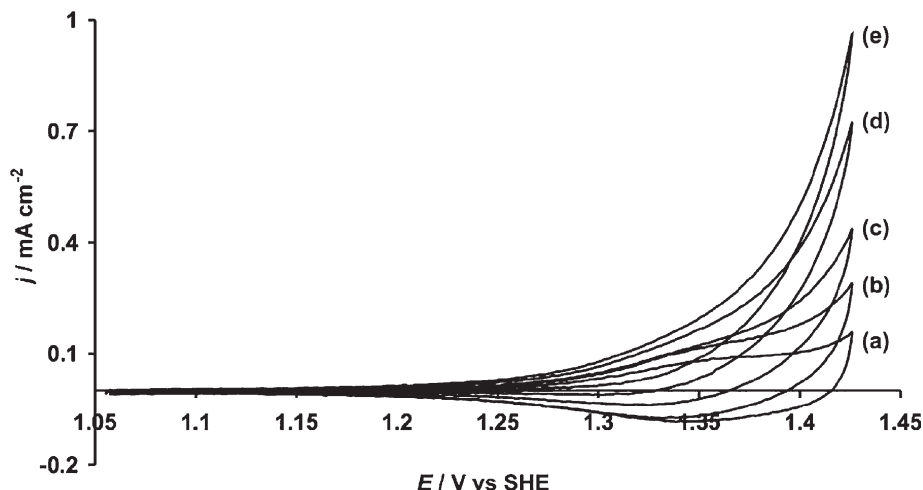


Fig. 7 Steady-state polarization curves between 1.3 and 1.5 V using TDIROF (IrO₂ loading: 0.35 mg cm^{−2}) for different concentration of formic acid: *a* 0 mM, *b* 195.33 mM, *c* 387.78 mM, *d* 577.4 mM, *e* 764.25 mM and *f* 948.41 mM. Supporting electrolyte: 1 M HClO₄. *T* = 25 °C

Fig. 8 Cyclic voltammograms recorded at 100 mV s^{-1} between 1.055 and 1.425 V using AIROF for different concentration of formic acid: *a* 0 mM, *b* 100 mM, *c* 250 mM, *d* 500 mM and *e* 750 mM. Supporting electrolyte: 1 M H_2SO_4 . $T = 25 \text{ }^\circ\text{C}$



This mechanism has been proved recently on TDIROF electrodes using ^{18}O labelling combined with DEMS measurements [14, 20].

Figure 8 shows CV obtained on AIROF in 1 M H_2SO_4 containing different concentration of formic acid. This figure clearly shows that the reduction peak related with the redox couple Ir(V)/Ir(IV) decreases strongly with increasing FA concentration. This is an indication that this redox couple is involved during FA oxidation on AIROF.

It is worthwhile to notice that the anodic oxide film was completely corroded at the end of these experiments.

4 Conclusions

The main conclusions can be summarized below:

- The surface redox activities involved on the AIROF are much faster than those involved on the TDIROF. Formation of a highly hydrated AIROF is certainly the main reason of the high surface activity of IrO_2 film electrodes obtained by the anodic polarization of Ir metal (AIROF).
- The investigation of the oxygen evolution reaction in acid media has shown that both films show similar mechanisms (same Tafel slope of 40 mV/decade) and specific electrocatalytic activity (similar normalized I–V curves).
- The involved surface redox couple during the anodic oxidation of formic acid (FA) depends strongly on the preparation mode of the IrO_2 anodes. In fact, on TDIROF the oxidation of FA and the OER compete

involving the same surface redox couple Ir(VI)/Ir(IV). However, this is not the case on the AIROF, where the oxidation of FA involves the Ir(V)/Ir(IV) surface redox couple and is not competing with the OER.

- Electrode stability measurements have shown that contrary to TDIROF, which are very stable under anodic polarization, the AIROF are rapidly corroded under anodic treatment. This corrosion is further enhanced in the presence of formic acid.

Acknowledgments The authors gratefully thank the Fonds National Suisse de la Recherche Scientifique for financial support as well as the Sensors, Actuators and Microsystems Laboratory, Institute of Microtechnology, University of Neuchâtel (SAMPLAB-UNINE) for providing the iridium electrodes.

References

1. Trasatti S, O'Grady WE (1981) In: Gerisher H, Tobias CW (eds) *Advances in electrochemistry and electrochemical engineering*. Wiley, New York, p 177
2. Comminellis Ch, Nerini A (1995) *J Appl Electrochem* 25:23
3. Beck F, Schultz H (1984) *Electrochim Acta* 29:1569
4. Trasatti S (2000) *Electrochim Acta* 45:2377
5. Beer H, Hinden JM (1985) EU Patent EP 0,046,449 B1
6. Hinden JM et al (1984) US Patent 4,444,642
7. Hüppauff M, Lengeler B (1993) *J Electrochem Soc* 140:598
8. Silva TM, Simões AMP, Ferreira MGS, Walls M, Da Cunha Belo M (1998) *Electroanal Chem* 441:5
9. Jaksic MM, Johansen B, Tunold R (1994) *Int J Hydrogen Energy* 19:321
10. Cukman D, Vukovic M (1990) *J Electroanal Chem* 279:283
11. Kötzt R, Neff H, Stucki S (1984) *J Electrochem Soc* 131:72
12. Kötzt R (1990) In: Gerischer H, Tobias CW (eds) *Advances in electrochemical science and engineering*. Verlag Chemie, Heidelberg, p 109
13. Fierro S, Nagel T, Baltruschat H, Comminellis Ch (2007) *Electrochem Commun* 9:1969
14. Fierro S, Nagel T, Baltruschat H, Comminellis Ch (2008) *Electrochem Solid-State Lett* 11(7):E20
15. Fierro S, Ouattara L, Herrera Calderon E, Comminellis Ch (2008) *Electrochem Commun* 10:955

16. Trasatti S (1980) In: Trasatti S (ed) Studies in physical and theoretical chemistry: electrodes of conductive metallic oxides Part A. Elsevier Scientific Publishing Company, Amsterdam, p 155
17. De Faria LA, Boodts JFC, Trasatti S (1996) J Appl Electrochem 26:1195
18. Vukovic M (1990) J Appl Electrochem 20:969
19. Gottesfeld S, Srinivasan S (1978) J Electroanal Chem 86:89
20. Fierro S et al (2008) Electrochim Acta. doi: [10.1016/j.electacta.2008.06.060](https://doi.org/10.1016/j.electacta.2008.06.060)



Electrochemical comparison between IrO₂ prepared by thermal treatment of iridium metal and IrO₂ prepared by thermal decomposition of H₂IrCl₆ solution

Stéphane Fierro*, Agnieszka Kapałka, Christos Comninellis

Institute of Chemical Sciences and Engineering, Swiss Federal Institute of Technology, ISIC-EPFL, CH-1015 Lausanne, Switzerland

ARTICLE INFO

Article history:

Received 14 October 2009

Received in revised form 10 November 2009

Accepted 10 November 2009

Available online 18 November 2009

Keywords:

IrO₂

Thermal decomposition of H₂IrCl₆

Thermal treatment of metallic Ir

Oxygen evolution

Formic acid oxidation

Surface redox activity

ABSTRACT

The surface redox activities, the oxygen evolution reaction (OER), the oxidation of formic acid (FA) and the anodic stability have been investigated and compared on IrO₂ electrodes prepared by two techniques: the thermal decomposition of H₂IrCl₆ precursor (TDIROF) and the thermal treatment of metallic iridium (TOIROF). It was found, that the surface redox activities involved on both IrO₂-based electrodes are similar. Concerning the oxygen evolution reaction and the oxidation of formic acid, both films show similar mechanism.

The electrode stability measurements have shown that both films are not corroded under strong OER or organics oxidation conditions and therefore, to summarize, both IrO₂-based films exhibit similar electrochemical behaviours.

© 2009 Elsevier B.V. All rights reserved.

1. Introduction

Iridium dioxide is known to be a good electrocatalyst for oxygen/chlorine evolution as well as electrochemical oxidation of organic compounds [1–3]. IrO₂ electrodes are usually prepared by thermal decomposition of the appropriate precursor solution (usually H₂IrCl₆) on an inert substrate such as titanium or tantalum [4,5]. The thermally prepared iridium dioxide electrodes (TDIROF) form part of the dimensionally stable anodes (DSA®) [1]. The big advantage of these electrodes is their long lifetime under oxygen evolution (OER) or organics electro-oxidation [6]. An alternative method of preparation of iridium dioxide electrodes is the anodic oxidation of metallic iridium (AIROF). In this method, the iridium dioxide film is grown at the metallic iridium electrode through potential cycling. It has been shown that on the contrary to TDIROF, AIROF rapidly corrodes under anodic polarization [6]. The corrosion is even more enhanced in the presence of organic compounds what makes AIROF unsuitable for large scale applications, e.g., in wastewater treatment.

In this paper, we compare TDIROF with IrO₂ film prepared by thermal treatment of metallic iridium (TOIROF). The electro-catalytic activity and stability of both electrodes is investigated. It is shown that the electrochemical behaviour of TOIROF is similar to TDIROF. Both electrodes are very stable under strong OER and or-

ganic oxidation conditions. Moreover, the surface redox activities involved during the OER and oxidation of formic acid are similar for both IrO₂-based films.

2. Experimental

All electrochemical experiments were performed in a classical three-electrode cell (70 ml) using an Autolab PGSTAT 30. The counter electrode was a Pt wire; the reference electrode was Hg/Hg₂SO₄/K₂SO₄ (sat.) (MSE; 0.65 V vs. SHE) and two different working electrodes were used:

- An IrO₂ electrode prepared by thermal treatment of iridium metal (TOIROF): an iridium film (0.1 μm) was deposited by sputtering on p-Si (0.0054 mm²) above a thin (0.02 μm) tantalum interlayer (p-Si/Ir). The thermally oxidized iridium oxide film (TOIROF) was formed by thermal treatment of the resulting iridium metal in air at 500 °C for 90 min.
- An IrO₂ electrode prepared by thermal decomposition of a precursor (TDIROF): the IrO₂ film (0.27 mg cm⁻²) was deposited on disc-shaped sandblasted p-Si (182.25 mm²) by the thermal decomposition of a H₂IrCl₆ (99.9%, ABCR) precursor aqueous solution in air at 500° (TDIROF).

The presence of iridium dioxide on the substrate was verified using XPS measurements (not presented).

All potentials in this work are with respect to the standard hydrogen electrode (SHE).

* Corresponding author.

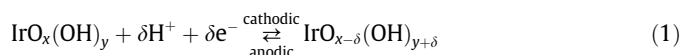
E-mail address: stephane.fierro@epfl.ch (S. Fierro).

3. Results and discussion

3.1. Surface redox activities

Fig. 1A and B show the cyclic voltammetry recorded for three potential windows, in the potential range between 0.0 V and 1.4 V, on TDIROF and TOIROF, respectively. The charge involved in the anodic scan is completely recovered during the cathodic scan ($q_+ = q_-$) for all the scan rates investigated (10–500 mV s^{-1}) and for both IrO_2 -based electrodes. Both CV show an axial symmetry (around the potential axis) only if the lower potential limit is higher than 0.4 V. In fact, at lower potential limits, a strong distortion of the CV around the potential axis is observed. This is an indication that the surface processes involved at low potentials (<0.4 V) are slow for both electrodes.

In a previous work [7], from apparent activation energy (E_a) measurements for the charging/discharging process using TDIROF, two contributions were considered for this process. The first contribution is a fast (instantaneous) process with zero activation energy related to the charging of the electrical double-layer at the electrode–electrolyte interface and the second corresponds to the slow diffusion of protons within the iridium oxide coating inducing surface redox activities (Eq. 1) with an activation energy around 2.4 kJ mol^{-1} [7].



These cyclic voltammetry measurements show that TDIROF and TOIROF have similar kinetics for the involved surface redox activity. In fact, on both iridium oxide based electrodes, the surface process is slow and can be related to reaction 1.

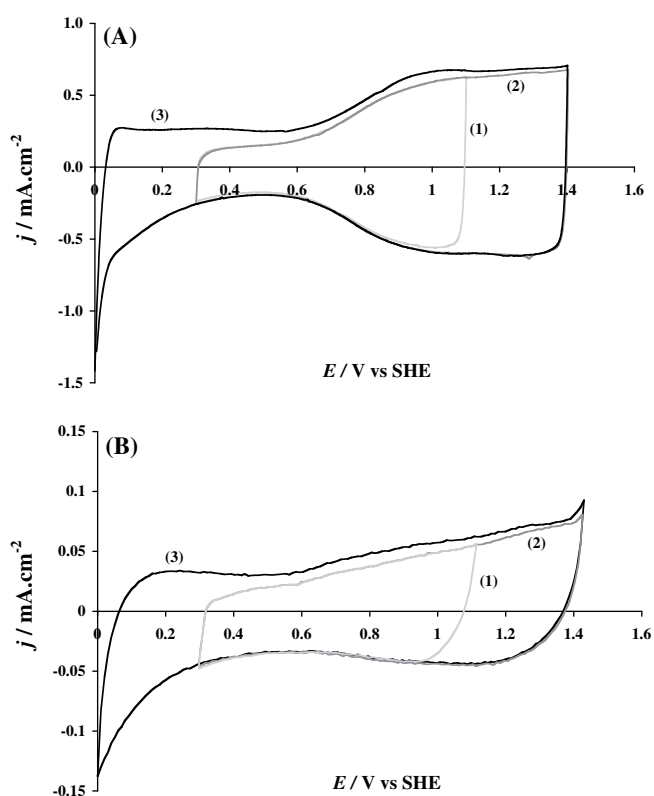


Fig. 1. Cyclic voltammograms recorded on (A) TDIROF (IrO_2 loading: 0.273 mg cm^{-2}) and (B) TOIROF at 100 mV s^{-1} for different potential windows (1) between 0.3 V and 1.1 V (2) between 0.3 V and 1.4 V (3) between 0 V and 1.4 V. Supporting electrolyte: 1 M HClO_4 , $T = 25^\circ\text{C}$.

These similarities are inherent to the preparation technique. In fact, both electrodes are produced under conditions involving thermal treatment in air at 500°C . It has been shown that this method yields anhydrous and highly porous IrO_2 [7–9].

However, Fig. 1A and B show that the current response obtained on TDIROF is almost one order of magnitude higher than the response obtained on TOIROF. This is certainly due to the higher 3D roughness factor (related to the IrO_2 loading) of TDIROF compared to TOIROF because all the coating participates actively in the charging/discharging process (Eq. 1) [7].

3.2. Intermediates involved in the oxygen evolution reaction (OER) and the oxidation of formic acid

Fig. 2 shows normalized polarization curves (the current is reported relative to the voltammetric charge measured from the CV curves between 0 V and 1.4 V at 50 mV s^{-1}) for the OER on (a) TOIROF electrodes and (b) TDIROF electrodes in 1 M HClO_4 . In the same figure, the Tafel plots obtained for the OER after IR drop correction for both type of IrO_2 electrodes (inset of Fig. 3) are also given. It can be seen that even at high overpotentials, the IR drop corrected Tafel plot gives a linear relation with a slope of about $40 \text{ mV decade}^{-1}$ for both IrO_2 -based electrodes.

It is worthwhile to notice that both electrode materials were not corroded by all these polarization measurements even after reaching high anodic potentials ($>1.5 \text{ V}$). This is an indication of the high anodic stability of TOIROF and TDIROF.

The fact that both normalized curves are almost the same proves that TOIROF and TDIROF have also almost the same specific electro-catalytic activity for the OER.

In acid medium, the following reaction path Eqs. (2)–(4) was proposed for the oxygen evolution reaction (OER) on active oxide electrodes [10].



where S stands for active sites and OH_{ads} , O_{ads} are adsorption intermediates.

This mechanism predicts the following Tafel slopes: $120 \text{ mV decade}^{-1}$ if step 2 is the rate determining step (rds), $40 \text{ mV decade}^{-1}$ for step 3 and $30 \text{ mV decade}^{-1}$ for step 4.

The measured Tafel slope indicates that formation of a higher oxide (step 3) is the rate determining step (rds) for both IrO_2 electrodes. This is an indication that TOIROF and TDIROF have the same

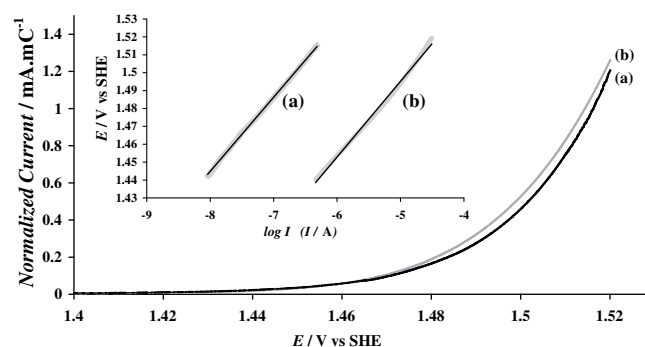
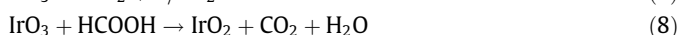
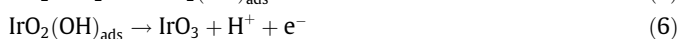
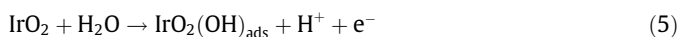


Fig. 2. Normalized steady state polarization curves using (a) TOIROF and (b) TDIROF (IrO_2 loading: 0.273 mg cm^{-2}). The current has been normalized relative to the voltammetric charge measured between 0 and 1.4 V at 50 mV s^{-1} . Inset: IR drop corrected Tafel plots for (a) TOIROF and (b) TDIROF. Supporting electrolyte: 1 M HClO_4 , $T = 25^\circ\text{C}$.

mechanism of oxygen evolution. In fact, the participation of the higher oxide in the OER on TDIROF via the $\text{IrO}_3/\text{IrO}_2$ redox couple has been demonstrated in another study using ^{18}O labelling together with differential electrochemical mass spectrometry (DEMS) measurements [11].

Figs. 3 and 4 shows steady state polarization curves obtained on TDIROF and TOIROF respectively in 1 M HClO_4 containing different concentration of formic acid (FA). The shift of these I - V curves toward less positive potentials in presence of FA is related with the involvement of the same redox couple $\text{IrO}_3/\text{IrO}_2$ in both the oxygen evolution reaction (Eq. 7) and FA oxidation (Eq. 8) competing during the process according to the reaction path given in Eqs. (5)–(8).



This mechanism has been proved recently on TDIROF electrodes using ^{18}O labelling combined with DEMS measurements [11,12].

The inset of Fig. 4 shows the Tafel plot corresponding to formic acid (100 mM) oxidation on TOIROF obtained after IR drop correction and subtraction of the current related to the oxygen evolution

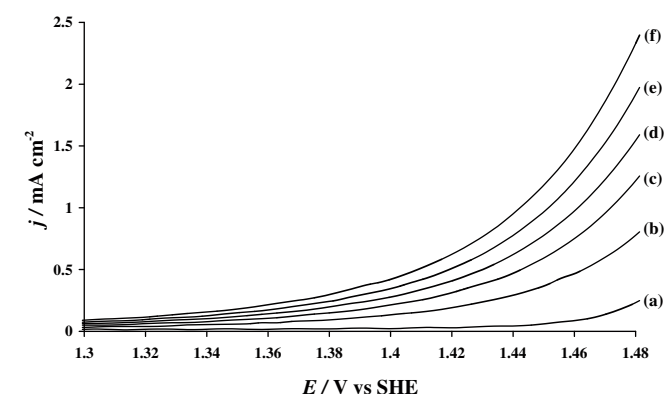


Fig. 3. Steady state polarization curves between 1.3 V and 1.5 V using TDIROF (IrO_2 loading: 0.35 mg cm^{-2}) for different concentration of formic acid: (a) 0 mM, (b) 195.33 mM, (c) 387.78 mM, (d) 577.4 mM, (e) 764.25 mM and (f) 948.41 mM. Supporting electrolyte: 1 M HClO_4 , $T = 25^\circ\text{C}$.

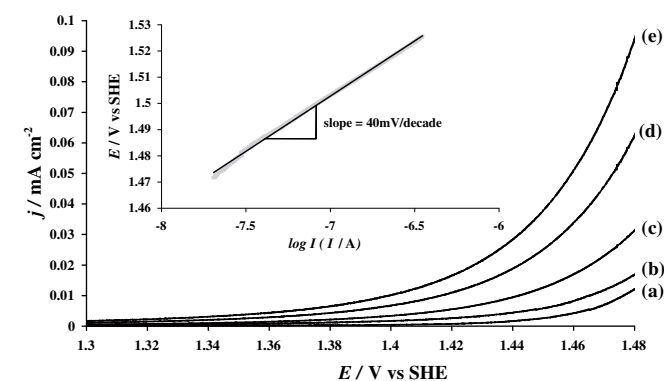


Fig. 4. Steady state polarization curves between 1.3 V and 1.5 V using TOIROF for different concentration of formic acid: (a) 0 mM, (b) 100 mM, (c) 250 mM, (d) 500 mM and (e) 750 mM. Supporting electrolyte: 1 M HClO_4 , $T = 25^\circ\text{C}$. Inset shows IR drop corrected and OER background subtracted Tafel slope recorded between 1.44 V and 1.52 V corresponding to oxidation of 100 mM of formic acid on TOIROF.

reaction. This figure shows clearly that on TOIROF, the same Tafel slope was reported for the oxidation of FA and the oxygen evolution reaction i.e. $40 \text{ mV decade}^{-1}$. This is an indication that the redox couple $\text{IrO}_3/\text{IrO}_2$ is involved in both processes on TOIROF, which is exactly the case of TDIROF as proved by DEMS measurements [11,12,14].

It is worthwhile to notice that the IrO_2 electrode prepared by thermal treatment of pure iridium (TOIROF) remained intact at the end of these experiments. This high stability toward organics oxidation has been also observed on TDIROF in previous studies [6,13,14].

4. Conclusions

This work concerns a comparative study of the electrochemical activity of iridium dioxide film electrodes prepared by two techniques: (a) thermal treatment of iridium metal in air (TOIROF) and (b) thermal decomposition of H_2IrCl_6 precursor solution on p-Si substrate (TDIROF).

The main conclusions are summarized below:

- The surface redox activities involved are similar for both IrO_2 -based films. These resemblances are inherent to the preparation conditions of both oxide films (thermal treatment in air at 500°C).
- The investigation of oxygen evolution reaction and formic acid oxidation in acid media has shown that both films show similar mechanism (same Tafel slope of $40 \text{ mV decade}^{-1}$) involving the same intermediate (the $\text{IrO}_3/\text{IrO}_2$ surface redox couple).
- Electrode stability measurements have shown that no corrosion was observed on both IrO_2 -based electrodes under strong OER and organic oxidation conditions.

Finally, it can be considered that the iridium oxide films prepared by thermal treatment of pure iridium (TOIROF) and by thermal decomposition of a precursor solution (TDIROF) exhibit similar electrochemical behaviours.

Acknowledgment

The authors gratefully thank the Fonds National Suisse de la Recherche Scientifique for the financial support as well as SAM-LAB-UNINE for providing the iridium electrodes.

References

- [1] S. Trasatti, *Electrochim. Acta* 45 (2000) 2377.
- [2] S. Trasatti, W.E. O'Grady, in: H. Gerischer, C.W. Tobias (Eds.), *Advances in Electrochemistry and Electrochemical Engineering*, John Wiley and Sons, New York, USA, 1981, p. 177.
- [3] F. Beck, H. Schulz, *Electrochim. Acta* 29 (1984) 1569.
- [4] H. Beer, J.M. Hinden, EU Pat. EP 0 046 449 B1, 1985.
- [5] J.M. Hinden et al., US Pat. 4,444,642, 1984.
- [6] L. Ouattara, S. Fierro, O. Frey, M. Koudelka, Ch. Comninellis, *J. Appl. Electrochem.* 39 (2009) 1361.
- [7] S. Fierro, L. Ouattara, E. Herrera Calderon, Ch. Comninellis, *Electrochem. Commun.* 10 (2008) 955.
- [8] T.M. Silva, A.M.P. Simões, M.G.S. Ferreira, M. Walls, M. Da Cunha Belo, *Electroanal. Chem.* 441 (1998) 5.
- [9] S. Trasatti, in: S. Trasatti (Ed.), *Studies in Physical and Theoretical Chemistry: Electrodes of Conductive Metallic Oxides Part A*, Elsevier Scientific Publishing Company, Amsterdam, 1980, p. 155.
- [10] L.A. De Faria, J.F.C. Boodts, S. Trasatti, *J. Appl. Electrochem.* 26 (1996) 1195.
- [11] S. Fierro, T. Nagel, H. Baltruschat, Ch. Comninellis, *Electrochem. Commun.* 9 (2007) 1969.
- [12] S. Fierro, T. Nagel, H. Baltruschat, Ch. Comninellis, *Electrochem. Solid-State Lett.* 11 (7) (2008) E20.
- [13] S. Fierro, L. Ouattara, E. Herrera Calderon, E. Passas-Lagos, H. Baltruschat, Ch. Comninellis, *Electrochim. Acta* 54 (2009) 2053.
- [14] S. Fierro, E. Passas-Lagos, E. Chatzisyseon, D. Mantzavinos, Ch. Comninellis, *Electrochem. Commun.* 11 (2009) 1358.



Contents lists available at ScienceDirect

Electrochemistry Communications

journal homepage: www.elsevier.com/locate/elecomMicroelectrode-array of IrO₂ prepared by thermal treatment of pure IrStéphane Fierro^{a,*}, Agnieszka Kapałka^a, Olivier Frey^b, Milena Koudelka^b, Christos Comninellis^a^a Institute of Chemical Sciences and Engineering, Swiss Federal Institute of Technology, ISIC-EPFL, CH-1015 Lausanne, Switzerland^b The Sensors, Actuators and Microsystems Laboratory, Institute of Microtechnology, University of Neuchâtel, SAMLAB-UNINE, Jaquet-Droz 1, 2007 Neuchâtel, Switzerland

ARTICLE INFO

Article history:

Received 15 January 2010

Received in revised form 5 February 2010

Accepted 8 February 2010

Available online xxx

Keywords:

Microelectrode-array

IrO₂

Capacitive current

Thermal treatment of pure Ir

ABSTRACT

In this paper, the IrO₂ electrode preparation technique consisting in thermal treatment of air with pure Ir was used in order to produce an IrO₂-based microelectrode-array (TOIROF-MEA) with low capacitive background current. The TOIROF-MEA was characterized using Fe(CN)₆^{4-/3-} as model redox couple. It was found that very low concentrations can be detected; this feature makes TOIROF-MEA suitable for analytical applications.

© 2010 Published by Elsevier B.V.

1. Introduction

IrO₂-based electrodes, produced by thermal decomposition of H₂IrCl₆ (TDIROF), are widely used for oxygen and chlorine evolution as well as electrochemical oxidation of organic compounds [1–4]. The main advantages of these electrodes are the high catalytic activity and long lifetime. These electrodes have been also proposed for analytical applications; however, a high capacitive background current inherent to these electrodes [5,6] gives strong limitations for traces analysis. The use of IrO₂ microelectrode might overcome this problem. Besides low capacitive current, microelectrodes have many other advantages, like small ohmic drop, superior mass transport (spherical diffusion) and possibility to work at very high scan rates [7].

Up to date, IrO₂ microelectrodes, used mainly as pH sensors, are prepared by anodic oxidation of metallic iridium (AIROF). However, AIROF electrodes suffer heavy corrosion under anodic polarization [8].

In this work, we characterize a IrO₂-based microelectrode-array (MEA), prepared by thermal treatment of pure iridium in air (TOIROF). Recently, it has been shown that TOIROF exhibits similar electrochemical behaviour to TDIROF [9]. Moreover, anodic treatment for long periods of time (several hours) and steady-state polarization curves recorded on TOIROF in acidic media and in the presence of formic acid have shown that the stability of TOIROF is also very similar to the one of TDIROF [9]. The TOIROF-MEA is investigated using Fe(CN)₆^{4-/3-} as model redox couple. It is shown that the high

capacitive current, usually recorded on IrO₂ macroelectrodes, can be considerably reduced when using TOIROF-MEA and very low concentration of the investigated redox couple can be detected.

2. Experimental

All electrochemical experiments were performed in a classical three-electrode cell (70 ml) using an Autolab PGSTAT 30. The counter electrode was a Pt wire; the reference electrode was Hg/Hg₂SO₄/K₂SO₄ (sat.) (MSE; 0.65 V vs. SHE) and the working electrode was a TOIROF microelectrode-array (MEA) prepared by thermal treatment of pure iridium in air. The interconnected iridium MEA chips were produced using thin film microsystems technology. The fabrication is based on a photolithographic process and is schematically illustrated in Fig. 1.

The substrate used is a (1 0 0)-oriented, 4-in. silicon wafer ((a) in Fig. 1) passivated by 200 nm thermally grown silicon dioxide, followed by 200 nm silicon nitride using low-pressure chemical vapour deposition (LPCVD). This results in a dense, pinhole-free insulation layer on the silicon surface ((b) in Fig. 1).

The metal layer is patterned by a lift-off process. Therefore a homogeneous photo-sensitive resist is spin-coated on the substrate and structured using a chrome mask to cover those areas, where the metal is not required ((c) in Fig. 1). Tantalum (20 nm) serving as adhesion layer and 100 nm iridium are evaporated in the same deposition process on the whole surface of the wafer ((d) in Fig. 1). The removal of the photoresist takes off the Ta/Ir above it and leaves a metal layer only where previously defined ((e) in Fig. 1). The structured iridium is covered by a silicon nitride (LPCVD, 200 nm) top passivation. The microelectrodes and contact pads are

* Corresponding author.

E-mail address: stephane.fierro@epfl.ch (S. Fierro).

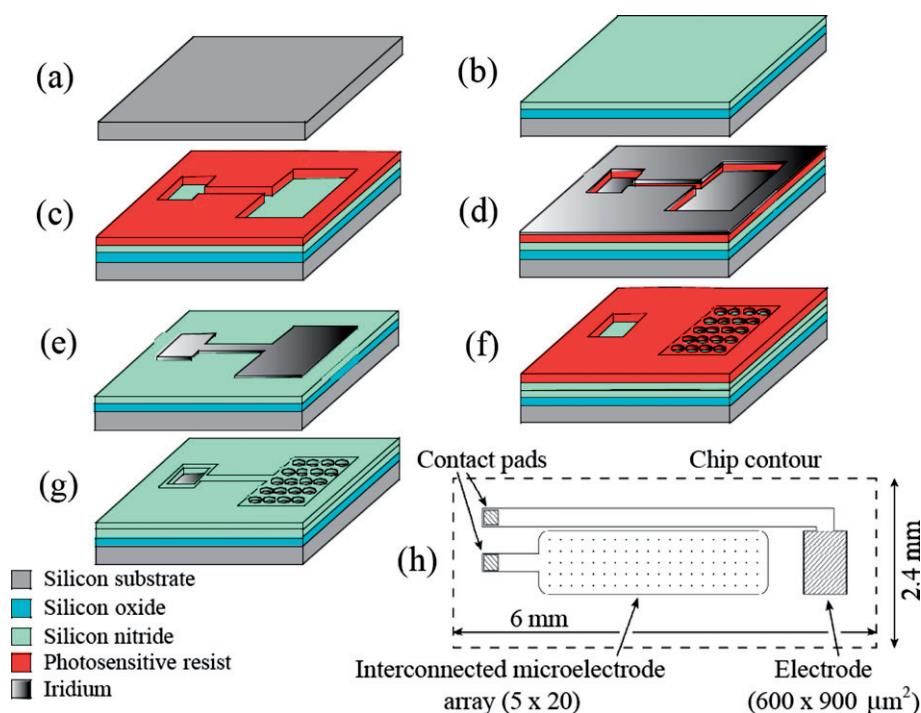


Fig. 1. Schema of the fabrication process of the iridium microchips (6 mm × 2.4 mm). (a) Silicon substrate, (b) pinhole-free insulation bi-layer deposited on the substrate, (c) deposition of photo-sensitive resist by spin coating and structuration of this resist using a chrome mask, (d) deposition of 20 nm tantalum adhesion layer followed by 100 nm of iridium, (e) removal of photoresist, (f) deposition of another insulation layer and photo-sensitive resist having the pattern of the electrode and the microelectrode-array, (g) the exposed insulation is removed by reactive ion etching and the remaining resist is stripped, (h) top view of the final interconnected iridium MEA chip.

created by removal of this insulation layer at specific sites. Therefore a second photopatterned resist is used as a mask. First, the silicon nitride is etched by reactive ion etching (RIE). Second, after resist stripping ((f) in Fig. 1), the wafer is immersed into concentrated H₃PO₄ (160 °C) for 10 min to completely expose the iridium sites and clean the metal surface ((g) in Fig. 1). Finally, the wafer is diced into single chips of the size of 2.4 × 6.0 mm². Two independent Ir structures are integrated on the chip: A square-shaped electrode with a geometric surface area of 0.54 mm² and an interconnected **microelectrode-array** consisting of 5 × 20 microdisks of 5 μm diameter (150 μm pitch). Each electrode structure is connected via wire bonds on the contact pads ((h) in Fig. 1).

The obtained pure Ir electrodes were treated in air at 500 °C for 90 min before the packaging process. The formation of IrO₂ film on metallic Ir by heat treatment in oxygen atmosphere in the temperature range between 500 and 800 °C has been previously reported [10–12]. The SEM photo of the obtained TOIROF-MEA is given as inset of Fig. 2.

3. Results and discussion

Voltammetric measurements performed on the TOIROF-MEA in the potential region of water stability showed that the capacitive current on this electrode is in the range of 10⁻² μA cm⁻² (Fig. 2)

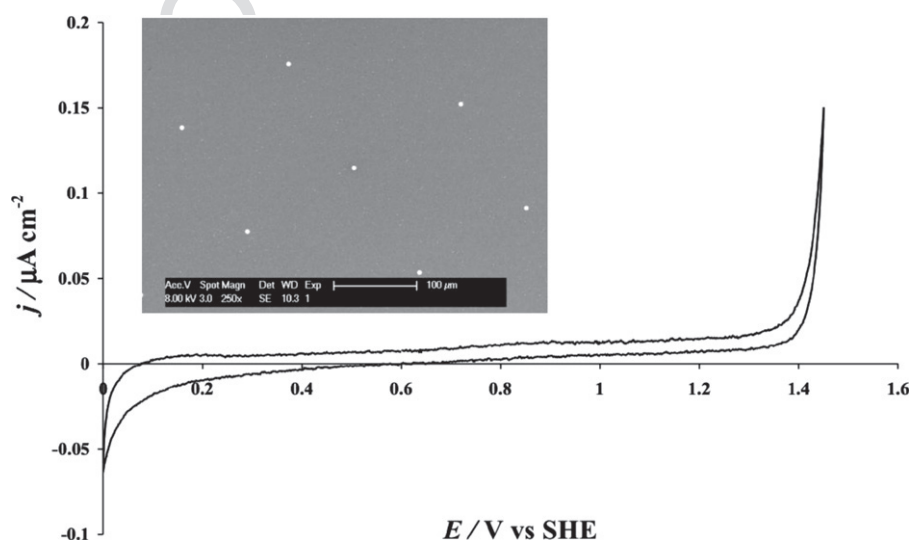


Fig. 2. Cyclic voltammogram recorded on TOIROF-MEA in 1 M H₂SO₄ at 10 mV s⁻¹, T = 25 °C. Inset shows a SEM photo of the TOIROF-MEA; the diameter of the single microelectrode in the array is 5 μm and the smallest spacing between microelectrodes is 150 μm.

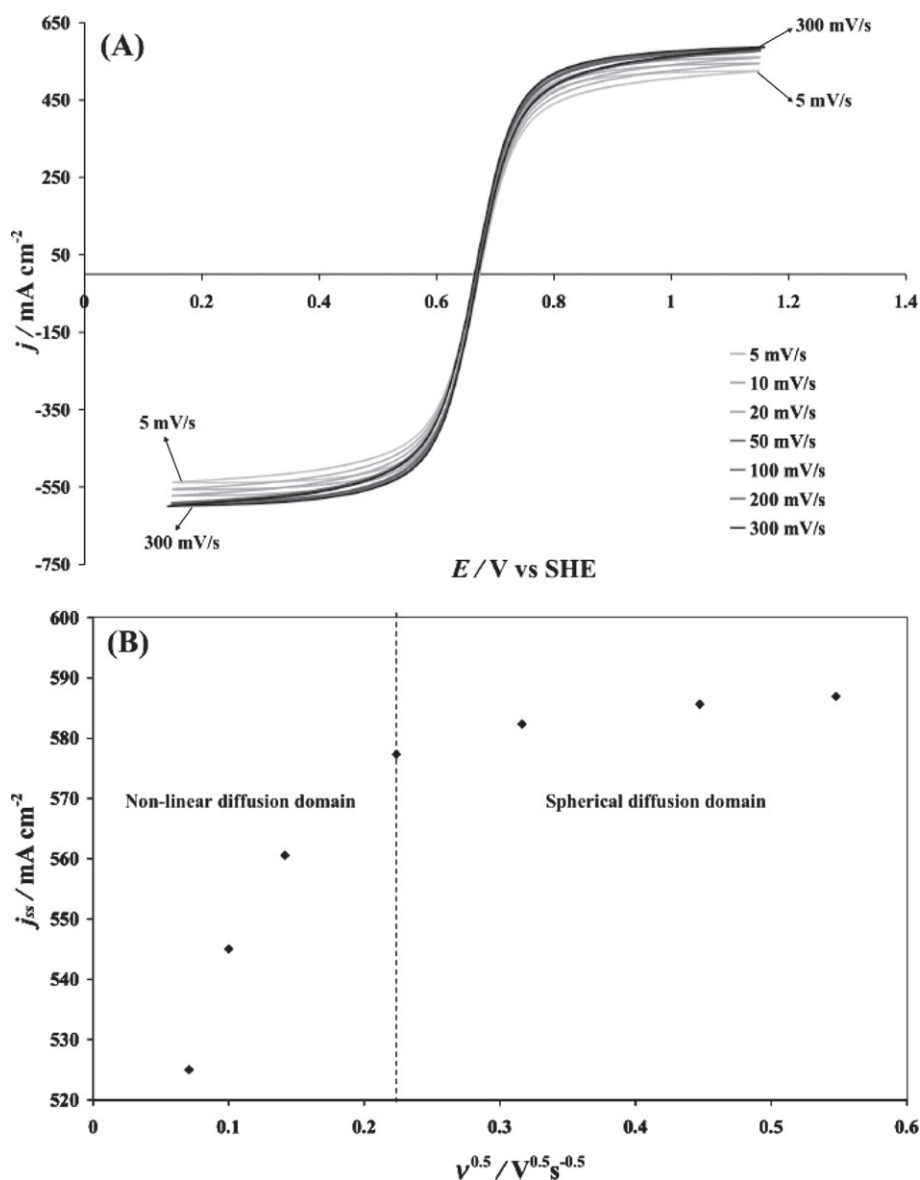


Fig. 3. (A) Cyclic voltammograms of the $\text{Fe}(\text{CN})_6^{4-/3-}$ redox couple recorded at the TOIROF-MEA in 1 M H_2SO_4 ; scan rates between 5 and 300 mV s^{-1} (5, 10, 20, 50, 100, 200 and 300 mV s^{-1}); concentration of $\text{Fe}(\text{CN})_6^{4-/3-}$ 50 mM, (B) anodic steady-state current densities (j_{ss}) plotted as a function of the square root of the scan rate. $T = 25^\circ\text{C}$.

05 and that the voltammetric charge is about 0.67 mC cm^{-2} . This cor-
 06 responds to $20 \mu\text{g IrO}_2 \text{ cm}^{-2}$. Therefore and considering a value of
 07 $31.1 \pm 2.9 \text{ mC}$ per mg of IrO_2 for the specific voltammetric charge
 08 [6,13], these results show that this technique of preparation (ther-
 09 mal treatment of Ir metal in air at 500°C) allow producing very
 10 thin coatings in contrast with the electrodes prepared by thermal
 11 decomposition of H_2IrCl_6 precursor [5]. In fact, even when using
 12 the spincoating deposition technique for the deposition of the pre-
 13 cursor, typical uniform coatings have a loading rarely inferior to
 14 $0.3 \text{ mg IrO}_2 \text{ cm}^{-2}$ [5]. Therefore, the low capacitive current and vol-
 15 tammetric charge measured on the TOIROF-MEA are related to the
 16 small size of the electrode and to its low loading. In fact, the small
 17 capacitive current is one of the main advantages of the IrO_2 -based
 18 electrode miniaturization [7].

19 Fig. 3A shows cyclic voltammetric measurements of the 50 mM
 20 $\text{Fe}(\text{CN})_6^{4-/3-}$ redox couple performed on the TOIROF-MEA at differ-
 21 ent scan rates (5–300 mV s^{-1}). Fig. 3B shows the corresponding
 22 anodic steady-state current densities plotted as a function of the
 23 square root of the scan rate. It can be seen that above 50 mV s^{-1} ,

Table 1

Characterization of TOIROF-MEA; v is the scan rate (mV s^{-1}), δ is the thickness of diffusion layer (μm), R ($=2.5 \mu\text{m}$) is the radius of the single microelectrode in the array, d ($=150 \mu\text{m}$) is the smallest distance between the microelectrodes in the array.

v (mV s^{-1})	δ (μm)	R/δ (-)	d/δ (-)
5	231.43	0.011	0.648
10	163.65	0.015	0.917
20	115.72	0.022	1.296
50	73.18	0.034	2.050
100	51.75	0.048	2.899
200	36.59	0.068	4.099
300	29.88	0.084	5.020

the current plateau does not depend on the scan rate indicating that the spherical diffusion dominates over the microelectrodes [7]. These conditions are referred to as diffusional independence [14], i.e. there is no overlap of adjacent diffusion zones. At the scan rates below 50 mV s^{-1} , anodic and cathodic steady-state current are dependent on the scan rate showing that there is an overlap

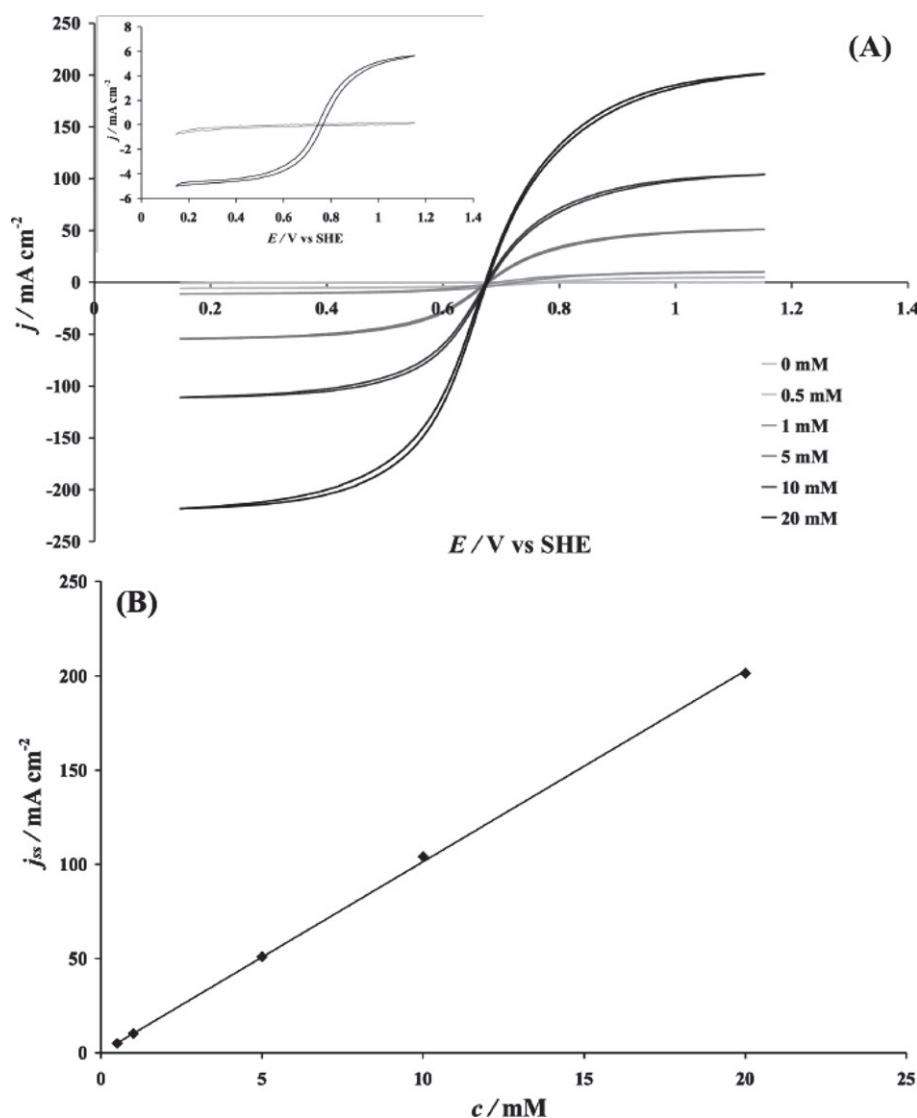


Fig. 4. (A) Cyclic voltammograms of the $\text{Fe}(\text{CN})_6^{4-/3-}$ redox couple (0–20 mM) recorded at the TOIROF-MEA in 1 M H_2SO_4 at 100 mV s^{-1} , (B) anodic steady-state current densities (j_{ss}) plotted as a function of the concentration of $\text{Fe}(\text{CN})_6^{4-/3-}$. $T = 25 \text{ }^\circ\text{C}$. Inset of (A) shows results obtained for 0 mM and 0.5 mM of $\text{Fe}(\text{CN})_6^{4-/3-}$.

of adjacent diffusion layers of individual microelectrodes [10,11]. Under these conditions, a non-linear diffusion with partial overlap dominates over the microelectrode-array, which can be associated with category 3 of diffusion profile, as detailed extensively by Davies et al. [15,16]. Similar conclusion can be made by comparing the thickness of the diffusion layer at a given scan rate (calculated with Eq. (1)) with a radius of the single microelectrode R in the array with a cubic packing geometry and the distance between the microelectrodes d [14–16]

$$\delta = \sqrt{2D \frac{\Delta E}{\nu}} \quad (1)$$

where D ($\text{m}^2 \text{ s}^{-1}$) is the diffusion coefficient, ΔE (V) is the potential difference between the onset oxidation potential at the potential of limiting current (Fig. 3), and ν (V s^{-1}) is the scan rate.

Table 1 gives the diffusion thickness δ (m) and the ratios R/δ and d/δ (–) as a function of potential scan rate. From this table it is clear that from 50 mV s^{-1} , the diffusion layer thickness exceeds clearly the size of the microelectrodes but it is smaller than the distance between two microelectrodes in the array, indicating domination of spherical diffusion at the scan rates above 50 mV s^{-1} .

Fig. 4A presents cyclic voltammetric measurements recorded on TOIROF-MEA for different concentrations of the $\text{Fe}(\text{CN})_6^{4-/3-}$ redox couple. The curves were recorded at 100 mV s^{-1} at which domination of spherical diffusion is expected. It can be seen that even at low $\text{Fe}(\text{CN})_6^{4-/3-}$ concentration (0.5 mM), the steady-state current is clearly observed. The detection of such low concentration can be considered as an advantage of the miniaturization of the IrO_2 macroelectrodes. In fact, on IrO_2 macroelectrodes, the detection of such low concentration is difficult due to the important capacitive background current.

Fig. 4B shows that the corresponding anodic steady-state current is proportional to the concentration of $\text{Fe}(\text{CN})_6^{4-/3-}$. Based on the theory of microelectrodes given in [7], the diffusion coefficient D of the $\text{Fe}(\text{CN})_6^{4-/3-}$ can be calculated using the following relation (Eq. (2)):

$$I_{ss} = 4 \cdot N \cdot n \cdot F \cdot r \cdot D \cdot c, \quad (2)$$

where I_{ss} is the steady-state current (A), N is the number of microelectrodes in the array (100), n is the number of exchanged electrons ($n = 1$), F is the Faraday constant (96,485 C), c is the bulk concentration of the redox couple and r is the radius of the single

73 microelectrode in the array. Using Eq. (1), the diffusion coefficient of
74 $\text{Fe}(\text{CN})_6^{3-}$ was calculated to be $1.03 \cdot 10^{-5} \text{ cm}^2 \text{ s}^{-1}$, which is in good
75 agreement with literature ($0.896 \cdot 10^{-5} \text{ cm}^2 \text{ s}^{-1}$ in 1 M KCl at 25 °C)
76 [7].

77 4. Conclusions

78 In this work, the characterization of an IrO_2 -based **microelec-**
79 **trode-array** prepared by thermal treatment of pure Ir (**TOIROF-**
80 **MEA**) is presented. The main conclusions are:

- 81 – This technique allows producing IrO_2 electrodes with very low
82 loadings ($\sim 20 \mu\text{g IrO}_2 \text{ cm}^{-2}$). As a consequence, the capacitive
83 current measured on the **TOIROF-MEA** is greatly reduced in con-
84 trast with the IrO_2 electrodes prepared by thermal decomposi-
85 tion of H_2IrCl_6 precursor.
- 86 – The characterization of the **TOIROF-MEA** using $\text{Fe}(\text{CN})_6^{4-/3-}$ has
87 revealed that even very small concentrations of the investigated
88 redox couple can be detected on this electrode. The diffusion
89 coefficient of $\text{Fe}(\text{CN})_6^{3-}$ obtained experimentally was found to
90 be in good agreement with the values reported in the literature.
91

92 Acknowledgement

93 The authors gratefully thank the Fonds National Suisse de la
94 Recherche Scientifique for the financial support.

References

- [1] S. Trasatti, W.E. O'Grady, in: H. Gerisher, C.W. Tobias (Eds.), *Advances in Electrochemistry and Electrochemical Engineering*, John Wiley and Sons, New York, USA, 1981, p. 177.
- [2] F. Beck, Ber. Bunsenges. Phys. Chem. 77 (1973) 353.
- [3] F. Beck, H. Schultz, *Electrochim. Acta* 29 (1984) 1569.
- [4] E. Lodowicks, F. Beck, *Chem. Eng. Technol.* 17 (1994) 338.
- [5] S. Fierro, L. Ouattara, E. Herrera Calderon, Ch. Comninellis, *Electrochem. Commun.* 10 (2008) 955.
- [6] S. Fierro, L. Ouattara, E. Herrera Calderon, H. Baltruschat, Ch. Comninellis, *Electrochim. Acta* 54 (2008) 2053.
- [7] L.R.F. Allen, J. Bard, *Electrochemical Methods: Fundamentals and Applications*, Wiley, New York, NY, 1980.
- [8] L. Ouattara, S. Fierro, O. Frey, M. Koudelka, Ch. Comninellis, *J. Appl. Chem.* 39 (2009) 1361.
- [9] S. Fierro, A. Kapałka, Ch. Comninellis, *Electrochem. Commun.* 12 (2010) 172.
- [10] C.U. Pinnow, I. Kasko, N. Nagel, S. Poppa, T. Mikolajick, C. Dehm, W. Höslér, F. Bleyl, F. Jahnel, M. Seibt, U. Geyer, K. Samwer, *J. Appl. Phys.* 91 (2002) 9591.
- [11] E. Raub, *Gmelin Handbuch der Anorganischen Chemie, Iridium*, Suppl. vol. 2, Springer, Berlin, 1978, p. 3.
- [12] K.L. Saenger, D.A. Neumayer, *J. Appl. Phys.* 89 (2001) 3132.
- [13] E. Herrera Calderon, Ph.D. Thesis, Swiss Institute of Technology (EPFL), No. 4181, 2008.
- [14] D. Menshukau, X.-J. Huang, N.V. Rees, F.J. del Campo, F.X. Muñoz, R.G. Compton, *Analyst* 134 (2009) 343.
- [15] T.J. Davies, S. Ward-Jones, C.E. Banks, J. Del Campo, R. Mas, F.X. Muñoz, R.G. Compton, *J. Electroanal. Chem.* 585 (2005) 51.
- [16] T.J. Davies, R.G. Compton, *J. Electroanal. Chem.* 585 (2005) 63.



Electrochemical behaviour of ammonia ($\text{NH}_4^+/\text{NH}_3$) on electrochemically grown anodic iridium oxide film (AIROF) electrode

Agnieszka Kapałka^{a,*}, Stéphane Fierro^a, Zacharias Frontistis^b, Alexandros Katsaounis^b, Olivier Frey^c, Milena Koudelka^c, Christos Comninellis^a, Kai M. Udert^d

^a Institute of Chemical Sciences and Engineering, Ecole Polytechnique Fédérale de Lausanne (EPFL), CH-1015 Lausanne, Switzerland

^b Department of Environmental Engineering, Technical University of Crete, GR-73100 Chania, Greece

^c The Sensors, Actuators and Microsystems Laboratory, Institute of Microtechnology, University of Neuchâtel, SAMLAB-UNINE, Jaquet-Droz 1, 2007 Neuchâtel, Switzerland

^d EAWAG, Ueberlandstrasse 133, 8600 Duebendorf, Switzerland

ARTICLE INFO

Article history:

Received 15 May 2009

Received in revised form 2 June 2009

Accepted 3 June 2009

Available online 9 June 2009

Keywords:

pH

Ammonia

Buffering

Hydrous IrO₂ oxide film

ABSTRACT

The electrochemical behaviour of ammonia ($\text{NH}_4^+/\text{NH}_3$) in sodium perchlorate at pH 9 has been investigated on electrochemically grown anodic iridium oxide film (AIROF) electrode. In base electrolyte at pH 9, the Ir(IV)/Ir(III) surface redox couple exhibits unusually large separation of the oxidation/reduction peaks ($\Delta E_p \sim 750$ mV) due to the local pH changes within the oxide film. These local pH changes are induced by protons released/consumed during the Ir(IV)/Ir(III) redox activity. As a consequence, the local pH within AIROF changed up to 10 units during potential cycling. The presence of ammonia at pH 9 prevents these local pH changes because $\text{NH}_4^+/\text{NH}_3$ buffer the solution inside the electrode. As a consequence, ΔE_p of Ir(IV)/Ir(III) was reduced to 100 mV. It has been shown further that ammonia oxidation is mediated by Ir(V), resulting in the appearance of anodic peaks in forward and backward scans.

© 2009 Elsevier B.V. All rights reserved.

1. Introduction

IrO₂ films are prepared either by thermal decomposition of the appropriate precursor solution on an inert substrate or they are grown electrochemically at metallic iridium electrodes through potential cycling. The thermally prepared iridium dioxide electrodes form part of the dimensionally stable anodes (DSA[®]) and have been widely investigated for applications such as metal electro-winning, oxygen evolution or electrochemical oxidation of organics [1–5]. The electrochemically grown anodic iridium oxide film (AIROF) exhibits a reversible Ir(IV)/Ir(III) oxidation state change in acidic media, which transforms the film from a colourless insulating material (Ir(III)) to a black metallic conductor (Ir(IV)). This particular feature has been widely investigated for applications in electrochromic devices [6–8]. Moreover, electrochemically grown IrO₂ have proved to be of potential interest in the area of electrocatalysis, for reactions such as chlorine evolution and oxygen evolution [9,10].

Most of the time the growth and activity of the electrochemically formed oxide films were studied in acidic media (H₂SO₄ or HClO₄ aqueous solution). However, it has been shown that the films grown in neutral or basic solutions were more stable against corrosion compared to the films grown in acidic media [11,12].

In this communication, we investigate the behaviour of AIROF in the absence and presence of ammonia in sodium perchlorate at pH 9. Recently, the electrochemical oxidation of ammonia has attracted much interest for ammonia removal from wastewater [13–15] as well as for ammonia sensing [16].

2. Experimental

The electrochemical measurements were carried out in a single-compartment three-electrode cell (70 mL) using an Autolab PGSTAT 30. The counter electrode was a Pt wire, the reference electrode was Hg/Hg₂SO₄/K₂SO₄ (MSE), and the working electrode was electrochemically grown anodic iridium oxide film electrode (AIROF, 0.54 mm²). AIROF was formed during potential cycling of a p-Si/Ir electrode at 100 mV s⁻¹ in 1 M NaClO₄ at pH 9 and 25 °C. The pH of the solution was adjusted with NaOH. More details about the preparation of AIROF are given in [17].

3. Results and discussion

3.1. Formation of an anodic iridium oxide film close to pH neutrality (pH 9)

Fig. 1 shows cyclic voltammograms (selected scans between 2 and 100) recorded on a p-Si/Ir electrode at 100 mV s⁻¹ in 1 M NaClO₄ + NaOH at pH 9. During successive scans, two anodic peaks

* Corresponding author. Tel.: +41 21 693 6164; fax: +41 21 693 6161.

E-mail address: agnieszka.ciecwiwa@epfl.ch (A. Kapałka).

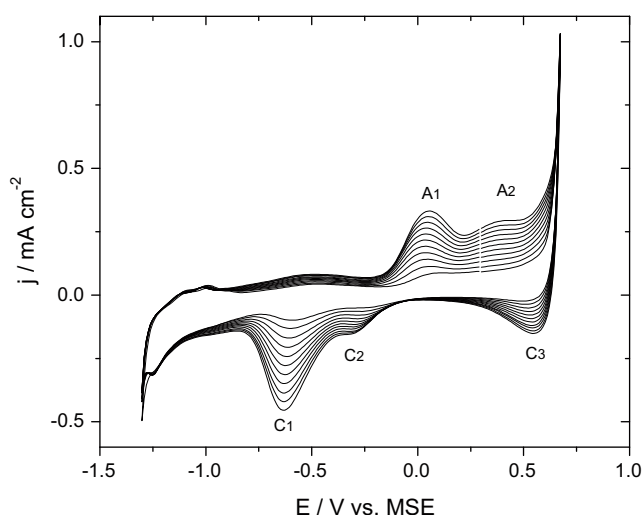
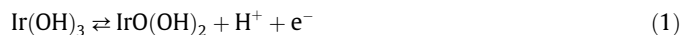


Fig. 1. Cyclic voltammograms (scans: 2, 10, 20, 30, 40, 50, 60, 70, 80, 90, 100) on p-Si/Ir electrode; scan rate 100 mV s^{-1} , electrolyte $1 \text{ M NaClO}_4 + \text{NaOH}$ at pH 9 and $25 \text{ }^\circ\text{C}$.

(A_1 and A_2) and three cathodic peaks (C_1 , C_2 and C_3) are formed. The cathodic peaks are strongly dependent on the upper sweep potential limit (E_p^1), as shown in Fig. 2. The cathodic peak at -0.6 V (C_1) is observed when E_p^1 is higher than -0.25 V . This is an indication that the anodic peak A_1 is related to C_1 . The C_2 peak appears clearly when E_p^1 is set above 0.5 V indicating the existence of the redox surface processes on AIROF also in the oxygen evolution region. C_3 peak appears when the E_p^1 is set above 0.25 V , thus, is related to A_2 .

The main redox process (A_1/C_1), centered at $\sim -0.4 \text{ V}$, can be attributed to Ir(IV)/(III) surface redox couple, according to Eq. (1) [18,19].



As separation of peaks A_1/C_1 (ΔE_p) is about 750 mV , it could seem that the behaviour of Ir(IV)/Ir(III) on AIROF in NaClO_4 is strongly irreversible. However, this contradicts the results obtained in basic and acidic media [20], in which ΔE_p indicates reversible character of Ir(IV)/Ir(III) couple.

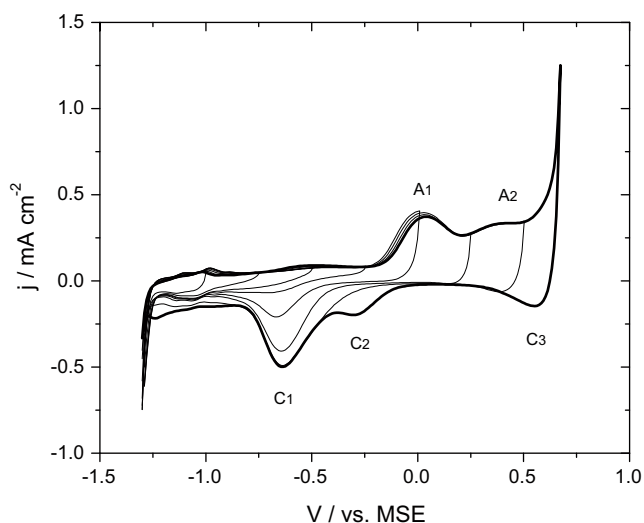


Fig. 2. Cyclic voltammograms with various upper sweep potential limit recorded on p-Si/Ir electrode; experimental conditions as in Fig. 1.

This apparent irreversibility of Ir(IV)/Ir(III) in NaClO_4 might be related to a change of the electrode environment during the potential sweep. Juodkazyte et al. [20] showed that the Ir(IV)/Ir(III) peaks are shifted negatively in alkaline solution by approximately 500 mV as compared to acidic ones. Moreover, it has been reported [20,21] that iridium oxide electrodes exhibit the pH-sensitivity ranging from 57 to 80 mV/pH . Therefore, ΔE_p of 750 mV in NaClO_4 might result from the pH change within the oxide film electrode [12] during the potential sweep. In fact, as iridium hydroxide is oxidized, protons are released (Eq. (1)) and the interior of the oxide film might become acidic. On the contrary, as iridium hydroxide is reduced, protons are consumed causing an increase of the pH inside the hydroxide. As a consequence, during potential cycling, the oxidation peak A_1 appears in the potential range characteristic for iridium oxide oxidation in acidic media [17] whereas the reduction peak C_1 appears at a potential characteristic for iridium oxide reduction in basic media [12] resulting in a high value of ΔE_p . Thus, considering $57\text{--}80 \text{ mV/pH}$ [21], the local pH changes within AIROF up to 10 units during the potential sweep in NaClO_4 at pH 9. It is important to note that the pH change inside the oxide is a gradual process going smoothly with increasing potential. This is the reason why the current density of C_1 (Fig. 2) increases progressively with the upper sweep potential limit in the vicinity of A_1 .

The couple A_2/C_3 can be attributed to Ir(V)/Ir(IV) surface redox couple, according to Eq. (2) [18,19].



As the potential further increases, Ir(V) is oxidized to Ir(VI) (Eq. (3)). Soon after, the oxygen is released (Eq. (4)) simultaneously to the corrosion of the electrode (Eq. (5)) [18].



Therefore, the cathodic peak C_2 might be related either to the reduction of the corrosion products that are present in the solution or to the reduction of adsorbed oxygen.

3.2. The buffering effect of ammonia

Fig. 3 shows cyclic voltammograms recorded on AIROF in the absence (curve 1) and presence (curve 2) of $100 \text{ mM NH}_4\text{ClO}_4$ in 1 M NaClO_4 at pH 9. It is interesting to see that in the presence

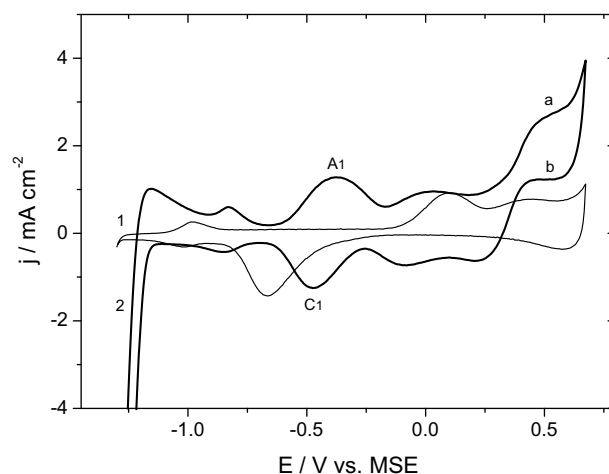


Fig. 3. Comparison of the voltammograms recorded in (1) $1 \text{ M NaClO}_4 + \text{NaOH}$ at pH 9 and (2) $100 \text{ mM NH}_4\text{ClO}_4 + 1 \text{ M NaClO}_4 + \text{NaOH}$ at pH 9 on an anodic iridium oxide film electrode (750 cycles) at 50 mV s^{-1} .

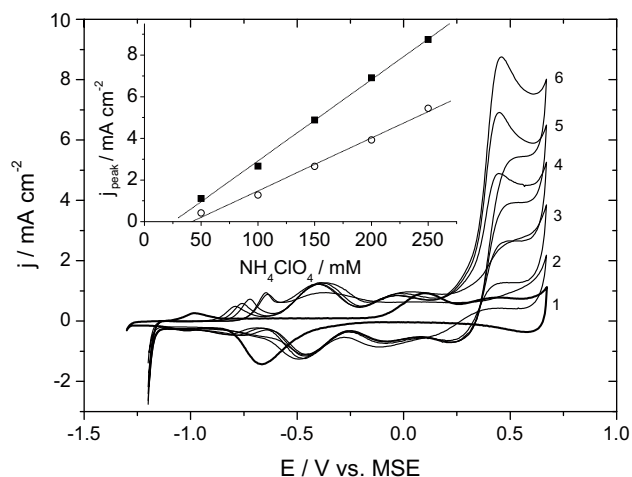


Fig. 4. Cyclic voltammograms of (1) 0 mM, (2) 50 mM, (3) 100 mM, (4) 150 mM, (5) 200 mM and (6) 250 mM NH_4ClO_4 in 1 M $\text{NaClO}_4 + \text{NaOH}$ at pH 9 and 25 °C recorded on an anodic iridium oxide film electrode at 50 mV s^{-1} . The inset shows the current peak that appears during the forward scan (■) and the reverse scan (○) as a function of the NH_4ClO_4 concentration.

of NH_4ClO_4 , ΔE_p of the A_1/C_1 redox couple becomes smaller ($\Delta E_p \sim 100 \text{ mV}$). To understand this apparent change, one has to consider the buffering effect of ammonia within the porous AIROF. As the $\text{p}K_a$ of ammonia is 9.25 at 25 °C [22], both, ammonium ion and molecular ammonia, coexist in the solution at pH 9. Therefore, $\text{NH}_4^+/\text{NH}_3$ acts as a buffer, maintaining a constant pH value inside the oxide film during its oxidation or reduction. Thus, in the presence of ammonia, the A_1/C_1 redox couple exhibits ΔE_p characteristic for alkaline solutions [12]. Therefore, in order to use AIROF in electrochromic devices in neutral solutions, it is essential to buffer the solution to prevent the electrode from the local pH changes during its oxidation/reduction.

3.3. Anodic oxidation of ammonia

The oxidation of ammonia on AIROF proceeds from 0.25 V vs. MSE resulting in the appearance of two well-defined anodic peaks: (a) in the forward scan and (b) in the backward scan (Fig. 3). Considering that the oxidation of ammonia involves Ir(V) [17], peak (b) might result from the oxidation of ammonia on freshly reduced Ir(VI) to Ir(V) .

As shown in Fig. 3, the oxidation of ammonia results in well-defined voltammetric response on AIROF that could be useful for the detection of ammonia. Recently, Compton et al. [16] reported the use of boron-doped diamond electrodes for ammonia sensing. Oxidation of ammonia on BDD proceeds in the same potential range as on AIROF giving an oxidation peak that increases linearly with the ammonia concentration. Fig. 4 shows a similar behaviour for the AIROF electrode; both anodic peaks (a and b) increase linearly with the concentration of NH_4ClO_4 . However, the lines do not

pass through the origin, probably due to the important changes of the background current caused by ammonia. These changes in the background current are certainly induced by the local pH changes in the hydrous iridium oxide film during its oxidation/reduction as well as during oxidation of ammonia. Indeed, at high potential the oxidation of ammonia itself induces considerable release of protons.

4. Conclusions

The presence of NH_4ClO_4 in NaClO_4 at pH 9 influences strongly the electrochemical response of IrO_2 film grown at p-Si/Ir. At potential $< 0.25 \text{ V}$ vs. MSE, ammonia is not electrochemically active, however, $\text{NH}_4^+/\text{NH}_3$ buffers the solution preventing from pH changes inside the porous electrode during a potential sweep. As a consequence, ΔE_p of the $\text{Ir(IV)}/\text{Ir(III)}$ redox couple remains in the range of 100 mV (typical value for alkaline solutions). At potential $> 0.25 \text{ V}$ vs. MSE, ammonia oxidation seems to be mediated by Ir(V) .

Acknowledgments

The authors thank Eawag for sponsoring the research with discretionary funding.

References

- [1] S. Trasatti, W.E. O'Grady, in: H. Gerisher, C.W. Tobias (Eds.), *Advances in Electrochemistry and Electrochemical Engineering*, John Wiley and Sons, New York, USA, 1981, p. 177.
- [2] S. Fierro, T. Nagel, H. Baltruschat, Ch. Comninellis, *Electrochem. Commun.* 9 (2007) 1969.
- [3] S. Fierro, T. Nagel, H. Baltruschat, Ch. Comninellis, *Electrochem. Solid-State Lett.* 11 (7) (2008) E20.
- [4] Ch. Comninellis, E. Plattner, *Chimia* 42 (1988) 250.
- [5] S. Fierro, E. Passas-Lagos, E. Chatzisympson, D. Mantzavinos, Ch. Comninellis, *Electrochem. Commun.* 11 (2009) 1358–1361.
- [6] S.H. Glarum, J.H. Marshall, *J. Electrochem. Soc.* 127 (1980) 1467.
- [7] S. Gottesfeld, J.D.E. McIntyre, G. Beni, J.L. Shay, *Appl. Phys. Lett.* 33 (2) (1978) 208.
- [8] S. Gottesfeld, J.D.E. McIntyre, *J. Electrochem. Soc.* 126 (1979) 742.
- [9] J. Mozota, B.E. Conway, *J. Electrochem. Soc.* 128 (1981) 2142.
- [10] L.D. Burke, in: S. Trasatti (Ed.), *Electrodes of Conductive Metallic Oxides*, Part A, Elsevier Publishing, New York, 1980.
- [11] L.D. Burke, R.A. Scannell, *J. Electroanal. Chem.* 175 (1984) 119.
- [12] P.G. Pickup, V.I. Birss, *J. Electrochem. Soc.* 135 (1988) 126.
- [13] L. Li, Y. Liu, J. Hazard. Mater. 161 (2009) 1010.
- [14] K.-W. Kim, Y.-J. Kim, I.-T. Kim, G.-I. Park, E.-H. Lee, *Electrochim. Acta* 50 (2005) 4356.
- [15] A. Anglada, A. Urriaga, I. Ortiz, *Environ. Sci. Technol.* 43 (2009) 2035–2040.
- [16] X. Ji, C.E. Banks, R.G. Compton, *Analyst* 130 (2005) 1345.
- [17] L. Ouattara, S. Fierro, O. Frey, M. Koudelka, Ch. Comninellis, *J. Appl. Electrochem.*, doi:10.1007/s10800-009-9809-2.
- [18] R. Kötz, H. Neff, S. Stucki, *J. Electrochem. Soc.* 131 (1984) 72.
- [19] R. Kötz, in: H. Gerischer, C.W. Tobias (Eds.), *Advances in Electrochemical Science and Engineering*, Verlag Chemie, Heidelberg, 1990.
- [20] J. Juodkazyte, B. Sebek, I. Valsiunas, K. Juodkazis, *Electroanalysis* 11 (2005) 947.
- [21] J. Hendrikse, W. Olthuis, P. Bergveld, *Transducers* 97, in: *International Conference on Solid-State Sensors and Actuators*, Chicago, June 16–19, 1997.
- [22] D.R. Lide, in: *CRC Handbook of Chemistry and Physics*, 86th ed., Taylor and Francis, Boca Raton, Florida, 2006, p. 1131.

**Electrochemical oxidation of ammonia ($\text{NH}_4^+/\text{NH}_3$) on thermally
and electrochemically prepared IrO_2 electrodes**

Agnieszka Kapałka^{1*}, Stéphane Fierro¹, Zacharias Frontistis², Alexandros
Katsaounis², Stefano Neodo¹, Christos Comninellis¹ and Kai M. Udert³

¹*Institute of Chemical Sciences and Engineering, Ecole Polytechnique Fédérale de
Lausanne (EPFL), CH-1015 Lausanne, Switzerland*

²*Department of Environmental Engineering, Technical University of Crete, GR-
73100 Chania, Greece*

³*Eawag, Swiss Federal Institute of Aquatic Science and Technology, 8600
Dübendorf, Switzerland*

*Corresponding author: agnieszka.cieciwa@epfl.ch

Abstract

The electrochemical oxidation of ammonia ($\text{NH}_4^+/\text{NH}_3$) in sodium perchlorate was investigated on IrO_2 electrodes prepared by two techniques: the thermal decomposition of H_2IrCl_6 precursor and the anodic oxidation of metallic iridium. The electrochemical behaviour of Ir(IV)/Ir(III) surface redox couple differs between the electrodes indicating that on the anodic iridium oxide film (AIROF) both, the surface and the interior of the electrode are electrochemically active whereas on the thermally decomposed iridium oxide films (TDIROF), mainly the electrode surface participates in the electrochemical processes.

On both electrodes, ammonia is oxidized in the potential region of Ir(V)/Ir(IV) surface redox couple activity, thus, may involve Ir(V). During ammonia oxidation, TDIROF is deactivated, probably by adsorbed products of ammonia oxidation. To regenerate TDIROF, it is necessary to polarize the electrode in the hydrogen evolution region. On the contrary, AIROF seems not to be blocked during ammonia oxidation indicating its fast regeneration during the potential scan. The difference between both electrodes may result from the difference in the activity of the iridium oxide surface redox couples.

Keywords: oxidation of ammonia; IrO_2 electrode; pH 9; deactivation; surface redox couple

Introduction

Discharges of ammonia to the aquatic environment cause eutrophication and fish toxicity. Today, large treatment plants with biological nitrification and denitrification are used to remove ammonia from municipal wastewater. Recently, the concept of urine separation has been proposed as a new technology to improve and simplify nitrogen removal from wastewater [1]. Several processes have been proposed and tested for nitrogen removal from urine, but none of them has been implemented on a large scale so far [2]. Recently, electrochemical removal of ammonia has been shown to be a promising method for degradation of ammonia along with organic compounds present in wastewater [3]. The process might also be well suited to remove ammonia and organic substances from urine. The main advantage of this technique is that no chemicals or bacteria are required. In fact, only electrical energy is consumed for elimination of pollutants.

The mechanism of ammonia electro-oxidation has been studied mainly on Pt electrodes and Pt-Me (Me = Ni, Ir, Ru, Cu) binary alloys for their applications in ammonia fuel cell [4]. The mechanism of ammonia electro-oxidation on Pt-based electrodes involves dehydrogenation of adsorbed ammonia and formation of N₂ as a final product (Eqs. (1)-(4)) [5].



Besides N₂, the oxygenated nitrogen species (such as NO and N₂O) might also be formed when the electrode surface becomes oxidized [4].

The mechanism of electro-oxidation of ammonia on metal oxide type electrodes, such as RuO₂ or IrO₂ is much less understood. It is known, however, that on these anodes ammonia is oxidized through several steps to various nitrogen compounds (Eq. (5)) [6, 7].



With this study, we aimed to gain a better understanding of the electrochemical oxidation of ammonia on IrO₂ electrodes. IrO₂ films were prepared either by thermal decomposition of the appropriate precursor solution on an inert substrate (TDIROF) or they were grown electrochemically on metallic iridium electrodes through potential cycling (AIROF). As reported in [8], the stability and the electro-catalytic activity of these electrodes differ due to the difference in the activity of the iridium oxide surface redox couples. In fact, iridium surface redox activities involved on the AIROF are much faster than those involved on the TDIROF [8]. Electro-oxidation of ammonia was studied in sodium perchlorate at pH 9 using cyclic voltammetry. As the pK_a of ammonia is 9.25 [9], both, ammonium ion and molecular ammonia, coexist in similar amounts at pH 9.

Experimental

The electrochemical measurements were carried out in a single-compartment three-electrode cell (50 mL) using an Autolab PGSTAT 30. The counter electrode was a Pt wire and the reference electrode was Hg/Hg₂SO₄/K₂SO₄ (MSE). All potentials in this work are given with respect to the MSE. The working electrode was either a Ti/IrO₂ electrode prepared by thermal decomposition of H₂IrCl₆ (TDIROF) or electrochemically formed anodic iridium oxide film (AIROF) electrode.

TDIROF electrodes were prepared by thermal decomposition, at 500°C, of a precursor solution of H₂IrCl₆ (250mM in i-propanol) on a titanium substrate, which was previously sandblasted and treated in boiling 1M oxalic acid for 1hour. The precursor solution was deposited on the inert substrate by spincoating using a SPIN150 wafer spinner (Semiconductor production systems, SPS, Germany). The spincoating technique allows creating thin films using the centripetal acceleration of the substrate induced by the application of a rotational movement. Due to the spinning, the solvent evaporates and after a certain time of spinning, a residual solid polymer film covers the substrate. This technique can lead to very uniform films of well-controlled thickness. In this work, the loading of the Ti/IrO₂ electrode was 1.1 mg cm⁻².

AIROF was formed during potential cycling (200 scans) of a p-Si/Ir electrode at 100mV s⁻¹ in 1M NaClO₄ at pH 9 and 25 °C. A p-Si/Ir electrode was prepared by sputtering on p-Si substrate (0.54 mm²) an iridium film (0.1 μm) using a thin (0.02 μm) tantalum interlayer.

All solutions were prepared using ultrapure distilled water without further purification. The pH of the solution was adjusted with NaOH.

The theoretical mole fractions of the ammonia and ammonium ion, coexisting in the solution at a given pH, were calculated using Eq. (6) [6].

$$[\text{NH}_3] = \frac{1}{1 + K_b[\text{H}^+]/K_w} \quad (6)$$

where

$$K_b = \frac{[\text{NH}_4^+][\text{OH}^-]}{[\text{NH}_3][\text{H}_2\text{O}]} = 1.8 \cdot 10^{-5} \quad (7)$$

$$K_w = [\text{H}^+][\text{OH}^-] = 1.0 \cdot 10^{-14} \quad (8)$$

Results and Discussion

1. Surface redox activities on AIROF and TDIROF

Figure 1 shows cyclic voltammograms recorded on AIROF (Fig. 1a) and TDIROF (Fig. 1b) in 1M NaClO₄ + NaOH at pH 9. On both electrodes, two redox couples, A₁/C₁ and A₂/C₂, are present. As discussed in literature [10, 11], the A₁/C₁ can be attributed to Ir(IV)/Ir(III) (Eq. (9)) whereas A₂/C₂ can be attributed to Ir(V)/Ir(IV) surface redox couple (Eq. (10)).



The main difference between both electrodes studied is the separation of the Ir(IV)/Ir(III) peaks (ΔE_p). On AIROF, ΔE_p of Ir(IV)/Ir(III) is about 750 mV. As reported previously [12, 13], such a high value of ΔE_p results from the pH changes within the oxide film. In fact, as iridium hydroxide is oxidized, protons are released and the interior of the oxide film become acidic. As iridium hydroxide is reduced, protons are consumed resulting in an increase of the pH inside the hydroxide. As a consequence, the oxidation peak A₁ appears in the potential range characteristic for iridium oxide oxidation in acidic media [8] whereas the reduction peak C₁ appears at the potential characteristic for iridium oxide reduction in basic media [13], resulting in large ΔE_p .

On TDIROF, ΔE_p of Ir(IV)/Ir(III) is about 150 mV, which is a typical value for alkaline solutions [13]. Hence, on the contrary to AIROF, Ir(IV)/Ir(III) response on TDIROF seems not to be influenced by the local pH changes within the oxide film. The possible explanation of such a difference between TDIROF and AIROF

would be that the interior of TDIROF is less accessible, hence, less electrochemically active. In fact, it has been reported that TDIROF is less hydrous and less porous compared to AIROF [8]. Thus, the observed differences in the electrochemical behaviour between TDIROF and AIROF might be related to the differences in the porosity of the iridium oxide film.

2. Electrochemical oxidation of ammonia on AIROF and TDIROF

Figure 2 shows cyclic voltammograms recorded on AIROF (Fig. 2a) and TDIROF (Fig. 2b) in the presence and absence of 250 mM NH_4ClO_4 in 1M NaClO_4 at pH 9. The electrochemical behaviour of ammonia on iridium hydroxide films depends strongly on potential, as discussed below.

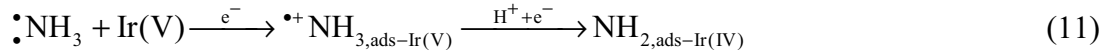
2.1 Below 0.25 V

Below 0.25 V, ammonia considerably influences the response of AIROF, whereas TDIROF seems to be less strongly affected. On AIROF, the ΔE_p of A_1/C_1 redox couple becomes smaller ($\Delta E_p \sim 100$ mV) compared to the situation without ammonia. This decrease of ΔE_p is caused by the simultaneous presence of NH_4^+ and NH_3 at pH 9 which buffers local pH changes within the AIROF electrode during oxidation and reduction [12]. These results confirm that on AIROF, both, the surface and the interior of the electrode, are electrochemically active, whereas on TDIROF, mainly the electrode surface participates in the electrochemical processes.

2.2 Above 0.25 V

On both electrodes, oxidation of ammonia proceeds from 0.25 V vs. MSE and results in the appearance of two anodic peaks: one in the forward scan (A_{3a}) and the

second in the backward scan (A_{3b}). These peaks are formed in the potential region of Ir(V)/Ir(IV) surface redox couple activity (Eq. (10)) indicating that the ammonia oxidation may involve this surface redox couple. In fact, ammonia having two free electrons can be oxidized on Ir(V) to its corresponding cation radical and be further dehydrogenated resulting in formation of Ir(IV), as shown in Eq. (11) [14].



In this potential range, however, Ir(IV) is not stable and it is fast re-oxidized to Ir(V) (Eq. (10)). As the potential further increases, Ir(V) is oxidized to Ir(VI) and oxygen is evolved during the reduction of Ir(VI) to Ir(IV) (Eqs. (12) and (13), respectively).



In the backward scan, Ir(VI) is reduced to Ir(V) allowing re-oxidation of ammonia. As a consequence, in the backward scan, the A_{3b} peak is formed. The A_{3b} peak intensity depends strongly on the upper potential sweep limit (E_p^a), as shown in Fig. 3: the higher is the E_p^a , the smaller is the A_{3b} peak. This can be explained by the fact that during oxygen evolution (Eq. (13)), the local pH at the electrode surface becomes more acidic inhibiting oxidation of ammonia. In fact, oxidation of ammonia is strongly pH dependent and does not proceed at $\text{pH} < 7$ (Fig. 4) at which mainly NH_4^+ is present.

3. Deactivation of TDIROF during ammonia oxidation.

Figure 5 shows the cyclic voltammograms with various lower sweep potential limits (E_p^c) recorded on AIROF and TDIROF in the presence of 250 mM NH_4ClO_4 in 1M NaClO_4 at pH 9. On AIROF, the A_{3a} and A_{3b} peaks intensities remain constant when E_p^c changes (Fig. 5a). On the contrary, both anodic peaks (A_{3a} and A_{3b})

decrease on TDIROF as the lower potential sweep limit decreases. This is an indication that the TDIROF is deactivated during ammonia oxidation, if E_p^c is not sufficiently low. In fact, it has been reported that the intermediates generated during oxidation of ammonia may remain on the electrode surface decreasing the electroactivity of the electrode [4]. Thus, TDIROF seems not to be regenerated as fast as AIROF during the potential scan. The difference between both electrodes may result from the difference in the activity of the iridium oxide surface redox couples, as discussed in the introduction.

To regenerate the TDIROF surface it is necessary to polarize the electrode in the hydrogen evolution region (HER). Otherwise, the successive scanning would cause deactivation of the electrode, followed by a decrease of the ammonia oxidation rate, as shown in Fig. 6. The regeneration of the electrode surface during HER may result from the reduction of remaining intermediates on the electrode surface [4].

4. Effect of the concentration on the ammonia oxidation.

Figure 7 shows cyclic voltammograms recorded on AIROF (Fig. 7a) and TDIROF (Fig. 7b) in the absence and presence of 50-250 mM NH_4ClO_4 in 1M NaClO_4 at pH 9. On both electrodes, AIROF and TDIROF, A_{3a} and A_{3b} peaks increase with the ammonia concentration.

On AIROF, oxidation peaks increase linearly with the concentration of ammonia (inset of Fig. 7a). However, the line does not pass through the origin, probably because the local pH changes during ammonia oxidation affect the background current. In fact, the oxidation of ammonia itself induces considerable release of protons, as shown in Eqs. (1)-(4).

On TDIROF, oxidation peaks increase linearly with ammonia concentrations up to 150 mM NH_4ClO_4 (inset of Fig. 7b) and the line passes through the origin. However, at the higher ammonia concentrations (> 150 mM), the increase of the oxidation peaks is slowed down indicating the saturation of the active sites for ammonia oxidation. These results are consistent with Fig. 5b and 6 showing deactivation of TDIROF during ammonia oxidation.

Conclusions

The electrochemical oxidation of ammonia on IrO_2 electrodes proceeds in the potential region of Ir(V)/Ir(IV) surface redox activity resulting in formation of two anodic peaks: one in the forward scan and the second in the backward scan. The anodic peak in the backward scan results from oxidation of ammonia on freshly reduced Ir(VI) to Ir(V).

During ammonia oxidation, TDIROF is deactivated, probably, by adsorbed products of ammonia oxidation. On the contrary, AIROF seems not to be blocked during ammonia oxidation indicating its fast regeneration during the potential scan. The difference between both electrodes may result from the difference in the activity of the iridium oxide surface redox couples.

To regenerate the TDIROF surface it is necessary to polarize the electrode in the hydrogen evolution region, where intermediates on the electrode surface are reduced. The polarization of the electrode in the oxygen evolution region causes a decrease of the local pH at the electrode surface, reducing the ammonia oxidation rate. In fact, oxidation of ammonia is strongly pH dependent and seems not to proceed below pH 7 at which mainly NH_4^+ is present.

Acknowledgments

The authors thank the Institute of Microtechnology at University of Neuchâtel, SAMLAB-UNINE, for preparing p-Si/Ir electrodes.

Reference

1. Larsen TA, Maurer M., Udert KM, Lienert J (2007) *Water Science and Technology* 56:229
2. Maurer M., Pronk W, Larsen TA (2006) *Water Research* 40:3151
3. Monica MD, Agostizno A, Ceglie A (1980) *J Appl Electrochem* 10:527
4. Vooy's ACA, Koper MTM, Van Santen RA, Van Veen JAR (2001) *J Electroan Chem* 506:127
5. Gerischer H, Mauerer A (1970) *J Electroan Chem* 25:421
6. Kim KW, Kim, YJ, Kim IT, Park GI, Lee EH (2005) *Electrochem Acta* 50: 4356
7. Kim KW, Kim, YJ, Kim IT, Park GI, Lee EH (2006) *Water Research* 40:1431
8. Ouattara L, Fierro S, Frey O, Koudelka M, Comninellis C (2009) *J Appl Electrochem* 39:1361
9. Lide DR (2006) *Handbook of Chemistry and Physics*, 86th ed., Taylor and Francis, Florida, p.1131
10. Kötzt R, Neff H, Stucki S (1984) *J Electrochem Soc* 131:72
11. Kötzt R, in Gerischer H., Tobias C W (1990) *Advances in electrochemical science and engineering*, Verlag Chemie, Heidelberg
12. Kapalka A, Fierro S, Frontistis Z, Katsaounis A, Frey O, Koudelka M, Comninellis C, Udert KM (2009) *Electrochem Commun* 11:1590
13. Pickup PG, Birss VI (1988) *J Electrochem Soc* 135:126
14. Deinhammer RS, Ho M, Anderegg JW, Porter MD (1994) *Langmuir* 10:1306

Figure captions:

Figure 1

Cyclic voltammograms recorded on (a) AIROF at 100 mV s^{-1} and (b) TDIROF at (—) 100 mV s^{-1} and (⋯) 300 mV s^{-1} ; solution $1 \text{ M NaClO}_4 + \text{NaOH}$ at pH 9 and 25°C .

Figure 2

Cyclic voltammograms in the absence (⋯) and presence (—) of ammonia recorded on (a) AIROF and (b) TDIROF; scan rate 100 mV s^{-1} ; solution $250 \text{ mM NH}_4\text{ClO}_4 + 1 \text{ M NaClO}_4 + \text{NaOH}$ at pH 9 and 25°C .

Figure 3

Cyclic voltammograms with various upper sweep potential limits recorded on TDIROF in the presence of ammonia. Experimental conditions as in Fig. 2.

Figure 4

Cyclic voltammograms recorded on TDIROF in the presence of ammonia at various pH; scan rate 100 mV s^{-1} ; solution $100 \text{ mM NH}_4\text{ClO}_4 + 1 \text{ M NaClO}_4 + \text{NaOH}$ at pH (1) 8, (2) 9, (3) 9.5, (4) 10, (5) 10.5, (6) 11.5 and 25°C . The inset shows: (■) the current peak density as a function of pH including additional experiments and (—) the mole fraction of the ammonia-ammonium ion, calculated from Eq. (6), as a function of pH.

Figure 5

Cyclic voltammograms with various lower sweep potential limits recorded on (a) AIROF and (b) TDIROF in the presence of ammonia. Experimental conditions as in Fig. 2.

Figure 6

Successive cyclic voltammograms (20 scans) recorded on TDIROF (a) from -0.7 V to 0.8V vs. MSE and (b) from -1.4V to 0.8V vs. MSE. Experimental conditions as in Fig. 2.

Figure 7

Cyclic voltammograms of (1) 0 mM, (2) 50 mM, (3) 100mM, (4) 150 mM, (5) 200 mM, (6) 250 mM NH_4ClO_4 in 1M NaClO_4 + NaOH at pH 9 and 25 °C recorded on (a) AIROF and (b) TDIROF at 50 mV s^{-1} . The insets show the current peak density as a function of the ammonia concentration.

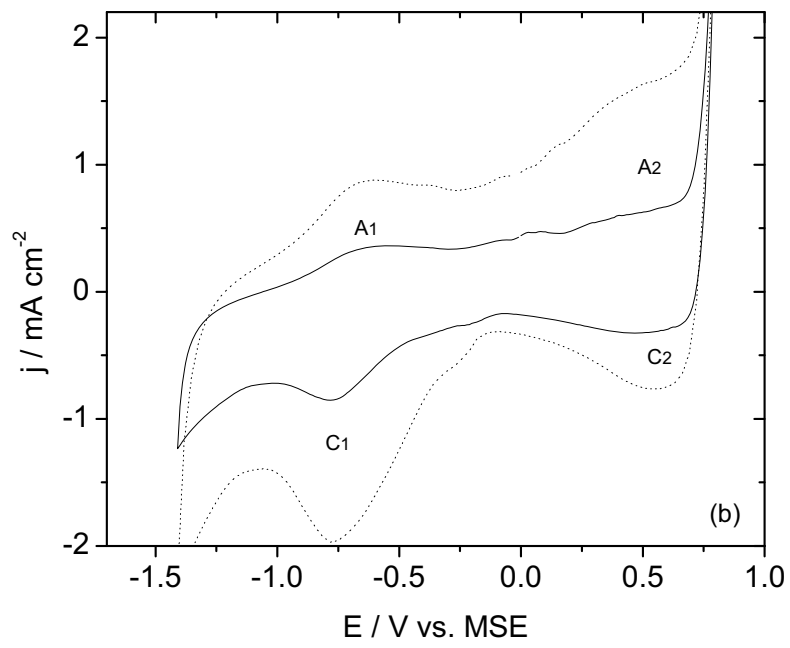
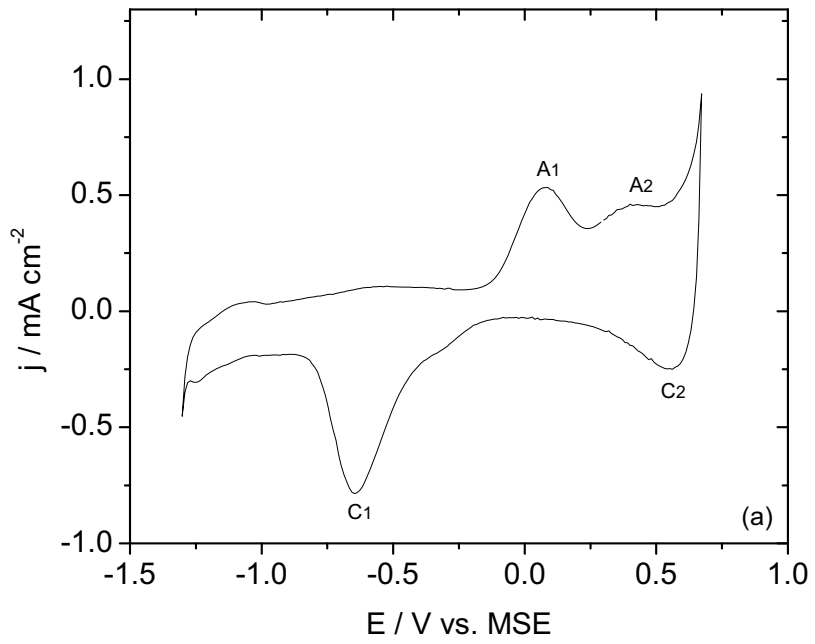


Figure 1

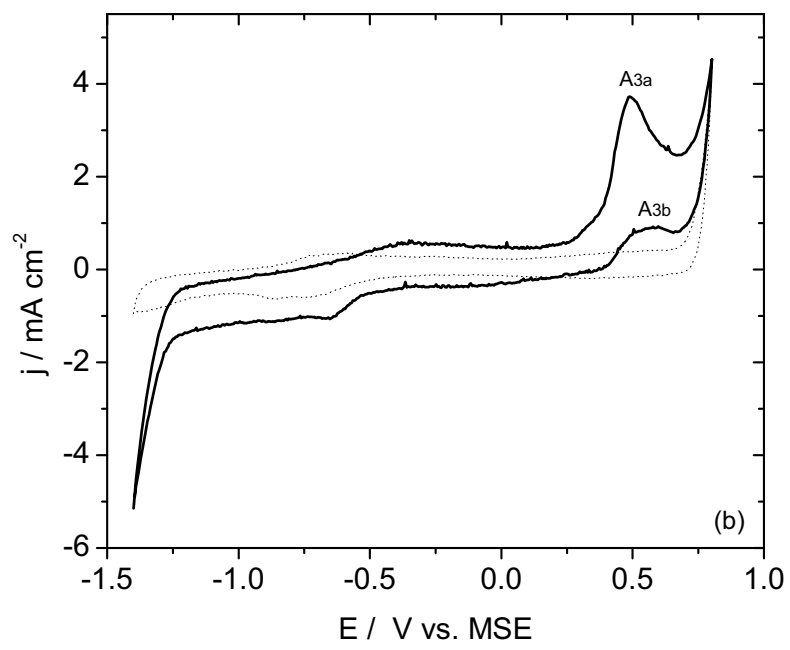
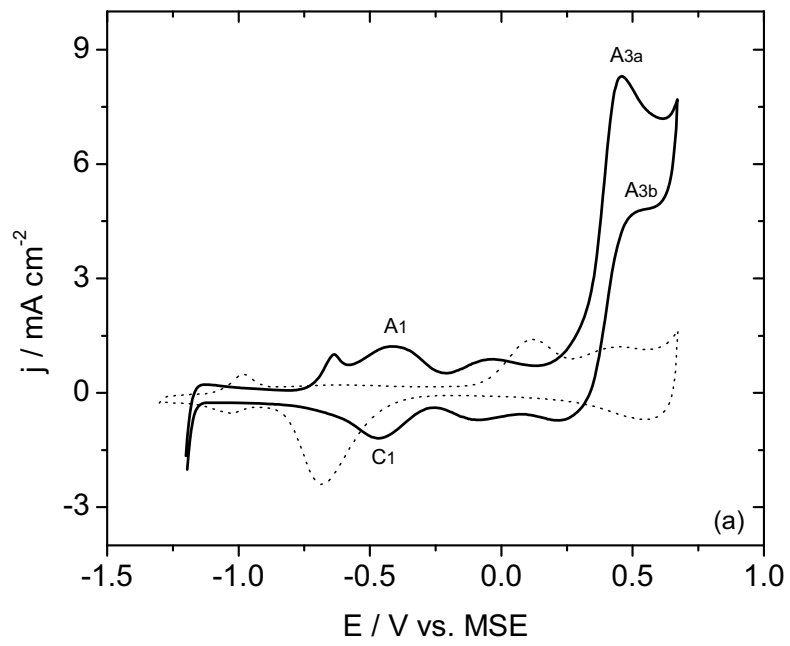


Figure 2

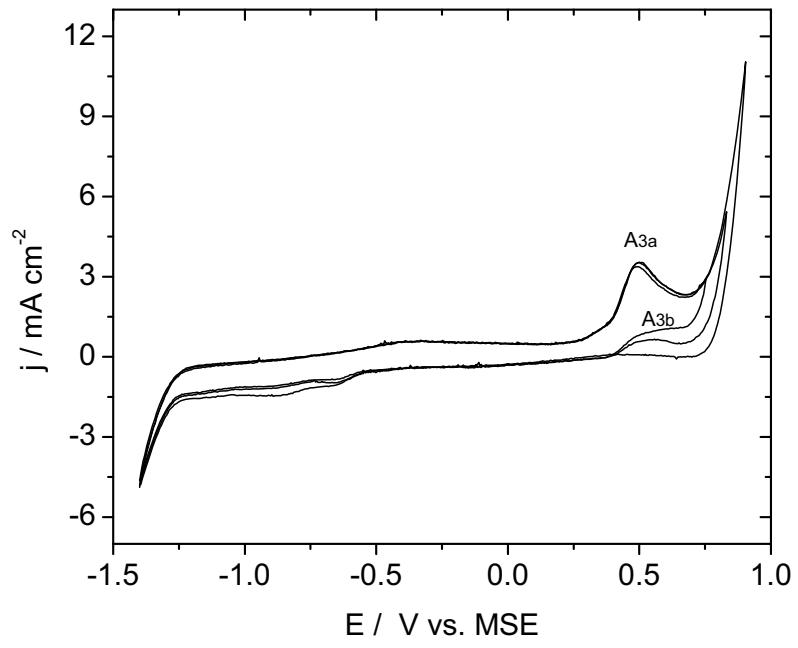


Figure 3

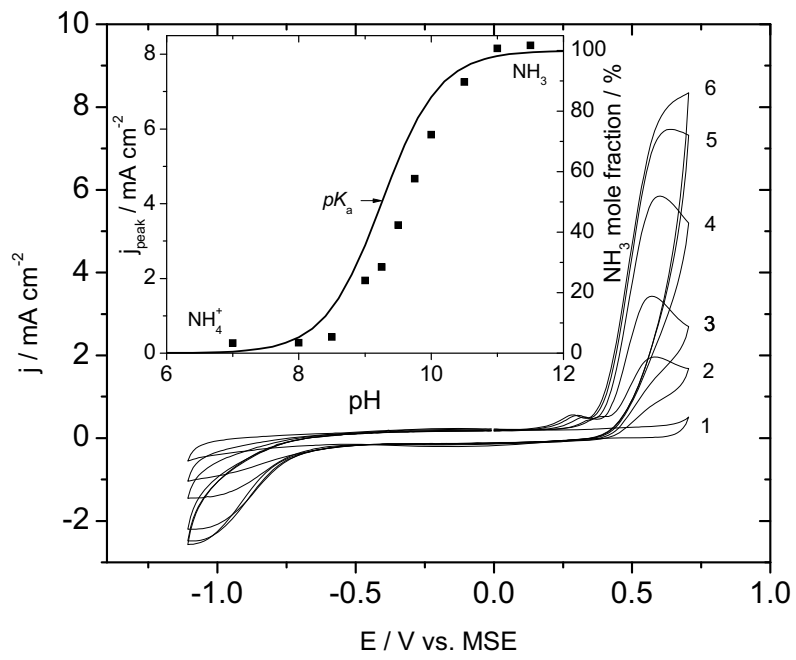


Figure 4

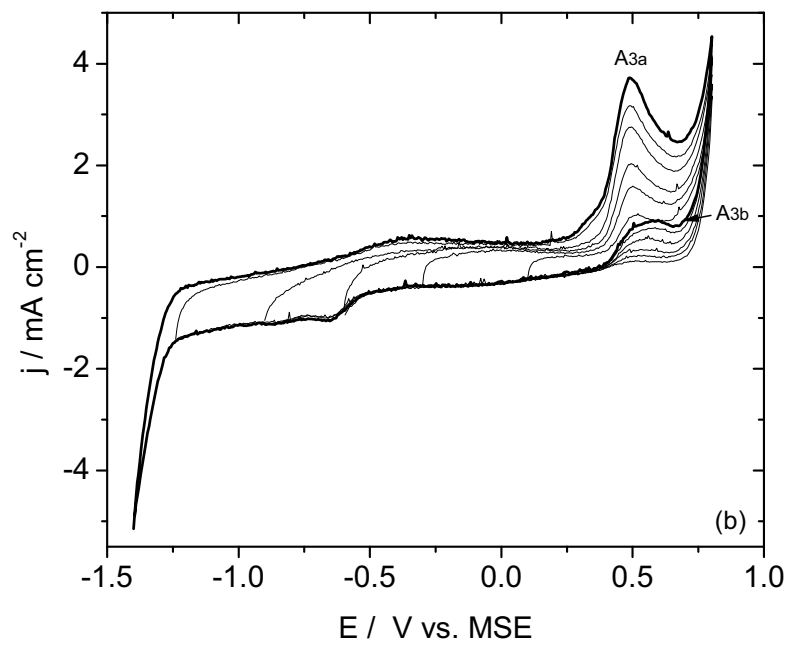
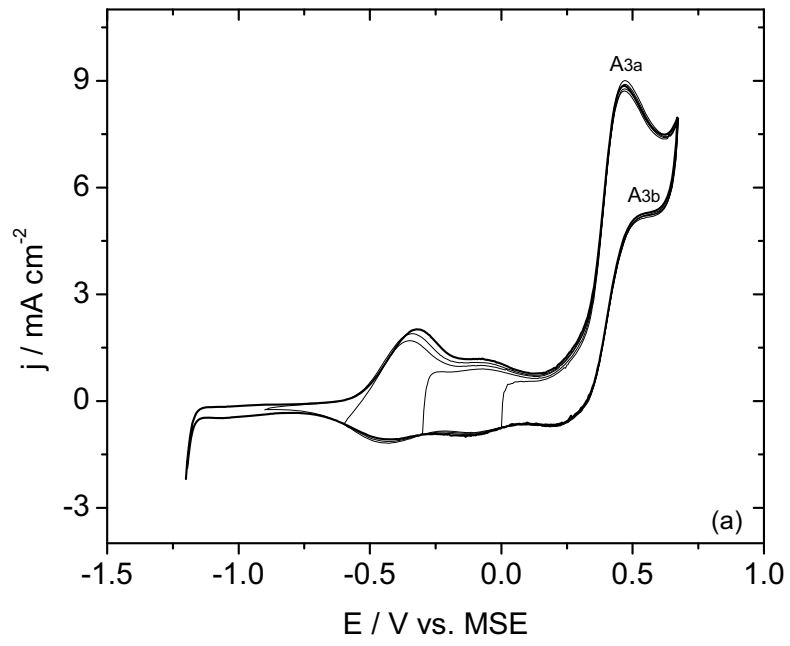


Figure 5

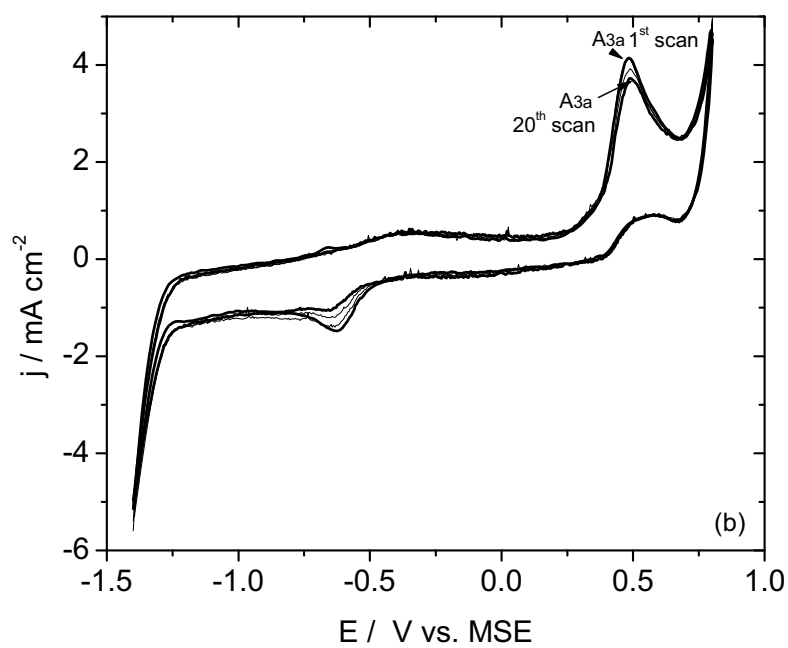
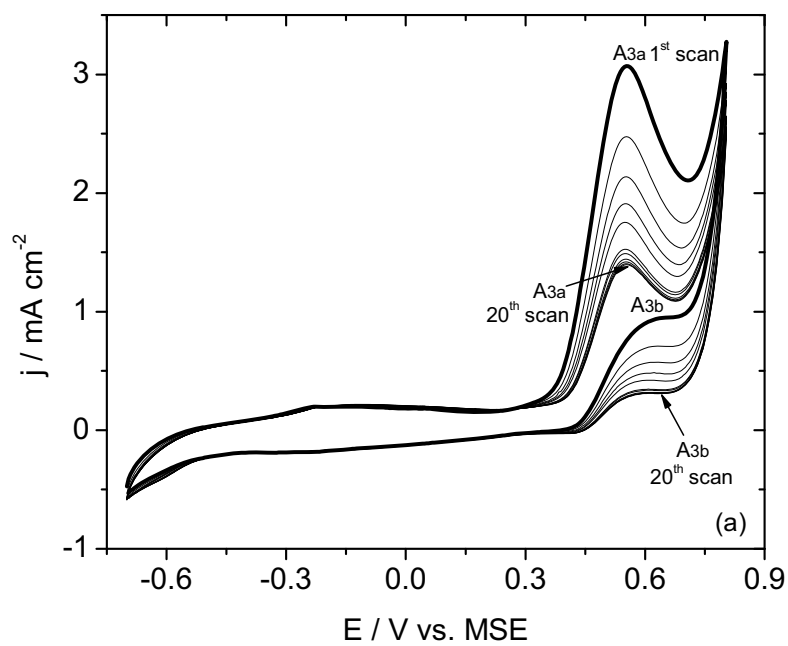


Figure 6

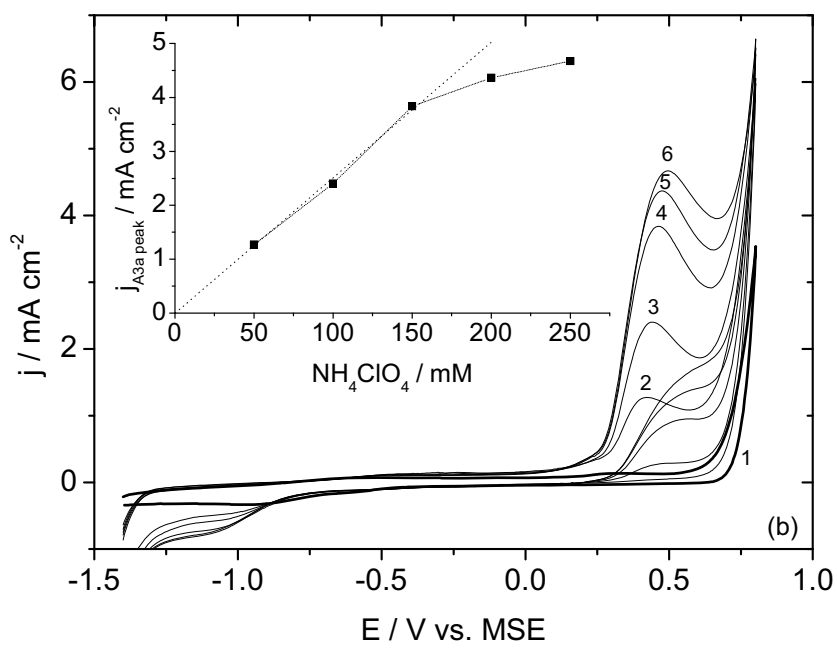
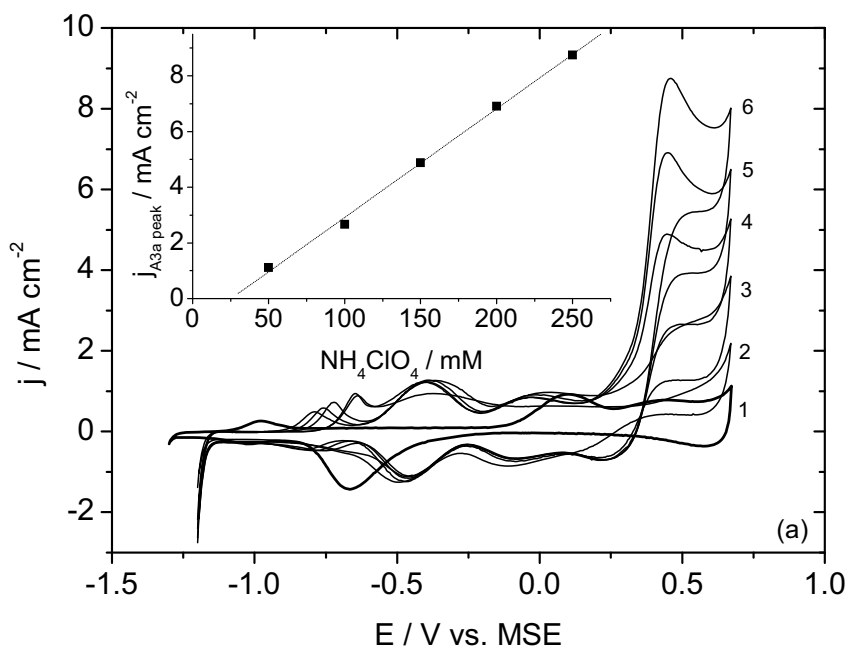


Figure 7

Curriculum vitae

Fierro Stéphane Gaël

57, chemin du Bois-Gentil

1018 Lausanne Switzerland

Tel. : 0041(76) 376 86 74



Email : stephane.fierro@epfl.ch

Born September 10, 1979

Swiss and Spanish citizenship

Education:

- 2007→2010: EPFL assistantship and PhD student in the group of electrochemical engineering (GGEC) from Pr.Comninellis
- 2000→2006: EPFL section of chemical and biological engineering
Master of Science in chemical and biological engineering
- 1999→2000: C.M.S (preparation program for EPFL admission test)
EPFL (Swiss institute of technology Lausanne Switzerland)
Admission at EPFL
- 1995→1998: French high school of Caracas Venezuela
French high school degree in scientific section (Baccalauréat général scientifique avec mention)
- 1993→1995: De Candolle College Geneva Switzerland
Scientific section
- 1990→1993: St-Louis College Corsier Geneva Switzerland
Scientific section

Languages:

Complete fluency in French, English and Spanish

Working command of German

Working experience:

- 2005→2005: employment: scientific project in electrochemistry for BASF in Ludwigshafen am Rhein Germany

